COO-3060-2

MITNE-130

USE OF GAMMA SPECTROSCOPY FOR NEUTRONIC ANALYSIS OF LMFBR BLANKETS

by

Chang-Sun Kang, Norman C. Rasmussen, Michael J. Driscoll

November, 1971

Department of Nuclear Engineering

Massachusetts Institute of Technology

Cambridge, Massachusetts 02139

Contract AT(11-1)-3060

U.S. Atomic Energy Commission

USE OF GAMMA SPECTROSCOPY FOR NEUTRONIC ANALYSIS OF LMFBR BLANKETS

by

Chang-Sun Kang

Norman C. Rasmussen

Michael J. Driscoll

November, 1971

Department of Nuclear Engineering

Massachusetts Institute of Technology

Cambridge, Massachusetts 02139

COO - 3060 - 2

MITNE - 130

Contract AT(11-1)-3060

U. S. Atomic Energy Commission

DISTRIBUTION LIST

Contract AT(11-1)-3060

U. S. Atomic Energy Commission, Headquarters
Division of Reactor Development and Technology
Reactor Physics Branch (3 copies)

U. S. Atomic Energy Commission
Cambridge Office (2 copies)

Dr. Paul Greebler, Manager
Nuclear Energy Division
Breeder Reactor Department
General Electric Compnay
310 DeGuigne Drive
Sunnyvale, California 94086 (1 copy)

Dr. Harry Morewitz, Manager
LMFBR Physics and Safety Projects
Atomics International
P.O. Box 309
Canoga Park, California 91305 (1 copy)

Mr. Malcolm Dyos, Manager
Nuclear Development, LMFBR Project
Westinghouse Electric Corporation
Advanced Reactors Division
Waltz Mill Site
P.O. Box 158
Madison, Pennsylvania 15663 (1 copy)

Dr. Robert Avery, Director
Reactor Physics Division
Argonne National Laboratory
9700 South Cass Avenue
Argonne, Illinois 60539 (1 copy)

Dr. Charles A. Preskitt, Jr.
Mgr., Atomic and Nuclear Department
Gulf Radiation Technology
P.O. Box 608
San Diego, California 92112 (1 copy)

ABSTRACT

It was the purpose of the present investigation to extend and apply Ge(Li) gamma-ray spectroscopy to the study of fast reactor blankets. The focal point for this research was the Blanket Test Facility at the MITR and Blanket No. 2, a realistic mockup of the blanket-reflector region of a large liquid metal cooled fast breeder reactor.

It was found that Ge(Li) detectors can be simultaneously used as both high energy neutron spectrometers and continuous gamma-ray spectrometers. The broadened internal conversion spectral line at 691.4 KeV has been analyzed for the former purpose, and the Compton recoil continuum has been analyzed and unfolded for the latter. This development makes the Ge(Li) spectrometer an extremely valuable shield analysis tool.

The moisture content of the sodium chromate used in the blanket mockup has been confirmed to be less than 0.1 w/o by prompt activation analysis.

Prompt capture and inelastic gamma, and decay gamma spectra emitted by the blanket were also analyzed to perform a neutron balance with mixed results. The inability to resolve U-238 prompt capture gammas made it necessary to use the low energy Np-239 decay gammas, with the attendant uncertainties due to large self-shielding corrections. Lack of data on the variation of prompt gamma yield with neutron energy for all blanket constituents also contributed to the uncertainties, which together made it impossible to develop this method to the point where reliable practical application can be recommended.

ACKNOWLEDGEMENTS

The work described in this report was made possible through the support of the M.I.T. LMFBR Blanket Physics Project which is sponsored by the United States Atomic Energy Commission. The same report has been also submitted by C. S. Kang in partial fulfillment of the requirements for the ScD degree at M.I.T.

Overall direction of this work has been shared by Professors M. J. Driscoll and N. C. Rasmussen. Special thanks are offered to Mr. Albert Supple, Dr. Yoshiyuti Hukai, Mr. Timothy Leung and Mr. Nestor Ortiz.

Greatly acknowledged are the assistance, patience and cooperation of the M.I.T. Reactor Machine Shop Staff, Radiation Protection Officers, Reactor Operation Personnel and M.I.T. Information Processing Center. Thanks are extended also to Miss Cindi Mitaras for the typing of this report.

TABLE OF CONTENTS

LIST OF FIGURES

LIST OF TABLES

Chapter I

INTRODUCTION

The development of high energy resolution lithium-drifted germanium detectors for gamma-ray measurements is a significant experimental advance which has been widely applied. Considerable previous work using these detectors for gamma-ray spectroscopy has been carried out at MIT, including prompt- and decay-gamma activation analysis (H2), and physics and burnup analysis of thermal reactor fuel (O1, H3, S1). It is the purpose of the present investigation to extend and apply these techniques to the study of fast reactor blankets as part of AEC sponsored research in this area at MIT.

The focal point for the research is the Blanket Test Facility at the MITR, which is powered by the thermal neutron flux from the MITR thermal column. The present work is concerned exclusively with measurements in Blanket No. 2, a mockup of a typical large LMFBR blanket. The only modification to the blanket design necessary for these studies was insertion of a 2-inch diameter beam hole through the blanket reflector. The experimental apparatus including Blanket No. 2 is described in Chapter II.

The general concern of the reactor physicist is

determination of the neutron reaction rates entering into the overall neutron balance; and the same objective is also paramount in the specific area of blanket physics research. Thus the first application investigated, as reported in Chapter III, is mainly concerned with the determination of neutron reaction rates in Blanket No. 2. These include the neutron capture rates, the inelastic scattering rates, and the fission rates. Both decay and prompt gamma-rays from Blanket No. 2 are analyzed for this purpose. The major constituents contributing useful gamma-rays were found to be U-238, Na, Cr, Fe, and O.

One not entirely anticipated result worthy of note was the complete disappearance of the U-238 prompt capture line at 4.059 MeV, which is so prominent in thermal neutron spectra.

Investigations have recently attributed persistent errors uncovered in analysis of LMFBR critical experiments to unanticipated moisture in graphite used to simulate carbide fuel (L4, P1). Small amounts of hydrogen can be important because it is so much better a moderator than any LMFBR constituent and can therefore soften the neutron energy spectrum. Since the water content of the LMFBR blanket materials could thereby have a significant effect upon the neutron energy

spectrum in the blanket, it is very important to know exactly how much moisture is contained in its constituent materials. Chapter IV treats the determination of the moisture content of sodium chromate, which is the major potential carrier for moisture in Blanket No. 2. Prompt activation analysis with thermal neutrons was used for this analysis.

Chapter V treats the application of gamma-ray spectroscopy to determine the neutron energy spectrum leaking from Blanket No. 2. Three methods are considered in this chapter:

1) An energy shift method using low-Z materials,

2) A prompt activation method, and

3) The germanium atomic recoil method.

The third method is developed in detail and applied to measure the neutron energy spectrum from Blanket No. 2.

In most experiments with Ge(Li) detectors for gamma-ray measurements, the dominance of the Compton recoil continuum in the detectors is regarded as an unwanted and troublesome complication. R. Gold (G1), however, showed that this feature can be exploited for continuous gamma-ray spectroscopy, and that it is therefore a useful tool for shielding analysis. Chapter VI is mainly concerned with the application of his

method to analysis of the continuous gamma-ray spectra from Blanket No. 2. Use of a fairly large Ge(Li) crystal (17 c.c.) made possible analysis of very high energy gamma-rays (up to 10 MeV).

In general, then, Chapters III and IV are concerned with extension of conventional photo-peak analysis into the realm of LMFBR blanket applications, while chapters V and VI introduce some more novel capabilities of the Ge(Li) detector. In a sense these latter applications can be considered to be "free information" obtained in the conventionally oriented gamma-ray spectra from Blanket No. 2. They are, however, of considerable interest in their own right. Since we have now shown that it is possible to use the Ge(Li) detector as a simultaneous spectrometer for both gamma-rays and neutrons, it deserves increased consideration as a shield analysis tool.

In Chapter VII, this and other conclusions and recommendations are summarized. The bibliography follows immediately after, and data and computer programs are introduced in Appendices.

Chapter II

EXPERIMENTAL APPARATUS

In this chapter the experimental apparatus concerned with the present work is discussed. First the Blanket Test Facility at the MITR is described, and the description of the Ge(Li) detectors and the associated electronics follows. Energy calibration and non-linearity correction are discussed next.

2-1 Blanket Test Facility

The Blanket Test Facility (BTF) is located at the rear of the graphite-lined cavity at the end of the MITR thermal column. A detailed description of the BTF is given in Reference F1. The front component in the BTF is a converter assembly, composed of a fission plate, filter and back scatter regions. Powered by the thermal neutron flux from the MITR thermal column, the converter generates a fast neutron flux similar to LMFBR core leakage spectra for testing mockups of LMFBR blankets. The converter assembly consists of a graphite backscatter-moderator region composed of 4 inch by 4 inch reactor grade graphite stringers, and a fuel region, which serves as both fission plate and filter, composed of 0.5-in. - diameter, aluminum clad UO_2 fuel rods in a close-packed, triangular pitch array. The active

fuel region is 48 in. high and 60 in. wide, and has U-235 enrichments of 1.0999% and 1.99%.

The simulated blanket assembly is installed directly behind the converter assembly. BTF Blanket No. 2 is an accurate mock-up of a typical LMFBR blanket composition. A detailed description of Blanket No. 2 is given in reference L1. Figure 2-1 shows the schematic plan view of the Blanket Test Facility with Blanket No. 2 in place. Blanket No. 2 is installed directly behind the converter assembly, which provides the simulated core leakage spectrum. Two 2-ft. - thick heavy concrete shield doors are used to close-off the irradiation cave containing the converter and blanket assemblies. A 2-in.-diameter hole, 4 in. below mid-plane, has been drilled through the blanket reflector to provide a beam hole for fast neutron and gamma-ray spectrum measurements. This beam hole is aligned with the holes through four masonite and steel laminated plugs in the port 12CH1 penetrating the shield doors, so that the measurements can be done externally. Lead collimators containing various-sized holes have been made up to fit into the holes of the masonite and steel laminated plugs.

Blanket No. 2 is composed of 25 subassemblies which contain steel-clad uranium metal fuel rods and anhydrous

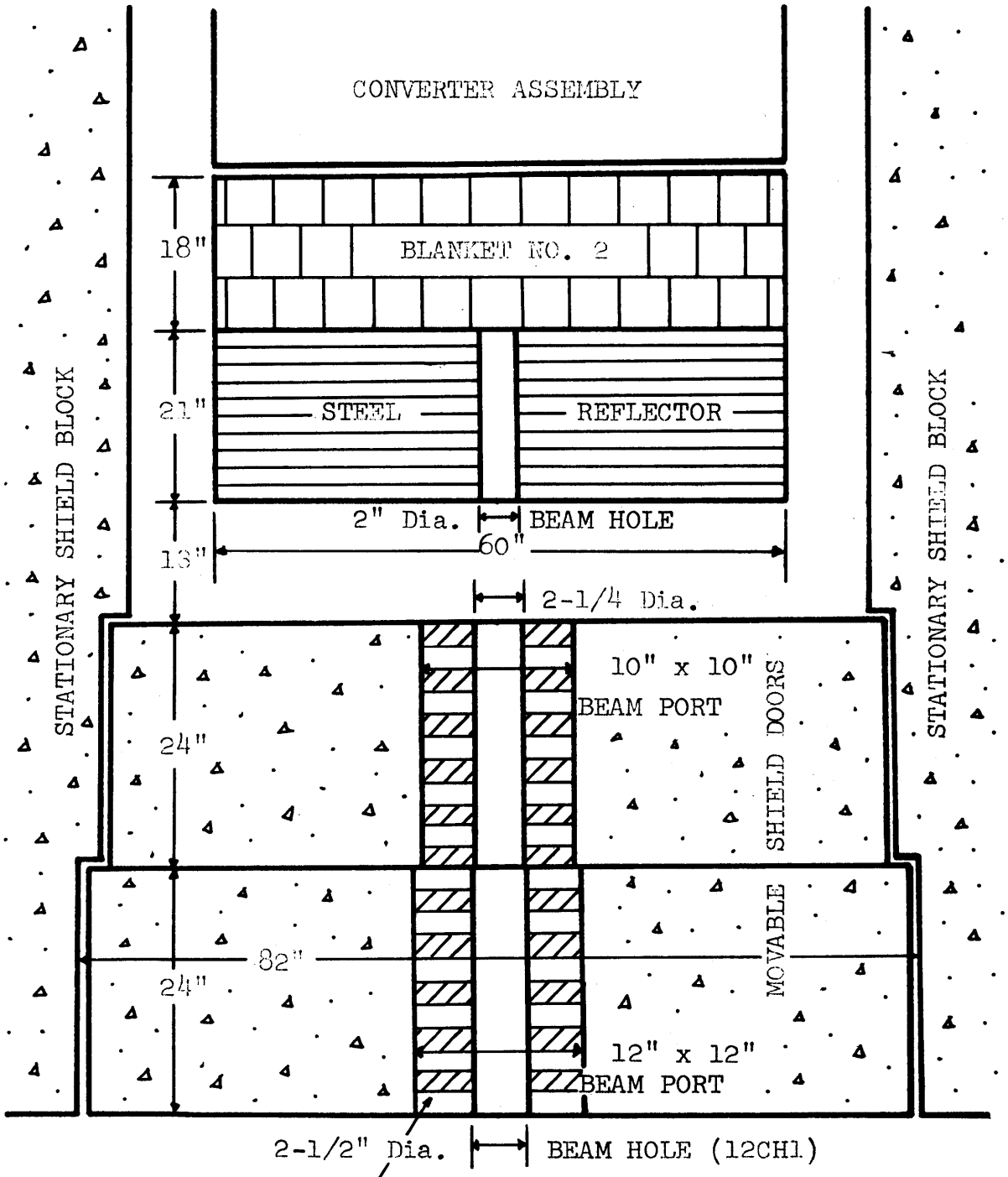

FIG. 2-1 Schematic Plan View of Blanket Test Facility and Blanket No. 2

sodium chromate powder (plus several outer subassemblies which are filled with a mixture of iron punchings and anhydrous borax powder). Each subassembly is loaded with 121 uranium metal fuel rods arranged on a square lattice spacing of 0.511 in.; the 1/4-in. - diameter uranium metal fuel is clad in low-carbon steel tubing. The inter-rod volume in each subassembly is filled with anhydrous sodium chromate (Na_2CrO_4) powder. Figure 2-2 shows a cross-sectional view through a subassembly.

The homogeneous atom densities in Blanket No. 2 are given in Table 2-1, where they are compared with the atom densities in a realistic blanket. As can be seen the homogenized compositions are in good agreement, confirming that Blanket No. 2 is a realistic mockup of an actual LMFBR blanket.

2-2 Ge (Li) Detectors and the Associated Electronics

The main detector used in this work was a Ge(Li) detector, which has been described by V. Rogers in Reference R1. This detector has an active volume of 17 c.c. It has a relatively large dead region, the overall efficiency is fairly high, and it had a better energy resolution than any other detectors available to the author. The detector was operated at liquid nitrogen temperature ($77^{o}K$) with a reverse bias of -700 V. The

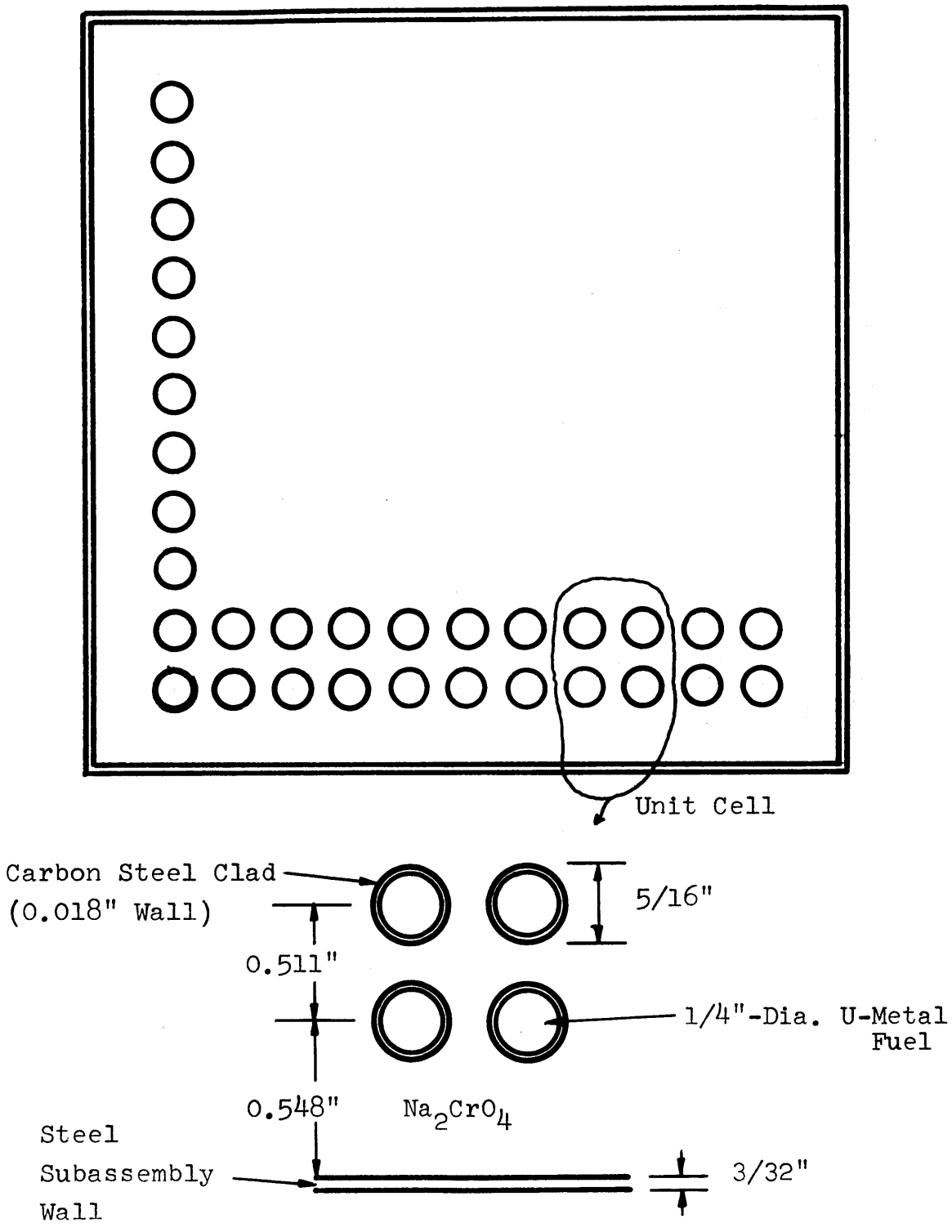

Fig. 2-2 Blanket No. 2 Subassembly

TABLE 2-1

Homogenized Atom Densities in BTF Blanket No. 2

Nuclide	Blanket No. 2		Equivalent Realistic* Blanket	
U-235	0.000088		0.000016	
U-238	0.008108		0.008131	
O	0.016293		0.016293	
Na	0.008128		0.008128	
Cr	0.004064		0.003728	
Fe	0.013750	0.017814	0.012611	0.017814
Ni	0.000000		0.001475	
H	0.000073		0.000000	
C	0.000096		0.000082	

Reference: L1

* Composed of 37.0 V/O depleted UO_2 (at 90% of theoretical density), 20.7 V/O Type 316 stainless steel, 32.0 V/O sodium and 10.3 V/O void.

exact bias voltage was determined by optimizing the energy resolution and the efficiency. The energy resolution of this detector varied from a full width at half maximum, FWHM, of 3.5 KeV to 7.0 KeV according to the gamma-ray energies (511 KeV and 7724 KeV, respectively). To reduce noise it is usually sufficient to have a solid electrical ground between the detector and the preamplifier. In particular it is strongly suggested that the ground of the system be completely isolated from external electronic contacts. One has also to allow a certain period of time after one moves the detector or refills the dewar with liquid nitrogen in order to prevent boiling noise. Many otherconsiderations have been discussed in References O1, H2, H3 and H4.

Generally there are three major methods of operation of the Ge(Li) spectrometer in the detection of gamma-rays: the direct or free mode, the Compton suppression mode and the pair spectrometer mode. The free mode method of operation, which was used throughout this work, consists of using the detector and its associated electronics to drive the analyzer. No gating of the analyzer is done, and no coincidence or timing of the detected pulses is carried out. Figure 2-3 shows the schematic electronics

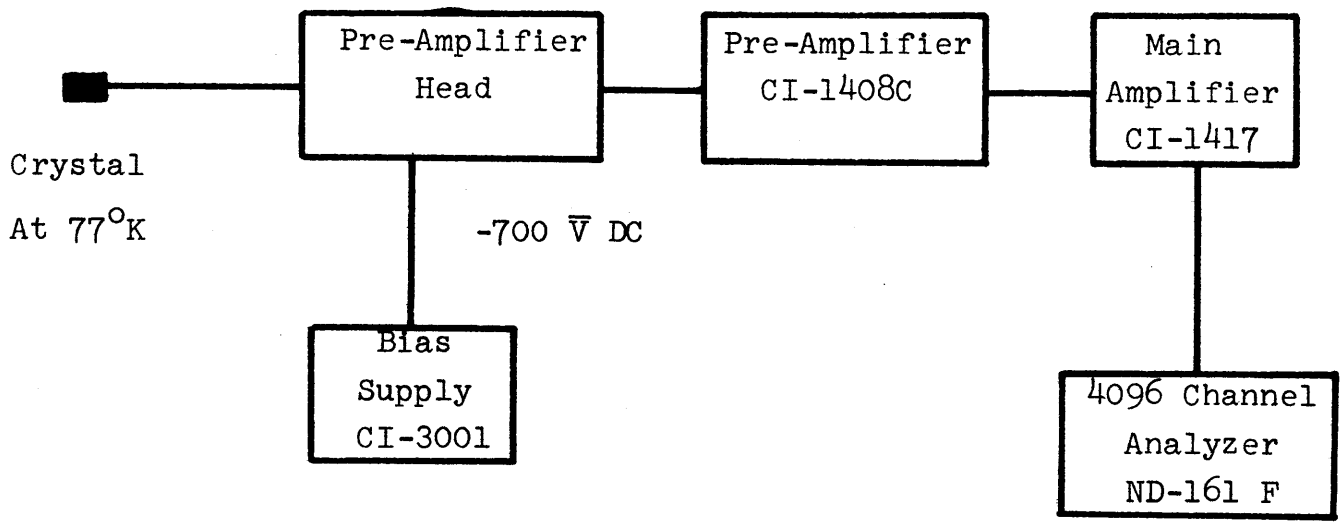

Fig. 2-3 BLOCK DIAGRAM OF DETECTOR ELECTRONICS FOR OPERATION IN THE FREE MODE

diagram for free mode operation of the Ge(Li) detector.

The free mode method of operation is preferable in the case of very low counting statistics even though it incurs a higher background.

2-3 Energy Calibration Standards and Non-linearity Correction

In the present work two accurately known calibration peaks are used to obtain a linear fit between the channel number of the peak center and gamma-ray energy. Consequently the non-linearity of the detector and electronic amplifiers must be checked.

An experimental method is used to check for system non-linearity. This set-up consists of using a pulser connected to the test input of the CI-1408C preamplifier, to simulate a spectrum of many peaks equally spaced in energy. Analyzing such a spectrum gives an indication of the system energy linearity (H1,O1). The method works well provided that the pulser is stable enough so as not to obscure the effect being measured. The pulser consists of a mercury relay precision pulse generator (RCL Model 20900), whose output amplitude is determined by the equally spaced triggering bias voltage provided by an EDC Model MV-100N Precision Millivolt Standard (0-10 V output) with 0.01% accuracy. To increase pulse amplitude a 6 V standard dry cell is connected in series. A series

of equally spaced pulses were analyzed for energy separation, and compared against what the separation would be if the system were perfectly linear. This analysis thus produced a set of linearity correction factors. The subroutine LINEAR of the computer code GAMANL (R2) performs this analysis. Figure 2-4 shows a plot of these correction factors versus channel number obtained through the subroutine LINEAR for the various gain settings of the main amplifier. The linearity data was checked from time to time throughout these experiments, but the linearity correction data did not change noticably, as V. Orphan has also reported in Reference 01.

The two known calibration peaks must be known very accurately to obtain a linear fit between the peak center and gamma-ray energy. Table 2-2 indicates the energy calibration standards used in the present work. The accuracies of the standards were 1.0 KeV or better in all cases. Any pair of lines from Table 2-2 were used according to the situation. The electron annihilation line and the Ar^{41} decay line were prominent whenever the reactor was at power. In the case of decay gamma-ray analysis Co^{60} or Na^{24} lines were mainly used for the energy calibration.

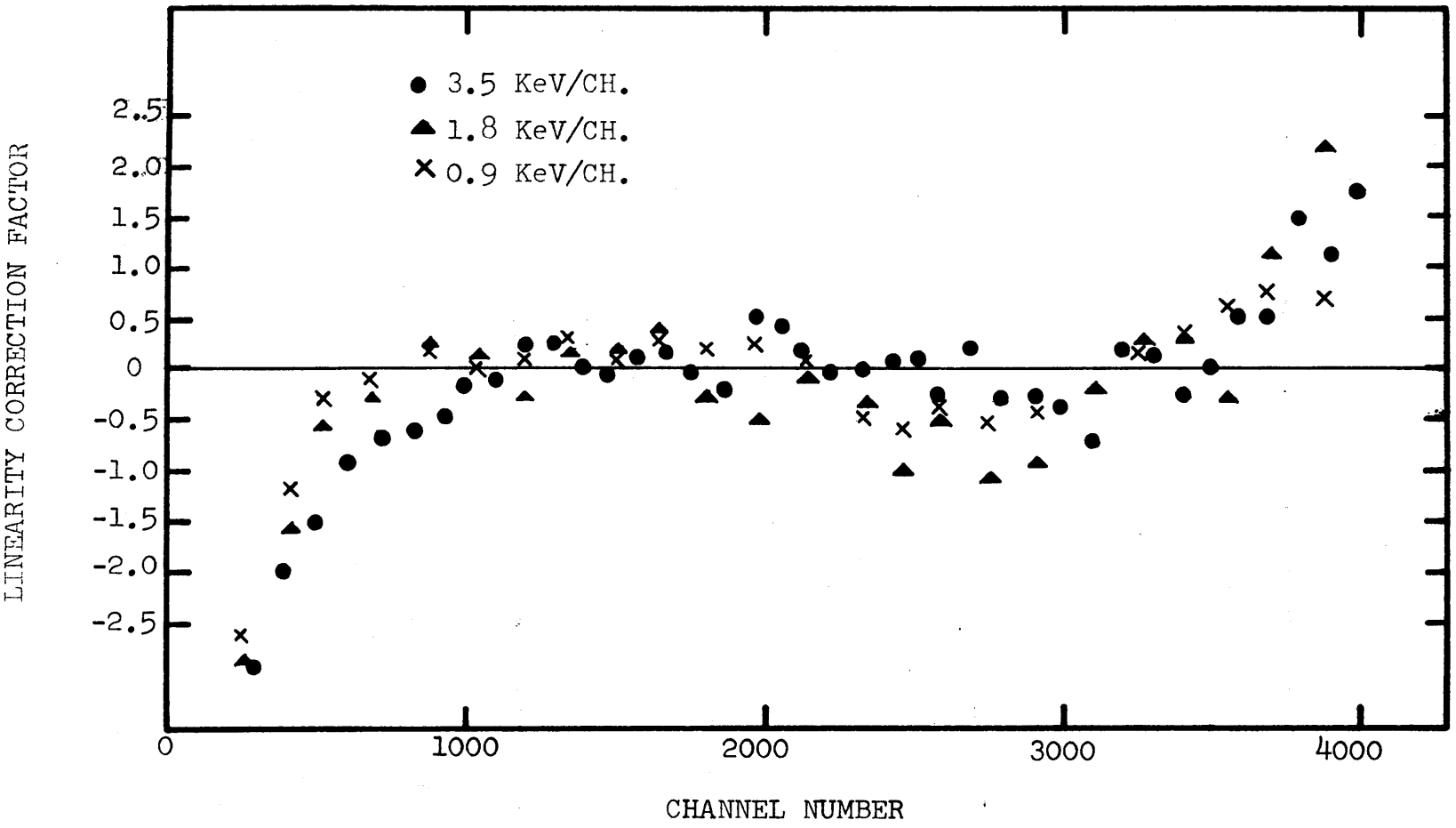

Fig. 2-4 Linearity Correction as a Function of Channel Number for Free Mode Operation

TABLE 2-2

ENERGY CALIBRATION STANDARDS

ENERGY(KeV)	REMARK	REFERENCE
511.006 ± 0.005	Annihilation of Electron-Positron	a
1173.226 ± 0.040	Co^{60} Decay	b
1293.64 ± 0.04	Ar^{41} Decay	c
1332.48 ± 0.05	Co^{60} Decay	b
1368.53 ± 0.04	Na^{24} Decay	b
2753.92 ± 0.12	Na^{24} Decay	b
6018.2 ± 1.0	Fe Capture Line	d
7278.8 ± 1.0	Fe Capture Line	d

References

a Electron rest mass from 1963 atomic constants.

b Murray G., et al., Nucl. Phys. G3 (1965) 353.

c White, D., et al., "Precision Measurements of Gamma-Rays from Co^{60}, Ar^{41}, and Cr^{53} (n,γ) Cr^{54}", Nucl. Inc. and Meth. 66 (1968) 70-76.

d Orphan V., et at.,"Study of Thermal Neutron Capture Gamma-Rays Using a Ge(Li) Spectrometer", MITNE-80 (Jan. 1970).

Most data are analyzed through the computer code GAMANL(R2) and plotted using the CAL-COMP provided by the MIT Information Processing Center. The gamma-ray spectra from Blanket No. 2 will be analyzed in the following chapters, and, in particular, the reaction rates in Blanket No. 2 will be discussed in the next chapter.

Chapter III

DETERMINATION OF NEUTRON REACTION RATES IN LMFBR BLANKET NO. 2

3-1 Introduction

In this chapter, Ge(Li) gamma-ray spectroscopy is used to determine neutron reaction rates in the LMFBR blanket mockup, and thereby to deduce the neutron balance in the blanket. These experimental results will be compared with calculated values, other experimental values, or both. Obtaining a variety of independent experimental support for calculated parameters is particularly important in the present case because of the necessity for establishing credibility for mockup experiments in lieu of studies on real blankets.

The neutron reaction rates of interest may be categorized as capture, scattering, and fission rates. The capture rate may be obtained by analyzing the prompt capture gamma-rays and short-lived decay gamma-rays from the blanket. Inelastic scattering rates, using the characteristic prompt inelastic gamma-rays, and the fission rate, using the short-lived fission product decay gamma-rays, will also be analyzed in this chapter.

Blanket No. 2 is mainly composed of U-238, Na, Cr, Fe, and O. By analyzing various gamma-rays from Blanket No. 2, one can determine the reaction rates of these major blanket constituents. The results can then be compared with the values obtained using foil activation methods.

Through observation of the prompt capture gamma-rays emitted by Blanket No. 2, the information listed in Table 3-1 was found to be identifiable. Somewhat unexpectedly the major thermal neutron capture gamma-ray lines of U-238 were not observable in the spectra from Blanket No. 2 even though calculations and foil irradiations showed that over 90% of all captures were in U-238. Hukai identified more than 35 thermal neutron prompt capture gamma-ray lines of U-238 in Reference H3. Groshev et al. (G2) also showed about 30 thermal neutron prompt capture gamma-ray lines of U-238 in the energy region of 3-4.5 MeV. In particular, the complete disappearance of the very prominent thermal neutron prompt capture gamma-ray line at 4.059 MeV was hardly expected. Yost et al. (Y1) have reported calculations which lead one to expect a decrease in the prompt capture gamma-ray yield of U-238 at 4-4.25 MeV by a factor of five. But the essentially complete disappearance observed for the 4.059 MeV line, and the other U-238 thermal capture

lines as well is still unexplainable. This complete disappearance of the U-238 capture line at 4.059 KeV made it difficult to deduce the capture rate of U-238 in the blanket. However, observation of many short-lived decay gamma-ray lines from Np-239 provided an alternate method for obtaining the capture rate of U-238 (Section 3-4). The observable decay gamma-ray lines from Blanket No. 2 are shown in Table 3-2. Analysis of the low energy Np-239 decay gamma-rays presents some difficulties as compared to the higher energy prompt gamma-rays, as will be explained subsequently. Other problems also arise.

The analysis of gamma-rays from the blanket is very different from the conventional analysis of gamma-rays emitted by small samples. The neutron flux, hence the capture rate, inside the blanket varies precipitously with depth, as does the transmission probability of the escaping gamma-rays. Particularly when dealing with low energy gamma-rays the heterogeneity of the blanket composition is also a major consideration.

Comparison of Tables 3-1 and 3-2 shows that sodium activity is prominent in both prompt and decay gamma-rays spectra. This enables one to inter-normalize the prompt and decay gamma-ray data and synthesize the

TABLE 3-1

OBSERVABLE PROMPT GAMMA-RAYS FROM BLANKET NO.2

Nuclei	Capture Line	Inelastic Line
U-238	None Resolved	None Resolved
Fe	More than 20 prominent peaks including 7631.6 KeV line	845 KeV
Na	870.6 KeV 6395.4 KeV	438 KeV
Cr	835.1 KeV 7939.3 KeV 8884.1 KeV	1433.9 KeV
O	None Resolved	6127.8 KeV
C	4945.2 KeV	None Resolved

Table 3-2

OBSERVABLE SHORT-LIVED DECAY GAMMA-RAYS

FROM BLANKET NO. 2

NUCLEI	ENERGY(KeV)	YIELD(%)*	T 1/2
Na^{24}	1368.7 2753.9	100 102	15 hrs.
Cr^{51}	322		27.8 d
Fe^{59}	1286.6		45.0 d
Np^{239}	106.1 209.8 228.2 277.6 315.9 334.3	22.8 4.1 12.7 14.1 1.5 2.0	2.3 d

* YIELD defined here is the number of gammas per 100 disintegrations. The reference is C. Lederer, J. Hollander, and I. Perlman Table of Isotopes, 6th edition, John Wiley and Sons, Inc. 1967

results into a single neutron balance. Although chromium and iron also appear in both spectra, they are not particularly suitable for this purpose due to the long half-life of Cr^{51} and Fe^{59}, which results in accumulation of interfering residual activity over a long previous irradiation history.

3-2 Theory

The geometric configuration of the Blanket Test Facility is described in the preceding chapter, and in LMFBR Blanket Physics Project Progress Report No. 1 (Li). Figure 3-1 shows the schematic overall plan view of the Blanket and the Ge(Li) detector set-up, where X_B, X_R, X_F and X_L are the thicknesses of blanket, reflector, LiF and lead, respectively, and X_A is the distance from the outside surface of the blanket to that of the shielding door.

The number of prompt gamma-rays of interest with energy E_γ produced per second at the position X in the blanket is given by the following equation:

$$C_\gamma(X) = \int_E N \left(\frac{I\gamma(E)}{100} \right) \sigma(E) \phi(E,X) \, dE, \qquad (3\text{-}1)$$

where

$I\gamma(E)$ - is the number of prompt gamma-rays with energy $E\gamma$ emitted per 100 neutron reactions

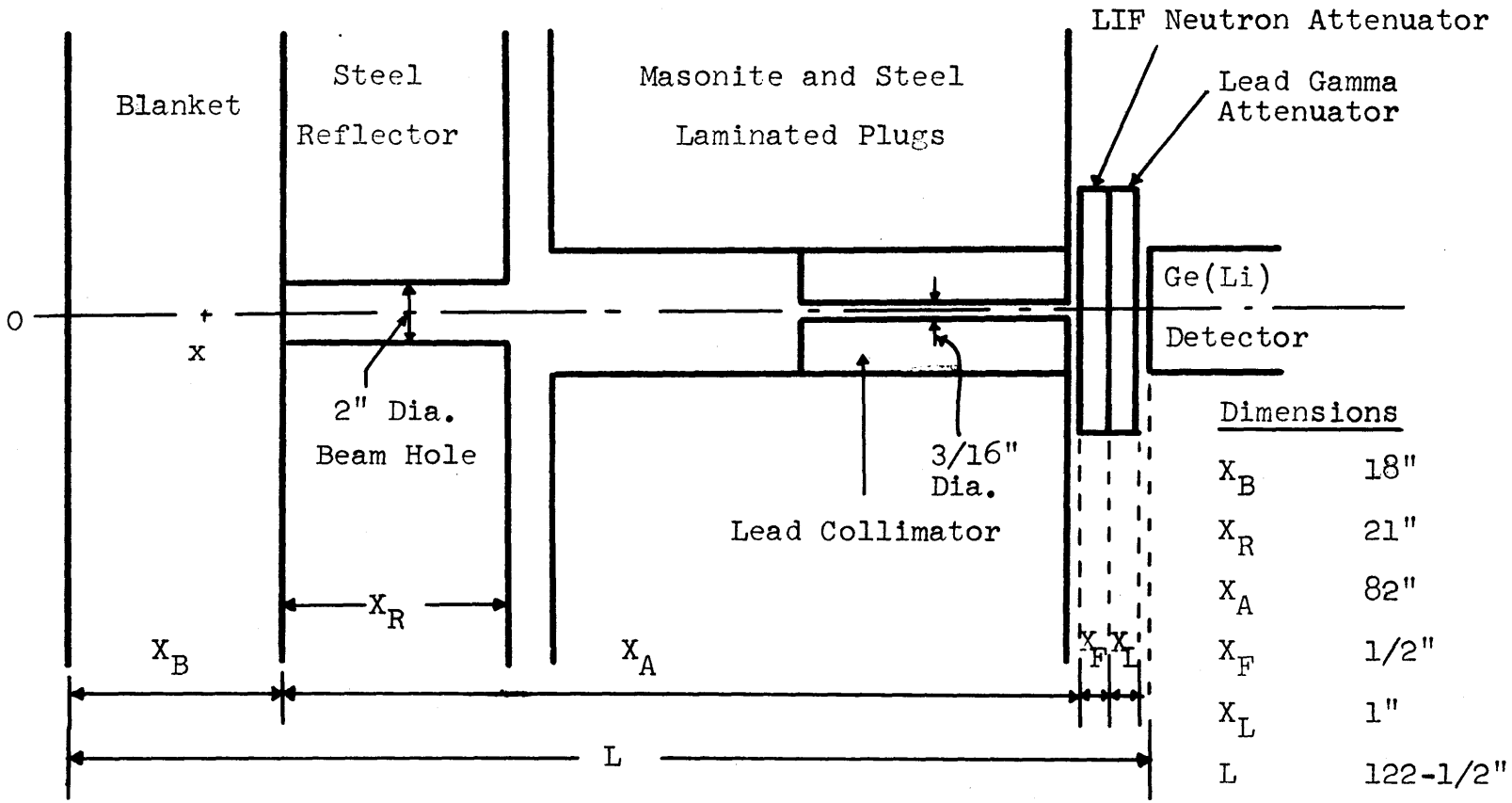

Fig. 3-1 Schematic Overall Plan View of Blanket No. 2 and Detection Setup

(capture or inelastic scattering) of energy E,

N - is the number of target nuclei of interest per c.c of the blanket (the medium is assumed to be completely homogeneous),

$\sigma(E)$ - is the neutron cross-section for a certain reaction (capture or inelastic scattering) of the element of interest at the neutron energy E, and

$\phi(E,X)$ - is the one-dimensional axial flux of neutrons having energy E at the position X in the blanket.

For a first step we may assume that the gamma-ray yield intensity function $I\gamma(E)$ is constant overall neutron energies. This may not be a very good approximation for certain constituents. However the efficiency curve for iron peaks shows that $I\gamma(E)$ does not vary appreciably with respect to the energy of the incoming neutrons. This will be discussed further in Section 3-3-1.

Secondly the separability of variables for the neutron flux $\phi(E,X)$ is assumed as follows:

$$\phi(E,X) = \phi(E)\ \psi(X) \qquad (3\text{-}2)$$

where $\phi(E)$ - is the neutron energy spectrum and

$\psi(X)$ - is the average one-group axial flux distribution in the blanket, which is normalized as follows:

$$\int_0^{X_B} \psi(X)\, dX \equiv 1.$$

Calculations show that the collapsed one-group flux varies very smoothly with position (Appendix A). Hence separability of the neutron flux $\phi(E,X)$ is quite an appropriate assumption for present purposes.

A homogeneous blanket medium and a steady state flux in the blanket is already assumed.

Hence, Equation 3-1 becomes

$$C\gamma(X) = \left(\frac{I\gamma}{100}\right) \psi(X) \int_E N\, \sigma\, (E)\, \phi\, (E)\, dE \qquad (3\text{-}3)$$

Now define the average reaction rate over the neutron energy in the blanket, R, as follows:

$$R \equiv \int_E N\, \sigma\, (E)\, \phi\, (E)\, dE \qquad (3\text{-}4)$$

This reaction rate, R, is classified into various kinds of reactions according to the specification of N and σ. N specifies the material of interest in the blanket and σ specifies both the material and mode of reaction.

The total area of the gamma-ray peak of interest with energy $E\gamma$ observed by the detector during the time interval, T, is given by the following equation:

$$A\gamma = \left(\int_o^{X_B} C\gamma\,(X)\; S\gamma\,(X)\; dX \right) \cdot T \cdot F\gamma \cdot E\gamma \cdot \Omega \qquad (3\text{-}5)$$

or

$$A\gamma = R \cdot \left(\frac{I\gamma}{100} \right) \cdot S\gamma \cdot T \cdot E\gamma \cdot F\gamma \cdot \Omega \qquad (3\text{-}6)$$

where

$$S\gamma \equiv \int_o^{X_B} \Psi\,(X)\; S\gamma\,(X)\; dX\,, \qquad (3\text{-}7)$$

T - is the counting time,

$E\gamma$ - is the intrinsic detection efficiency of the Ge(Li) detector and the associated electronics for gamma-ray energy $E\gamma$,

$F\gamma$ - is the correction factor for attenuation of gamma-rays with energy $E\gamma$ by air or any other materials placed in the flight path of the gamma-ray beam from the blanket surface to the detector,

Ω - is the geometric solid-angle correction factor, and

$S\gamma\,(X)$ - is the correction function for self-absorption of gamma-rays with energy $E\gamma$ in the blanket, which is a function of position.

3-3 Prompt Capture Gamma-Rays

3-3-1 Total Efficiency

From Eq. 3-6 the total peak area at $E\gamma$ observed by the detector may be rewritten as:

$$A\gamma = \left(\frac{I\gamma}{100} \right) \cdot R \cdot \varepsilon\gamma \cdot T \qquad (3\text{-}8)$$

where $\varepsilon\gamma$ is the total efficiency which is defined by

$$\varepsilon\gamma \equiv S\gamma \cdot F\gamma \cdot \varepsilon\gamma \cdot \Omega \ . \qquad (3\text{-}9)$$

The total efficiency function, $\varepsilon\gamma$, represents the contribution of the gamma-ray energy dependent terms and the constant terms to the reaction rate calculation. The function $\varepsilon\gamma$ is computed by using an array εj that stores all the terms for the j-th gamma-ray energy value, Ej. The εj array values are determined by using the measured data on system efficiency, self-absorption and the variation of the neutron flux in the blanket, and the attenuation of the gamma-ray beam during the flight to the detector. The determination of the total efficiency curves to be used with the data involves consideration of complicated effects taking place during the flight from birth to detection. Thus the total efficiency of the setup has been determined experimentally instead of by calculation.

Since we are dealing for the most part with prompt gamma-rays of fairly high energy, a homogeneous medium was assumed and all heterogeneous effects on the self-absorption correction factor are neglected. Since the same detector and geometry was used for all prompt gamma-ray experiments on Blanket No. 2, the same efficiency curve applies. The total efficiency array Ej that stores all the terms for j-th energy value is:

$$\varepsilon_j = \frac{A_j}{\left(\frac{I_j}{100}\right) \cdot R \cdot T} \quad , \qquad (3\text{-}10)$$

where Aj and Ij are the arrays of $A\gamma$ and $I\gamma$, respectively, for the j-th gamma-ray energy value.

Figure 3-2 shows the total efficiency curve for the detection system, which is obtained from the iron prompt capture gamma-ray data from Blanket No. 2, employing the yield intensity array Ij for thermal neutrons. Note that the observed total efficiency array data lie on the efficiency curve for thermal neutron capture (O1, H3, H4) except for a few of the peaks. The most prominent shift in yield occurs with the peak at 7278.9 KeV, which is considerably displaced from the thermal efficiency curve. This shows that some peaks do indeed change in yield intensities as the neutron energy

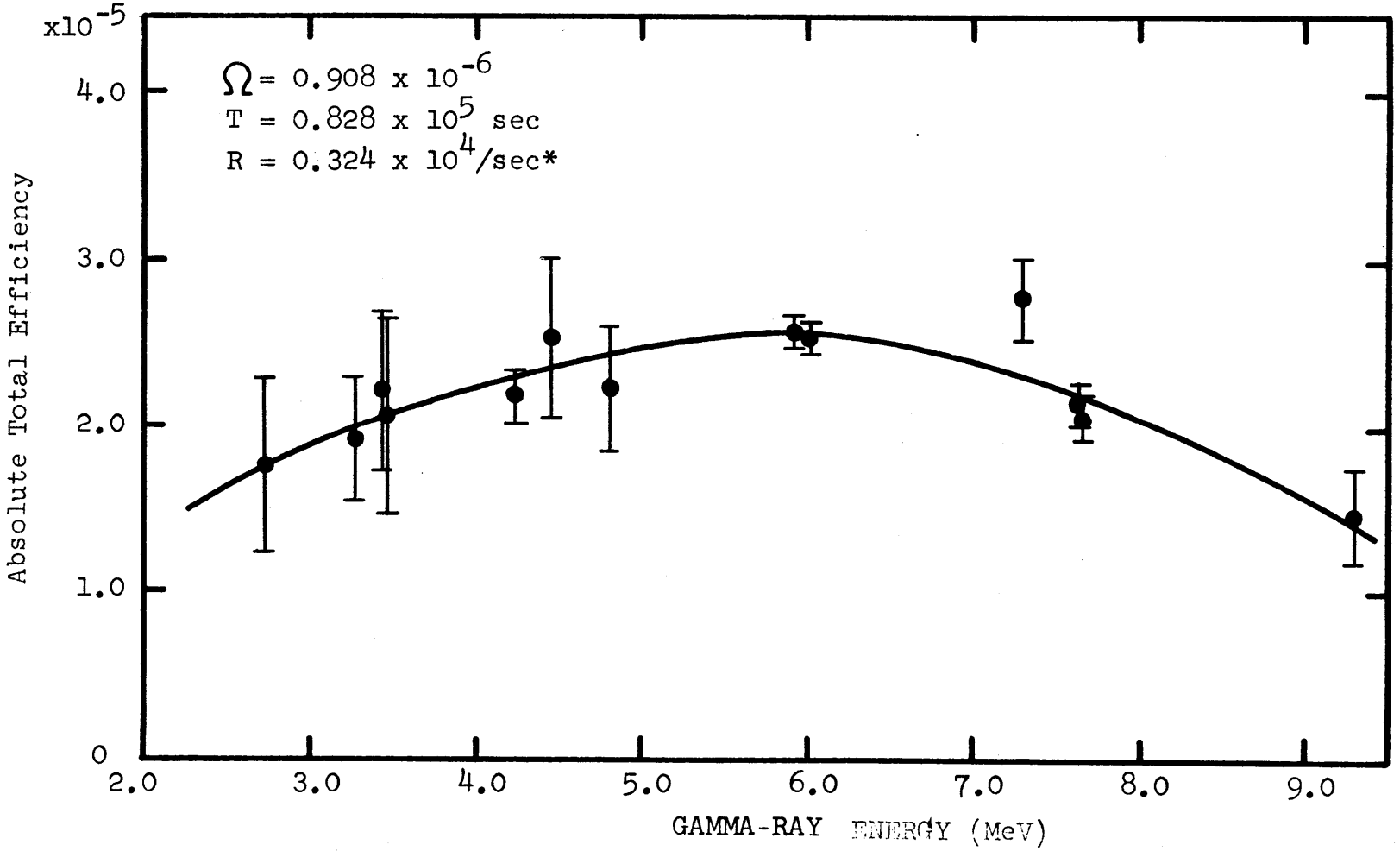

Fig. 3-2 Total Efficiency Curve of Detection System for High Gamma-Energies

(* $R = N \bar{\sigma} \bar{\phi}$: $N = 0.01375$, $\bar{\sigma} = 0.00867$, $\bar{\phi} = 2.72 \times 10^8$)

changes, while a substantial number of others do not. It is very important to know that there are some gamma-ray peaks which maintain an invariant yield regardless of the neutron energy. Otherwise data interpretation would be hopelessly complicated due to the paucity of prompt gamma-ray yield data for all but thermal neutron energies.

Run number 105 is used to get the total efficiency data. Appendix I shows all GAMANL output data for the prompt and decay gamma-ray spectra from Blanket No. 2.

A background run has been performed with the 2-in. diameter beam hole in the reflector plugged to check background (especially Fe). The counting rate was so small that no significant contribution from the reflector is observed. As the diameter of the collimators was decreased, the signal ratio of Na and Cr prompt capture lines to Fe prompt capture lines improved a great deal.

3-3-2 Data Analysis

Table 3-3 shows the major background lines observed in spectra from Blanket No. 2. Among these background peaks Ar-41 at 1293.6 KeV was always so prominent that it was used as an energy calibration, together with the

Table 3-3

PRINCIPAL BACKGROUND GAMMA-RAYS

ENERGY (KeV)	REMARKS
476.3	B-12 Decay
511.0	Annihilation
595.0	Ge-74 Inelastic
691.4	Ge-72 Internal Conversion
1173.2	Co-60 Decay
1293.6	Ar-41 Decay
1332.6	Co-60 Decay
1460.5	K-40 Decay or Ar-40 Inelastic
1778.9	Al-28 Decay
4945.2	C Capture, Prompt Gamma
7367.7	Pb Capture, Prompt Gamma
7723.8	Al Capture, Prompt Gamma

annihilation peak at 511 KeV. There are also two interesting background peaks at 595 KeV and 691.4 KeV. They are, respectively, an inelastic scattering gamma line and the internal conversion line of Ge caused by interaction of incident fast neutrons with the Ge(Li) detector itself. The line at 691.4 KeV is analyzed in considerable detail in Chapter V, since it permits inference of the fast neutron spectrum. The prompt capture line of carbon at 4945.2 KeV is observed, originating perhaps in the masonite 12CH1 port shield or even in the distant converter assembly itself; the other lines are general background lines which are all possible emissions from the structual materials around the facility.

Table 3-2 showed the prompt capture gamma-rays of Fe, Na, and Cr which were observable in the spectra of Blanket No. 2. Iron always showed more than 20 peaks in every spectrum obtained from Blanket No. 2. It should be noted that the shielding for the facility is magnetite concrete and the blanket reflector is pure iron. Therefore one can expect iron prompt capture lines from almost everywhere. In this case, if one is interested in the iron peaks due only to the blanket, a judicious choice of collimator design and careful alignment of

the beam holes between the blanket assembly and the two movable shielding doors is called for. A specially built 2-ft. long and 3/16 in. internal diameter collimator was used in order to view only the bottom of the exposed blanket surface at the beam hole. This collimator eliminated most of the background iron lines from the side wall of the iron reflector. Sodium showed two prompt capture gamma-ray peaks at 870.6 KeV and 6395.4 KeV, and two major decay gamma-ray lines at 1368.7 KeV and 2754.2 KeV. These two decay gamma-rays made it possible to relate the prompt capture gamma-rays and the decay gamma-rays, and to deduce the reaction rate of U-238, as is discussed in Section 3-4. Chromium showed three prompt capture gamma-rays at 835.1-, 7939.3-, and 8884.1- KeV.

The neutron capture reaction rate calculation for iron in Blanket No. 2 is shown in Table 3-4, and that for Na, and Cr is shown in Table 3-5. Two runs, No. 104 and 105, are compared in both tables. GAMANL output data for runs, No. 104 and 105, are presented in Appendix I. Two different sized collimators, 5/16 in. dia. and 3/16 in. dia., were used in runs No. 104 and 105, respectively. Run number 105 in Table 3-4 shows that the reaction rate, R, lies within a $\pm 6\%$ error except for the

TABLE 3-4

REACTION RATE CALCULATIONS FOR IRON IN BLANKET NO. 2

RUNS NO. 104 and 105

ENERGY(KeV)	YIELD(%)	EFFICIENCY(10^{-4})	Run No. 104 AREA	Run No. 104 RELATIVE REACTION RATE	Run No. 105 AREA	Run No. 105 RELATIVE REACTION RATE
1613.0	5.85	0.665			1014.9	3.23
4218.8	4.02	0.235	553.6	2.74	2446.8	3.13
5920.5	8.29	0.254	2203.9	4.90	5694.1	3.26
6018.5	8.08	0.254	1598.1	3.64	5443.3	3.20
7278.9	4.60	0.222	716.8	3.28	3383.7	4.00
7631.6	27.19	0.211	4073.3	3.32	15793.5	3.32
7645.6	22.14	0.211	3100.3	3.10	12244.9	3.16

Table 3-5

REACTION RATE CALCULATIONS FOR Na AND Cr

IN BLANKET NO.2, RUNS NO. 104 AND 105

RUN NUMBER			104		105	
ENERGY(KeV)	YIELD(%)	EFF.(10^{-4})	AREA	R	AREA	R
870.6(Na)	25.39	0.908*	3220.4	0.590	5838.0	0.305
6395.4(Na)	25.69	0.247	330.2	0.243	1533.4	0.292
835.1(Cr)	24.04	0.937*	3385.1	0.608	6778.7	0.363
7939.3(Cr)	11.41	0.200	--	--	446.2	0.236
8884.1(Cr)	24.14	0.163	202.9	0.241	1238.0	0.380

* Total Efficiency data for low energy gamma-rays are calculated in Section 3-5-2

peak at 7278.9 KeV, which indicates that good collimation is very important in this experiment. This also confirms the accuracy of the measured reaction rates.

As mentioned previously, the calculation is based upon the key assumption that the yield intensity does not change with neutron energy. In Section 3-5-2 we show that certain peaks from sodium and chromium do not change in yield intensity. The calculation of the capture reaction of U-238 in Blanket No. 2 is discussed in the next section. This is done by analyzing the low energy short-lived decay gamma-rays from Np-239.

3-4 Decay Gamma-Rays

3-4-1 Induced Radioactivity in the Blanket

Consider a neutron capture reaction at the position $\underline{r}$ in the blanket, at time t, which will produce a radioactive nuclide A which decays into a stable nuclide B. The rate of decay, dA/dt, of a nuclide A is given by the following equation:

$$\frac{dA(\underline{r},t)}{dt} = \int_E N(\underline{r})\ \sigma_c\ (E)\ \phi\ (E,\underline{r})\ dE - A\ (\underline{r},t)\ \lambda_A, \tag{3-11}$$

where λ_A is the radioactive decay constant of nuclide A, and the remaining terms are the same as previously described. Now the separability of variables for the

neutron flux is again assumed, and Eq. 3-11 can be written

$$\frac{dA(\underline{r},t)}{dt} = R \cdot n(\underline{r}) \cdot \psi(\underline{r}) - A(\underline{r},t)\,\lambda_A , \qquad (3\text{-}12)$$

where

$n(\underline{r}) = N(\underline{r})/N$; the heterogeneity function,

$$R = \int_E N\,\sigma_c(E)\,\phi(E)\,dE, \qquad (3\text{-}13)$$

is defined as the capture rate, and N is the homogenized concentration. After the irradiation for the time interval t_1, the number of radioactive nuclei, A, at the position $\underline{r}$ in the blanket, at time t is therefore:

$$A(\underline{r},t) = \frac{R\,\psi(\underline{r})\,n(\underline{r})}{\lambda_A}\left(e^{-\lambda_A t} - e^{-\lambda_A(t_1+t)}\right). \qquad (3\text{-}13)$$

In a number of cases a radioactive nuclide A, which is produced by a neutron capture reaction decays into a nuclide B which is also radioactive. In this case the number of radioactive nuclei, B, at the position $\underline{r}$ in the blanket, at time t after an irradiation for the time interval t_1 is:

$$B(\underline{r},t) = \frac{R\,\psi(\underline{r})\,n(\underline{r})}{\lambda_B - \lambda_A}\left(e^{-\lambda_A t} - e^{-\lambda_A(t+t_1)}\right.$$

$$\left. + \frac{\lambda_A}{\lambda_B} e^{-\lambda_B(t+t_1)} - \frac{\lambda_A}{\lambda_B} e^{-\lambda_B t}\right), \qquad (3\text{-}14)$$

where λ_A and λ_B are the radioactive decay constants of nuclides A and B, respectively.

Na^{23} is in the former group of radioactive nuclides and Np-239 is in the latter group. Hence, Equations 3-13 and 3-14 can be thought of as giving the number of the radio-active nuclei of interest produced by a neutron capture reaction of sodium and U-238, respectively.

Now the number of decay gamma-rays of interest with energy $E\gamma$ produced at the position $\underline{r}$ in the blanket, at time t is given by the following equation:

$$C\gamma\ (\underline{r},t) = \left(\frac{I\gamma}{100}\right)\ \lambda_\eta \eta(\underline{r},t), \qquad (3\text{-}15)$$

where $I\gamma$ - is the number of decay gamma-rays with energy $E\gamma$ emitted per 100 <u>disintegrations</u> of the nuclide of interest. Hence, the total area under the decay gamma-ray peak of interest observed by the detector at energy $E\gamma$ during the time interval between t_s and t_f is given by the following equation:

$$A\gamma = \left(\int_{t_s}^{t_f} dt \int_{\Delta V} dV\ C\gamma(\underline{r},t) S\gamma(\underline{r})\right) \cdot F\gamma \cdot \epsilon\gamma \cdot \Omega, \qquad (3\text{-}16)$$

where ΔV is the volume of blanket which can be seen by the detector through the beam hole. Substituting Eq. 3-15 into Eq. 3-16, the total area is:

$$A\gamma = \left(\frac{I\gamma}{100}\right) \cdot \lambda_\eta \cdot \left(\int_{t_s}^{t_f} dt \int_{\Delta V} dV\ \eta(\underline{r},t)\ S\gamma\ (\underline{r})\right)$$

$$\cdot\ F\gamma \cdot \epsilon\gamma \cdot \Omega. \qquad (3\text{-}17)$$

According to decay modes, $\eta(\underline{r},t)$ may be Equation 3-13 or Equation 3-14. However Equation 3-17 will be:

$$A\gamma = \left(\frac{I\gamma}{100}\right) \cdot R \cdot T \cdot S\gamma \cdot F\gamma \cdot E\gamma \cdot \Omega , \qquad (3\text{-}18)$$

where

$$T_{Na} = \int_{t_s}^{t_f} \left(e^{-\lambda_{Na} t} - e^{-\lambda_{Na}(t_1+t)}\right) dt, \qquad (3\text{-}19)$$

$$T_{Np} = \int_{t_s}^{t_f} \frac{\lambda_{Np}}{\lambda_{Np} - \lambda_U} \left(e^{-\lambda_U t} - e^{-\lambda_U (t+t_1)} + \frac{\lambda_U}{\lambda_{Np}}\right.$$

$$\left. e^{-\lambda_{Np}(t+t_1)} - \frac{\lambda_U}{\lambda_{Np}} e^{-\lambda_{Np} t}\right) dt, \qquad (3\text{-}20)$$

$$S\gamma^{Na} = \int_{\Delta V} dV \ \psi(\underline{r}) \ n_{Na}(\underline{r}) \ S\gamma^{Na}(\underline{r}), \qquad (3\text{-}21)$$

and

$$S\gamma^{U} = \int_{\Delta V} dV \ \psi(\underline{r}) \ n_{U}(\underline{r}) \ S\gamma^{U}(\underline{r}). \qquad (3\text{-}22)$$

All terms will be discussed further, one-by-one in the two following sections.

3-4-2 Correction Factors

From Equation 3-18 one can see that four factors are involved to account for all processes anticipated from the birth of the gamma-rays to their detection by the Ge(Li) detector. In the previous case of the high energy gamma-ray analysis, we combined all these four factors into one factor, the so-called total efficiency. But when one deals with low energy gamma rays the heterogeneity effect does not allow combination of all factors into a single factor since the self-absorption correction factor will be very different according to where the gamma-rays originate. In this section two correction factors, $F\gamma$ and $S\gamma$, are discussed and the intrinsic efficiency, $\epsilon\gamma$, and the solid angle factor, Ω, will be discussed in the next section.

$F\gamma$ is the attenuation correction factor for gamma-rays of energy $E\gamma$ by air, LiF, lead, or any other materials placed in the flight path of the gamma-ray beam from the blanket surface to the detector. If we assume that there are air, LiF and lead, thickness of X_A, X_F, and X_L, respectively

between the surface of the blanket and the Ge(Li) detector surface (ref. Fig. 3-1), the attenuation correction factor is given by

$$F\gamma = e^{-(\mu_\gamma^A \ X_A + \mu_\gamma^F \ X_F + \mu_\gamma^L \ X_L)} \qquad (3\text{-}23)$$

where μ_γ^A, μ_γ^F, and μ_γ^L are the total linear attenuation coefficients of air, LiF, and lead, respectively, for gamma-rays of energy $E\gamma$.

The treatment of the self-absorption factor is somewhat different than that of ordinary small samples, since the gamma-ray emitting "sample" is as large as the blanket itself. Furthermore, when dealing with decay gamma-rays the heterogeneity effect of the blanket can no longer be ignored, since the energy of the gamma-rays is typically much lower than that of prompt gamma-rays, and in the range where gamma-ray attenuation coefficients are very large. The self-absorption correction factor is defined as the ratio of the total number of gamma-rays of interest with energy $E\gamma$ appearing at the outside surface of the blanket per second to the total number of gamma-rays of interest with the same

energy $E\gamma$ produced throughout the blanket per second. This factor is dependent on the thickness, the composition, the structural order of the blanket, the neutron flux shape in the blanket, and the energy of the gamma-rays of interest. Therefore the self-absorption correction factor is completely different according to where the decay gamma-rays originate, U-fuel rods or Na_2CrO_4 filling. Calculations of self-absorption correction factors for gamma-rays from both U-fuel rods and Na_2CrO_4 filling are done in Appendix E. Computer codes SELFN and SELFU are also presented in Appendix E. The computer programs perform the double integration of Equations 3-21 and 3-22, The calculated values are compared with the measured values of the attenuation coefficients in a fuel rod lattice in SELFU. Figure 3-3 shows the calculated self-absorption correction factors for gamma-rays from Na_2CrO_4 by SELFN. Figure 3-4 shows the calculated (circular dots) and measured (triangular dots) self-absorption correction factors for gamma-rays from U-fuel rods of Blanket No. 2 by SELFU.

Gamma-ray linear attenuation coefficients of Na_2CrO_4 and Uranium were independently obtained by a series of measurements (Appendix B). A test box was prepared to measure the actual attenuation factor of the fuel rod cell. Obviously all curves of Figures 3-3 and

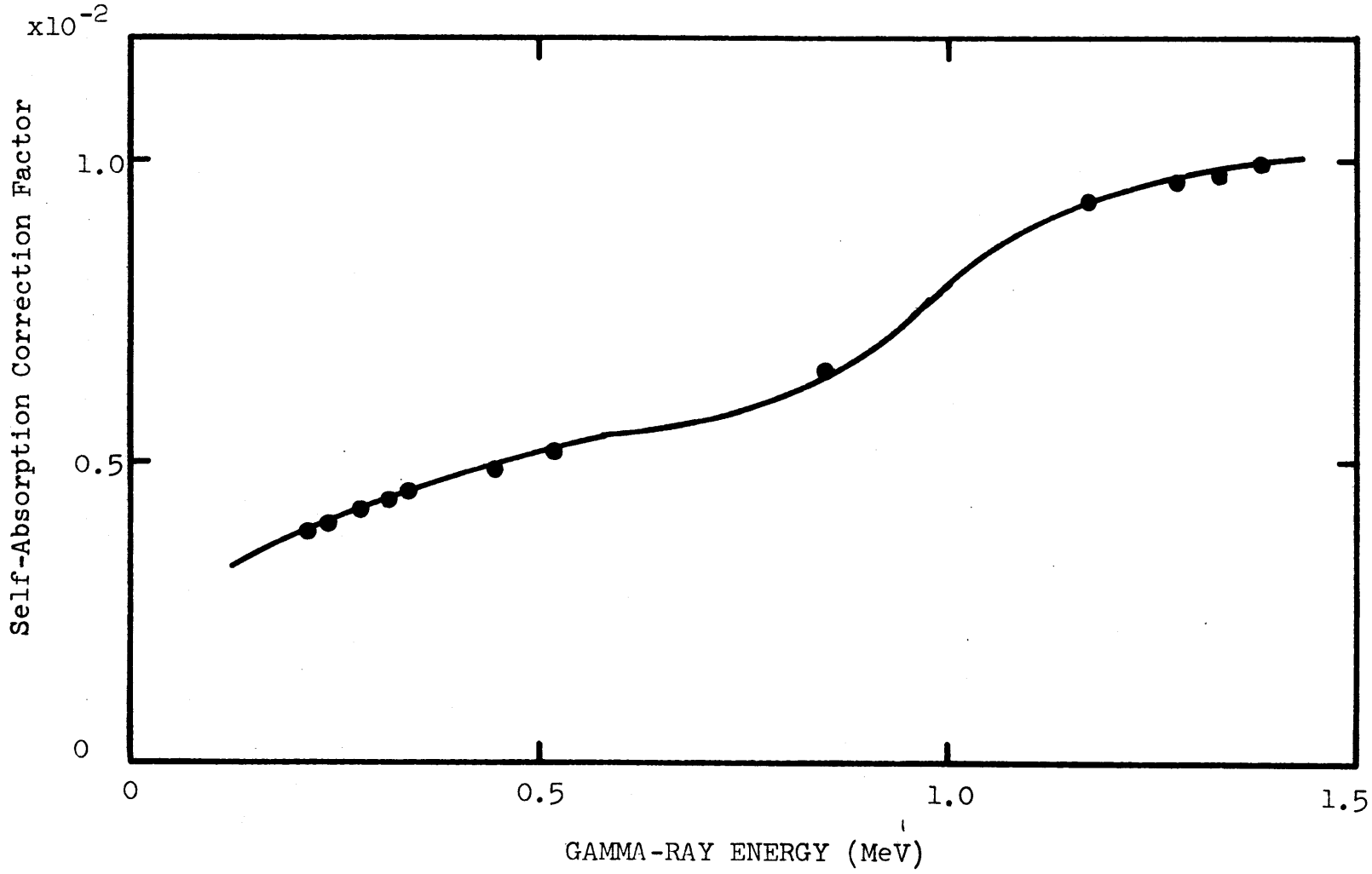

Fig. 3-3 Self-Absorption Correction Factors for Gamma-Rays from Na_2CrO_4 of Blanket No. 2 (calculated by SELFN)

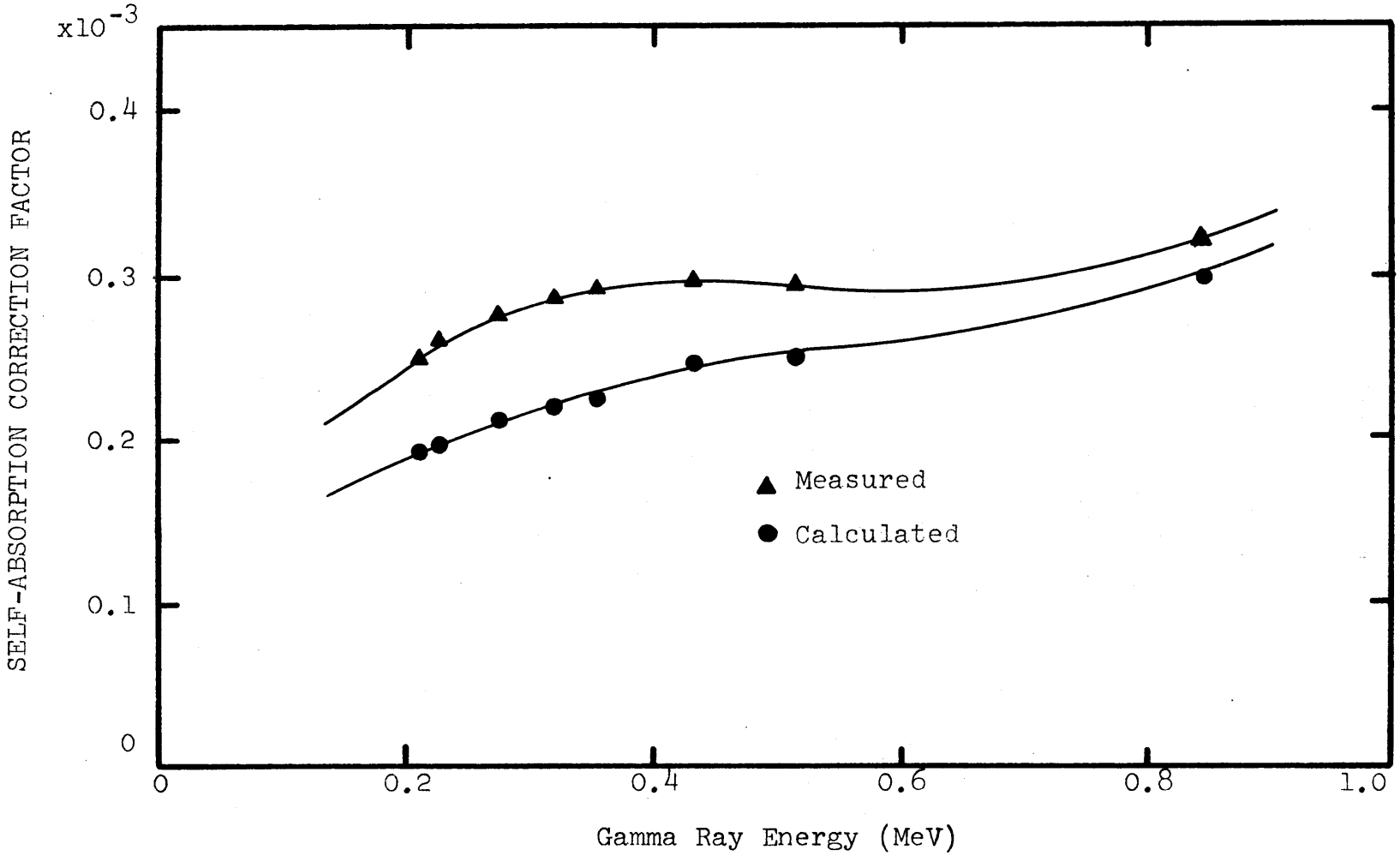

Fig. 3-4 Self-Absorption Correction Factor for Gamma-Rays from U-Fuel Rods of Blanket No. 2 (Calculated by SELFU)

3-4 ought to converge to the same value, since the heterogeneous effect decreases as the gamma-ray energy increases. When the calculation of the self-absorption factor for gamma-rays of Np-239 is carried out, neither possible structural disorder nor scattered gamma-rays were considered. Furthermore the uncertainty increases as the energy of the gamma-rays decreases, because of the high linear attenuation coefficients. Calculation shows that most of the Np-239 gamma-ray contribution comes from the first row of fuel rods, but the actual measurement showed that the contributions from other rows of fuel rods were not negligible. This indicates that small changes in fuel pin structure would produce a considerable change in the calculated self-absorption factors.

The intrinsic efficiency data can be obtained by a series of experiments without major difficulty. This will be discussed in the next section.

3-4-3 Intrinsic Efficiency

The intrinsic efficiency factor is the number of counts recorded at the energy $E\gamma$ in the multi-channel analyzer per gamma-ray arriving at the surface of the Ge(Li) detector. Figure 3-5 shows the schematic setup for the efficiency measurements. An adjustable calibrated

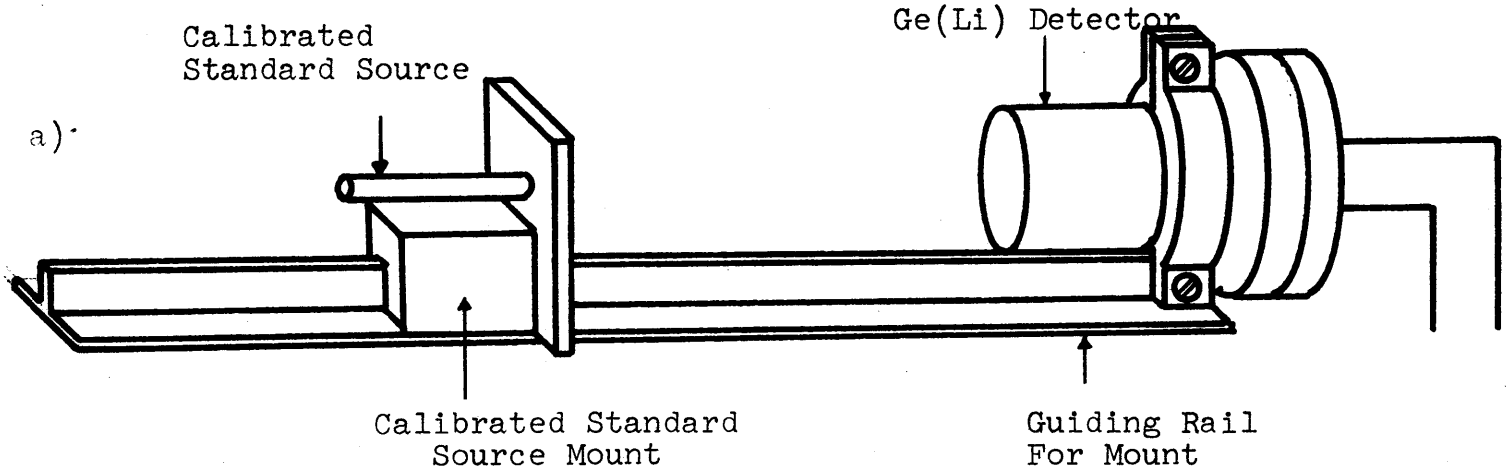

b) Plan View

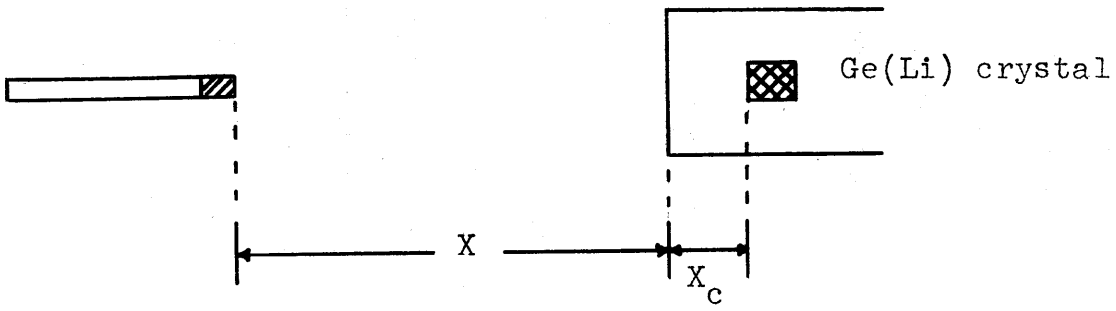

Fig. 3-5 Schematic View of the Setup for the Efficiency Measurements

source mounting system made of aluminum is used with the 17 c.c. crystal detector so it could be mounted with fixed reference to the crystal.

The intrinsic efficiency of the detection system including the solid-angle correction factor, $\varepsilon = \varepsilon_\gamma \Omega$, may be written as follows:

$$\varepsilon = A\gamma/Ao \cdot Cd \cdot \left(\frac{I\gamma}{100}\right) \cdot F\gamma \cdot T \qquad (3\text{-}24)$$

where

Ao - is the initial activity from the calibrated standard source,

Cd - is the decay correction factor for the time of initial calibration to the time of the experiment.

The geometric component of the intrinsic efficiency can be exactly expressed by the following equation since the effective distance from the source to the detector depends on the size of the crystal and the distance from the aluminum wall to the crystal (ref. Fig. 3.5(b)).

$$\varepsilon = \frac{C}{(X + X_c)^2}, \qquad (3\text{-}25)$$

or $$\varepsilon^{-1/2} = A_o + A_1 X, \qquad (3\text{-}26)$$

where

C, A_o, and A_1 - are constants with respect to the distance,

X - is the distance between the source and the surface of the detector, and

X_c - is the distance between the crystal and the surface of the detector face.

Equation 3-26 is a linear equation with respect to the distance, X, where A_o and A_1 are functions of the gamma-ray energy.

Efficiency runs were made using a series of calibrated sources purchased from the New England Nuclear Corporation. Table 3-6 shows the information supplied by the manufacturer for the sources which were used in the measurement. A dozen runs were made at various distances from the detector with each source. Figure 3-6 shows the resultant inverse of the square root of the efficiency versus the distance from the surface of the detector. All slopes and intercepts were obtained using a linear least square fit with very satisfactory results. A computer program INTEF calculate the intrinsic efficiency of the system (Appendix D). Using the computer program INTEF the detector efficiency of the 17 c.c. Ge(Li) crystal was obtained and plotted in

Table 3-6

STANDARD SOURCES

(NEW ENGLAND NUCLEAR CORPORATION)

ISOTOPE	INITIAL ACTIVITY (μCi)	CALIBRATION DATE	HALF-LIFE	ENERGY* (KeV)	YIELD** (%)
Co^{57}	10.7	3-1-69	272 d	122.05±0.05 136.40±0.06	87 10.5
Cs^{137}	12.4	9-2-69	30 y	661.595±0.076	85
Mn^{54}	10.5	3-1-69	314 d	834.9 ± 1.1	100
Co^{60}	7.5	9-2-69	5.26 y	1173.226±0.040 1332.48 ±0.05	99 99
Na^{22}	9.4	3-1-69	2.60 y	511.006±0.005 1275.0 ±0.8	180 99

* References are on Table 2-2

** C. Lederer et al., "Table of Isotopes" 6th Ed., John Wiley and Sons, Inc. (1967)

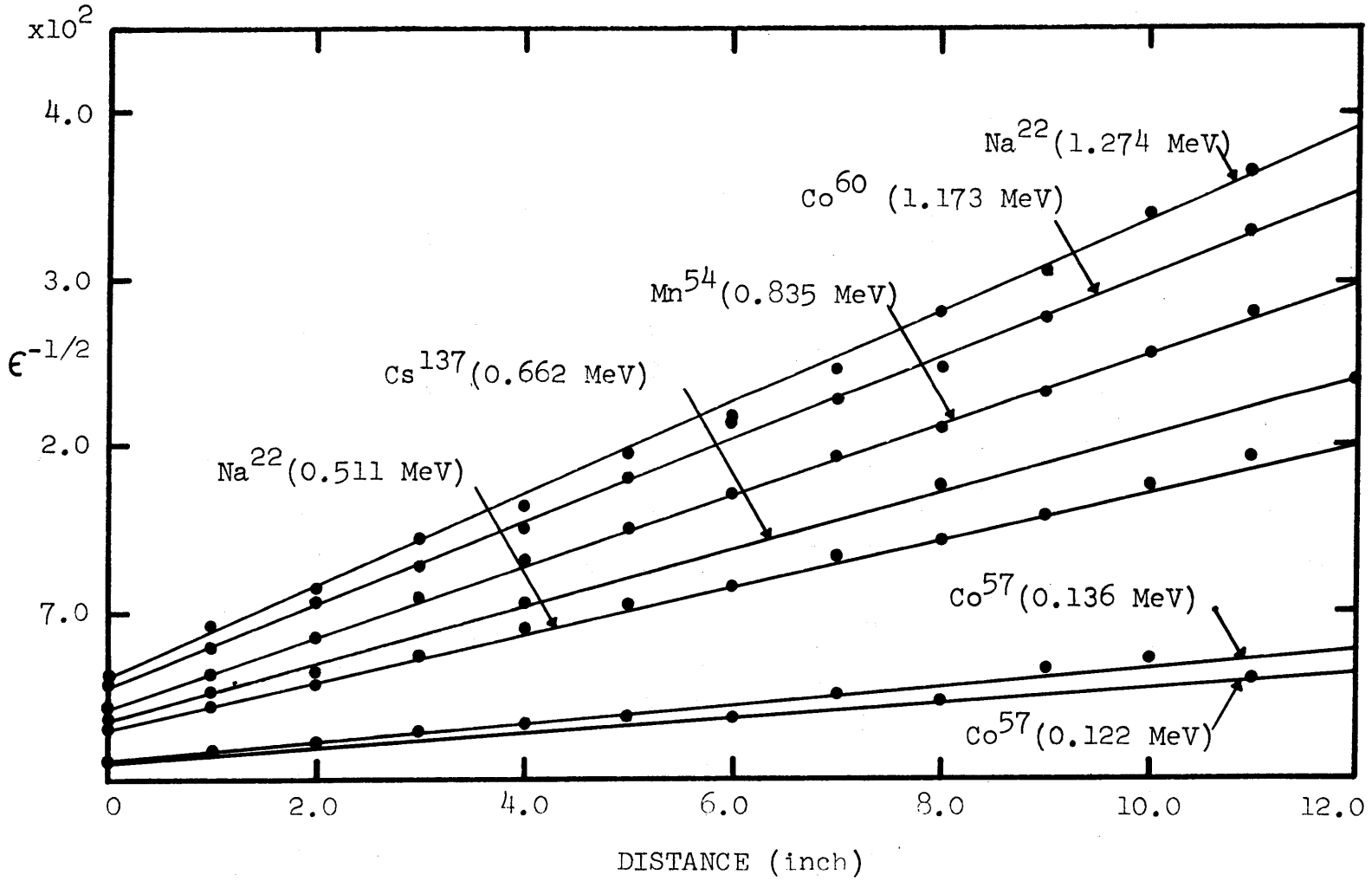

Fig. 3-6 Variation of Intrinsic Efficiency with Distance from Detector

Figure 3-7. The triangular points in Figure 3-7 are the data reported by Odette (02) for the same detector and the same sources. The good agreement between the two calculations demonstrates excellent consistency in the efficiency measurements. It would have been desirable to have more standard sources especially in the range between 136 KeV and 511 KeV. However interpolation should be adequate in this region. The estimated error in this experiment is on the order of 5-10%, most of which is attributable to the uncertainty in the initial activity of the sources.

The measurement of intrinsic efficiency by this method is much more accurate and reliable than that using a single fixed position for the gamma-ray sources. In this method one can not only have better statistics than any other method, but also correct the efficiency for the effective distance between the gamma-ray source and the detector.

3-4-4 Capture Reactions in Na and U-238

Two radioactive isotopes, Na-24 and Np-239, are of primary interest in the analysis of the blanket decay gamma-ray spectra. The Na-24 decay gamma-ray lines at 1368 KeV and 2754 KeV are used to internormalize the prompt capture gamma-rays and the decay gamma-rays in

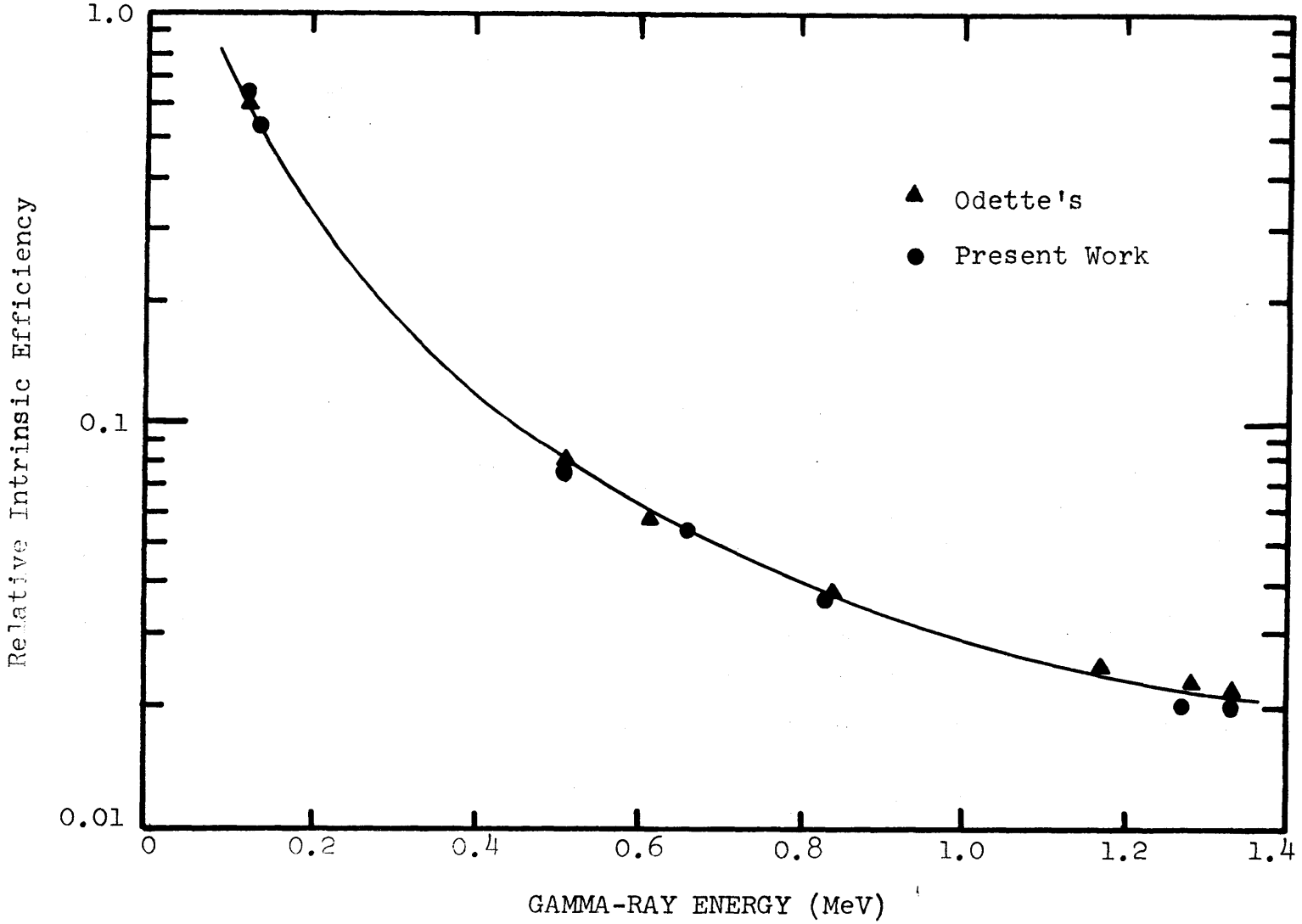

Fig. 3-7 Intrinsic Efficiency of 17 c.c. Ge(Li) Detector

the analysis of the neutron capture reactions. Since the capture reaction rate of sodium in the blanket is already known through analysis of the prompt capture gamma-rays, the neutron capture rate of U-238 can be obtained by analyzing the decay gamma-rays from Np-239 along with the decay gamma-rays of the sodium.

When a neutron is captured by a Na^{23} nucleus, Na^{24} is formed, which will decay into a stable nuclide, Mg^{24}, which a half-life of 15 hrs. This radioactive decay is accompanied by the emission of two prominent gamma-rays. The neutron capture rate of sodium, therefore, can be obtained by analyzing the gamma-rays from Na^{24} decay.

Np-239 comes from the β-decay of U-239, which is formed by the neutron capture reaction of U-238.

$$\text{U-238} + {}_0n^1 \rightarrow \text{U-239} \xrightarrow[23.5\text{m}]{\beta} \text{Np-239} \xrightarrow[2.35\ \text{d}]{\beta} \text{Pu-239} \quad (3\text{-}27)$$

Np-239 is radioactive itself and decays into Pu-239 by β-decay, coincident with the emission of more than 30 gamma-ray peaks (L2). The following peaks are the most prominent.

E_o(KeV)	106.14	209.8	228.2	277.6	315.9	334.3
$I\gamma$ (%)	22.8	4.1	12.7	14.1	1.5	2.0

These peaks were all observed in the short-lived decay gamma-ray spectra of blanket No. 2(see Runs No. 99, 102, and 103 in Appendix I). Table 3-7 shows the capture reaction rates of U-238 and Na deduced from analysis of decay gamma-rays from Np-239 and Na-24, respectively. Two different successive runs, No. 102 and 103, were analyzed for various gamma-rays from Np-239. Both runs are analyzed using the computer program GAMANL and plotted in Appendix I. Table 3-7 shows that run-to-run reproducibility is good, but that the resultant capture rate inferred tends to increase with increasing gamma-ray energy. This difference results mainly from the difference between the calculated and real self-absorption correction factor.

3-5 Inelastic Scattering Gamma-Rays

3-5-1 Inelastic Scattering Rates

Other observable gamma-rays in the prompt gamma-ray spectra from Blanket No. 2 are inelastic gamma-rays. Inelastic scattering plays an important role in reducing the energy of fast neutrons in LMFBR's, and is therefore an important phenomenon to investigate. In inelastic scattering a neutron of energy E enters the nucleus to form a compound nucleus. It is then re-emitted with a lower energy, leaving the original target nucleus in an excited state. The excited state subsequently decays

TABLE 3-7

THE CAPTURE RATES OF U-238 AND Na IN BLANKET NO. 2

USING VARIOUS DECAY GAMMA-RAYS FROM Np-239 AND Na-24

RUN NUMBER					102				103		
ISOTOPE	$E\gamma$ (KeV)	$I\gamma$ (%)	$S\gamma$* (10^{-3})	$\epsilon_\gamma\Omega$** (10^{-4})	$F\gamma$	T	$A\gamma$	R	T	$A\gamma$	R
Np^{239}	209.8	4.1	0.245	2.8	0.993	243.0	2621.3	0.386	363.8	4189.8	0.386
	228.2	12.7	0.255	2.45	0.992	243.0	9109.7	0.465	363.8	14680.5	0.507
	277.6	14.1	0.271	1.90	0.992	243.0	13059.0	0.735	363.8	19007.5	0.727
	334.3	2.0	0.290	1.65	0.992	243.0	1685.3	0.720	363.8	2393.5	0.708
Na^{24}	1368.5	100.0	9.943	0.19	0.993	406.6	2167.5	0.288×10^{-2}	229.0	1466.8	0.346×10^{-2}

* Calculated by Computer Codes, SELFN and SELFU. (Appendix E)

** Measured and calculated by INTEF. (Appendix D)

by gamma-ray emission. Inelastic scattering is impossible below the threshold energy or, rather, until the neutron energy exceeds (A + 1)/A times the energy of the first excited state, where A is the mass number of the target nucleus.

The energy of the first and the second excited states of the materials of Blanket No. 2 are given in Table 3-8. In general the threshold energy for inelastic scattering decreases as A increases. The excited levels of U-238 are noticeably lower than those of the other materials.

The inelastic scattering process can be analyzed by the measurement of the gamma-rays emitted by the excited target nucleus, since every inelastic scattering event is accompanied by the emission of gamma-rays, the energy of which corresponds to the excited levels of the target materials.

In a manner similar to that used for the calculation of capture reaction rates, the number of inelastic gamma-rays of interest having energy $E\gamma$ produced per second at the position $\underline{r}$ in the blanket is given by the following equation:

$$C\gamma\ (\underline{r}) = \int_E N(\underline{r})\ \sigma_i\ (E)\ \phi\ (E,\underline{r})\ dE \qquad (3\text{-}28)$$

TABLE 3-8

ENERGY OF FIRST AND SECOND EXCITED STATES*

NUCLEUS	FIRST EXCITED STATE(MeV)	SECOND EXCITED STATE(MeV)
O-16	6.05	6.13
Na^{23}	0.438	2.08
Cr^{52}	1.434	2.37
Fe^{56}	0.845	2.085
U^{238}	0.045	0.145

* Nuclear Data Table

As a first approximation we assume that the intensities of the γ-rays from the first excited level are proportional to the total inelastic scattering rate. Hence, the peak area of the gamma-rays having energy $E\gamma$ observed by the detector during the time interval, T, is given by:

$$A\gamma = R \cdot \varepsilon\gamma \cdot T \qquad (3\text{-}29)$$

where $\varepsilon\gamma = F\gamma \cdot S\gamma \cdot \epsilon\gamma \cdot \Omega$; the total efficiency of the Ge(Li) detection system, which includes all correction factors and the intrinsic efficiency.

One can actually observe all the inelastic gamma-rays corresponding to the first excited states, in the gamma-ray spectra from Blanket No. 2, except for that of U-238. Since the energy levels of U-238 are very dense and are nearly describable as a continuum state even at the low energies involved, it is impossible to distinguish the peaks of the U-238 inelastic gamma-rays against the very high background level in the low energy region of the gamma-ray spectra from Blanket No. 2.

The gamma-rays from inelastic scattering have low energies except for those of O^{16}. This means that the measured total efficiency data can be applied only to O^{16}

inelastic scattering since the measured efficiency data for low energy gamma-rays are not available. The calculated total efficiency data must be used for the rest of the elements, where heterogeneous effects are again of concern.

3-5-2 Calculation of Total Efficiency for Low Energy Gamma-Rays

This section is mainly concerned with the calculation of the total efficiency for the low energy region of the gamma-rays from Blanket No. 2. The calculation can be done by using the intrinsic efficiency of the detector and the self-absorption correction factor of the system. Since the heterogeneous effect is large for low energy gamma-rays, the calculation of the total efficiency for the gamma-rays from Na_2CrO_4 should again be different from that for the U-fuel rod. First of all consider the capture rate of sodium in the blanket. As seen in the previous sections, the capture rate of sodium can be analyzed using both the prompt capture gamma-rays and the decay gamma-rays. This allows one to correct the intrinsic efficiency and the total efficiency.

Figure 3-8 shows the calculated total efficiency of the system for low energy gamma-rays. This efficiency data can be normalized to the measured total efficiency

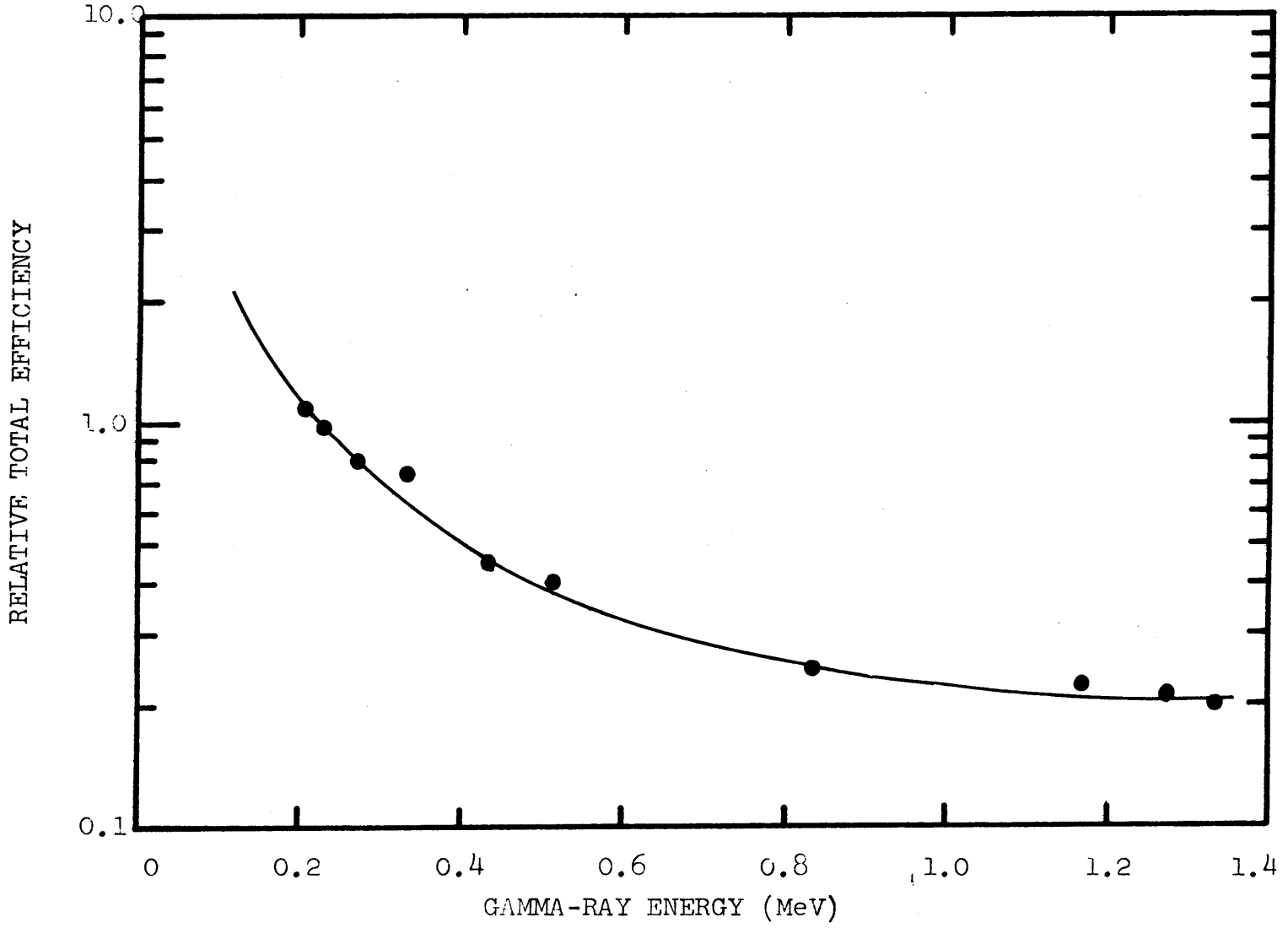

Fig. 3-8 Calculated Total Efficiency for Low Energy Gamma-Rays, Which Originate from Na_2CrO_4

data obtained from iron lines. The normalization is done by manipulation of low and high energy capture gamma-ray lines from sodium and chromium. Table 3-9 shows the normalization factors which have been calculated using three sets of low-high energy prompt capture gamma-ray lines. Set No. 1 belongs to sodium and Sets No. 2 and No. 3 to chromium. The values for the total efficiency are read from Figs. 3-2 and 3-8. These normalization factors between the measured efficiency data for the high energy gamma-rays and the calculated efficiency data for the low energy gamma-rays made it possible to compare the reactions involving high energy gamma-rays with those of low energy gamma-rays.

The three sets of normalization factor calculations illustrate a very important point. The factors of Sets No. 1 and No. 3 are very similar to each other, and the factor of Set No. 2 is very different from the others. This shows that the yield intensity of some prompt capture gamma-rays changes with incident neutron energy, while the yield of others does not. This also confirms that in the calculation of the capture rates of sodium and chromium in Section 3-3-2 the assumption of fixed yield for the specific gamma-rays in question was well-founded.

TABLE 3-9

CALCULATION OF NORMALIZATION FACTOR

SET	Eγ(KeV)	Iγ(%)	Aγ	$\varepsilon\gamma$	Normalization Factor
1	870.6	25.39	5838.0	2.3	4.14
	6395.4	25.69	1533.4	2.47	1
2	835.1	24.04	6778.7	2.37	6.08
	7939.3	11.41	446.2	2.00	1
3	835.1	24.04	6778.7	2.37	3.77
	8884.1	24.14	1238.0	1.63	1

* Average normalization factor is chosen to be 3.95, which is the average value of Sets No. 1 and 3.

Table 3-10 gives the resultant inelastic scattering rates of Na, Cr, Fe and O in Blanket No. 2. Run No. 105 is analyzed for this purpose (Appendix I).

3-6 Fission in the Blanket

3-6-1 Short Lived Fission Product Gamma-Rays

The primary interest is focused on short-lived fission products in Blanket No. 2 for the purpose of investigating the fission rates in the blanket. Use of long-lived fission products raises a complicated problem of unknown amount of accumulation of counts, and the use of exceptionally short-lived fission products, on the other hand, would raise the problem of poor counting statistics because of rapid decay.

Several leakage spectra were measured using the 2-in. diameter beam hole through the reflector of Blanket No. 2 (without any collimators) for about 24 hours of counting time. Runs No. 99, 102, and 103 in Appendix I are measured in this manner. For these spectra the blanket had been cooled for over a week prior to the 23 hours irradiation to get rid of the short-lived fission product gamma-rays due to previous irradiation, and it was then cooled for 100 minutes, counted for 20 hours, and counted again during the next 43 hours. (Runs No. 102 and 103, respectively). The computer

TABLE 3-10

INELASTIC GAMMA-RAYS IN BLANKET NO. 2, RUN NO. 105

($T = 8.24 \times 10^4$ sec)

Nuclide	$E\gamma$ (KeV)	$A\gamma$	$\mathcal{E}\gamma$ (10^{-4})	R (10^2)
Na^{23}	438	3515.6	1.777	2.39
Cr^{52}	1433.9	2114.3	0.771	3.33
Fe^{56}	845	12530.3	0.932	16.32
O^{16}	6127.8	1072.4	0.250	5.19

code GAMANL (R2) was used to analyze the data and the annihilation peak at 511 KeV and the Ar^{41} decay peak at 1.2936 KeV are used for the purpose of energy calibration. The identification of the peaks was based upon the data of Heath (H1) and Gordon (G3). Table 3-11 gives the energies, the corresponding fission products and their half-lives for the principal lines of Run No. 99 (see Appendix I). More than 45 fission product gamma-ray lines were observed in the spectra of Runs No. 99, 102 and 103 from Blanket No. 2. Out of these many short-lived fission products only a few are really suitable for present purposes. Useful peaks are not chosen solely on the basis of the relative difference in their fission yield nor on the basis of the gamma-ray yield and the energy. Other parameters must be considered such as the fission yields of all the radioactive precursors that decay to the fission product of interest as well as the fission product itself, the decay constant, and also the yield of the gamma-ray. Also the half-lives of all precursors of the fission product of interest must be very short compared to that of the fission product itself.

Table 3-12 shows the decay chains which are selected for the present work. The numbers under the symbols

TABLE 3-11

SHORT-LIVED FISSION PRODUCT GAMMA-RAYS

FROM BLANKET NO. 2

LINE NUMBER*	ENERGY(KeV)	FISSION PRODUCT	HALF-LIFE
1	213.2	Ru^{97}	2.9 d
2	230.9	Te^{132}	78 h
4	251.5	Xe^{135}	9.2 h
5	264.9	Y^{93}	10.1 h
8	296.5	Ce^{143}	33 h
9	304.3	La^{140}, Ba^{140}	40.2 h, 12.8 d
16	435.1	La^{140}, Ba^{140}	40.2 h, 12.8 d
18	530.6	I^{133}	20.8 h
19	541.6	Rh^{101m}**, Sb^{129}	4.5 d, 4.5 h
23	658.22	Nb^{97}	73m
24	667.1	I^{132}, I^{126}, Cs^{132}	23 h, 13 d, 6.5 d
26	743.3	Nb^{97m}	1.0 min.

* The line numbers correspond to the peak numbers of Run No. 99 in Appendix I.

** The superscript m refers to isometric states.

TABLE 3-11

(concluded)

LINE NUMBER	ENERGY(KeV)	FISSION PRODUCT	HALF-LIFE
28	772.2	I^{132}	2.3 h
29	811.8	Sb^{129}	4.5 h
30	816.5	La^{140}, Ba^{140}	40.2 h, 12.8 d
33	846.8	I^{134}	52 m
37	1024.8	Sr^{91}	9.7 h
40	1147.6	Zr^{97}, I^{130}	17 h, 12.4 h
42	1261.3	I^{135}, Sb^{129}	6.7 h, 4.5 h
43	1282.5	I^{135}	6.7 h
47	1384.9	Sr^{92}	2.7 h
53	1587.6	Pr^{142}	19.2 h
54	1595.7	La^{140}, Ba^{140}	40.2 h, 12.8 d
55	1677.5	I^{135}	6.7 h

TABLE 3-12

FISSION PRODUCT DECAY CHAINS OF INTEREST TO THE PRESENT WORK

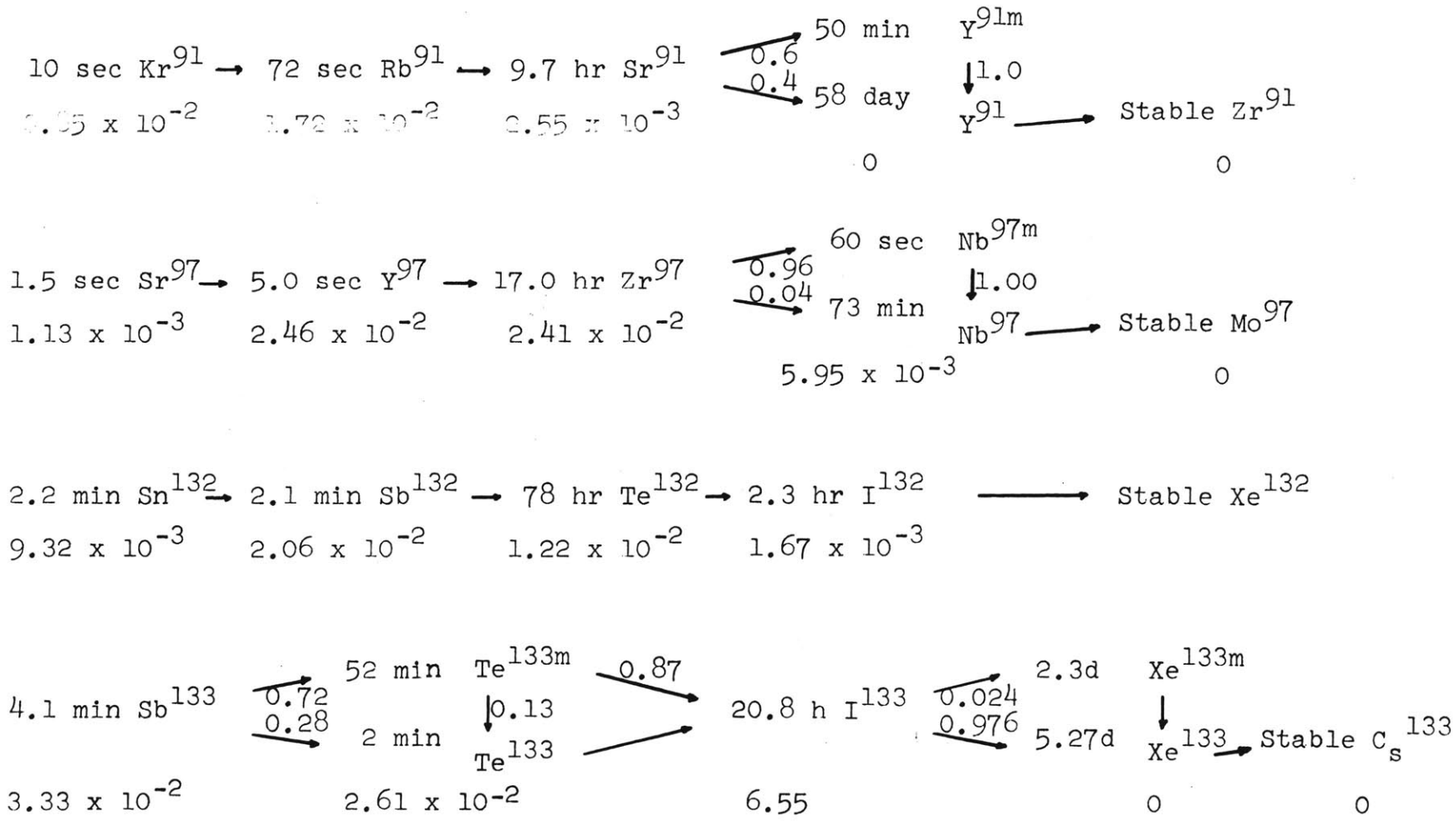

of the various isotopes are the yields of the fission products (Tl). Table 3-13 shows the principal lines of these fission products and their corresponding intensity yields. The peak areas of these lines of Run No. 99 are reported in the table.

3-6-2 Fission Rates

Short-lived fission product gamma-rays make possible the estimation of the total fission rate in Blanket No. 2. There are two major contributions to the fission process in the blanket: from U-235 fission, and from U-238 fission. These two fissions will be treated as a total fission in the blanket in the present work.

As an example consider the fission product decay chain 97. The first two fission products, Sr^{92} and Y^{97} have such short half-lives that their activity will die out within a few minutes. Then the 17 hr. Zr^{97} gives rise to 1147.6 KeV gamma-rays when it decays into Nb^{97}. Hence the total area recorded under this peak is:

$$A\gamma = \left(\frac{I\gamma}{100}\right) \cdot R \cdot S\gamma \cdot T \cdot F\gamma \cdot \varepsilon\gamma \cdot \Omega \cdot Y\gamma \qquad (3\text{-}30)$$

where

R - is the total fission rate in the blanket,

$Y\gamma = Y_{Sr} + Y_{Y} + Y_{Zr}$; total fission yield up to Zr,

$T = \int_{t_s}^{t_f} \left(e^{-\lambda Zr\, t} - e^{-\lambda Zr (t_1+t)}\right) dt$, and the

remaining terms are the same as defined before.

TABLE 3-13

PRINCIPAL FISSION PRODUCT GAMMAS OF INTEREST

ISOTOPE	ENERGY(KeV)	GAMMA-YIELD(%)	AREA(Aγ)*
Sr^{91}	1024.8	30	328.5 ± 19%
Zr^{97}	1146.7	2	144.2 ± 28.1%
Nb^{97m}	743.3	100	1014.7 ± 9.1%
Nb^{97}	658.2	99	1861.6 ± 7.1%
Te^{132}	230.9	100	12485.1 ± 2%
I^{132}	667.1	95	797.8 ± 7.1%
	772.1	82	607.9 ± 17.3%
I^{133}	530.6	100	1112.5 ± 9.8%

* Area data are Run No. 99 (See Appendix I).

Therefore from the measured value of $A\gamma$ for the 1147.6 KeV from Zr^{97}, one can deduce the fission rate, R.

The gamma-ray of Te^{132} at 230.9 KeV submerged by a strong peak of Np-239 at 228.2 KeV, and Sr^{91} at 1024.8 KeV and Zr^{97} at 1146.7 KeV introduce too high error ($\pm$ 19% and $\pm$ 28.1%). Therefore Te^{132}, Sr^{91} and Zr^{97} are not suitable for analysis.

Table 3-14 shows the gamma-rays chosen and the deduced total fission rates from different fission product gamma-rays. The estimated reaction rates are larger for I^{132} than for the other peaks analyzed since the I^{132} peak at 667.1 KeV overlaps the Cs^{132} peak at the same energy.

Except for these two peaks, the calculated reaction rate varies from 0.7×10^9/sec. to 1.6×10^9/sec. The calculation was based upon thekey assumption that the yields of thermal U-235 fission apply in the present work. Most of the error introduced in this work is attributable to the difference of fission yields between thermal and fast neutron induced fission, between U-235 and U-238, and the uncertainty of the calculated self-absorption correction factors.

3-7 Summary

So far neutron capture, inelastic scattering, and fission rates in Blanket No. 2 have been discussed in

TABLE 3-14

FISSION RATE CALCULATIONS FOR RUN NO. 99

ISOTOPE	ENERGY(KeV)	$Y\gamma(10^{-2})$*	$I\gamma(\%)$	T	$S\gamma(10^{-4})$	$\epsilon\gamma\ (10^{-4})$	$A\gamma$	$R(10^{9})$
Nb^{97m}	743.3	5.49	100	407.42	3.01	2.14	1014.7	0.738
Nb^{97}	658.2	6.08	99	431.72	2.92	1.95	1861.6	1.255
I^{132}	667.1	4.38	95	167.27	2.93	1.97	797.8	1.98
	772.1	4.38	82	167.27	3.05	2.20	607.9	1.51
I^{133}	530.6	3.60	100	380.10	2.91	1.66	1112.5	1.68

* The reference is for thermal neutron fission of U-235 (Reference G3)

turn. The results are summarized in Table 3-15, and normalized and compared with theoretical and other experimental values (L5) in Table 3-16.

Even though the complete disappearance of the U-238 prompt capture lines made it difficult to deduce the capture rate of U-238, it is encouraging that one can nevertheless deduce most of the pertinent neutron reaction rates in Blanket No. 2. The neutron capture rates of iron, chromium, sodium, and U-238 were analyzed in this chapter, and the inelastic scattering rates of sodium, chromium, iron and oxygen also were analyzed as well as the total fission rate in the blanket.

The measured reaction rate of iron is higher than calculated as might be expected, since iron is a major constituent in the reflector and shielding , and background interference is therefore possible in spite of the good collimation of the gamma-ray beam. The big difference in the capture rate of chromium is unexplainable. All that can be said is that for chromium the present method is preferable to foil activation, (T. Leung's method), since the Cr^{50} nuclide activated in the foil method is only 4.3% of natural chromium, while all chromium isotopes are represented in the prompt capture gamma spectrum.

Leung assumed that the capture cross section in all chromium isotopes was the same in the energy range of interest, and thus his total chromium capture rate is just 1/0.043 of the measured Cr^{50} capture rate. While this is undoubtedly more accurate than, say, scaling the activities proportional to the known thermal cross sections for the chromium isotopes, it is at best qualitative. The prompt capture gamma method on the other hand would be an accurate approach if capture gamma yields were either known at high energy or known not to change from their cataloged thermal values.

In regard to the high iron activation, it should be noted that the extraneous source must come from the near vicinity of the flight-path. This was demonstrated by carrying out a background run with the facility at power but with the 18 inch long steel plug inserted into the reflector beam hole. The measured iron line background was found to be far less than the signal obtained during operation with the open flight-path. Thus the steel reflector or the iron laminae in port 12CH1 are the likely sources of the background problem. The latter source could be eliminated by replacing the port shielding with a lead-lithiated plastic combination.

TABLE 3-15

REACTION RATES IN BLANKET NO. 2

REACTION	RELATIVE REACTION RATE	REMARK (Gamma-rays)
Fe (n,γ)	3.13 - 4.00	More than 20 prompt γ-peaks analyzed
Cr (n,γ)	0.24 - 0.38	835.1-, 7939.3- and 8884.1 KeV
Na (n,γ)	0.30 - 0.31	870.6-, 6395.4- and 1368.7 KeV
U^{238}(n,γ)	50.7 - 72.7	Np-239 decay γ-rays at 209.8-228.2-, 277.6-, and 334.3- KeV
Na (n,n')	2.39 $\pm$ 16.7%	438.0 KeV
Cr (n,n')	3.33 $\pm$ 14.0%	1433.9 KeV
Fe (n,n')	16.32 $\pm$ 4.5%	845.0 KeV
O (n,n')	5.19 $\pm$ 16.7%	6127.8 KeV
U (n,f)	7.38 - 19.8	Fission Product Decay Gamma-Rays from Nb^{97m}, Nb^{97}, I^{132} and I^{133}

TABLE 3-16

NEUTRON BALANCE IN BLANKET NO. 2

REACTION	ANISN		T. LEUNG(L5)		PRESENT WORK
$U^{238}(n,\gamma)$*	1.0000		1.0000		1.0000
Fe (n,γ)	0.0036		--		0.0346 ± 0.0042
Na (n,γ)	0.0025		0.0022		0.0029 ± 0.0001
Cr (n,γ)	0.0650		0.0740		0.0030 ± 0.0007
$U^{235}(n,\gamma)$	0.0016		--		-----
$U^{238}(n,f)$	0.0485	0.1069	0.0520	0.1130	0.1326 ± 0.0612
$U^{235}(n,f)$	0.0584		0.0610		
Na (n,n')	0.0271		--		0.0232 ± 0.0039
Cr (n,n')	0.0081		--		0.0324 ± 0.0046
Fe (n,n')	0.0418		--		0.1590 ± 0.0071
O (n,n')	0.0001		--		0.0504 ± 0.0084

* All values reported relative to U-238.

The capture reaction rates of sodium and the fission rate are in good agreement with calculated values and with T. Leung's results from the foil activation method. (Note that the results in Table 3-16 are normalized to self-shielded in-rod U-238 activities; thus Leung's entries have been re-normalized to account for the fact that the values tabulated in Ref. (L5) are for unshielded U-238 foils.)

The inelastic scattering rates are in poor agreement with the theoretical results except for sodium. This is mainly because the inelastic scattering cross-section is not the same as the production cross-section for the gamma-ray corresponding to the first excited level. Other sources of error are the uncertainties in the high energy neutron spectrum deep in the blanket and in the inelastic scattering cross-sections.

Chapter IV

DETERMINATION OF HYDROGEN CONTENT OF LMFBR BLANKET MATERIALS

4-1 Introduction

Since the hydrogen content of the LMFBR blanket materials has a significant effect upon the neutron energy spectrum in the blanket assembly (F1), it is very important to know exactly how much hydrogen is contained in its component materials. Because of the high neutron slowing down power of hydrogen the moisture which is absorbed or contained in the materials causes depletion of fast neutrons and enhancement of epithermal neutrons in the blanket. I. Forbes (I1) has calculated the effect of hydrogen in the blanket and converter assembly.

The ANISN code was used to make 16-group, 1-D, S_8 calculations of the neutron capture and fission rates of U-238 through the blanket and steel reflector of Blanket No. 2. The U-238 capture (a typical capture reaction) and fission (a typical threshold reaction) rates were calculated for chromate water contents of 0.0 w/o, 0.1 w/o, 0.2 w/o and 0.5 w/o. Figure 4-1 shows, for a given sodium chromate water content, the

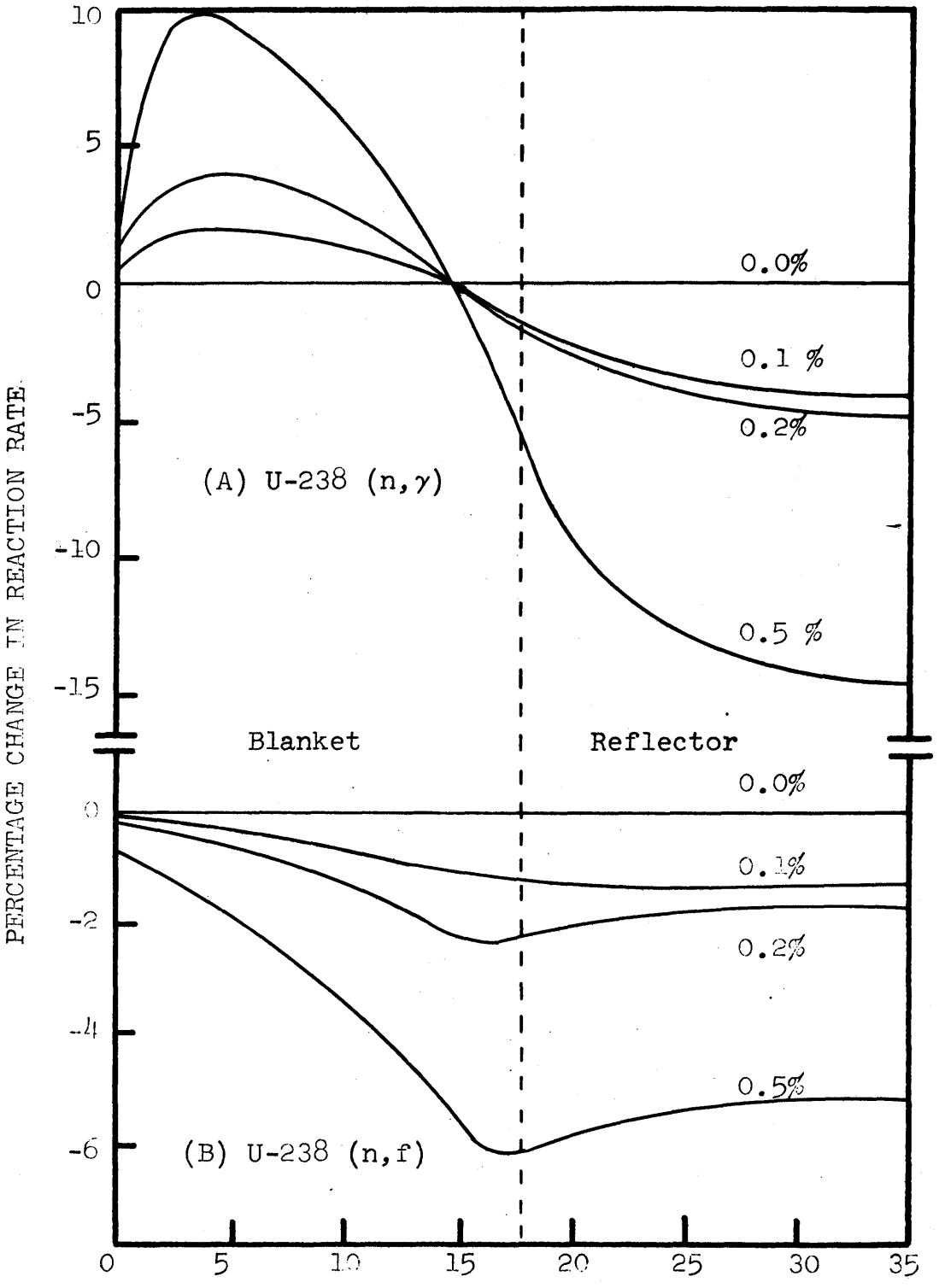

Fig. 4-1 Percentage Error in Reaction Rates in Blanket No. 2 as a Function of the Sodium Chromate Water Content Weight Percentage

amount by which the U-238 capture and fission rates through Blanket No. 2 differ from the zero water content case. It is seen that the error in the capture and fission rates due to the hydrogen content of the chromate is reduced to about the limit of precision in the experimental determination of the activities only when the water content of the sodium chromate is 0.1 w/o or less. As can be seen, a good knowledge of the moisture content of blanket materials is quite important since as little as 0.1 w/o H_2O can change the U-238 capture rate by as much as $\pm$ 5%.

The good energy resolution of Ge(Li) detectors makes possible the accurate measurement of moisture content using the prompt capture gamma-ray of hydrogen. In fact, in most thermal neutron prompt capture analysis carried out at MIT the hydrogen characteristic line was always so prominent that it was used as an energy calibration line in almost every experiment.

This chapter investigates the possible application of prompt activation analysis in competition with physical/chemical analyses, to assess the accuracy and efficiency of the method, not only for the present specific application, but also for more general industrial or scientific applications. The prompt

activation analysis method has been improved both as regards the detector itself, and the associated detection system.

4-2 Theory

When a proton captures a neutron, the binding energy of the deuteron appears as a gamma-ray of about 2.223 MeV.

The probability of this process, i.e., the thermal neutron capture cross-section of hydrogen is (H6):

$$\sigma_c \ (2200) = (0.332 \pm 0.002) \text{ b.}$$

However the capture cross-section of hydrogen decreases so rapidly with energy that high energy neutrons cannot be effectively used to analyze the hydrogen content in a material.

The only possible prompt gamma-radiation emitted as a result of thermal neutron capture in the hydrogen is at 2.223 MeV, since there is no other excited bound state in the deuteron. The precise energy of this hydrogen gamma-ray is very important to the present work in many respects. Table 4-1 shows the energy of the thermal neutron prompt capture gamma-rays of hydrogen reported by various experimenters. The value of 2.223 MeV is obviously a well-established and reliable result.

As already noted, the characteristic hydrogen peak

TABLE 4-1

THE ENERGY OF THE HYDROGEN THERMAL NEUTRON CAPTURE GAMMA-RAY LINE

Reference	Instrument	Energy (KeV)
Bell and Elliot (B2, B3)	Magnetic β Spectrometer with a Uranium Photoelectric Converter	2229 ± 7
Monahan et al. (M1)	NaI Scintillation Spectrometer	2217.2 ± 1.5
Motz et al. (M2)	Magnetic Compton Spectrometer	2223.0 ± 1.0
Chupp et al. (C1)	2m Bent Crystal Spectrometer	2223.3 ± 1.5
Kazi et al. (K1)	2m Bent Crystal Spectrometer	2224.2 ± 1.5
Knowles (K2)	Double Flat Crystal Spectrometer	2223.18 ± 0.14
Greenwood et al. (G6)	Ge(Li) Detector	2223.29 ± 0.07

at 2.223 MeV is a sensitive indicator of hydrogen content. The total area under this peak is:

$$A\gamma = \int_V dv \int_T dt \int_E dE\ \Gamma(E)\ \Sigma_c(\underline{r},E)\ \phi\ (\underline{r},E,t)\ \cdot\ \varepsilon_\gamma \qquad (4\text{-}1)$$

where

V - is the volume of the sample,

T - is the neutron irradiation time,

$\Gamma(E)$ - is the number of characteristic prompt gamma-rays emitted per capture of a neutron having energy E,

$\Sigma_c(\underline{r},E)$ - is the macroscopic neutron capture cross-section of hydrogen at the position $\underline{r}$ and at neutron energy E,

$\phi(\underline{r},E,t)$ - is the neutron flux in which the sample is immersed at the position $\underline{r}$ for neutrons having energy E, at time t, and

ε_γ - is the total gamma-ray detection efficiency of the experimental system, which includes all correction factors, the solid angle factor, and the intrinsic detection efficiency.

For the present application we may confidently assume that the irradiated sample is small enough to neglect the variation of reaction rate with position, and the neutron flux is also nearly constant throughout

the time interval T. Equation 4-3 may then be written:

$$A\gamma = V\ T\ \varepsilon r \int_E \Gamma(E)\ \Sigma_c(E)\ \phi\ (E)\ dE \qquad (4\text{-}2)$$

by making use of the definitions:

$$\int_T dt\ \phi\ (\underline{r},E,t) \equiv \phi(\underline{r},E) \cdot T \qquad (4\text{-}3)$$

and

$$\int_V dV\ \Sigma_c(\underline{r},E)\ \phi\ (\underline{r},E) \equiv \Sigma_c(E) \cdot \phi\ (E) \cdot V \qquad (4\text{-}4)$$

Since a highly thermal neutron flux is used, we may also assume the energy spectrum is Maxwellian, and thereby define an effective averaged one-group cross-section. Hence, the intensity of the hydrogen characteristic prompt capture gamma-ray line at 2.223 MeV is given by the following equation:

$$A\gamma = V \cdot T \cdot \varepsilon\gamma \cdot \Gamma^{th} \cdot \Sigma_c{}^{th} \cdot \phi^{th}, \qquad (4\text{-}5)$$

where the superscript "th" refers to the thermal neutrons. The macroscopic capture cross-section of hydrogen is given by:

$$\Sigma_c{}^{th} = 2 \cdot N_A\ \frac{m}{M \cdot V}\ \sigma_c{}^{th} \qquad (4\text{-}6)$$

where

N_A - is Avogadro's number,

m - is the total equivalent H_2O mass in the sample,

M - is the molecular weight of water, and

σ_c^{th} - is the microscopic thermal neutron capture cross-section.

From Eq. 4-5 the area, $A\gamma$, may be written:

$$A\gamma = C\gamma \cdot m \qquad (4\text{-}7)$$

where

$$C\gamma = 2 \cdot N_A \cdot T \cdot \varepsilon\gamma \cdot \Gamma^{th} \cdot \phi^{th} \cdot \frac{1}{M} \cdot \sigma_c{}^{th}.$$

Now we can see from Eq. 4-7 that the intensity of the hydrogen characteristic line is directly proportional to the moisture content of a material. Since $C\gamma$ contains a variety of factors subject to uncertainty, it is preferable to employ a comparison technique to obtain absolute results. The same sample is re-irradiated with a small known amount of hydrogeneous material, Δm, added to it, for the same interval, T. The new peak area of the hydrogen characteristic line becomes:

$$A\gamma' = (m + \Delta m)\, C\gamma \qquad (4\text{-}8)$$

Hence, from these two consecutive experiments hydrogen content in a material is given by:

$$m = \frac{\Delta m}{R-1} \quad , \qquad (4\text{-}9)$$

where

Δm - is the mass of the known amount of hydrogeneous material added, and

R - is the ratio of the two photopeak areas, A'/A.

4-3 Experimental Setup and Procedure

4-3-1 Irradiation Facility and Detection Setup

The prompt activation analysis facilities using thermal neutron beam port 4TH1 of the MIT Research Reactor have been described in detail by Y. Hukai (H3), T. Harper (H4) and V. Orphan (O1). The front irradiation facility was used in this experiment. This facility was constructed by T. Harper (H4) as part of his doctoral thesis research. The primary shielding material used is heavy concrete, together with masonite and boral which are used to thermalize and capture stray neutrons. Lead is used for shielding and collimation of gamma-rays in the access ports of the facility. The thermal neutron beam coming from the reactor port can be interrupted just preceding the irradiation position by a boral and lead shutter.

The neutrons from the reactor core are scattered by a graphite plug, 3-7/8 in. diameter and 40 in. long, placed inside the 4TH1 beam port, which is tangential to the reactor core tank; the resulting scattered neutrons form a beam for the external irradiation facilities. The cadmium ratio for gold at the front irradiation position was measured and found to be 54 (H3). To reduce the gamma-ray background from the beam port, a 1-1/2 in. long lead plug was placed in the beam port.

The sample is inserted into the irradiation position through one of the side access ports in the shielding; the prompt capture gamma-rays coming from the sample are collimated vertically by a set of lead collimators. Figure 4-2 shows a schematic view of the sample position which can be adjusted horizontally.

A planar, hexagonal-shaped, 7C.C.Ge(Li) detector with 5 C.C. of active volume was used (Ref. H3). The electronics associated with the 7C.C. detector was the standard arrangement for free mode operation. The signal from the Ge(Li) cryostat is amplified by a CI-1408C preamplifier which is connected through the pre-amplifier head, followed by a CI-1417 main amplifier, and thereafter fed into a Nuclear Data ND-161F 4096 Channel Analyzer. -500 $\overline{V}$ was supplied as the detector

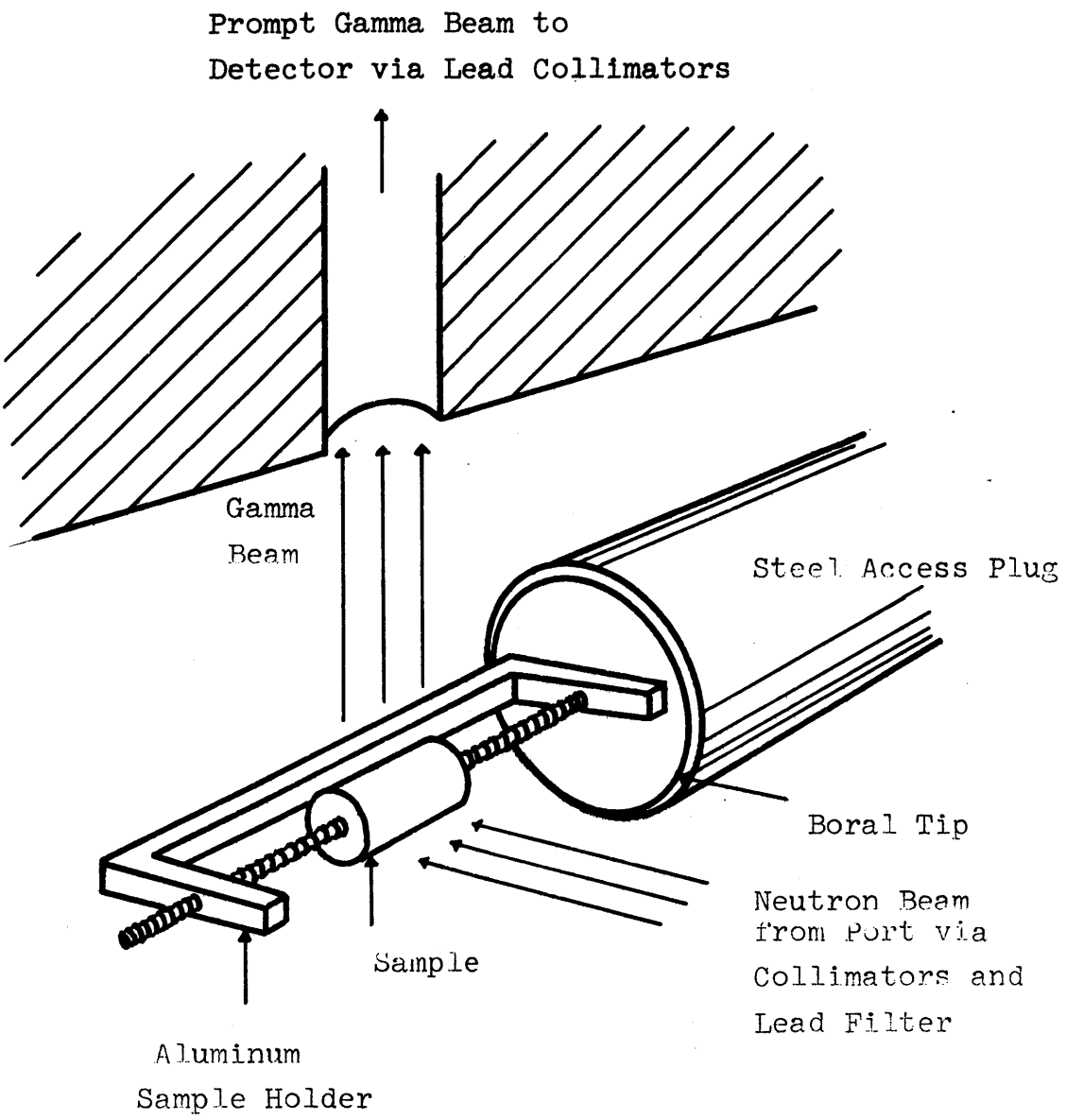

Fig. 4-2 Schematic of Sample Position in Front Irradiation Facility

bias voltage.

4-3-2 Operating Procedure

Crucible drying experiments showed that the water content of the technical grade "anhydrous" sodium chromate, as delivered by the supplier, had a water content of about 0.8 w/o. This was clearly unacceptable in terms of its effect upon blanket neutronics, and was sufficient motivation for confirmation of this analysis by an independent method.

The sodium chromate samples were prepared in 3/4 in. diameter and 2 in. long aluminum cans, and sealed air-tight. The uniformity of the neutron flux over the region occupied by the sample position in the front facility was checked by Y. Hukai (H3). The size of the present sample was kept within the allowable limits assuring uniformity of the neutron flux. To add a known amount of hydrogen to the sample, Mylar tape was used. During each irradiation the fluctuation of the incident neutron flux and the variation of the irradiation time interval was monitored using another characteristic line from the sample. Right adjacent to the hydrogen characteristic line at 2.223 MeV, chromium has a prompt capture line at 2.239 MeV (R3). The total thermal cross-section of chromium is 3.10 b and the capture gamma-ray

yield per 100 thermal neutron captures is 7.45 at this energy. This chromium prompt capture line at 2.239 MeV was used as a monitor line to check the fluctuation of the neutron flux and the irradiation time interval between two successive experiments. Taking the ratio of the intensity of the chromium lines between two experiments will cancel out all such fluctuation between two experiments. A background run was also performed: no significant peak was found at 2.223 MeV, which is encouraging in terms of use of the prompt activation method to measure the moisture content in a material using this irradiation facility. The monitoring method of this experiment using another adjacent line such as chromium at 2.239 MeV is more reliable and more convenient than the foil monitoring method employed in most other studies using this facility. Since the monitor line originates from the sample itself, no error can be introduced by position difference, which is not always true in the foil monitoring method. Further the foil method requires extra work, such as keeping track of irradiation, cooling and counting times, weighing the foils, etc.

4-4 Data Analysis

Figure 4-3 shows the prompt capture gamma-ray

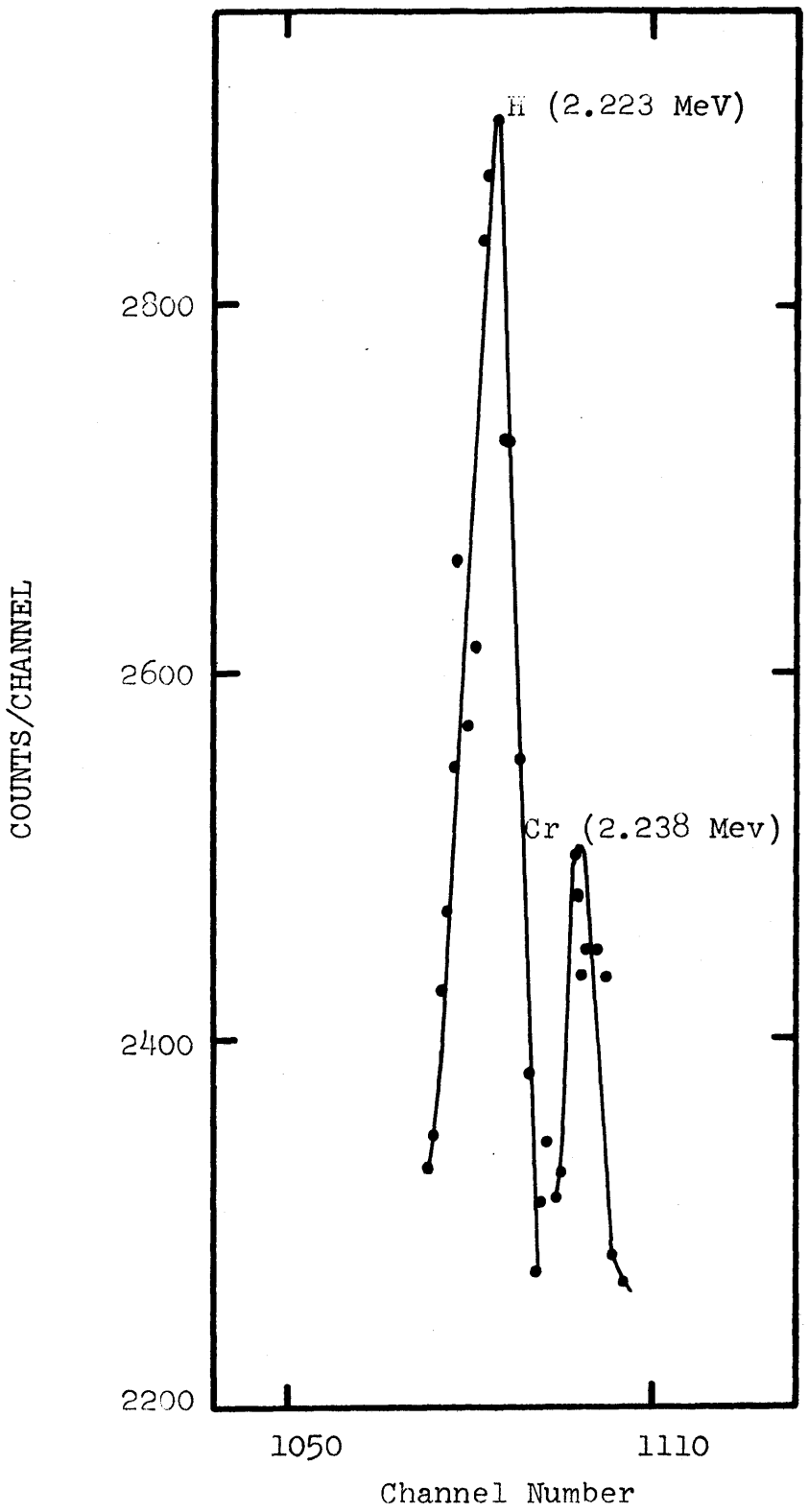

Fig. 4-3 Spectrum of H and Cr of Na_2CrO_4 with Known Amount of Hydrogen Added, Run No. 38

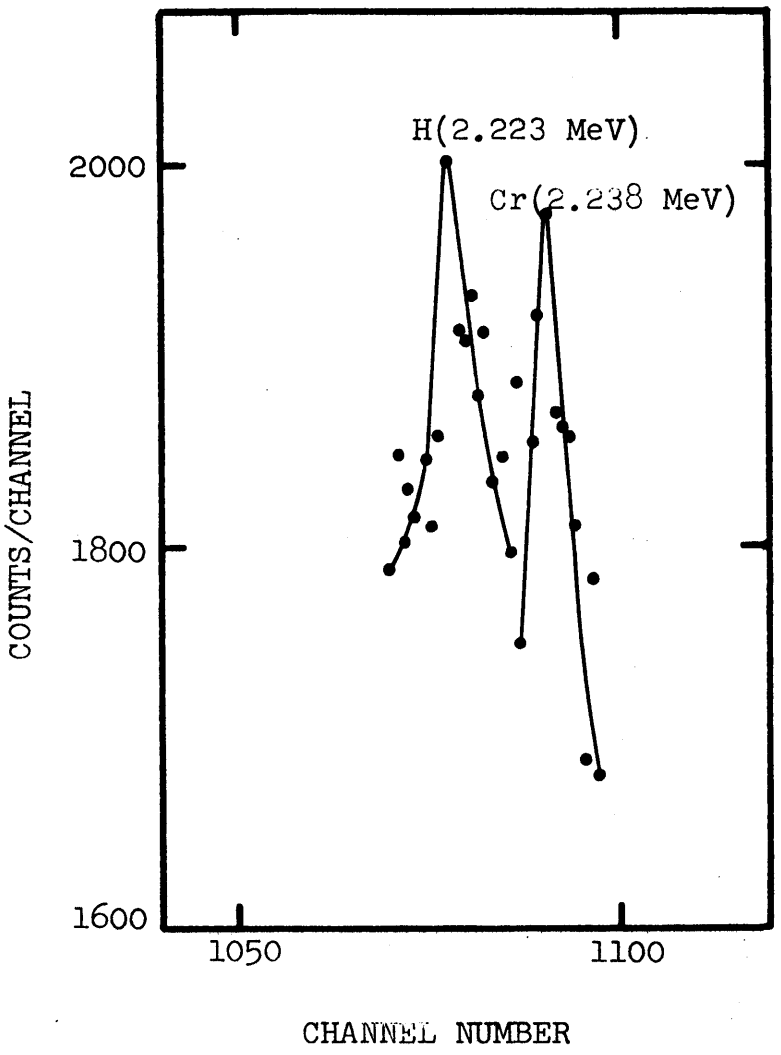

Fig. 4-4 Spectrum of H and Cr of Na_2CrO_4, Run No. 40

spectrum of $Na_2C_rO_4$ with Mylar tape added. The high peak on the left is the H-line at 2.223 MeV, and the small peak at the right is the Cr-line at 2.239 MeV. Figure 4-4 shows the same lines from $Na_2C_rO_4$ without any Mylar tape. Both experiments had the same irradiation time of 468 minutes. Because of the addition of a small amount of hydrogeneous material, we can see the large augmentation of the H-line at 2.223 MeV. The $Na_2C_rO_4$ sample consisted of:

$Na_2C_rO_4$	12.3718 gm
Al - can	11.6660 gm
Mylar Tape	0.7710 gm
Total	24.8088 gm

The Mylar tape was added at the center of the aluminum can. The first run (Run No. 38) was made with the prepared sample with Mylar tape added, and the following run (Run No. 40) was made with the sample after taking off the Mylar tape. A background run (Run No. 39) was also made with an aluminum can without any $Na_2C_rO_4$ sample. The background subtracted total counts of the H-line and Cr-line are as follows:

Run Number	38	40
Description	with Mylar	without Mylar
C_r-Monitor line	1042 ± 32	1133 ± 34
H-line	3889 ± 62	443 ± 21

Hence the amount of hydrogen which is contained in 12.3718 gm of $Na_2C_rO_4$ sample was 0.095 ± 0.015 gm (Mylar Tape equivalent; the hydrogen content in Mylar tape is almost the same as that in the same weight of water). As a result the moisture content in the Na_2CrO_4 was 0.77 ± 0.12 w/o (Mylar-tape equivalent). The water content of the sodium chromate delivered by the supplier was determined to be 0.83 ± 0.04 w/o from the crucible drying tests. In order to reduce this contamination the entire shipment of sodium chromate was baked at 400°F for eight hours in a domestic electric oven. Since sodium chromate has a low dehydration temperature (about 300°F), a simple oven drying procedure was good enough. After baking, the weight of the sodium chromate was measured and found to be decreased by about 0.75%. The dried chromate was ground and stored in sealed cans prior to loading it into the subassemblies of Blanket No. 2. Samples from the dried sodium chromate loaded into the blanket subassemblies

were confirmed to be $\leq$ 0.1 w/o by both crucible drying tests and prompt activation methods. No resolvable line was observed using the prompt activation method and dried sodium chromate samples. It is estimated that as little as 0.1 w/o would have been detectable.

This prompt activation analysis of hydrogen insures the detection of all possible hydrogen in $Na_2C_rO_4$, while the crucible drying tests could miss bound hydrogen, such as in NaOH impurity, a very likely contaminent in sodium chromate. Furthermore it was also very encouraging that no H-line was detectable in the gamma spectra from Blanket No. 2.

Chapter V

DETERMINATION OF THE NEUTRON LEAKAGE SPECTRUM FROM BLANKET No. 2

5-1 Introduction

The following two chapters will focus on the analysis of information that can be obtained from the spectra from Ge(Li) detectors by means other than convectional photo-peak analysis, namely measurement of neutron energy spectra and the continuous gamma-ray spectra of the Compton recoil continum. The measurement of the neutron energy spectrum leaking from Blanket No. 2 will be discussed in this chapter.

Reactor physics has as its chief concern the process of neutron multiplication, absorption and leakage. Consequently the spatial and energy variation of the neutron population is of considerable interest. These dual objectives are in fact the subject of two other detailed investigations on Blanket No. 2 (L5,03). In effect the present work parallels these other approaches in all respects, but with the restriction that a gamma-ray spectrometer is the tool rather than foil activation, He-3 or Proton recoil methods. Reaction rate measurements were already discussed in a previous chapter; the measurement of the neutron spectrum is

the concern of the present one.

The evaluation of techniques for the measurement of the leakage neutron spectrum from Blanket No.2 has focused on three methods,

1. An energy shift-method using low-Z materials,
2. A prompt activation method, and
3. The analysis of Ge interval conversion spectra at 691.4 KeV.

The first two methods will be discussed in the last section of this chapter and the third method will be developed and applied. The final technique developed will permit measurement of the neutron energy spectrum above 700 KeV using a comparison method in which spectra are unfolded by comparison with the neutron spectrum from a Cf-252 standard neutron source. All response kernel matrices (which will be discussed in Section 5-2) will be compared to and corrected by the spectra from Cf-252. To effect the unfolding a series of linear equations will be solved by the so-called iterative unfolding method (G7).

5-2 Theory

5-2-1 Internal Conversion Spectrum at 691.4 KeV

In most experiments using Ge(Li) gamma-ray detectors for fast neutron prompt capture analysis two spectral

lines undergo broadening in a manner which is not observed in applications involving thermal neutron activation analysis. These two spectral lines are at 595 KeV and 691.4 KeV, and are well-broadened on the high energy side compared with any other photo-peaks. In particular the peak at 691.4 KeV shows broadening of almost 100 KeV (FWHM is less than 4 KeV), so much that it will be referred to as a "spectrum" rather as a "peak" in this chapter.

The spectrum at 691.4 KeV is produced by the internal conversion of Ge^{72} nuclei excited by inelastic scattering events with the neutrons incident on the Ge(Li) detector. Internal conversion is an alternative mode of deexcitation which always competes with gamma-ray emission if the nuclear excitation energy is small and the angular momentum change is large (E4). In the case of the Ge^{72} nucleus since $0^+ \rightarrow 0^+$ transitions are forbidden in any radiative process, all the transition must proceed by internal conversion (E5). The other spectrum, at 595 KeV is, on the other hand, produced by gamma-ray emission of Ge^{74}, which is caused by inelastic scattering reactions with the fast neutrons incident on the Ge(Li) detector.

This de-excitation energy from Ge^{72} or Ge^{74} is

accompanied by the ionization energy deposited by recoil Ge atoms, which broadens the peaks at 595 KeV and 691.4 KeV. The appreciable broadening of both the gamma-ray lines from Ge^{74} at 595 KeV and the conversion electron line from Ge^{72} at 691.4 KeV is a well substantiated phenomenon reported previously by several investigators, including Hukai at MIT (C2, C3, H3). In this chapter the focus will be mainly on the analysis of the internal conversion spectra of Ge^{72} at 691.4 KeV, since the Ge^{74} line is contaminated by superposition of photons from higher energy events.

5-2-2 Broadening of 691.4 KeV Spectrum

When a Ge(Li) detector is exposed to fast neutrons, inelastic scattering events will occur and the Ge^{72} nuclei will recoil to conserve momentum. The observed line-broadening is due to the amount of electronic excitation produced by the recoiling Ge atom when the de-excitation of the excited state is coincident in time (within the charge collection time of the detecting system, typically about 20 μsec) with the slowing down of the recoiling Ge atom (which occurs in 0.3 μsec).

The lower limit to the observable energy loss is fixed by the intrinsic energy resolution of Ge(Li) detectors and

their associated electronics. Actually the spectra at 691.4 keV will be given by summation of the hole-electron pairs produced in the Ge crystal by the 691.4 keV internal conversion transition and the hole-electron pairs produced by the recoiling Ge atom.

Jones et al. studied the energy lost to ionization by recoiling Ge atoms in Ge(Li) detectors (C2, C3). They supported Lindhard's conjecture (L3) of an electronic stopping power proportional to v for particle energies down to very low energy. There was a satisfactory agreement with the theory of Lindhard et al.

Figure 5-1 shows the comparison of the experimental values of Jones et al. with the theoretical curves which represent the solution of the equations given by Lindhard et al.

Therefore the electronic energy loss of the recoiling atoms can be expressed by

$$E'' = f(E'), \qquad (5\text{-}1)$$

where E'' is the energy lost ionization and E' is the energy of the recoiling atom. In other words, the broadened energy, E'', of Ge^{72} internal conversion spectra is a known function of the energy of the recoiling atom, E'. In the present work the experimental formula of

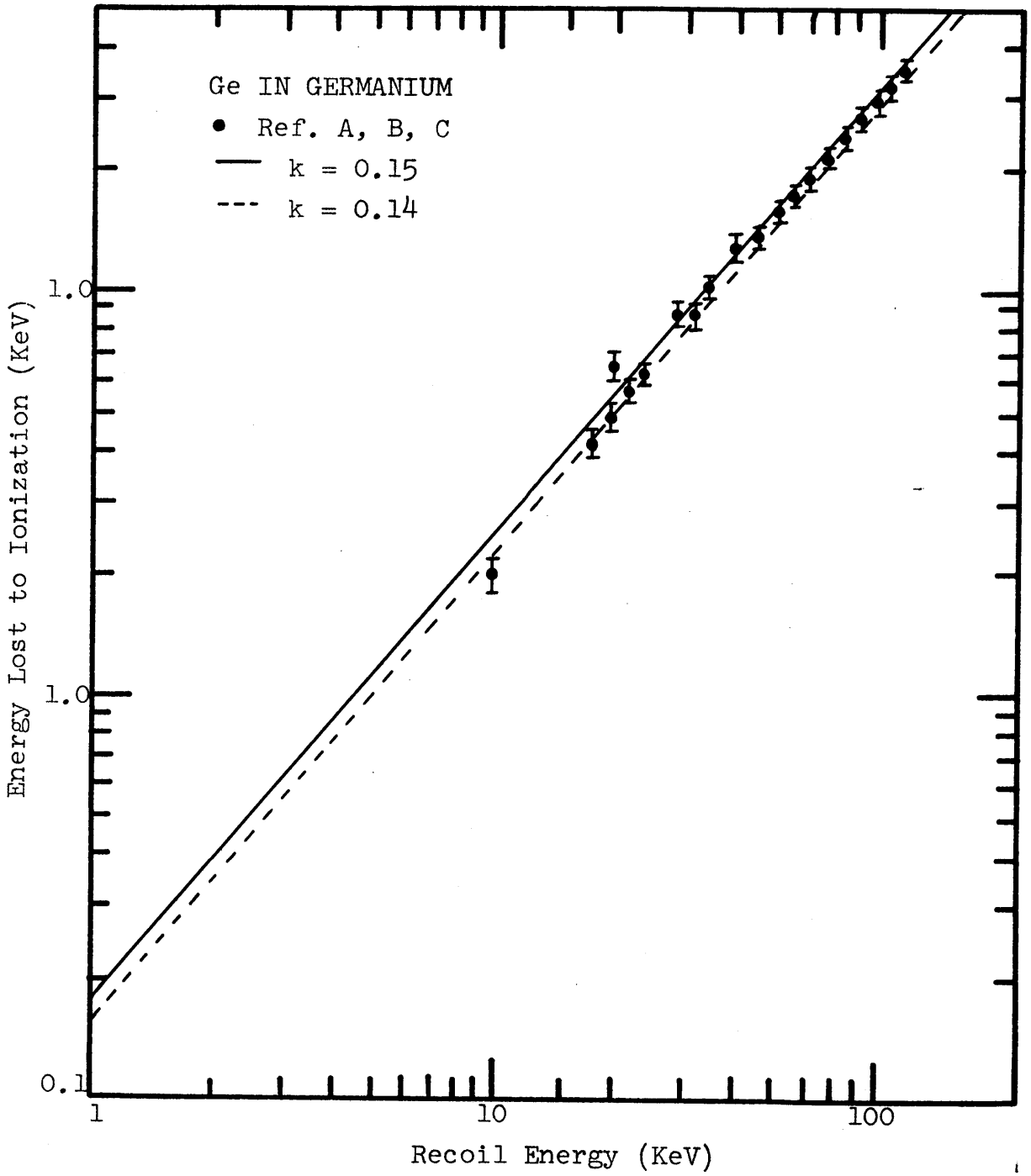

Fig. 5-1 The Energy Lost to Ionization vs. the Recoil Energy of Germanium

Ref. A - Chaseman et al., Phys. Rev. Letters, 20, 1430 (1968)
Ref. B - Chaseman et al., Phys. Rev. Letters, 15, 245 (1965)
Ref. C - Chaseman et al,, Phys. Rev. 154, 239 (1967)

Jones et al. is used for this functional relationship. This semi-empirical formula is:

$$E'' = a\ (E')^b \qquad (5\text{-}2)$$

where

$$a = 0.170 \text{ and } b = 1.163.$$

5-2-3 Integral Equation Formulation

Let $\phi\ (E,\underline{\Omega})$ be the steady-state angular neutron flux at energy E in the direction $\underline{\Omega}$. Here ϕ possesses the customary units of an angular flux, namely neutrons per unit area per unit time per unit energy per steradian. It is also assumed that the angular flux does not vary rapidly over the region of the Ge(Li) detector. For example, when the detector is far away from the neutron source we can assume the flux is independent of the angular direction. Let $dN(\underline{\Omega}')$ be the number of Ge recoils per unit time arising in the solid angle $d\underline{\Omega}'$ at $\underline{\Omega}'$. Introducing the differential cross-section per steradian per free neutron, $d\sigma/d\underline{\Omega}'$, one has

$$dN(\underline{\Omega}') = N\ d\underline{\Omega}' \int_E \frac{d\sigma}{d\underline{\Omega}'}\ (E,\underline{\Omega}')\ \phi\ (E)\ dE \qquad (5\text{-}3)$$

where N is the total number of Ge^{72} nuclei in the detector, and all solid angles are in the center of

mass system. Since in a beam experiment the neutron flux is mono-directional, $\underline{\Omega}'$ simply denotes the cosine of the angle between the original neutron direction and the germanium nucleus recoil direction. Consequently one can transform from the variable $\underline{\Omega}'$ to the final state germanium nucleus recoil energy E', since the observable production rate of germanium nuclei obtained from a Ge(Li) detector is the number of germanium nuclei per unit time arriving in a final state energy interval dE', at E'. In this case, Eq. 5-3 becomes

$$dN(E') = N\, dE' \int P(E \rightarrow E')\, \phi(E)\, dE, \qquad (5\text{-}4)$$

where

$$P(E \rightarrow E') = \frac{d\sigma}{d\underline{\Omega}'}\,(E,\underline{\Omega}')\,\frac{\partial \underline{\Omega}'}{\partial E'} \qquad (5\text{-}5)$$

is defined so that $P(E \rightarrow E')\, dE'$ is the probability that a germanium nucleus will be recoiled with an energy between E' and E' + dE' when the nucleus is struck by a neutron of energy E.

This representation of the recoiling kernal can be written in the following form:

$$P(E \rightarrow E') = -\frac{2\pi\, \sigma(E,\Theta)}{\sigma(E)}\,\frac{d\mu}{dE'} \qquad (5\text{-}6)$$

where

$$d\Omega = -2\pi\, d\mu \tag{5-7}$$

$$\sigma(E) = \int_{4\pi} \sigma(E,\theta)\, d\Omega \text{ and} \tag{5-8}$$

$\sigma(E,\theta)$ is the differential recoiling cross-section of the germanium nucleus by neutrons having energy E through an angle θ.

Hence the spectra of the recoil germanium atom becomes

$$I_R(E') = \frac{dN(E')}{dE'} \tag{5-9}$$

or

$$I_R(E') = N \int P(E,E')\, \phi(E)\, dE \tag{5-10}$$

Equation 5-13 is the desired integral equation relating the germanium recoil spectrum, $I_R(E')$, to the neutron energy spectrum, $\phi(E)$, and Eq. 5-2 relates the measured ionization loss by the stopping of recoiling germanium atoms in the germanium, E", with the energy of the recoiled germanium , E'.

In the next section the recoiling kernel, $P(E \rightarrow E')$, will be discussed. The integral equation is solved numerically using a computer code, SPECT (see Appendix F).

5-2-4 Recoiling Kernel P(E→E')

Since the Ge^{72} nucleus has well resolved and widely spaced inelastic levels at 691.4 -, 835 - keV, etc.*, classical collision theory can be applied as discussed by Donohew (D1). While this may not be adequate at high energies, this kernel will be corrected by using a measured response function.

By applying the conservation of mass-energy and of linear momentum to the collision between a neutron of unit mass and a nucleus of mass A, a relationship between the neutron energy before and after the collision and the recoiling angle can be derived. The velocity of the recoiling nucleus after the collision is given by:

$$(V')^2 = V_d^2 + V_{cm}^2 - 2V_d V_{cm} \cos \Theta , \qquad (5\text{-}11)$$

where

V' - is the velocity of the recoiling nucleus in the laboratory system,

V_d - is the velocity of the recoiling nucleus in the center-of-mass system,

V_{cm} - is the velocity of the center of mass in the laboratory system, and

Θ - is the scattering angle in the center of mass system.

* Nuclear Data Tables

Using the conservation of mass-energy, the following relationship can be obtained:

$$\frac{E'}{E} = \frac{A}{(A+1)^2} \left[D^2 + 1 - 2 D\mu \right] \qquad (5\text{-}12)$$

where

μ = COS Θ ; Θ - scattering angle in the C-system,

$$D = \sqrt{1 + \frac{A+1}{A} \frac{Q}{E}} \qquad (5\text{-}13)$$

E - is the energy of neutrons before the collision in the L-system,

E' - is the energy of recoiling nuclei after the collision in the L-system, and

Q - is the energy of the inelastic level.

Hence, the differentiation of E' with respect to μ becomes:

$$\frac{dE'}{d\mu} = - \frac{2DA}{(A+1)^2} E \qquad (5\text{-}14)$$

And the possible energy range should lie between the values of $\Theta = 0$ and $\Theta = 2\pi$. In other words the energy of the recoiling nuclei is confined to be:

$$\alpha_1 E \leq E' \leq \alpha_2 E \qquad (5\text{-}15)$$

where

$$\alpha_1 = A\left(\frac{D-1}{A+1}\right)^2 \text{ and} \qquad (5\text{-}16)$$

$$\alpha_2 = A\left(\frac{D+1}{A+1}\right)^2 .$$

Hence the recoiling kernel, Equation 5-6, becomes:

$$P(E \rightarrow E') = \begin{cases} \dfrac{\pi(A+1)^2 \ \sigma(E, \theta)}{D \cdot A \cdot E \ \ \sigma(E)} & \alpha_1 E \leq E' \leq \alpha_2 E \\ 0 & \text{otherwise} \end{cases} \qquad (5\text{-}18)$$

For isotropic recoil within the C-system, the recoiling kernel becomes:

$$P(E \ \ E') = \begin{cases} \dfrac{(A+1)^2}{4ADE} & \alpha_1 E \leq E' \leq \alpha_2 E \\ 0 & \text{otherwise} \end{cases} \qquad (5\text{-}19)$$

This assumption is very good near the threshold energy. The distribution becomes increasingly anisotropic as the energy of the incident neutrons increases. However this is not a bad initial assumption. This anisotropic effect will also be corrected for by introducing the response function using a Cf-252 standard neutron source.

5-2-5 Response Diagonal Matrix and Constraints

In the numerical treatment of integral equations of the type encompassing Eq. 5-10, it is customary to introduce a matrix representation. For a particular

value $E' = E_i'$, Eq. 5-10 can be written as follows:

$$I_R(E_i') = N \int_{E'/\alpha_2}^{E'/\alpha_1} P(E, E_i')\, \phi(E)\, dE \qquad (5\text{-}20)$$

where all the terms are the same as those defined before. As a first approximation we can assume the neutron flux $\phi(E)$ is a known function within the energy interval. This function may be any appropriate trial function (such as a constant, a linear function, a cubic polynomial, etc). For this work a constant average flux is assumed in the energy interval. Then Eq. 5-20 can be approximated as:

$$I_R(E_i') = \sum_{j=1}^{N} C_{ij}\, \phi_j \qquad (5\text{-}21)$$

where

$$C_{ij} = \begin{cases} \displaystyle\int_{E_j'/\alpha_2}^{E_j'/\alpha_1} P(E,E_i')\, dE & i = j \\ 0 & i \neq j \end{cases} \qquad (5\text{-}22)$$

Using constraints imposed by collision theory, one can obtain a particularly advantageous representation. More specifically, given a recoil germanium atom of energy E', the permissible range of initial neutron energies is bound from below by (E6);

$$(E)_{min} = \frac{1}{4E'\cdot A} \left\{ Q + E' \quad (1 + A) \right\}^2, \qquad (5\text{-}23)$$

where

$E' \geq \frac{Q}{1 + A}$; the threshold energy.

This constraint helps solve the matrix equation by trial and error. The bound energy in E-space, which corresponds to E'_j in the E'-space, is

$$(E_j)_{min} = \frac{1}{4E'_j\cdot A} \left\{ Q + E'_j \ (1 + A) \right\}. \qquad (5\text{-}24)$$

Finally, the matrix equation may be expressed:

$$[I_R] = [C] \ [\phi], \qquad (5\text{-}25)$$

where

$$I_R = \text{col} \left\{ I_{R1}, I_{R2}, \ldots\ldots\ldots I_{RN} \right\},$$

$$C = \text{dia} \left\{ C_{11}, C_{22}, \ldots\ldots\ldots C_{NN} \right\}, \text{and}$$

$$\phi = \text{col} \left\{ \phi_1, \phi_2, \ldots\ldots\ldots \phi_N \right\}.$$

When we assume that the neutron energy spectra from Cf-252, $\phi_S(E)$, is known, the matrix equation becomes

$$[I_R] = [C] \ [\phi]_S \cdot \qquad (5\text{-}26)$$

where $[\phi]_S$ = the known flux column vector from Cf-252.

The measured spectra can be written:

$$[I_R] = [C]_M [\phi]_M \qquad (5\text{-}27)$$

where $[\phi]_M$ = the neutron flux column vector deduced from the measured $[I_R]$ spectrum vector using Cf-252

irradiation. From Eqs. 5-26 and 5-27, the corrected response diagonal matrix becomes

$$[C] = [C]_M [\lambda]^T \tag{5-28}$$

where the elements of $[\lambda]$ are

$$\lambda_{ii} = \frac{\phi_{Mi}}{\phi_{Si}} \tag{5-29}$$

This corrected response diagonal matrix will enable us to cover the entire energy range of the incident neutrons without incurring distortion due to analytical or numerical shortcomings of the unfolding technique. The actual solution is accomplished by a computer code SPECT, described in Appendix F.

5-3 Data Analysis

5-3-1 Cf-252 Standard Neutron Source

It is very important to have an exact neutron spectrum available as a reference. In common with a growing number of other applications Cf-252 has been selected for the present work. In Cf-252 spontaneous fission, an average of approximately two neutrons per fragment are released. These neutrons have the typical shape of fission neutron spectra. For fission sources, the spectrum shape is frequently taken to be Maxwellian,

$$\phi(E) \sim \sqrt{E} \exp\left(-\frac{E}{T_c}\right) \qquad (5\text{-}30)$$

so that it is completely specified by the single parameter T_c, the Maxwellian temperature. A number of measurements of this parameter have been made for Cf-252 fission neutron sources, and these are summarized in Table 5-1. The fourth temperature listed in Table 5-1 is an average of three earlier measurements. The last three are the results of more recent studies, obtained using techniques very similar to one another. It can be seen that there is wide disagreement between No. 6 and No. 5 or No. 7. For the present work the temperature from H. Condé or L. Green ($T_c = 1.390 \pm 0.04$) is chosen because these results represent more recent work. The Cf-252 neutron source has a most probable energy of 700 KeV and a 2.58 yr. effective half-life, and the average number of neutrons emitted per fission is 3.77.

The use of a Cf-252 source to deduce the response function of the detecting system and to correct the calculated response matrix is described in the following section.

5-3-2 Experimental Procedure and Data Analysis

The runs with Cf-252 neutron sources were made in the well-isolated, low background accelerator vault in

TABLE 5-1

Cf-252 Fission Neutron Spectrum Parameter

Number	T_c (Maxwellian Temp., MeV)	Reference
1	1.57 ± 0.05	S3
2	1.37 ± 0.03	B4
3	1.42 ± 0.05	S3
4	1.466 ± 0.100	R4
5	1.390 ± 0.04	C4
6	1.592	M3
7	1.390 ± 0.04	G8

building NW-12 at MIT. The source was placed in the middle of the 31.5 ft. by 19 ft. by 12 ft. high vault in order to minimize back-scattering of neutrons by the vault walls. The detector used here was the same 17 c.c. Ge(Li) crystal previously discussed. Two different Cf-252 neutron sources were available. One is a point source, which is mounted on the top of a 1/4 in. diameter, 2 in. long aluminum rod. The other is mounted in a 7/8 in. diameter, 1-1/2 in. long lead cylinder. Both sources gave the same spectra at 691.4 KeV, except for the accompanying fission gamma-ray background in that energy region. Furthermore it was found that the spectra at 691.4 KeV are not appreciably affected by varying the direction of the incident neutron beam relative to the Ge(Li) crystal axis. In any case, after subtracting the background from the broadened spectrum the spectrum has the shape shown in Fig. 5-2. Figure 5-2 is the broadened spectrum at 691.4 KeV produced by bombardment of the Ge(Li) crystal by the Cf-252 fission neutron source. In the present work the energy resolution, the full width at the half-maximum (FWHM), is eight channels. The broadening by the Ge(Li) recoil is shown to be more than 150 channels in Fig. 5-2. Since the energy per channel of this run is 0.425 KeV/CH, the broadening is

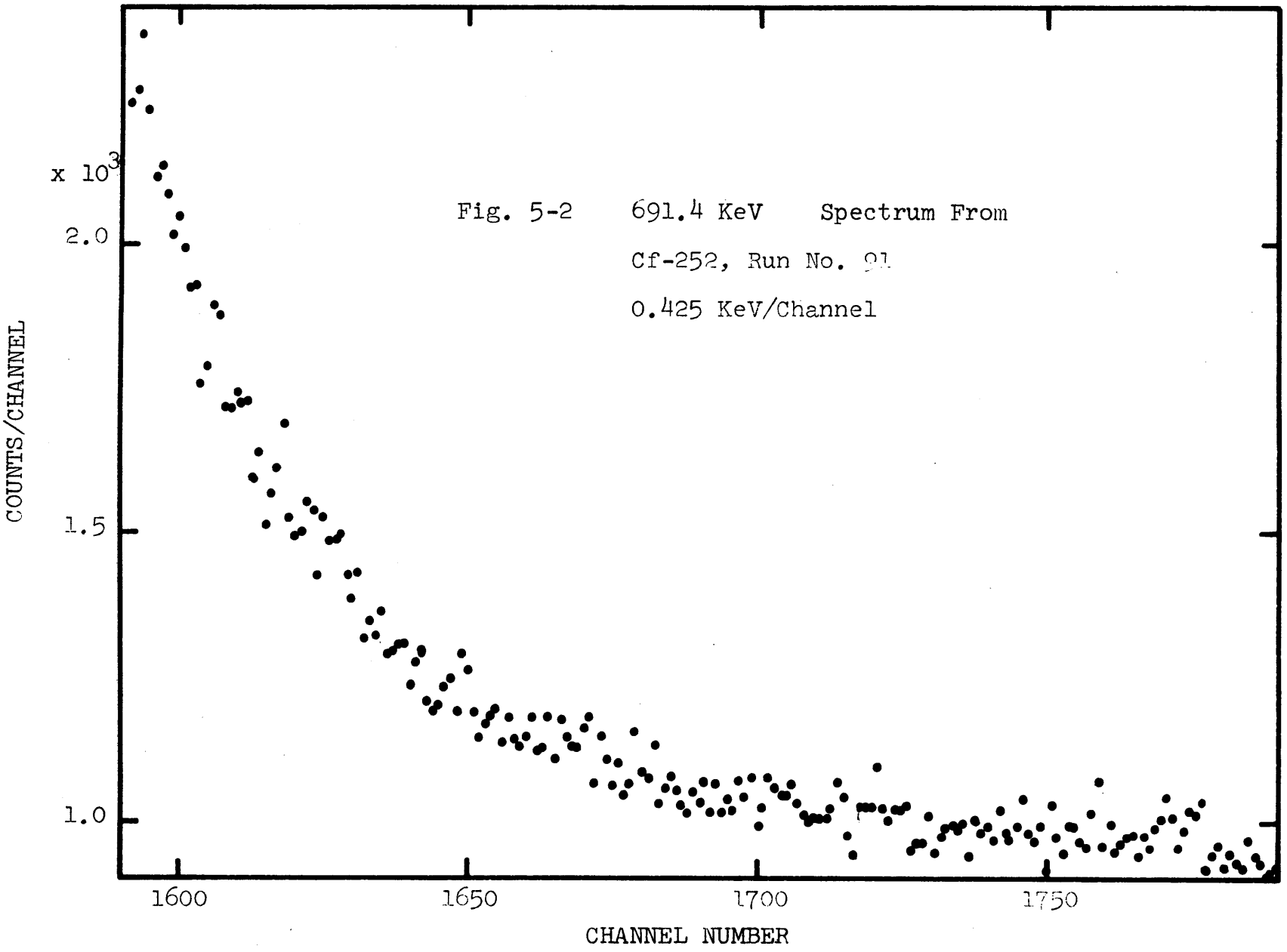

Fig. 5-2 691.4 KeV Spectrum From Cf-252, Run No. 91
0.425 KeV/Channel

more than 64 KeV on the higher energy side, with better than 4 KeV energy resolution.

Figure 5-3 shows the neutron energy spectra of Cf-252; the dots show the theoretical, or "true" Cf-252 fission neutron energy spectrum and the crosses show the deduced inelastic collision density spectrum, $\sigma_{in}\ \phi$, from the measured broadened gamma spectrum at 691.4 KeV. Since the inelastic scattering cross-section data are not well established, it is better to include the cross-section in the so-called response matrix. The response correction matrix is calculated from these two independent spectra.

Figure 5-4 shows a broadened gamma spectrum at 691.4 KeV produced by neutrons leaking from Blanket No. 2. This original continuous broadened spectrum from Blanket No. 2 is analyzed with the help of the correction matrix, obtained using the Cf-252 standard neutron source. The analyzed neutron spectra of Runs No. 107 and 106 from Blanket No. 2 are shown in Figs. 5-5 and 5-6, respectively. This analysis is done by a computer program SPECT (see Appendix F). Since the internal conversion transition is a threshold reaction, one can only obtain the neutron spectrum above the threshold energy of the reaction. Both Figs. 5-5 and 5-6 exhibit large depressions in the neutron flux at 2.2 MeV and 3 MeV. These depressions are

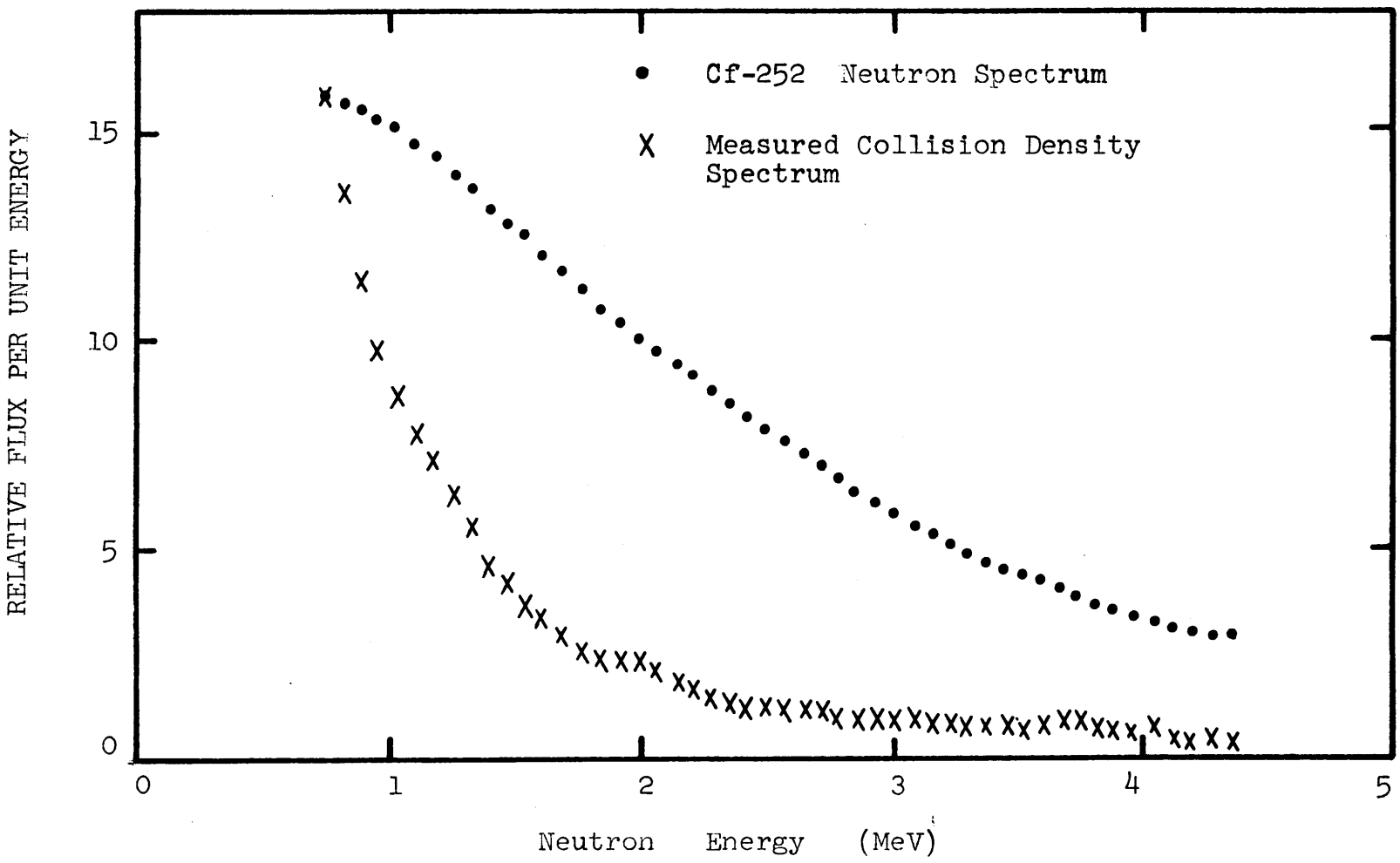

Fig. 5-3 Comparison of the Cf-252 Neutron Spectrum with the Measured Collision Density Spectrum

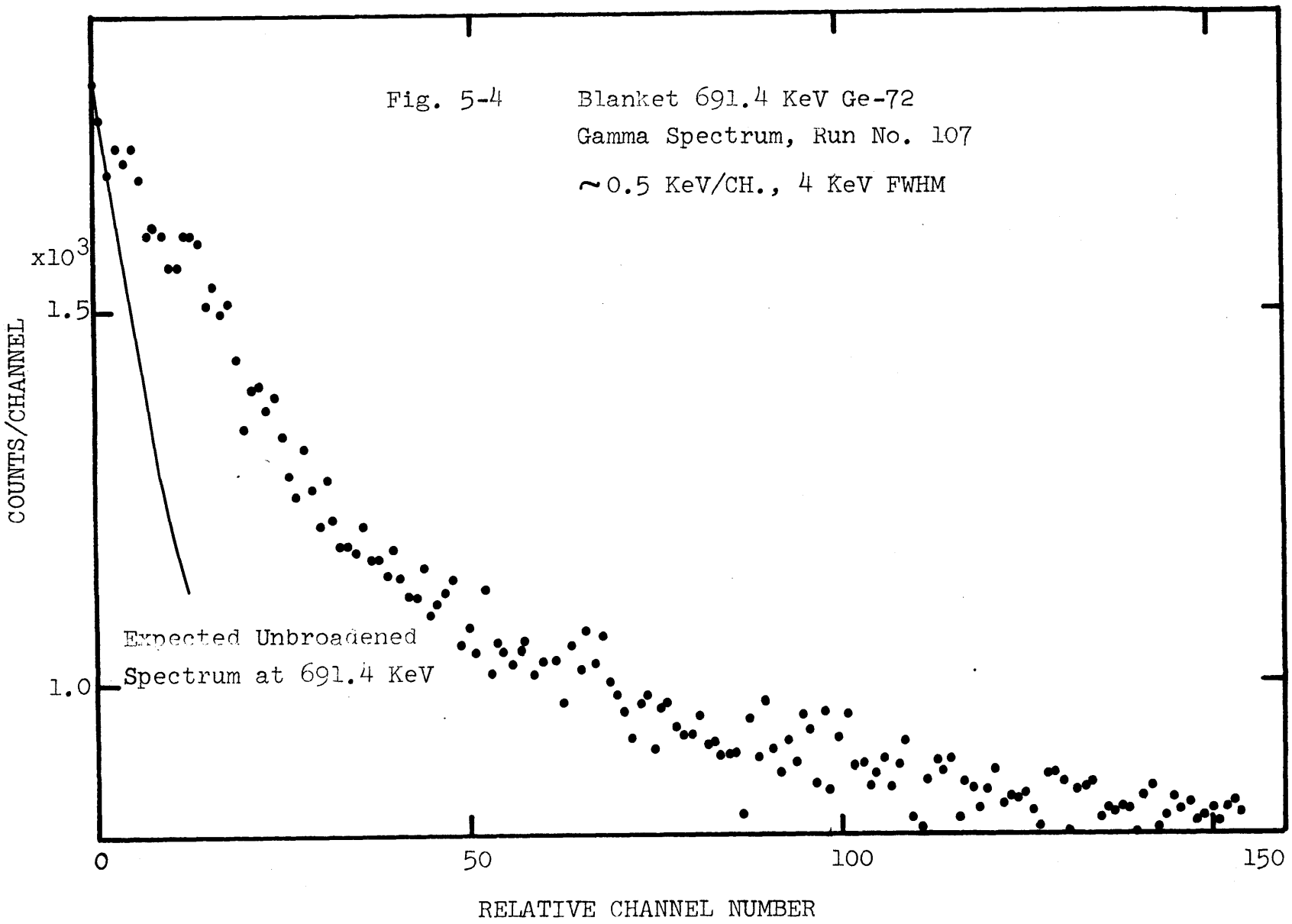
Blanket 691.4 KeV Ge-72
Gamma Spectrum, Run No. 107
~0.5 KeV/CH., 4 KeV FWHM
x10^3
1.5
1.0
COUNTS/CHANNEL
Expected Unbroadened
Spectrum at 691.4 KeV
0
50
100
150
RELATIVE CHANNEL NUMBER

Fig. 5-4

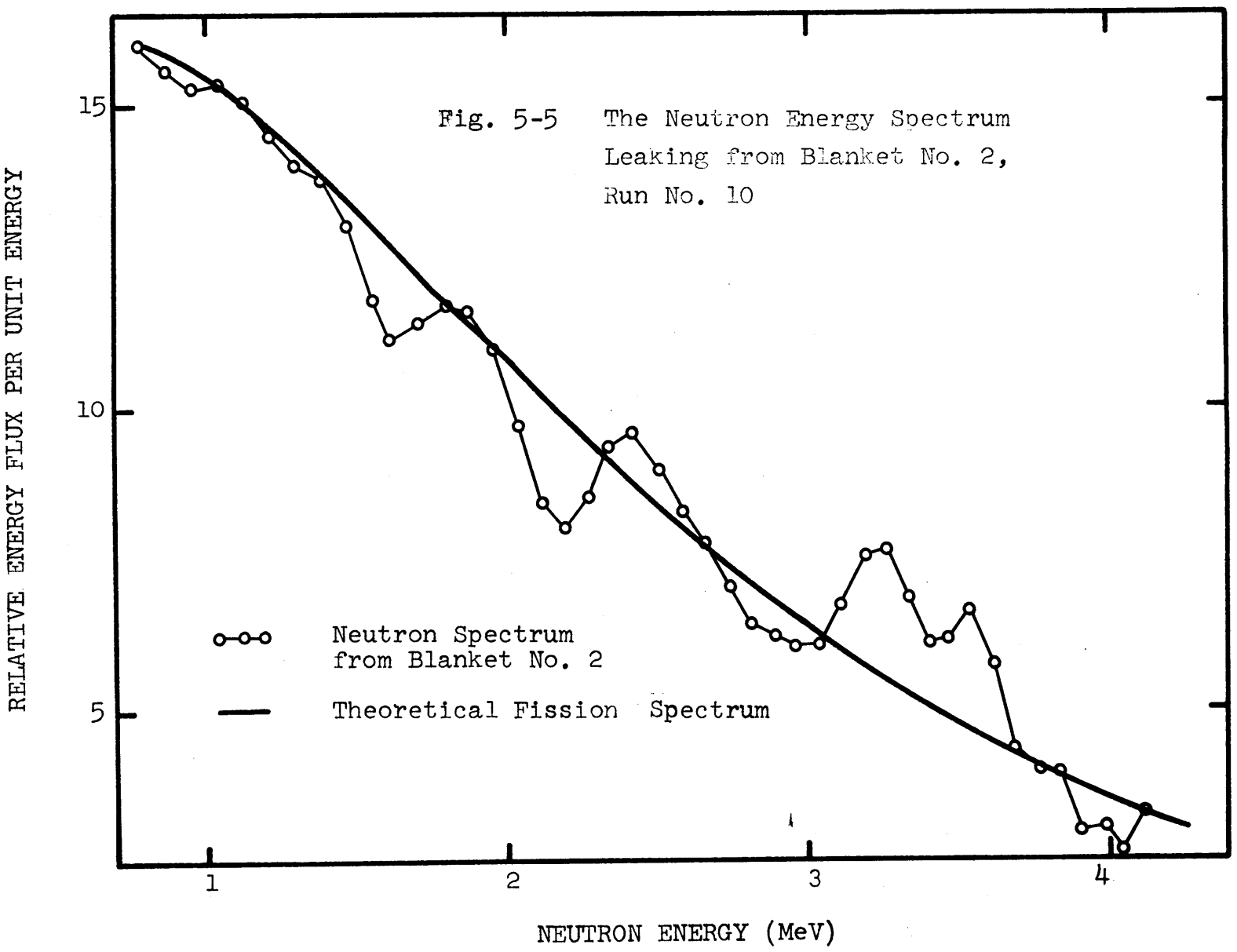

Fig. 5-5 The Neutron Energy Spectrum Leaking from Blanket No. 2, Run No. 10

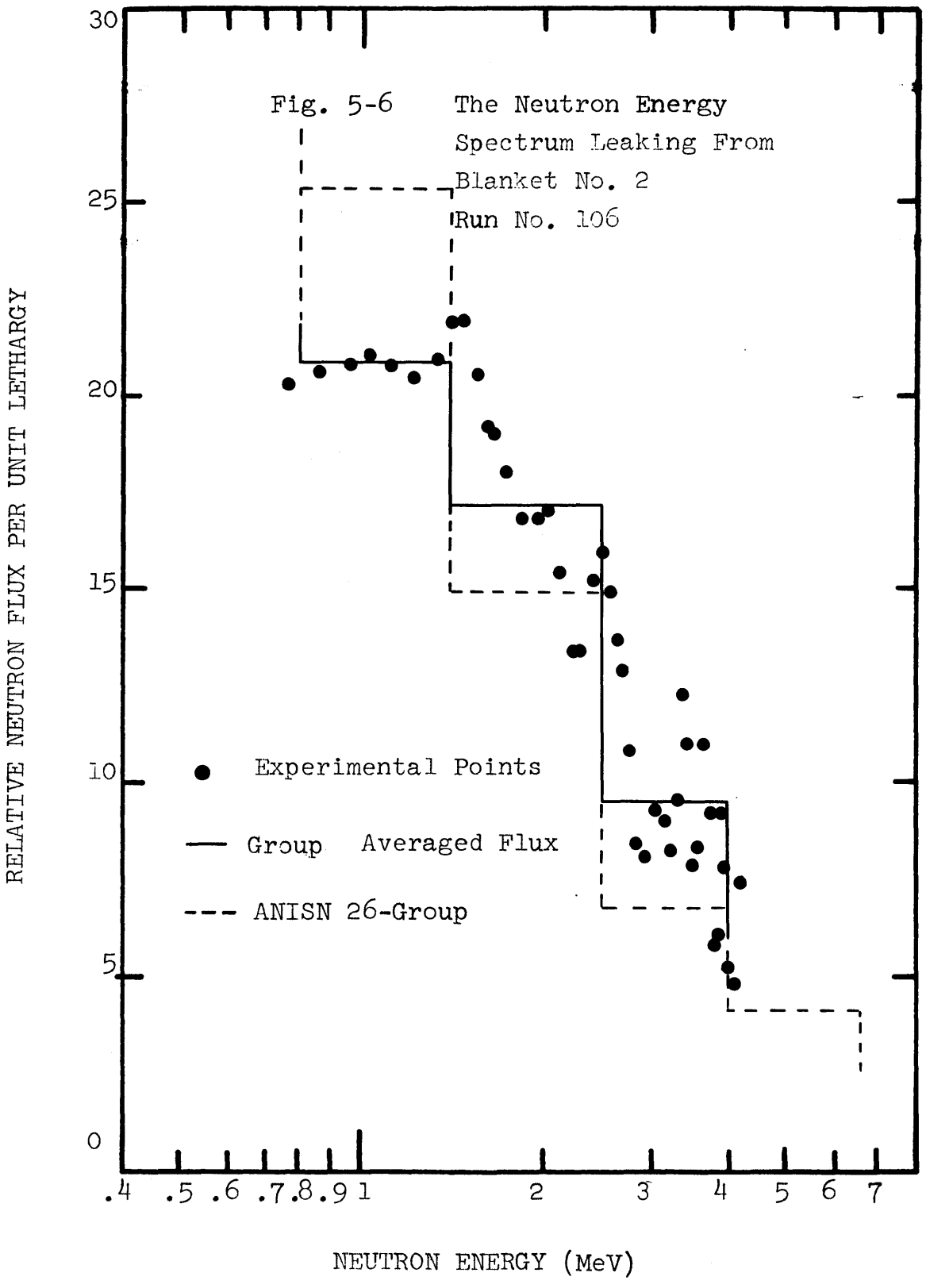
Fig. 5-6 The Neutron Energy Spectrum Leaking From Blanket No. 2 Run No. 106
Experimental Points
Group Averaged Flux
ANISN 26-Group
RELATIVE NEUTRON FLUX PER UNIT LETHARGY
NEUTRON ENERGY (MeV)
0
5
10
15
20
25
30
.4
.5
.6
.7
.8
.9
1
2
3
4
5
6
7

also observed in the neutron spectrum in ZPR-3 Assembly 48 deduced by both MC^2 calculation and proton-recoil measurement at ANL (Y2). This is attributable to high energy resonances at these energies. Oxygen, chromium and sodium all have large scattering resonances in this energy range. The spectrum from the blanket is compared with the typical fission neutron spectrum in Fig. 5-5 and with the ANISN 26 group flux in Fig. 5-6, respectively.

Methods are suggested to cover the low energy section of the neutron energy spectrum in the next section.

5-4 Some Other Methods for Extracting Neutron Spectra from Gamma-Ray Spectra

There are other possible approaches to unfolding neutron spectra from gamma-ray spectra. For example, Forsberg exploited the fact that the capture gamma-ray yield changes according to the energy of the incident neutrons (F3). Here two additional methods for obtaining neutron energy spectra using gamma-ray spectroscopy will be discussed.

5-4-1 Energy Shift Method

The analytical relationship between the Q-value, and the kinetic energy of the incident and compound particle, as measured in the laboratory system, can be deduced. We

consider here the non-relativistic case, in which the kinetic energy, E, of the incident and compound particles is small compared with the rest mass-energy MC^2. As an example, consider a neutron of energy E_n and mass M_n hitting a target nucleus and being captured by the target, releasing a prompt capture gamma-ray. Conservation laws for nuclear reactions give the following equation (E7):

$$E\gamma = X \pm \sqrt{X^2 - Y} \qquad (5\text{-}31)$$

where

$$X = C\sqrt{2 M_n E_n} \cos\theta - M_c C^2, \qquad (5\text{-}32)$$

$$Y = 2\left[(M_n - M_c) C^2 \cdot E_n - Q M_c C^2\right], \qquad (5\text{-}33)$$

$E\gamma$, E_n - are the energies of the prompt capture gamma-rays, and the incident neutrons, respectively,

M_n, M_c - are the masses of a neutron and the compound nucleus formed, respectively,

Q - is the Q-value of the reaction,

C - is the velocity of light,

θ - is the trajectory angle of the compound nucleus after the neutron is captured.

The energetically possible solutions are those for which $E\gamma$ is real and positive. Two special cases of interest will be examined.

Case I : Thermal neutron bombardment, i.e., $E_n \approx 0$.

$$E\gamma = M_c C^2 \left(\sqrt{1 + \frac{2Q}{M_c C^2}} - 1 \right) \qquad (5\text{-}34)$$

Or if we expand in a power series, the gamma-ray energy can be approximated, as expected, by:

$$E\gamma = M_c C^2 \left(\frac{Q}{M_c C^2} - \frac{1}{2} * \frac{Q^2}{(M_c C^2)} + \text{---} \right) \qquad (5\text{-}35)$$

$$\approx Q$$

Hence in thermal neutron capture reactions, one can see a gamma-ray, the energy of which corresponds to Q, as well as cascades of gamma-rays. In the special case of hydrogen the Q-value is 2.223 MeV, which can be seen prominently in every thermal prompt capture gamma-ray spectrum involving hydrogeneous targets.

Case II: The target is hydrogen and the detector is placed at a 90° angle to the direction of the neutron beam, i.e., $M_c = 2M_n$ and $\theta = \pm 90^\circ$,

$$E\gamma = (Q + \frac{En}{2}) - \frac{1}{4} \frac{(Q + E_n/2)^2}{M_n C^2} + \text{.....} \qquad (5\text{-}36)$$

Hence the shift of the gamma-ray energy from the thermal capture line at 2.223 MeV depends on the energy of the incident neutrons. This effect may make it possible to deduce the incident neutron energy spectrum. However this method has several disadvantages. The first one is that the capture cross-section of hydrogen decreases very rapidly (roughly as $E^{-1/2}$) as the energy of the neutrons increases. The second disadvantage is that the possibility of scattering is much higher than that of capture. Thus for thick targets moderation and subsequent capture is actually preferred to initial capture. (see calculation in Appendix I). In order to avoid this problem a very thin target is called for, which, again because of the small σ_a, results in very low detection efficiency.

5-4-2 Prompt Activation Method

A very well-known method for analysis of neutron energy spectra is that of foil activation analysis. In this method one can choose a number of special elements, irradiate them for a certain time, and count the decay gamma-rays after a certain cooling period. A direct analogy to this approach is possible, using prompt instead of decay gamma-rays. In fact, rather than target foils one can use gamma-rays given off by the normal constituents of the assembly itself. Prompt gamma-rays from a typical

multiplying assembly include the inelastic gamma-rays, the prompt capture and fission gamma-rays, and the very short lived decay gamma-rays. Applications involving inelastic gamma-rays appear very encouraging.

Most cross-sections for higher energy neutrons are very small, except for the scattering cross-section. Further, in the case of prompt capture gamma-rays the yield changes according to the energy of the incident neutrons. Because these varying yields are not well known, this complication will lead one to use inelastic gamma-rays for prompt activation analysis of the present sort. Further production of gamma-rays by inelastic scattering increases as the neutron energy increases. Furthermore, the cross-section for gamma-ray production by inelastic scattering is well known for many elements (Rl) such as F, Ta, Fe, Nb, W, Sc, etc.

The total gamma-ray intensity of a peak of interest due to inelastic scattering can be expressed by:

$$I_i = \epsilon_i \int \Sigma_i(E)\, \phi\,(E)\, dE\,, \qquad (5\text{-}37)$$

where

I_i - is the total intensity of the inelastic gamma-ray peak i,

ϵ_i - is the total efficiency of the detection system for the gamma-ray peak i,

$\Sigma_i(E)$ - is the macroscopic inelastic gamma-ray producing cross-section for the gamma-ray peak i at the neutron energy E, and

$\phi(E)$ - is the incident neutron flux having energy E.

Many approaches are appropriate for solving integral equations of the type Eq. 5-37. Here one of the simpler treatments will be introduced. The unknown flux $\phi(E)$ may be expanded in a series of known functions as follows:

$$\phi(E) = \sum_j a_j u_j(E), \tag{5-38}$$

where

a_j - are unknown coefficients, and

$u_j(E)$ - appropriate known trial functions.

Substituting Eq. 5-38 into Eq. 5-37 gives:

$$I_i = \epsilon_i \sum_j a_j \Sigma_{ij}, \tag{5-39}$$

where

$$\Sigma_{ij} = \int \Sigma_i(E)\, u_j(E)\, dE. \tag{5-40}$$

The matrix elements, Σ_{ij}, can be computed and Eq. 5-40 becomes a well known form of matrix equation if one can choose N well-resolved inelastic gamma-ray peaks.

$$[I] = [\Sigma] [A] , \tag{5-41}$$

where

$$[I] = \text{col} \{ I_1/\ _1,\ I_2/\ _2,\ ----,\ I_N/\ _N \},$$

$[\Sigma]$ = NXN matrix, the elements of which are defined in Eq. 5-43, and

$$[A] = \text{col} \{ a_1, a_2, ---, a_N \}.$$

Therefore the spectrum coefficient vector $[A]$ is given by:

$$[A] = [\Sigma]^{-1} [I] . \tag{5-42}$$

Equation 5-42 can be solved in so far as the matrix $[\Sigma]$ is not singular, which can be accomplished by proper choice of the peaks. An advantage of this procedure is that one can use a large number of peaks, since some materials such as Ta, Nb, Sc have almost ten prominent inelastic gamma-ray peaks (R1). Furthermore thermal neutrons no longer interfere with the experiment. However several disadvantages are incurred. One is that we cannot get any information on neutron spectra lower than about 100 KeV because inelastic scattering is a

threshold reaction. Another disadvantage is that the gamma-ray production cross-section is not well determined which may introduce large errors in the unfolding unless methods using Cf-252 standards are again developed. Further, gamma-ray background problems are often severe because inelastic gamma-rays are typically of lower energy than prompt capture gamma-rays or even some decay gamma-rays.

Chapter VI

GAMMA-RAY DOSIMETRY

6-1 Introduction

The radiation environment of a reactor is not exclusively composed of neutrons; gamma-rays are also an important component. The intensity and energy spectrum of the gamma-rays in the blanket are of practical interest in such areas as gamma-ray heating, shielding, and radiation damage.

In most experiments with Ge(Li) detectors for gamma-ray measurements, the dominance of the Compton recoil continuum in the detectors is regarded a very unwanted and troublesome complication. R. Gold (G5), however, showed how this background signal can be exploited for continuous gamma-ray spectroscopy. He used the well-defined integral equation, which relates the Compton distribution of the recoil electrons and the incoming continuous gamma-ray spectrum, and solved the integral equation numerically using an iterative unfolding method for response matrices (G7). R. Gold used a small Si(Li) crystal (200 mm^2 area by 5 mm depletion depth) and focused his major effort on low energy gamma-rays (lower than 1.5 MeV) in his work.

For many purposes, such as shielding and radiation damage, high energy gamma-rays are also very important. The present work will cover the high energy region of the gamma-ray spectrum from Blanket No. 2 (up to 10 MeV). The main objective of the work reported in this chapter is the measurement of the continuous gamma-ray spectrum leaking from Blanket No. 2.

The continuous gamma-ray spectrum is contributed by not only the gamma-rays produced in the fission process but also the gamma-rays resulting from neutron interactions with the structural materials. Depending on the type of material used, the spectrum of gamma-rays can be considerably enhanced, both in energy and intensity, by the production of inelastic scattering and capture gamma-rays. Thus, when stainless steel was substituted for aluminum as the structural and cladding material in the pool-type ORNL Bulk Shielding Reactor (S4), it was expected that the spectrum of gamma-rays emitted by the core would harden since the gamma-rays above 5 MeV originate primarily from thermal neutron capture in the components of the stainless steel such as Fe^{57} at 5.91, 6.02, and 7.6 MeV, Fe^{58} at 10.16 MeV, Cr^{54} at 8.88 MeV and 9.72 MeV, and Ni^{59} at 8.53 and 8.99 MeV.

We should also point out that the subject gamma spectrum is obtained "free" in every gamma-ray spectrum measured on Blanket No. 2, just as were the neutron spectra using the 693.5 KeV germanium internal conversion. These two by-products of the gamma-ray spectra suggest the possibility of using Ge(Li) detectors as simultaneous neutron - gamma spectrometers in LMFBR shielding studies.

6-2 Theory

The measured electron recoil spectrum due to Compton scattering by the incoming gamma-rays to the Ge(Li) detector is given by:

$$I(E) = \int_{E'_{min}}^{E'_{max}} K(E,E') \; \phi(E') \, dE', \qquad (6\text{-}1)$$

where the function K(E,E') is customarily called the response function of the detection system, which is the Compton scattering kernel defined by the Klein-Nishina formula in the form (N1):

$$K(E,E') = \frac{\pi r_o^2}{(E'-E)} \left\{ \left(\frac{E}{E'^2} \right)^2 + 2 \left(\frac{E'-E}{E'} \right)^2 + \frac{(E'-E)}{E'^3} \cdot \left[(E-1)^2 - 1 \right] \right\}, \qquad (6\text{-}2)$$

where r_o is the classical electron radius, and ϕ (E') is the total photon flux at energy E'.

Equation 6-1 is well-known as a non-singular Fredholm equation of the first kind. The solution of this kind of integral equation may be treated numerically. It is customary to introduce a matrix formulation using the energy-group approximation. One divides the E-space into N equally spaced energy intervals, whose mid-bin energies are E_1, E_2, ----,E_{N-1}, E_N. For a particular value at $E = E_i$, Equation 6-1 becomes

$$I_i = \int_{E'_{min}}^{E'_{max}} K(E_i, E')\, \phi(E')\, dE', \qquad (6\text{-}3)$$

where

$$I_i = I(E_i). \qquad (6\text{-}4)$$

If one divides the integral term of Equation 6-3 into N small energy intervals, Eq. 6-3 can be rewritten as:

$$I_i = \sum_{j=1}^{N} \int_{\Delta E'_j} K(E_i, E')\, \phi(E')\, dE', \qquad (6\text{-}5)$$

where

$\Delta E'_j = E_j^{U'} - E_j^{L'}$, and $E_j^{U'}$ and $E_j^{L'}$ are the upper and lower limits bounding the j-th bin, E'_j, of E'-space.

Using physical constraints imposed by the Compton scattering process (E-6), one can rewrite Eq. 6-5 as follows:

$$I_i = \sum_j \int_{\Delta E'_j} K(E_i, E') \, \phi(E') \, dE', \qquad (6\text{-}6)$$

where

$$j = i, \; i+1, \; ----, \; N.$$

If one can assume that the photon flux ϕ is a constant over the small region $\Delta E'_j$, then Eq. 6-6 can be approximated by:

$$I_i = \sum_j K_{ij} \, \phi_j \, , \qquad (6\text{-}7)$$

where

$$I_i = \int_{\Delta E_i} I(E) \, dE / \Delta E_i , \qquad (6\text{-}8)$$

$$K_{ij} = \int_{\Delta E'_j} K(E_i, E') \, dE', \qquad (6\text{-}9)$$

and $$\phi_j = \phi(E'_j). \qquad (6\text{-}10)$$

Or in the matrix form, the equation becomes:

$$[I] = [K] \; [\phi] \qquad (6\text{-}11)$$

where

$$[I] = \text{col} \; \{I_1, I_2, \; -----, \; I_N\} , \qquad (6\text{-}12)$$

$$[\phi] = \text{col}\ \{\phi_1, \phi_2, \text{----}, \phi_N\}\ , \qquad (6\text{-}13)$$

and

$[K]$ is the upper triangular matrix, whose elements are

$$K_{ij} = \int_{\Delta E'_j} K(E_i, E')\, dE' \ ; \quad j = i, i+1, \text{---}, N. \qquad (6\text{-}14)$$

The upper triangular matrix Eq. 6-11 can be solved without any difficulty. Equation 6-11 may be written by:

$$I_N = K_{NN}\phi_N$$

$$I_{N-1} = K_{N-1,N-1}\,\phi_{N-1} + K_{N-1N}\,\phi_N$$

$$I_2 = K_{22}\,\phi_2 + K_{23}\,\phi_3 + \text{---} + K_{2N}\,\phi_N$$

$$I_1 = K_{11}\,\phi_1 + K_{12}\,\phi_2 + \text{---} + K_{1N}\,\phi_N \qquad (6\text{-}14)$$

These equations can be solved exactly in order once all integral terms such as I_i and K_{ij} are computed and provided. R. Gold introduced an iterative unfolding method (G7) to solve this matrix equation.

The continuum gamma-ray analysis is performed by a computer code COMPT (Appendix H) which performs the integrations to form the electron and photon vector array by Simpson's rule (H7), the formulation of the matrix equation and the solution of the upper triangular

matrix equation using an iterative unfolding method.

6-3 Data Analysis

The electron-recoil spectrum observed with any given detector is not necessarily identical to the Compton continuum. It has been generally demonstrated that effects of finite detector size introduce a completely independent unfolding problem (G4). The detector should be chosen as large as possible consistent with requirements of good energy resolution, low noise, and the counting rate. By choosing the largest possible detector, one can obtain higher sensitivity and reduce the complexity of the finite size effect unfolding problem. A 17 c.c. Ge(Li) crystal is used in this present measurement. A detector of this size does not give rise to appreciable finite-size effects, since the electron range in the energy region of interest is not comparable with the detector thickness. In fact, for a very high electron energy of 10 MeV, the range in germanium is only approximately 8 mm (E1) Getting rid of the finite-size problem makes the entire process very much simpler. R. Gold suggested an electronic Pulse Shape Discrimination (PSD) method to reduce the finite-size problem (G5). However he used a thin Si(Li) detector, 5 mm thick by 200 mm^2 area. A detector of this size introduces non-negligible finite-size effects,

especially in the high energy region.

Figure 6-1 shows the observed Compton recoil continuum spectrum from Blanket No. 2, which has been analyzed by GAMANL. GAMANL was used to perform the smoothing of the original gamma-ray spectrum from Blanket No. 2 using Fourier Transforms, and to subtract all analyzed discrete peaks from the spectrum. This output, the analyzed background data of the spectrum, became the input to the computer code COMPT, which performed the analysis of the Compton recoil continuum gamma-ray spectrum. These background data of a typical gamma-ray spectrum from Blanket No. 2 are given in Appendix H.

Figure 6-2 shows the gamma-ray continuum leaking from Blanket No. 2 obtained through the computer program COMPT (Appendix H). In Figure 6-2 the component of the spectra due to prompt neutron captures in the blanket structural materials is evident in the peaks appearing above 5 MeV. The photons above 5 MeV originate primarily from prompt neutron capture in the iron, which is the cladding and main structural material in Blanket No. 2, its reflector, and the surrounding shielding. Two prominent Fe^{57} lines of almost equal intensity, with energies of 5.921 and

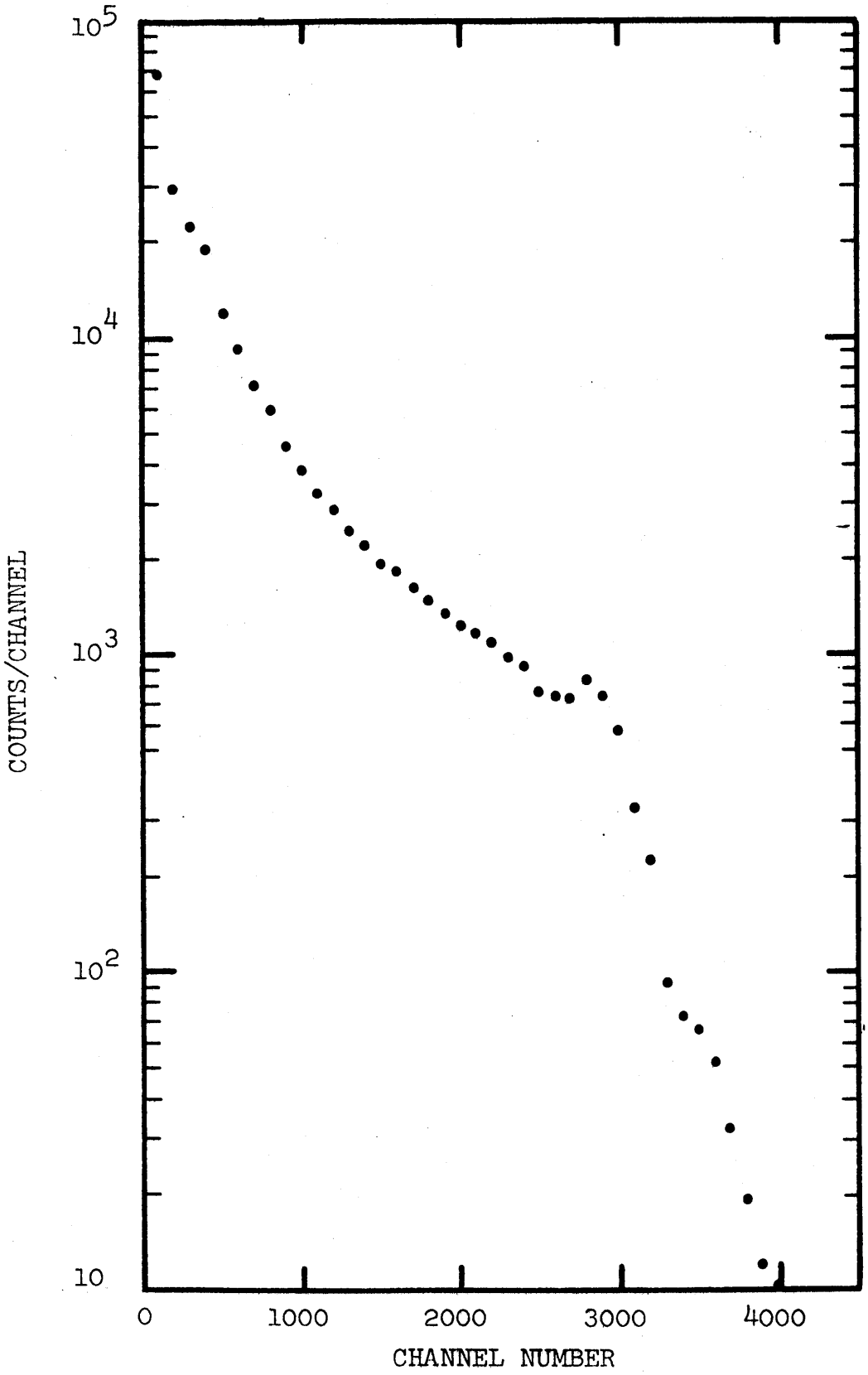

Fig. 6-1 Gamma-Ray Continuum from Blanket No. 2, Run No. 105

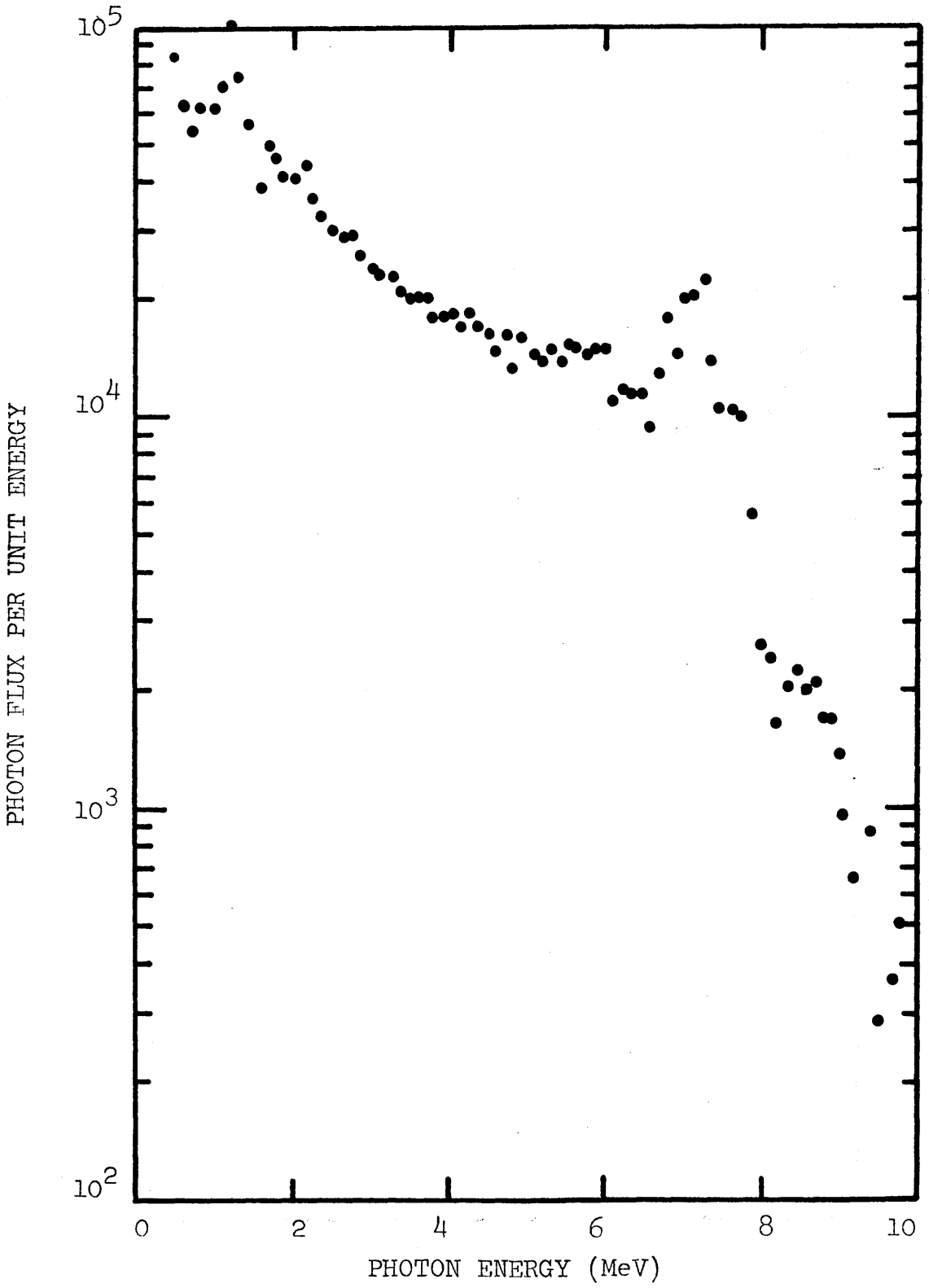

Fig. 6-2 The Gamma-Ray Spectrum Leaking from Blanket No. 2, Run No. 105

6.019 MeV, contribute to the spectrum. Other Fe^{57} capture gamma-rays, at 7.632 and 7.646 MeV, appear as the most distinct contribution in the high energy spectrum. These high energy iron prompt capture peaks are responsible for the large continuum flux up to 7.5 MeV. Above this energy the flux decreases abruptly. The distribution between 8.5 and 9 MeV is composed of gamma-rays from Cr^{54} at 8.881 MeV, plus a possible weak contribution of gamma-rays from Fe^{57} at 8.872 MeV. Above 9 MeV, the major contribution comes from Cr^{54} at 9.716 MeV and from Fe^{58} at 10.16 MeV. Below 5 MeV the spectrum in Figure 6-2 is apparently contributed by gamma-rays that constitute the expected continua of prompt fission and fission product gamma-rays plus a contribution by neutron capture and inelastic scattering in sodium, chromium, uranium, iron, etc.

The first bump at 1.2 MeV in Figure 6-2 is due to the high background gamma-ray from Ar^{41} at 1.294 MeV. The second bump at 7.3 MeV is due to the most distinct peak of iron prompt capture, the 7.64 MeV doublet. The third bump at 8.5 MeV is due to the prompt capture gamma-ray from Cr^{54} at 8.882 MeV. The analysis has been done in a very straight forward manner, neglecting the finite size problem. This finite size effect should not

be appreciable in this measurement. Most errors introduced in unfolding the spectrum are in the high energy region, and are caused mainly by neglecting the finite-size problem.

Chapter VII

CONCLUSIONS AND RECOMMENDATIONS

7-1 Conclusions

The present work was a study of the application of gamma-ray spectroscopy to the investigation of fast reactor blankets. This AEC sponsored work was carried out on Blanket No. 2 of the M.I.T. Blanket Test Facility. As a result of this study the following conclusions were reached:

1. Ge(Li) detectors can be used to determine simultaneously the fast neutron spectrum ($E_n > .8$ MeV) and the high energy gamma-ray spectrum. This information can be obtained from a single spectrum from a Ge(Li) detector. The neutron spectrum is obtained from an analysis of broadened Ge lines and the gamma-ray spectrum from an analysis of the Compton distribution. This information about the high energy portion of each spectrum would be particularly useful in shielding studies.

2. The hydrogen content of materials in a fast system can be accurately determined by prompt activation analysis using the hydrogen capture gamma-ray. This information is particularly useful since small hydrogen impurities can have important effects on the neutron spectrum in fast facilities.
3. The determination of the reaction rates in various components of the fast facility can in principle be determined by analysis of a combination of capture inelastic, and decay gamma-rays. In this study it was found that this method did not give a high degree of accuracy. The accuracy was limited by lack of knowledge of the gamma-ray yield as a function of neutron energy. Another serious limitation discovered was that no capture lines from U-238 could be identified in the fast neutron spectrum even though a number can be measured in a thermal neutron spectrum.

This means that capture gamma-rays from the dominant capture mode in the blanket cannot be detected in measurements of the type carried out in this study. For this reason this method does not appear promising for applications of the type investigated.

It was shown that the reaction rate in U-238 could be determined from the decay gamma-rays of Np-239. However the low energy of these gamma-rays (100-300 KeV) led to vary large self absorption corrections, which are difficult to determine accurately. This comment also applies to the gamma-rays from inelastic neutron scattering.

7-2 Recommendations

Based upon the results of this investigation, a number of both specific and general recommendations are suggested:

1. It is suggested that in future work at M.I.T. the possibility of using a long-nose dewar to hold the Ge(Li) crystal closer to the blanket be investigated. This will increase the counting rate of the detecting system and reduce the statistical error.

2. It is recommended that a study of prompt capture yield changes of U-238, sodium, chromium and other LMFBR constituents be made as a function of neutron energy if further development of prompt gamma analysis methods is attempted. It should be noted, however, that this will be a very tedious and expensive task. Similarly, further study of the relationship between the gamma-ray production and inelastic scattering cross-section would be necessary. In any event it is recommended that successful extraction of U-238 prompt capture gamma lines be deomonstrated before embarking upon the preceding work.
3. Analysis and unfolding of the broadened inelastic scattering spectrum of Ge^{74} at 595 KeV, and comparison with the spectrum unfolded using the 691.4 KeV spectral line would appear useful.

4. Development of external target methods to reduce background (especially Fe prompt capture gamma-rays, which cause great problems in all spectra) is suggested.
5. Further study of the energy shift method using low-Z materials for measurement of neutron spectra is probably not warranted based upon its demonstrable low efficiency.
6. Finite size effects of the Ge(Li) crystal (Gl) should be investigated in more detail in regard to the Compton recoil continuum analysis.

REFERENCES

B1 E. Barrington, A. Pope and J. Story, "The data in the Winfrith Nuclear Data Library", AEEW-R, 351, 5 (1964)

B2 R. E. Bell and L. G. Elliot, "Gamma-Rays from the Reaction H (n,γ) D and the Binding Energy of the Deuteron," Phys. Rev., 74, 1552 (1948)

B3 R. E. Bell and L. G. Elliot, "Gamma-Rays from the Reaction H (n,γ) D and the Binding Energy of the Deuteron", Phys. Rev., 79, 282 (1950)

B4 T. W. Bonner, "Measurements of Neutron Spectra from Fission", Nucl. Phys., 23 116 (1961)

C1 E. L. Chupp, R. W. Jewell, Jr. and W. John, "Binding Energy of the Deuteron Measured with a Bent Crystal Spectrometer," Phys. Rev., 121 , 234 (1961)

C2 C. Chaseman, K. Jones and R. Rinstein, "Measurement of the Energy Loss of Germanium Atoms to Electrons in Germanium at Energies below 100 KeV," Phys. Rev. Letters, 15, 245 (1965)

C3 C. Chaseman, K. Jones, "Band-Gap Effects in the Stopping of Ge^{72} Atoms in Germanium," Phys. Rev. Letters, 21, 1430 (1968)

C4 H. Conde and G. During, "Fission Neutron Spectra", Arkiv for Fysik, 29, 313 (1965)

D1 J. Donohew, "Inelastic Scattering in Fast Reactor Materials", ScD Thesis, MIT Nucl. Eng. Dept. (1970)

E1 R. D. Evans, "The Atomic Nucleus", McGraw-Hill Book Co. (1955) (Chapt. 21, Sec. 3)

E2 R. D. Evans,"The Atomic Nucleus, " McGraw-Hill Book Co. (1955) (Chapt. 10, Sec. 4)

E3 R. D. Evans, "The Atomic Nucleus," McGraw-Hill Book Co. (1955) (Chapt. 12, Sec. 2)

E4 R. D. Evans, "The Atomic Nucleus", McGraw-Hill Book Co. (1955) (Chapt. 6, Sec. 5)

E5 R. D. Evans, "The Atomic Nucleus", McGraw-Hill Book Co. (1955) (Chapt. 6, Sec. 4)

E6 R. D. Evans, "The Atomic Nucleus", McGraw-Hill Book Co. (1955) (Chapt. 23, Sec. 2)

E7 R. D. Evans, "The Atomic Nucleus", McGraw-Hill Book Co. (1955) (Chapt. 12, Sec. 2)

F1 I. A. Forbes, J. J. Driscoll, T. J. Thompson, I. Kaplan and D. D. Lanning, "Design, Construction and Evaluation of a Facility for the Simulation of Fast Reactor Blankets", MIT-4105-2, MITNE-110 (February, 1970)

F2 H. Feshbach and J. Schwinger, "On a Phenomenological Neutron-Proton Interaction", Phys. Rev., 84, 194 (1951)

F3 C. W. Forsberg, "Determination of Neutron Spectra by Prompt Gamma-Ray Spectroscopy", M. S. Thesis, MIT Nucl. Eng. Dept. (June, 1971)

G1 R. Gold, "Compton Recoil Continuum Measurements for In-Core Gamma-Ray Spectroscopy", Reactor Phys. Div. Annual Report (July 1, 1967 - June 30, 1968), ANL-7410 PP. 373-377

G2 L. Groshev, et al., "Compendium of Thermal Neutron Capture Gamma-Ray Measurements", Part III for Z=68 to Z=94, Nucl. Data, Section A, Vol. 5, No. 3-4 February 1969)

G3 G. Gordon, J. Harvey and H. Nakahara, "Measuring Fission Spectra with Semiconductor Detectors", Nucleonics, No. 12, 62 (December 1966)

G4 R. Gold and E. Bennett, "Effects of Finite Size in 4π-Recoil Proportional Counters", Nucl. Instr. and Meth., 63, 285 (1968)

G5 R. Gold, "Compton Recoil Gamma-Ray Spectroscopy", Nucl. Instr. and Meth., 84, 176 (1970)

G6 R. C. Greenwood and W. W. Black, "The Binding Energy of the Deuteron Determined from Measurement of the Hydrogen Neutron Capture Gamma-Ray Energy", Phys. Letters, 21, 702 (1966)

G7 R. Gold, "An Iterative Unfolding Method for Response Matrix," ANL-6984 (December 1964)

G8 L. Green, "Transmission Measurement of the Cf-252 Fission Neutron Spectrum", Nucl. Sci. and Eng., 37 232-242 (1969)

G9 T. N. E. Greville, "Spline Functions, Interpolation, and Numerical Quadrature," Mathematics Research Center, U. S. Army

H1 R. Heath, et al., "Instrumental Requirements for High Resolution Gamma-Ray spectroscopy Using Ge(Li) Detectors", IEEE Trans. Nucl. Sc., NS-13, 445 (June, 1966)

H2 J. Hamawi and N. Rasmussen, " Investigation of Elemental Analysis Using Neutron-Capture Gamma-Ray Spectra", MITNE-107 (1969)

H3 Y. Hukai, N. Rasmussen and M. Driscoll, "Some Applications of Ge(Li) Gamma-Ray Spectroscopy to Fuel Element Assay", MIT-3944-5, MITNE-113 (April 1970)

H4 T. Harper, Jr. and N. Rasmussen, "Determination of Thermal Neutron Capture Gamma Yields", MITNE-104 (July 1969)

H5 R. Heath, "The Potential of High Resolution Gamma Ray Spectrometry for the Assay of Irradiated Reactor Fuel", WASH-1076, 115 (1967)

H6 A. Horsley, "Neutron Cross Sections of the Proton in the Energy Range 0.0001 eV-20 MeV", AWRE-0-23/65 (1965)

H7 F. Hildebrand,"Methods of Applied Mathematics," 2nd Edition Prentice Hall (Chapt. 3,sec. 15)

H8 F. Hildebrand, "Introduction to Numerical Analysis", McGraw Hill (Chapt. 7, sec. 2)

K1 A. H. Kazi, N. Rasmussen and H. Mark, "Measurement of the Deuteron Binding Energy using a Bent-Crystal Spectrograph", Phys. Rev., 123, 1310 (1961)

K2 J. W. Knowles, "Diffraction Angle Measurements Bearing on the Deuteron Binding Energy and on the X-Unit-to-Milliangstrom Conversion Constant", Can. J. Phys., 40, 257 (1962)

L1 "LMFBR Blanket Physics Project Progress Report No. 1", MITNE-116, MIT-4105-3 (June 1970)

L2 C. Lederer, J. Hollander and I. Perman, "Table of Isotopes", 6th Ed., John Wiley and Sons, Inc. (1967)

L3 J. Lindhard, V. Nielsen, M. Scharff and P. Thomson, "Integral Equations Governing Radiation Effects", Kgl. Danske Videnskab. Selskab., 33, No. 10 (1963)

L4 M. M. Leving, "Report from Atomic Energy Establishment, Winfrith," Issued by B.N.L. (February 1970)

L5 T. C. Leung, M. J. Driscoll, I. Kaplan and D. D. Lanning, "Neutronics of a LMFBR Blanket Mock-Up", C00-3060-1 MITNE-127, to be issued

M1 J. E. Monahan, S. Raboy and C. C. Trail, "Measurement of the Energy of the Gamma Radiation from Neutron Capture by Hydrogen", Nucl. Phys., 24, 400 (1961)

M2 H. T. Motz, R. E. Carter and P. C. Fisher, "Gamma-Ray Energy Measurements with a Compton Spectrometer", Bull. Amer. Phys. Soc., 4, 477 (1959)

M3 J. Meadows, "Cf-252 Fission Neutron Spectrum from 0.003 to 15.0 MeV", Phys. Rev., 157, 1076 (1967)

N1 A. Nelms, "Graphs of the Compton Energy-Angle Relationship and the Klein-Nishina Formula from 10 KeV to 500 KeV," NBS Circular 542 (1953)

O1 V. Orphan and N. Rasmussen, "Study of Thermal Neutron Capture Gamma-Rays Using a Ge(Li) Spectrometer", MITNE-80 (January 1967)

O2 G. Odette, "Measurement of the Fast Neutron Radiation Hardening Energy Response Function in Iron", ScD Thesis, MIT Nucl. Eng. Dept. (September 1970)

O3 N. Ortiz, I. C. Rickard, M. J. Driscoll and N. C. Rasmussen, "Instrumental Methods for Neutron Spectroscopy in LMFBR Applications", C00-3060-3, MITNE-129, to be issued.

P1 P. Palmedo, H. Ludewig and A. Aronson, " Effect of Hydrogen Content of Graphite in Fast Critical Experiments", ANS Trans., Vol. 13, No. 1, P. 253 (June 1970)

R1 V. Rogers, "Neutron Inelastic Scattering Cross-sections", PhD Thesis, MIT Nucl. Eng. Dept. (February 1969)

R2 N. Rasmussen, T. Harper, Jr. and T. Inouye, "GAMANL, A Computer Program Applying Fourier Transforms to the Analysis of Gamma Spectra", MIT-3944-2, MITNE-97 (August 1968)

R3 N. Rasmussen, Y. Hukai, T. Inouye and V. Orphan, "Thermal Neutron Capture Gamma-Ray Spectra of the Elements", MITNE-85 (January 1969)

R4 "Reactor Physics Constants," ANL-5800, 2nd Ed., U. S. Government Printing Office (July 1963)

S1 J. A. Sovka and N. C. Rasmussen, "Nondestructive Analysis of Irradiated MITR Fuel by Gamma-Ray Spectroscopy", AFCRL-65-787, MITNE-64 (October 1965)

S2 J. Stehn, M. Goldberg, B. Magurno and R. Wienerchasman, BNL-325 (3rd Ed., Supplement No. 2) Vol. 1 (1964)

S3 A. B. Smith, P. R. Fields and J. H. Roberts, "Spontaneous Fission Neutron Spectrum of Cf-252," Phys. Rev., 108, 411 (1957)

S4 E. G. Silver and J. Lewin, "Safeguard Report for a Stainless-Steel Reactor for the BSF (BSR-I)", ORNL-2470 (July 1958)

T1 M. Trammel and W. Henninger, "Nuclear Data Library for the Fission Product Program", Astronuclear Lab., Westinghouse, WANL-TME-574 (November 1966)

W1 V. Weisskopf, "Statistics and Nuclear Reactions", Phys. Rev. 52, 295 (1937)

Y1 K. Yost, J. White and C. Fu, "Neutron Energy Dependent Capture Gamma-Ray Yields for U-238 and Ta-181," ANS Trans. (Winter 1970) 866, Vol. 13, No. 2

Y2 T. J. Yule and E. F. Bennett, "Measured Neutron Spectra in a Number of Uranium and Plutonium-Fueled Reactor Assemblies", Nucl. Science and Eng. 46, 236-243 (1971)

Appendix A

CALCULATION OF BLANKET AXIAL NEUTRON FLUX

Application of 1-group diffusion theory gives the following equation:

$$D \nabla^2 \phi - (\Sigma_a - \nu\Sigma_f) \phi = 0, \qquad \text{(A-1)}$$

or

$$\nabla^2 \phi - K^2 \phi = 0, \qquad \text{(A-2)}$$

where

$$K^2 = \frac{\Sigma_a - \nu\Sigma_f}{D} \qquad \text{(A-3)}$$

Reference L5 shows that the neutron flux in the blanket is well represented by the solution of the diffusion equation:

$$\phi (x, y, z, E) = \cos \left(\frac{\pi z}{A}\right) \cos \left(\frac{\pi y}{B}\right) \phi (E,X). \qquad \text{(A-4)}$$

Assuming the separability of energy and position, $\phi(E,X) = \phi (E) \psi (x)$; the 1-group axial neutron flux is further assumed to be in the form:

$$\psi(x) \sim e^{-\Gamma x}, \qquad \text{(A-5)}$$

(than effectively infinite medium is assumed) A semi-log plot of the total neutron flux in Blanket No. 2 calculated by the ANISN code in the S8 option using 26-groups is shows in Fig. A-1. As can be seen, the simple one-group

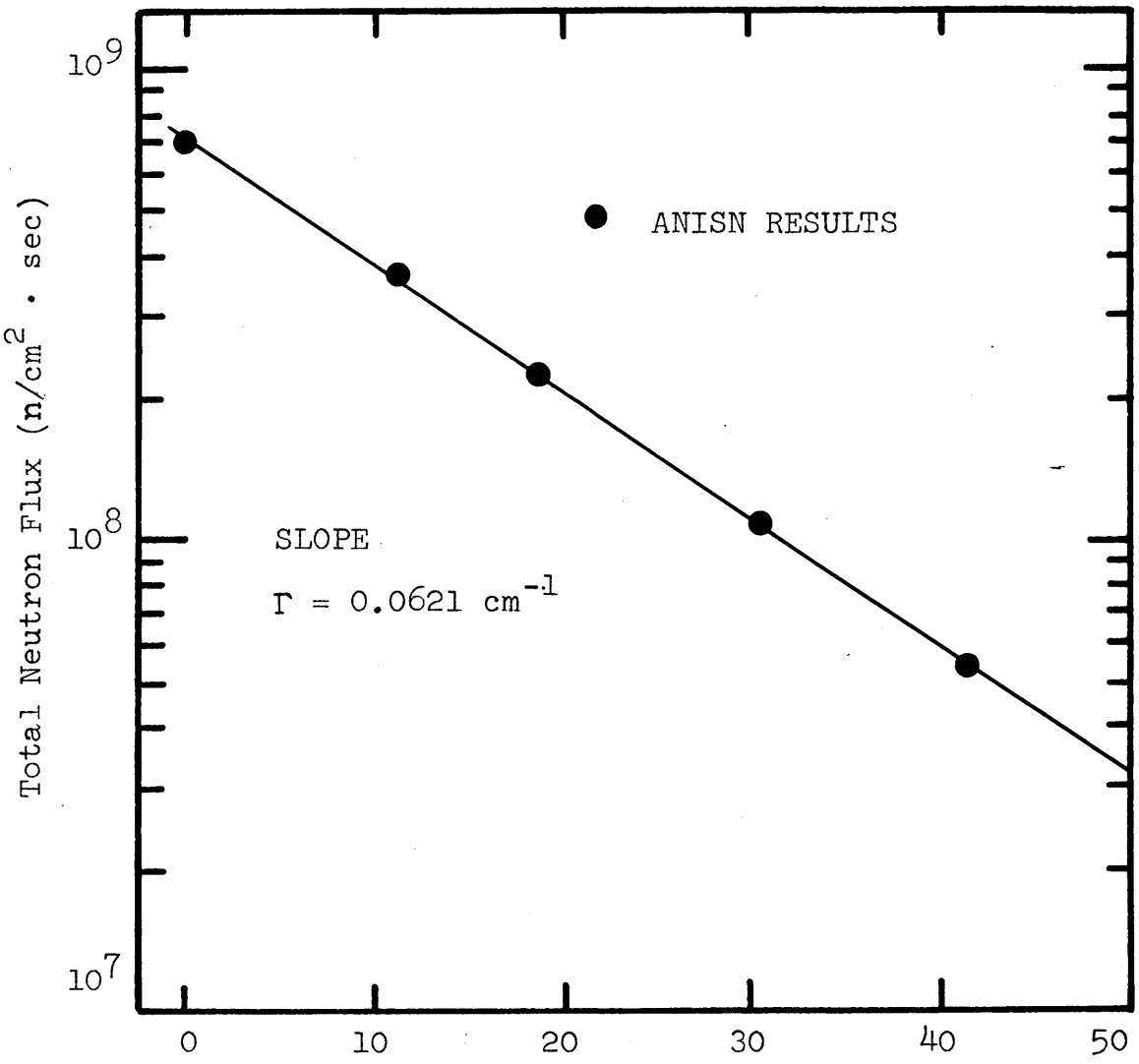

Fig. A-1 Total Axial Neutron Flux of Blanket No. 2 Calculated by S8, 26-Group ANISN vs. Distance into Blanket

model is a quite good representation of the multigroup results. Therefore the one dimensional neutron flux across Blanket No. 2 is given by the following equation:

$$\Psi(x) = \Psi_o \, e^{-\Gamma x} \tag{A-7}$$

where

$$\Psi_o = 7.06049 \times 10^8 \text{ n/sec. CM}^2, \tag{A-8}$$

and

$$\Gamma = 0.0621 \text{ CM}^{-1} \tag{A-9}$$

The average neutron flux over the blanket is:

$$\bar{\Psi} = \int_o^{X_B} \Psi_o \, e^{-\Gamma x} \, dx \, / \, X_B$$

$$= 2.72 \times 10^8 \text{ n/sec. CM}^2 \tag{A-10}$$

The normalized neutron flux is:

$$\Psi (x) = \Psi (x) \, / \int_o^{X_B} 4(x) \, dx$$

$$= 0.0662 \, e^{-0.0621 \, x} \tag{A-11}$$

The normalized flux distribution $\Psi(x)$ of Eq. A-11 across Blanket No. 2 is used in the text whenever the axial flux variation needs to be taken into account.

Appendix B

MEASUREMENTS OF GAMMA-RAY LINEAR ATTENUATION COEFFICIENTS

At the outset it should be noted that the gamma ray attenuation data experimentally determined here did not agree with the established data (R4). In particular, the attenuation coefficients of uranium for low energy gamma-rays are not well resolved yet. Table B-1 shows the attenuation coefficients of uranium for some discrete gamma-ray energies.

Three gamma-ray sources were used in these measurements. For high energy gamma-rays (1 - 1.5 MeV) Co^{60} and Na^{22} standard sources were used and for low energy gamma-rays highly depleted uranium foils (18 ppm U-235) having a total weight of 0.61 gms, were irradiated to produce a 2.35 day half-life Np-239 gamma-ray source. Varying the thickness of uranium attenuators, a series of measurements were done with each gamma source. The thickness of uranium attenuators was varied by combination of .005 inch thick and .02 inch thick uranium foils. The same 17 c.c. crystal was used as a Ge(Li) detector for this purpose. Output data for each gamma-source were fitted by the linear least square method in semi-log rectangular coordinates using a subroutine LILSQ

TABLE B-1

GAMMA-RAY LINEAR ATTENUATION

COEFFICIENTS OF URANIUM

Gamma Sources	Energy (Kev)	Linear Attenuation Coeff. (cm^{-1})	
		Present Work	Reference*
Np-239	209.8	25.5	20.6
	228.2	20.6	18.1
	277.6	13.0	8.75
	315.9	10.4	7.88
	334.3	8.51	7.21
Co-60	1173.0	1.29	1.23
	1332.5	1.04	1.11
Na-22	1274.5	1.13	1.13
Na-24	1368.5	1.00**	

* Reference: "Reactor Physics Constants", ANL-5800, Table 8-10

** Extrapolated by three measured values from Co^{60} and Na^{22}.

(Appendix D). Table B-2 shows the measured gamma-ray linear attenuation data for varying thicknesses of Na_2CrO_4, a major constituent of Blanket No. 2, and the attenuation data of iron from the literature.

TABLE B-2

GAMMA-RAY LINEAR ATTENUATION COEFFICIENTS

OF Na_2 Cr O_4 and Fe

ENERGY(KeV)	LINEAR ATTENUATION COEFFICIENTS(cm^{-1})	
	Na_2CrO_4 (Measured)	Fe (Reference)*
209.8	0.207	1.060
228.2	0.204	1.014
277.6	0.202	0.890
315.9	0.199	0.815
334.3	0.197	0.795
1173.0	0.126	0.433
1332.5	0.121	0.414
1274.5	0.122	0.405
1368.5	0.120**	0.401

* Reference: "Reactor Physics Constants", ANL-5800, Table 8-10

** Extrapolated by three measured values from Co^{60} and Na^{22}.

Appendix C

CALCULATION OF FAST NEUTRON CAPTURE RATE OF HYDROGEN

The fast neutron capture rate of hydrogen is calculated in this appendix, and compared with that of lower-energy neutron capture. In the reaction with fast incident neutrons the probability of incident neutrons undergoing capture by a sample is

$$Pi = \frac{\Sigma_a^o}{\Sigma_a^o + \Sigma_s^o} ,$$

or

$$Pi \approx \frac{\Sigma_a^o}{\Sigma_s^o} , \qquad (c\text{-}1)$$

since $\Sigma_a^o \ll \Sigma_s^o$ for fast neutrons. The probability of a scattered neutron undergoing capture on its first flight out of the sample is

$$Pi = \Sigma_a^* \bar{\ell} \qquad (C\text{-}2)$$

where Σ_a^* is the average absorption cross-section of hydrogen for scattered neutrons, and $\bar{\ell}$ is the mean chord length of escaping neutrons; which is $\bar{\ell} = 4/3\ R$ for an infinite cylindrical rod with radius R for a uniform internal scattering source. Hence the ratio of the probability of capture reactions by scattered lower

energy neutrons to that of the incident higher energy neutrons is:

$$R = \frac{\Sigma_a^* \bar{l}}{\Sigma_a^o / \Sigma_s^o} \qquad (C\text{-}3)$$

or

$$R = (\Sigma_s^o \bar{l}) \left(\frac{\Sigma_a^*}{\Sigma_a^o}\right) \qquad (C\text{-}4)$$

Now the average absorption cross – section can be expressed by

$$\Sigma_a^* = \int_{E=0}^{E_o} \Sigma_a(E)\ P(E)\ dE \qquad (C\text{-}5)$$

where

E_o is the maximum incident energy,

$\Sigma_a(E) = \Sigma_a^o \frac{1}{\sqrt{E}}$, and

$P(E)\ dE = \frac{dE}{E}$ for hydrogen.

Integration of Eq. C-5 shows that the ratio of the average absorption cross-section for scattered neutrons to the average for the initial incident neutrons is:

$$\frac{\Sigma_a^*}{\Sigma_a^o} = 2. \qquad (C\text{-}6)$$

Therefore Eq. C-4 can be rewritten

$$R = 2\,\Sigma_s^o\,\bar{\ell}. \qquad \text{(C-7)}$$

Thus since $\Sigma_s^o \approx 2\ CM^{-1}$ for scattering by a hydrogeneous substance and $\bar{\ell} \approx 1$ CM for a reasonably sized sample, the ratio of the probability of capture reactions by scattered lower energy neutrons to that for the incident higher energy neutrons is:

$$R = 4. \qquad \text{(C-8)}$$

This shows that the hydrogeneous sample target should be very thin to overcome the capture contribution by the scattered neutrons.

Appendix D

COMPUTER PROGRAM INTEF

INTEF calculates the intrinsic efficiency of a Ge(Li) detection system using a series of runs with calibrated gamma-ray sources. All data are fitted by the linear - least square method. Typical input and output data follow immediately after the program. Input data consists of the energy of the peak, the half-life of the standard source, the initial activity of the source, the yield of the gamma-ray, the cooling time interval, the gamma-attenuation coefficient of the lucite-source-holder, the number of input peaks and the distance and peak area array. Output data give the two coefficients of the least-square fitted linear equation, which will calculate the intrinsic efficiency as a function of the distance from the detector.

```
C      INTRINSIC EFFICIENCY CALCULATION
       REAL A(21),EFF(21),R(21),EFC(21),EROR(21),CONST(21),COEFF(21),
      1ENERG(21)
       READ (5,3) N
     3 FORMAT (I5)
       DO 200 J=1,N
       READ (5,1) EN,AO,TH,Y,TC,SL,M
     1 FORMAT (F10.4,F5.1,4E10.3,I5)
C
C      EN -  ENERGY OF THE PEAK IN KEV
C      TH - HALF-LIFE OF THE RADIOACTIVE MATERIAL IN DAYS
C      AO - INITIAL ACTIVITY IN MICRO-CURIES
C      Y  - YIELD OF GAMMA-RAY
C      TC - COOLING TIME IN DAYS
C      SL - GAMMA-ATTENUATION CEFFICIENT OF LUCITE
C      N  - NO. OF DIFFERENT ENERGY GROUPS
C      M  - NO. OF INPUT PEAKS
C      A  - PEAK AREA ARRAY
C      EFF- EFFICIENCY ARRAY
C      R  - DISTANCE ARRAY IN INCHES
C
C      INITIAL ACTIVITY
       AO=AO*(3.7E+04)
       WRITE (6,10) EN
       WRITE (7,10) EN
    10 FORMAT ('1',14X,'ANALYSIS OF ',F10.4,'KEV')
       WRITE (6,11) AO
       WRITE (7,11) AO
    11 FORMAT ('0',14X,'THE INITIAL ACTIVITY (DIS/SEC) ',E10.5)
C
C      DECAY CORRECTION FACTOR CALCULATION
       CD=0.693/TH
       CD=CD*TC
       CD=EXP(-CD)
       WRITE (6,12) CD
       WRITE (7,12) CD
```

```
   12 FORMAT (15X,'THE DECAY CORRECTION FACTOR     ',E10.5)
C
C      GAMMA-RAY YIELD
       Y=Y/100.
       WRITE (6,13) Y
       WRITE (7,13) Y
   13 FORMAT (15X,'THE GAMMA-RAY YIELD             ',E10.5)
C
C      LUCITE ATTENUATION CORRECTION
       CL=1.905
C      CL IS THE THICKNESS OF LUCITE IN CM
       CL=CL*SL
       CL=(1-EXP(-CL))/CL
       WRITE (6,14) CL
       WRITE (7,14) CL
   14 FORMAT (15X,'THE LUCITE ATTENUATION FACTOR  ',E10.5)
C
C      TOTAL COUNTING TIME
       TD=16.
C      TD IS THE TOTAL COUNTING TIME IN MINUTES
       TD=TD*60.
       WRITE (6,15) TD
       WRITE (7,15) TD
   15 FORMAT (15X,'TOTAL COUNTING TIME (SEC)       ',E10.5)
       WRITE (6,16)
       WRITE (7,16)
   16 FORMAT (15X,'*****************************************')
C
C      CONSTANT TERM CALCULATION
       C=AC*CD*Y*CL*TD
       WRITE (6,17) C
       WRITE (7,17) C
   17 FORMAT (15X,'CONSTANT TERM                   ',E10.5)
C
C      EFFICIENCY CALCULATION
       DO 100 I=1,M
```

```
      READ (5,2) R(I),A(I)
    2 FORMAT (10X,F5.2,E12.4)
      EA=A(I)/C
      EA=SQRT(EA)
      EFF(I)=1/EA
  100 CONTINUE
C
C     CALCULATION OF COEFFICIENTS OF LINEAR EQUATION.  SUBROUTINE
C     LILSQ DOES THE LINEAR LEAST SQUARE FIT.
C
      CALL LILSQ (R,EFF,M,C0,C1)
C
      WRITE (6,18)
      WRITE (7,18)
   18 FORMAT ('0',6X,'DIST(IN)',6X,'AREA',8X,'1/SQRT(E)',5X,
     1'CALC. LSQ',5X,'RMS ERROR')
      DO 101 I=1,M
      EFC(I)=C1*R(I)+C0
      ER=EFC(I)-EFF(I)
      ER=ER*ER
      EROR(I)=SQRT(ER)/EFF(I)
      WRITE (6,19) I,R(I),A(I),EFF(I),EFC(I),EROR(I)
      WRITE (7,19) I,R(I),A(I),EFF(I),EFC(I),EROR(I)
   19 FORMAT (I5,4X,F5.2,4X,E10.5,4X,E10.5,4X,E10.5,4X,E10.5)
  101 CONTINUE
      WRITE (6,20) EN
      WRITE (7,20) EN
   20 FORMAT ('0',14X,'THE COEFFICIENTS OF LINEAR EQUATION FOR ',
     1F10.5,'KEV')
      WRITE (6,21) C0
      WRITE (7,21) C0
   21 FORMAT (15X,'C0 = ',E12.5)
      WRITE (6,22) C1
      WRITE (7,22) C1
   22 FORMAT (15X,'C1 = ',E12.5)
      ENERG(J)=EN
```

```
      CONST(J)=C0
      COEFF(J)=C1
  200 CONTINUE
C
C     OUTPUT ARGUEMENT.  THE DISTANCE BETWEEN DETECTOR AND BLANKET
C     IS 82 INCHES.  THE DIAMETER OF DETECTOR IS ONE INCH.
      RD=82.
      WRITE (6,23)
      WRITE (7,23)
   23 FORMAT ('1',14X,'THE COEFFICIENTS OF THE LINEAR EQUATIONS')
      WRITE (6,24)
      WRITE (7,24)
   24 FORMAT ('0',6X,' ENERGY ',6X,' C0 ',8X,'    C1    ',5X,
     1'1/SQRT(E)',5X,'EFFCIENCY')
      DO 102 J=1,N
      EFF(J)=CONST(J)+RD*COEFF(J)
      A(J)=16*RD*RD/(EFF(J)*EFF(J))
      WRITE (6,25) J,ENERG(J),CONST(J),COEFF(J),EFF(J),A(J)
      WRITE (7,25) J,ENERG(J),CONST(J),COEFF(J),EFF(J),A(J)
   25 FORMAT (I5,4X,F5.0,4X,E10.5,4X,E10.5,4X,E10.5,4X,E10.5)
  102 CONTINUE
      CALL EXIT
      END
```

```
      SUBROUTINE LILSQ (R,EFF,M,C0,C1)
      REAL R(20),EFF(20)
C     C0 AND C1 ARE OUTPUT ARGUEMENTS
      C11=M
      C12=0.
      C13=0.
      C22=0.
      C23=0.
C
C     AUGMENTED MATRIX CALCULATION
      DO 1 I=1,M
      C12=C12+R(I)
      C13=C13+EFF(I)
      C22=C22+R(I)*R(I)
      C23=C23+R(I)*EFF(I)
    1 CONTINUE
C
C     SOLUTION OF LINEAR EQUATIONS
      DELTA=C11*C22-C12*C12
      C0=C13*C22-C12*C23
      C0=C0/DELTA
      C1=C11*C23-C13*C12
      C1=C1/DELTA
      RETURN
      END
```

INPUT DATA

```
  8
122.046   10.7 2.720E+02 8.700E+01 8.390E+02 2.629E-01    12          CO-57
  1        0.00  2.5583E+05                                           CO-57
  2        1.00  1.2781E+05                                           CO-57
  3        2.00  7.5504E+04                                           CO-57
  4        3.00  4.8634E+04                                           CO-57
  5        4.00  3.4280E+04                                           CO-57
  6        5.00  2.5014E+04                                           CO-57
  7        6.00  1.9085E+04                                           CO-57
  8        7.00  1.5594E+04                                           CO-57
  9        8.00  1.2346E+04                                           CO-57
 10        9.00  1.0497E+04                                           CO-57
 11       10.00  8.6703E+03                                           CO-57
 12       11.00  7.3452E+03                                           CO-57
136.465   10.7 2.720E+02 1.050E+01 8.390E+02 2.501E-01    12          CO-57
  1        0.00  3.0386E+04                                           CO-57
  2        1.00  1.5524E+04                                           CO-57
  3        2.00  9.3160E+03                                           CO-57
  4        3.00  5.4785E+03                                           CO-57
  5        4.00  3.6650E+03                                           CO-57
  6        5.00  2.8875E+03                                           CO-57
  7        6.00  2.4576E+03                                           CO-57
  8        7.00  1.5808E+03                                           CO-57
  9        8.00  1.3944E+03                                           CO-57
 10        9.00  1.0046E+03                                           CO-57
 11       10.00  7.9760E+02                                           CO-57
 12       11.00  8.9710E+02                                           CO-57
511.003    9.4 9.500E+02 1.800E+02 8.400E+02 1.452E-01    12          NA-22
  1        0.00  2.6354E+05                                           NA-22
  2        1.00  1.3212E+05                                           NA-22
  3        2.00  7.8911E+04                                           NA-22
  4        3.00  5.2503E+04                                           NA-22
  5        4.00  3.6728E+04                                           NA-22
```

6	5.00	2.7353E+04					NA-22
7	6.00	2.1800E+04					NA-22
8	7.00	1.6785E+04					NA-22
9	8.00	1.4317E+04					NA-22
10	9.00	1.1215E+04					NA-22
11	10.00	9.1938E+03					NA-22
12	11.00	8.0320E+03					NA-22
661.632	12.4	1.095E+04	8.500E+01	6.530E+02	1.287E-01	9	CS-137
1	0.0	2.1378E+05					CS-137
2	1.00	1.0501E+05					CS-137
3	2.00	6.3264E+04					CS-137
4	4.00	2.8875E+04					CS-137
5	8.00	1.0415E+04					CS-137
6	12.00	5.6206E+03					CS-137
7	16.00	3.5152E+03					CS-137
8	20.00	2.3264E+03					CS-137
9	24.00	1.6302E+03					CS-137
834.861	10.5	3.140E+02	1.000E+02	8.400E+02	1.186E-01	12	MN-54
1	0.00	2.3517E+04					MN-54
2	1.00	1.1173E+04					MN-54
3	2.00	7.0034E+03					MN-54
4	3.00	4.3610E+03					MN-54
5	4.00	3.1072E+03					MN-54
6	5.00	2.3204E+03					MN-54
7	6.00	1.8562E+03					MN-54
8	7.00	1.4476E+03					MN-54
9	8.00	1.1921E+03					MN-54
10	9.00	9.8490E+02					MN-54
11	10.00	8.0070E+02					MN-54
12	11.00	6.7400E+02					MN-54
1173.231	7.5	1.920E+03	1.000E+02	6.560E+02	1.056E-01	12	CO-60
1	0.00	5.7156E+04					CO-60
2	1.00	2.8621E+04					CO-60
3	2.00	1.6171E+04					CO-60
4	3.00	1.1242E+04					CO-60
5	4.00	8.2430E+03					CO-60

6	5.10	5.7040E+03					CO-60
7	6.00	4.1310E+03					CO-60
8	7.00	3.6896E+03					CO-60
9	8.00	3.0882E+03					CO-60
10	9.00	2.4640E+03					CO-60
11	10.00	1.9944E+03					CO-60
12	11.00	1.7756E+03					CO-60
1274.552	9.4	9.500E+02	9.900E+01	8.400E+02	1.002E-01	12	NA-22
1	0.00	4.1864E+04					NA-22
2	1.00	2.0105E+04					NA-22
3	2.00	1.1719E+04					NA-22
4	3.00	8.0215E+03					NA-22
5	4.00	5.8630E+03					NA-22
6	5.00	4.1760E+03					NA-22
7	6.00	3.4348E+03					NA-22
8	7.00	2.6650E+03					NA-22
9	8.00	2.1176E+03					NA-22
10	9.00	1.7538E+03					NA-22
11	10.00	1.4054E+03					NA-22
12	11.00	1.2153E+03					NA-22
1332.518	7.5	1.920E+03	1.000E+02	6.560E+02	9.775E-02	12	CO-60
1	0.00	4.6566E+04					CO-60
2	1.00	2.3654E+04					CO-60
3	2.00	1.3698E+04					CO-60
4	3.00	1.0008E+04					CO-60
5	4.00	6.8440E+03					CO-60
6	5.10	4.6320E+03					CO-60
7	6.00	3.6660E+03					CO-60
8	7.00	3.0460E+03					CO-60
9	8.00	2.4708E+03					CO-60
10	9.00	2.0490E+03					CO-60
11	10.00	1.7553E+03					CO-60
12	11.00	1.4958E+03					CO-60

OUTPUT DATA

ANALYSIS OF 122.0460KEV

THE INITIAL ACTIVITY (DIS/SEC)	.39590E 06
THE DECAY CORRECTION FACTOR	.11794E 00
THE GAMMA-RAY YIELD	.87000E 00
THE LUCITE ATTENUATION FACTOR	.78664E 00
TOTAL COUNTING TIME (SEC)	.96000E 03
**********	**********
CONSTANT TERM	.30676E 08

	DIST(IN)	AREA	1/SQRT(E)	CALC. LSQ	RMS ERROR
1	0.0	.25583E 06	.10950E 02	.10585E 02	.33348E-01
2	1.00	.12781E 06	.15492E 02	.15465E 02	.17583E-02
3	2.00	.75504E 05	.20157E 02	.20345E 02	.93597E-02
4	3.00	.48634E 05	.25115E 02	.25225E 02	.43945E-02
5	4.00	.34280E 05	.29915E 02	.30105E 02	.63801E-02
6	5.00	.25014E 05	.35020E 02	.34985E 02	.97471E-03
7	6.00	.19085E 05	.40092E 02	.39866E 02	.56465E-02
8	7.00	.15594E 05	.44353E 02	.44746E 02	.88491E-02
9	8.00	.12346E 05	.49847E 02	.49626E 02	.44420E-02
10	9.00	.10497E 05	.54059E 02	.54506E 02	.82584E-02
11	10.00	.86703E 04	.59482E 02	.59386E 02	.16182E-02
12	11.00	.73452E 04	.64625E 02	.64266E 02	.55586E-02

THE COEFFICIENTS OF LINEAR EQUATION

C0 = 0.10585E 02

C1 = 0.48801E 01

OUTPUT DATA

ANALYSIS OF 136.4650KEV

THE INITIAL ACTIVITY (DIS/SEC)	.39590E 06
THE DECAY CORRECTION FACTOR	.11794E 00
THE GAMMA-RAY YIELD	.10500E 00
THE LUCITE ATTENUATION FACTOR	.79550E 00
TOTAL COUNTING TIME (SEC)	.96000E 03
**********	**********
CONSTANT TERM	.37440E 07

	DIST(IN)	AREA	1/SQRT(E)	CALC. LSQ	RMS ERROR
1	0.0	.30386E 05	.11100E 02	.10041E 02	.95426E-01
2	1.00	.15524E 05	.15530E 02	.15404E 02	.80869E-02
3	2.00	.93160E 04	.20047E 02	.20768E 02	.35932E-01
4	3.00	.54785E 04	.26142E 02	.26131E 02	.42609E-03
5	4.00	.36650E 04	.31962E 02	.31494E 02	.14634E-01
6	5.00	.28875E 04	.36009E 02	.36857E 02	.23568E-01
7	6.00	.24576E 04	.39031E 02	.42221E 02	.81712E-01
8	7.00	.15808E 04	.48667E 02	.47584E 02	.22245E-01
9	8.00	.13944E 04	.51818E 02	.52947E 02	.21805E-01
10	9.00	.10046E 04	.61048E 02	.58311E 02	.44844E-01
11	10.00	.79760E 03	.68514E 02	.63674E 02	.70639E-01
12	11.00	.89710E 03	.64603E 02	.69037E 02	.68646E-01

THE COEFFICIENTS OF LINEAR EQUATION

C0 = 0.10041E 02

C1 = 0.53633E 01

OUTPUT DATA

ANALYSIS OF 511.0029KEV

THE INITIAL ACTIVITY (DIS/SEC)	.34780E 06
THE DECAY CORRECTION FACTOR	.54185E 00
THE GAMMA-RAY YIELD	.18000E 01
THE LUCITE ATTENUATION FACTOR	.87361E 00
TOTAL COUNTING TIME (SEC)	.96000E 03
**********	**********
CONSTANT TERM	.28450E 09

	DIST(IN)	AREA	1/SQRT(E)	CALC. LSQ	RMS ERROR
1	0.0	.26354E 06	.32856E 02	.31528E 02	.40410E-01
2	1.00	.13212E 06	.46404E 02	.45670E 02	.15815E-01
3	2.00	.78911E 05	.60044E 02	.59812E 02	.38691E-02
4	3.00	.52503E 05	.73611E 02	.73953E 02	.46426E-02
5	4.00	.36728E 05	.88011E 02	.88095E 02	.94852E-03
6	5.00	.27353E 05	.10198E 03	.10224E 03	.24689E-02
7	6.00	.21800E 05	.11424E 03	.11638E 03	.18737E-01
8	7.00	.16785E 05	.13019E 03	.13052E 03	.25351E-02
9	8.00	.14317E 05	.14097E 03	.14466E 03	.26222E-01
10	9.00	.11215E 05	.15927E 03	.15880E 03	.29408E-02
11	10.00	.91938E 04	.17591E 03	.17294E 03	.16855E-01
12	11.00	.80320E 04	.18820E 03	.18709E 03	.59312E-02

THE COEFFICIENTS OF LINEAR EQUATION

C0 = 0.31528E 02

C1 = 0.14142E 02

OUTPUT DATA

ANALYSIS OF 661.6318KEV

THE INITIAL ACTIVITY (DIS/SEC)	.45883E 06
THE DECAY CORRECTION FACTOR	.95952E 00
THE GAMMA-RAY YIELD	.85000E 00
THE LUCITE ATTENUATION FACTOR	.88685E 00
TOTAL COUNTING TIME (SEC)	.96000E 03
**********	**********
CONSTANT TERM	.31858E 09

	DIST(IN)	AREA	1/SQRT(E)	CALC. LSQ	RMS ERROR
1	0.0	.21378E 06	.38603E 02	.38304E 02	.77383E-02
2	1.00	.10501E 06	.55080E 02	.54984E 02	.17461E-02
3	2.00	.63264E 05	.70962E 02	.71663E 02	.98661E-02
4	4.00	.28875E 05	.10504E 03	.10502E 03	.16415E-03
5	8.00	.10415E 05	.17489E 03	.17174E 03	.18058E-01
6	12.00	.56206E 04	.23818E 03	.23845E 03	.15829E-02
7	16.00	.35152E 04	.30105E 03	.30517E 03	.13698E-01
8	20.00	.23264E 04	.37005E 03	.37189E 03	.49494E-02
9	24.00	.16302E 04	.44207E 03	.43860E 03	.78362E-02

THE COEFFICIENTS OF LINEAR EQUATION

C0 = 0.38304E 02

C1 = 0.16679E 02

OUTPUT DATA

ANALYSIS OF 834.8608KEV

THE INITIAL ACTIVITY (DIS/SEC)	.3885CE 06
THE DECAY CORRECTION FACTOR	.15663E 00
THE GAMMA-RAY YIELD	.10000E 01
THE LUCITE ATTENUATION FACTOR	.89508E 00
TOTAL COUNTING TIME (SEC)	.96000E 03
**********	**********
CONSTANT TERM	.52287E 08

	DIST(IN)	AREA	1/SQRT(E)	CALC. LSQ	RMS ERROR
1	0.0	.23517E 05	.47153E 02	.46109E 02	.22122E-01
2	1.00	.11173E 05	.68409E 02	.66864E 02	.22585E-01
3	2.00	.70034E 04	.86406E 02	.87618E 02	.14030E-01
4	3.00	.43610E 04	.10950E 03	.10837E 03	.10276E-01
5	4.00	.31072E 04	.12972E 03	.12913E 03	.45877E-02
6	5.00	.23204E 04	.15011E 03	.14988E 03	.15410E-02
7	6.00	.18562E 04	.16784E 03	.17063E 03	.16678E-01
8	7.00	.14476E 04	.19005E 03	.19139E 03	.70350E-02
9	8.00	.11921E 04	.20943E 03	.21214E 03	.12952E-01
10	9.00	.98490E 03	.23041E 03	.23290E 03	.10797E-01
11	10.00	.80070E 03	.25554E 03	.25365E 03	.73960E-02
12	11.00	.67400E 03	.27853E 03	.27441E 03	.14794E-01

THE COEFFICIENTS OF LINEAR EQUATION
C0 = 0.46109E 02
C1 = 0.20754E 02

OUTPUT DATA

ANALYSIS OF 1173.2310KEV

THE INITIAL ACTIVITY (DIS/SEC)	.27750E 06
THE DECAY CORRECTION FACTOR	.78917E 00
THE GAMMA-RAY YIELD	.10000E 01
THE LUCITE ATTENUATION FACTOR	.90583E 00
TOTAL COUNTING TIME (SEC)	.96000E 03
**********	**********
CONSTANT TERM	.19044E 09

	DIST(IN)	AREA	1/SQRT(E)	CALC. LSQ	RMS ERROR
1	0.0	.57156E 05	.57723E 02	.57303E 02	.72640E-02
2	1.00	.28621E 05	.81571E 02	.81959E 02	.47660E-02
3	2.00	.16171E 05	.10852E 03	.10662E 03	.17545E-01
4	3.00	.11242E 05	.13015E 03	.13127E 03	.85948E-02
5	4.00	.82430E 04	.15200E 03	.15593E 03	.25865E-01
6	5.10	.57040E 04	.18272E 03	.18305E 03	.18031E-02
7	6.00	.41310E 04	.21471E 03	.20524E 03	.44097E-01
8	7.00	.36896E 04	.22719E 03	.22990E 03	.11918E-01
9	8.00	.30882E 04	.24833E 03	.25455E 03	.25071E-01
10	9.00	.24640E 04	.27801E 03	.27921E 03	.43224E-02
11	10.00	.19944E 04	.30901E 03	.30386E 03	.16645E-01
12	11.00	.17756E 04	.32749E 03	.32852E 03	.31347E-02

THE COEFFICIENTS OF LINEAR EQUATION
C0 = 0.57303E 02
C1 = 0.24656E 02

OUTPUT DATA

ANALYSIS OF 1274.5518KEV

THE INITIAL ACTIVITY (DIS/SEC)	.34780E 06
THE DECAY CORRECTION FACTOR	.54185E 00
THE GAMMA-RAY YIELD	.99000E 00
THE LUCITE ATTENUATION FACTOR	.91035E 00
TOTAL COUNTING TIME (SEC)	.96000E 03
**********	**********
CONSTANT TERM	.16305E 09

	DIST(IN)	AREA	1/SQRT(E)	CALC. LSQ	RMS ERROR
1	0.0	.41864E 05	.62408E 02	.60164E 02	.35969E-01
2	1.00	.20105E 05	.90056E 02	.87587E 02	.27417E-01
3	2.00	.11719E 05	.11796E 03	.11501E 03	.24974E-01
4	3.00	.80215E 04	.14257E 03	.14243E 03	.98024E-03
5	4.00	.58630E 04	.16676E 03	.16986E 03	.18537E-01
6	5.00	.41760E 04	.19760E 03	.19728E 03	.16168E-02
7	6.00	.34348E 04	.21788E 03	.22470E 03	.31321E-01
8	7.00	.26650E 04	.24735E 03	.25213E 03	.19297E-01
9	8.00	.21176E 04	.27749E 03	.27955E 03	.74293E-02
10	9.00	.17538E 04	.30491E 03	.30697E 03	.67546E-02
11	10.00	.14054E 04	.34062E 03	.33439E 03	.18265E-01
12	11.00	.12153E 04	.36629E 03	.36182E 03	.12205E-01

THE COEFFICIENTS OF LINEAR EQUATION

C0 = 0.60164E 02

C1 = 0.27423E 02

OUTPUT DATA

ANALYSIS OF 1332.5178KEV

THE INITIAL ACTIVITY (DIS/SEC)	.27750E 06
THE DECAY CORRECTION FACTOR	.78917E 00
THE GAMMA-RAY YIELD	.10000E 01
THE LUCITE ATTENUATION FACTOR	.91241E 00
TOTAL COUNTING TIME (SEC)	.96000E 03
**********	**********
CONSTANT TERM	.19182E 09

	DIST(IN)	AREA	1/SQRT(E)	CALC. LSQ	RMS ERROR
1	0.0	.46566E 05	.64182E 02	.63106E 02	.16766E-01
2	1.00	.23654E 05	.90052E 02	.89999E 02	.59407E-03
3	2.00	.13698E 05	.11834E 03	.11689E 03	.12208E-01
4	3.00	.10008E 05	.13844E 03	.14378E 03	.38579E-01
5	4.00	.68440E 04	.16741E 03	.17068E 03	.19494E-01
6	5.10	.46320E 04	.20350E 03	.20026E 03	.15918E-01
7	6.00	.36660E 04	.22874E 03	.22446E 03	.18715E-01
8	7.00	.30460E 04	.25095E 03	.25136E 03	.16314E-02
9	8.00	.24708E 04	.27863E 03	.27825E 03	.13660E-02
10	9.00	.20490E 04	.30597E 03	.30514E 03	.26978E-02
11	10.00	.17553E 04	.33058E 03	.33204E 03	.44149E-02
12	11.00	.14958E 04	.35811E 03	.35893E 03	.22989E-02

THE COEFFICIENTS OF LINEAR EQUATION
C0 = 0.63106E 02
C1 = 0.26893E 02

FINAL OUTPUT DATA

THE COEFFICIENTS OF THE LINEAR EQUATIONS

	ENERGY	C0	C1	1/SQRT(E)	EFFCIENCY
1	122.	.10585E 02	.48801E 01	.41075E 03	.63766E 00
2	136.	.10041E 02	.53633E 01	.44983E 03	.53168E 00
3	511.	.31528E 02	.14142E 02	.11911E 04	.75826E-01
4	662.	.38304E 02	.16679E 02	.14060E 04	.54423E-01
5	835.	.46109E 02	.20754E 02	.17480E 04	.35212E-01
6	1173.	.57303E 02	.24656E 02	.20791E 04	.24888E-01
7	1275.	.60164E 02	.27423E 02	.23089E 04	.20182E-01
8	1333.	.63106E 02	.26893E 02	.22683E 04	.20909E-01

Appendix E

CALCULATION OF GAMMA-RAY SELF-ABSORPTION CORRECTION FACTORS FOR BLANKET NO. 2

E-1 Theory

The gamma-ray self-absorption correction factor is defined as the ratio of the total number of gamma-rays of interest with energy $E\gamma$ appearing at the outside surface of the blanket per second to the total number of gamma-rays of interest with the same energy $E\gamma$ produced throughout the blanket per second. Hence this factor is mainly dependent on the structure of the blanket and the origin of the gamma-rays of interest, for example, suppose that the gamma-ray of interest is one of the decay gamma-rays from Np-239, then the gamma-ray originates from the fuel rod and goes through Region A of the blanket, which is shown in Fig. E-1. However if the gamma is one of the decay gamma-rays from Na^{24}, the gamma-ray originates from Na_2CrO_4 and goes through Region A or Region B of the blanket. In other words, the gamma-ray self-absorption in Blanket No. 2 differs according to the energy of gamma-rays and the place of origin of the gamma-rays.

Figure E-1 shows the detail of the blanket structure seen by the detector, looking down the 2-inch diameter

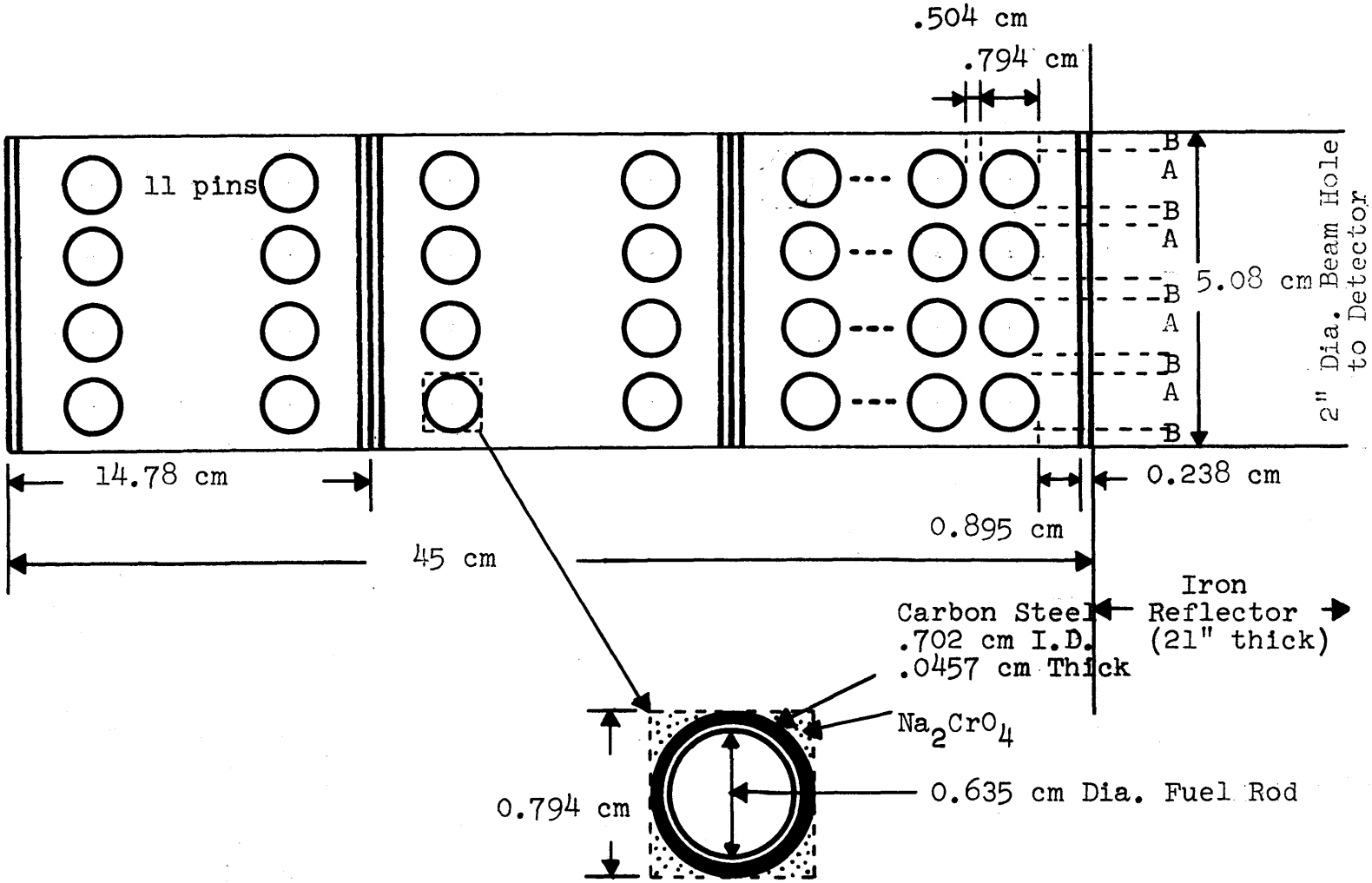

Fig. E-1 Top View of the Part of Blanket No. 2 Seen by the Detectors through the 2-in. dia. Beam Hole

beam hole penetrating the reflector. The structure is divided into two regions, A and B, where Region A contains the fuel pins and Na_2CrO_4, and Region B contains Na_2CrO_4 only.

Suppose the gamma-ray of interest with energy $E\gamma$ originates from Na_2CrO_4 in the blanket; the self-absorption correction factor is given by

$$S\gamma = \int_{\Delta V} dV \psi(\underline{r})\ n\ (\underline{r})\ S\gamma\ (\underline{r})$$

or

$$S\gamma = \int_{V_A} dV \psi(\underline{r})\ n\ (\underline{r})\ S\gamma\ (\underline{r}) + \int_{V_B} dV\ \psi(\underline{r})\ n\ (\underline{r}) S\gamma\ (\underline{r}) \qquad \text{(E-1)}$$

where V_A and V_B are volume fractions of Na_2CrO_4 in Region A and Region B, respectively.

Region B is a completely homogeneous medium of Na_2CrO_4, and so the self-absorption correction factor for Region B only is simply:

$$\begin{aligned}(S\gamma)_B = {} & \frac{V_B}{3} \cdot \left(\int_o^1 \psi\ (x)\ S\gamma\ (x)\ dx\ \right) \cdot e^{-\mu_\gamma^{Fe} \cdot d} \\ & + \frac{V_B}{3} \cdot \left(\int_o^1 \psi\ (x)\ S\gamma\ (x)\ dx\ \right) \cdot e^{-3\mu_\gamma^{Fe} \cdot d} \cdot e^{-\mu_\gamma^{N} \cdot l} \\ & + \frac{V_A}{3} \cdot \left(\int_o^1 \psi\ (x)\ S\gamma\ (x)\ dx\ \right) \cdot e^{-5\mu_\gamma^{Fe} \cdot d} \cdot e^{-2\mu_\gamma^{N} \cdot l}\end{aligned} \qquad \text{(E-2)}$$

where μ_γ^{Fe} and μ_γ^{N} are the linear attenuation coefficients of gamma-rays with energy $E\gamma$ for iron and Na_2CrO_4, respectively,

and d, l - are the thicknesses of the steel plate of the subassembly wall and the subassembly box less the thickness of its two steel walls.

The first term of Eq. E-2 is the contribution from the first subassembly; the second term from the second sub-assembly; and the third term from the third sub-assembly. The neutron flux shape, $\psi(x)$, is adequately approximated by an exponential function (see Appendix A):

$$\psi(x) = a\ e^{-\Gamma x} \qquad \text{(E-3)}$$

where

$a = 0.662$ and

$\Gamma = 0.0621\ \ cm^{-1}$.

And the self-absorption function, $S\gamma(x)$, is:

$$S\gamma(x) = e^{-\mu_{\gamma}^{N}\,(x_B - x)} \qquad \text{(E-4)}$$

where X_B is the thickness of the blanket, as usual.

Region A is somewhat more complicated. As one can see in Fig. E-2, Region A is divided into three parts, the steel plate (d), the end piece of Na_2CrO_4 (ln) at both ends of the subassembly, and successive eleven unit cells of fuel pin plus Na_2CrO_4 ($2R_N$). The geometry of the plate and the Na_2CrO_4 at both ends of the sub-assembly depends only on the axial x direction. However, that of the unit cell, which consists of a fuel

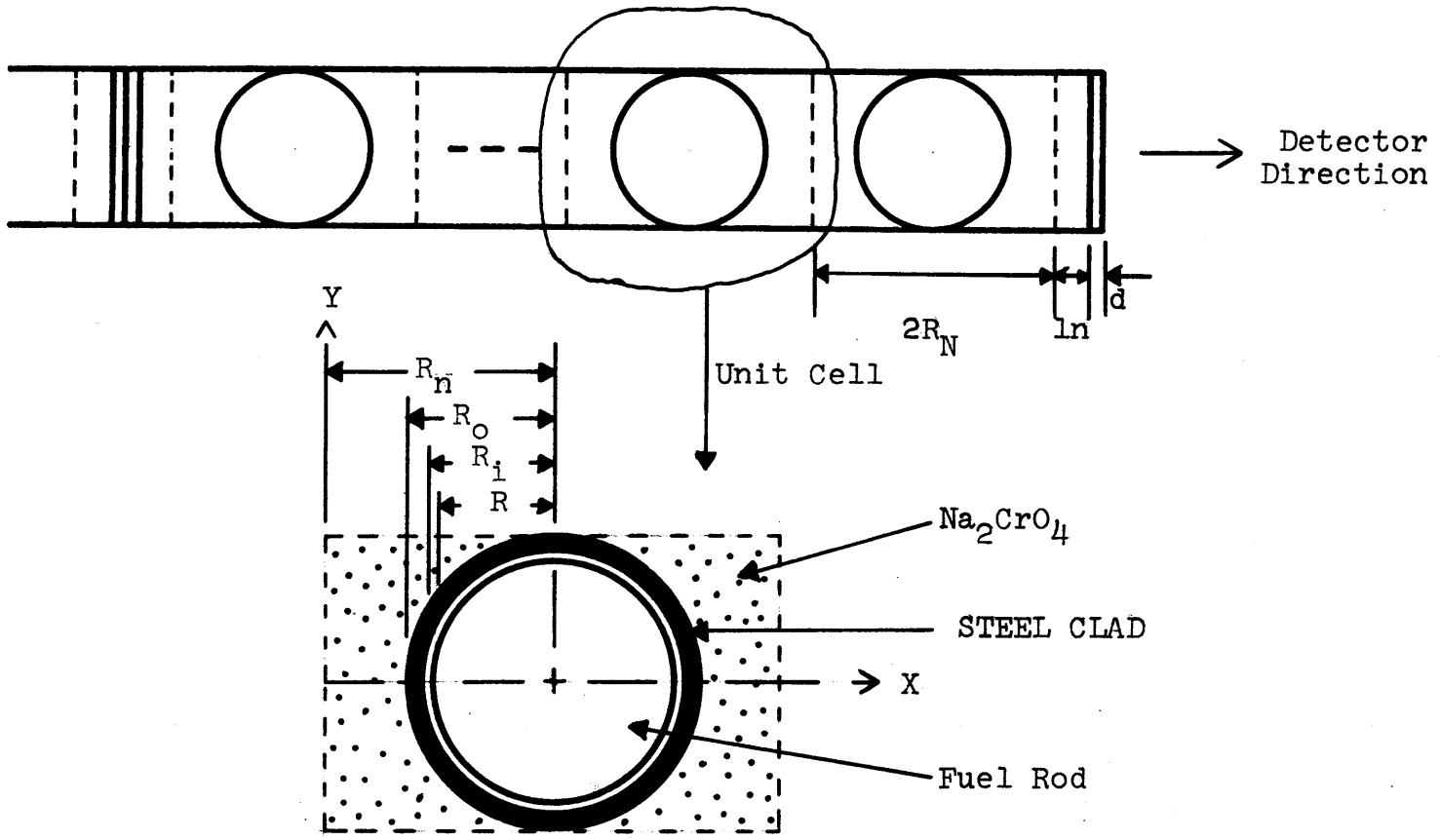

Fig. E-2 Top View of Region A of Blanket No. 2 Seen by the Detector, and a Unit Cell

pin and Na_2CrO_4, depends upon two directions, x and y.

In the unit cell of Fig. E-2,

the thickness of Na_2CrO_4 at y: $2(R_N-\sqrt{R_o^2-y^2})=2X_N(y)$

the thickness of Fe clad at y: $2(\sqrt{R_o^2-y^2} - \sqrt{R_i^2-y^2})$

$= 2X_{Fe}(y)$

the thickness of Fuel at y: $2\sqrt{R^2-y^2} = 2X_U(y)$.

Hence the self-absorption correction factor of the unit cell for the gamma-rays which originate from Na_2CrO_4 at the position y is:

$$S\gamma^U(y) = X_N(y) \int_o^{X_N(y)} \Psi(x)\, S\gamma(x,y)\, dx + X_N(y) \left(\int_o^{X_N(y)} \Psi(x)\, S\gamma(x,y)\, dx\right) \cdot e^{-(\mu_\gamma^{Fe} \cdot 2X_{Fe}(y) + \mu_\gamma^U \cdot 2X_U(y) + \mu_\gamma^N \cdot X_N(y))} \qquad \text{(E-5)}$$

where

$$S\gamma(x,y) = e^{-\mu_\gamma^N (X_N(y)-x)}.$$

The average self-absorption correction factor for the unit cell, $S\gamma^U$, can be obtained by integration of Eq. E-5

with respect to y. This resultant double integration can be performed numerically.

The attenuation factor of the unit cell for gamma-rays of energy Eγ at the position y is:

$$A_\gamma^U(y) = e^{-2(\mu_\gamma^{Fe} X_{Fe}(y) + \mu_\gamma^U \cdot X_U(y) + \mu_\gamma^N \cdot X_N(y))} \qquad \text{(E-6)}$$

Similarly the average attenuation factor for the unit cell, A_γ^U is obtained by integration of Eq. E-6.

Hence the total self-absorption correction factor for Region A is given by:

$$(S\gamma)_A = S_\gamma^{ln} \cdot A_\gamma^d \cdot V_{l_1} + S_\gamma^U \cdot A_\gamma^{ln} \cdot A_\gamma^d \cdot V_{l_2} + S_\gamma^U \cdot A_\gamma^U \cdot A_\gamma^{2ln} \cdot A_\gamma^d \cdot V_{l_2} + \text{------} \qquad \text{(E-7)}$$

where

$$S_\gamma^{ln} = \int_o^{ln} 4(x)\, e^{-\mu_N^\gamma (ln-x)}\, dx$$

$$A_\gamma^d = e^{-\mu_\gamma^{Fe} \cdot d}$$

$$A_\gamma^{ln} = e^{-\mu_\gamma^{Fe} \cdot ln}, \quad \text{and}$$

V_{l_1}, V_{l_2} are the volume fractions of Na_2CrO_4 in the first remaining Na_2CrO_4 part and the unit cell, respectively. Hence the total self-absorption correction factor for gamma-rays having energy $E\gamma$ which originate from Na_2CrO_4 is:

$$S\gamma = (S\gamma)_A + (S\gamma)_B \qquad \text{(E-8)}$$

This calculation is done by a computer program **SELFN.**

The self-absorption correction factor for gamma-rays which originate from the U-fuel rods should be treated differently since Region A is our only concern in this case. As for the decay gamma-rays of Np-239, which is formed in U-fuel rods, the self-abosorption correction factor of the unit cell (see Fig. E-2) for these gamma-rays of energy $E\gamma$ is:

$$S_\gamma^U = 2 \int_o^R S_\gamma^U (y)\, dy \qquad \text{(E-9)}$$

where

$$S_\gamma^U(y) = 2\, X_U(y) \left(\int_o^{X_U(y)} \phi(x)\, S_\gamma(x,y)\, dx \right) \cdot e^{-(\mu_\gamma^{Fe} \cdot X_{Fe}(y) + \mu_\gamma^N \cdot X_N(y))} \qquad \text{(E-10)}$$

and

$$S_\gamma(x,y) = e^{-\mu_\gamma^U (X_N(y) - x)}. \qquad \text{(E-11)}$$

Hence the total self-absorption correction factor for gamma-rays having energy $E\gamma$ which originate from U-fuel rods is:

$$S^{\gamma} = S_{\gamma}^{U} \cdot A_{\gamma}^{ln} \cdot A_{\gamma}^{d} \cdot V$$

$$+ S_{\gamma}^{U} \cdot A_{\gamma}^{U} \cdot A_{\gamma}^{ln} \cdot A_{\gamma}^{d} \cdot V$$

$$+ S_{\gamma}^{U} \cdot (A_{\gamma}^{U})^{2} \cdot A_{\gamma}^{ln} \cdot A_{\gamma}^{d} \cdot V$$

$$+ \text{-----} \qquad \text{(E-12)}$$

where V = 1/132; volume fraction of a single U-fuel rod. A computer program SELFU calculates the self-absorption factor for these gamma-rays.

E-2 Experimental Correction for Fuel Heterogenity

A mock-up experiment was performed to measured the actual attenuation factor of a single fuel rod. The calculated attenuation factor for the unit cell is inexact due to contributions by the statistical mis-alignment of fuel rod rows and streaming in the gap between fuel and clad. Hence the experimental determination was considered essential.

The test box was built from 6" x 6" x 21-1/2" by 1/16" thick steel plate. This box holds 44 fixed fuel

rods, 10 movable fuel rods and one irradiated rod (see Fig. E-3). This mocks up the five center rows of a real subassembly of Blanket No. 2. Sodium chromate fills the space between the rods. The irradiated rod contains a 1 inch long fuel rod at the center of an aluminum rod. This rod was irradiated in the 2CH1 irradiation facility of the MITR to produce a low energy gamma-ray source of Np-239. A series of measurements were carried out, changing the position of the irradiated rod along the center row of the test box. This was carried out in the isolated accelerator vault with a 35-c.c Ge(Li) crystal. Figure E-4 shows the gamma-ray transmission factors of a unit cell according to the gamma-ray energy. Here the transmission factor of a unit cell is defined by the ratio of transmitted gamma-rays through the unit cell to total incoming gamma-rays to the unit cell. These experimental data are fitted in the linear least-square sense.

E-3 Computer Programs SELFN and SELFU

Two computer programs, SELFN and SELFU, are listed together with typical input and output data. This program mainly performs numerical double integrations. Between two mesh points Simpson's rule is applied to perform a simple integration. The calculated values

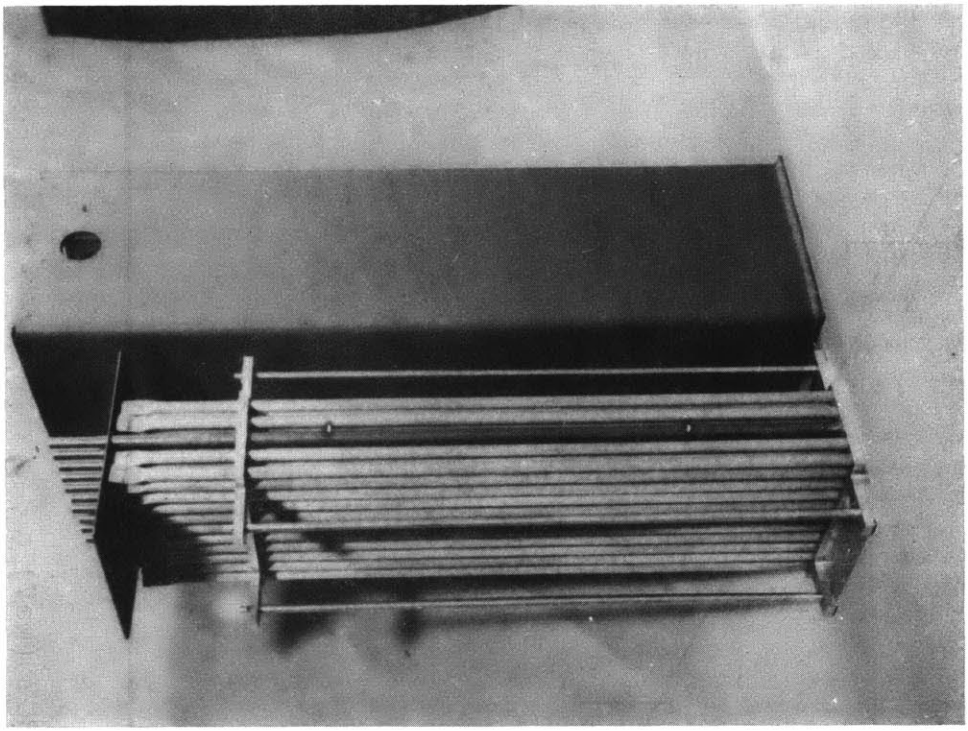

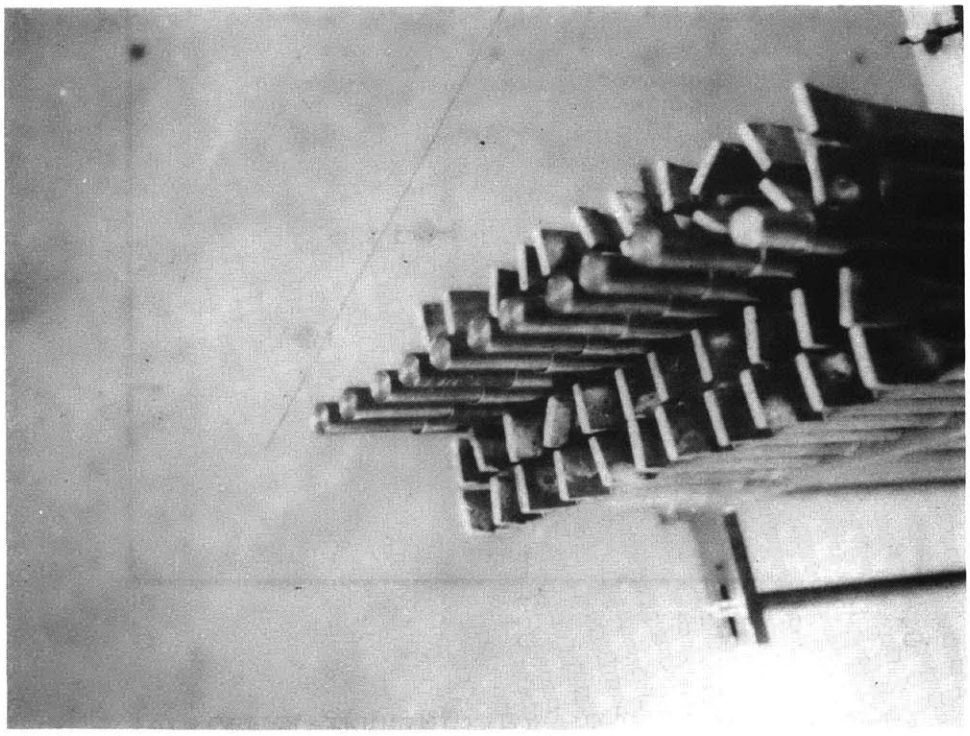

Fig. E-3 Views of Test Box and Its Fuel Rod Array

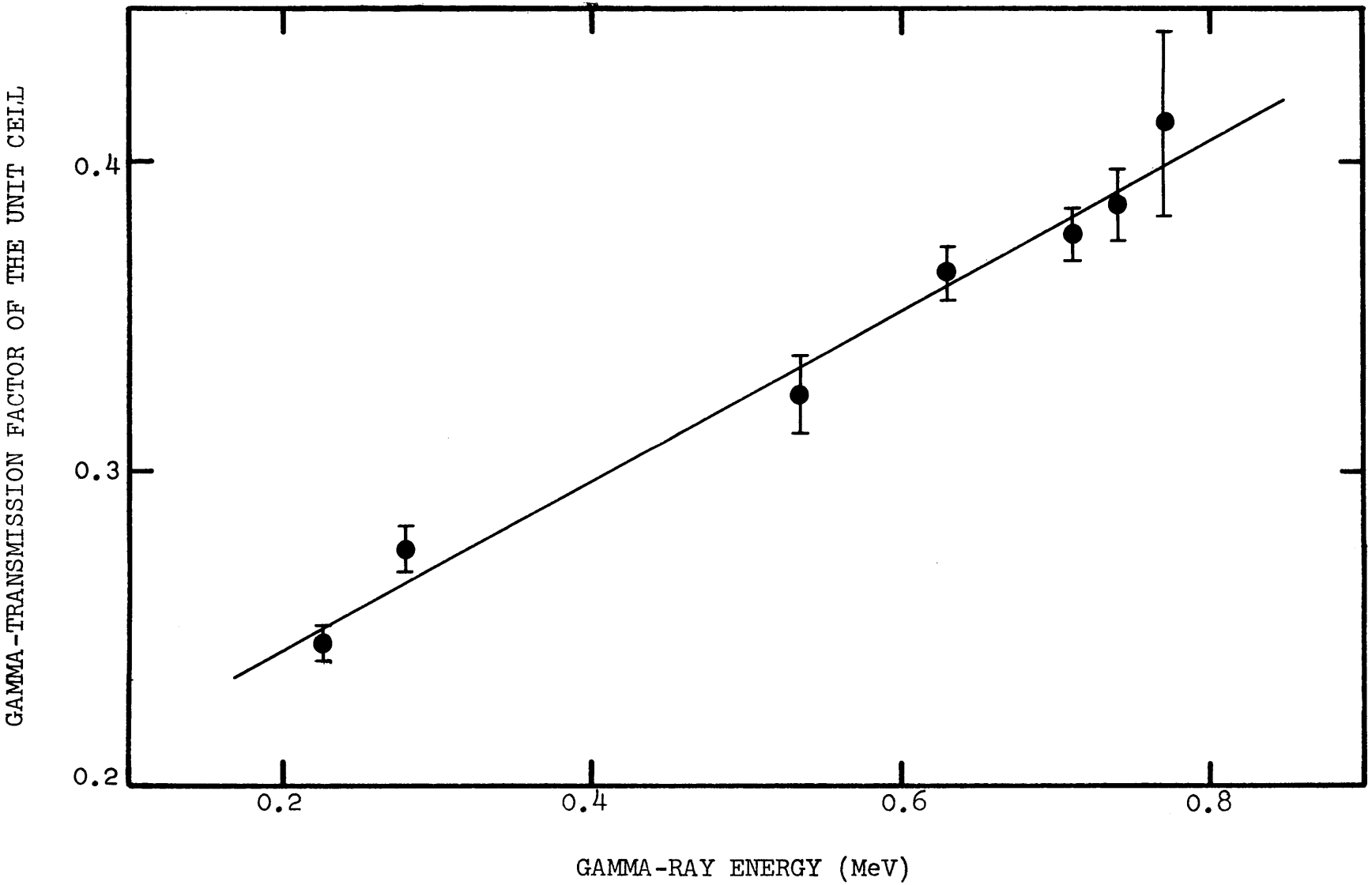

Fig. E-4 Gamma-Transmission Factor of a Unit Cell of Fuel Rods

are compared with the measured values in the program SELFU. Input data of SELFN consists of the energy of the peak and the measured gamma-ray linear attenuation coefficients of sodium chromate, iron cladding and uranium. Input data of SELFU consists of not only the energy peak and the linear attenuation coefficients, but also the measured total transmission factor of the unit cell. Output data includes the self-attenuation factor of each region and the total averaged attenuation factor of the blanket, which is compared with the measured value in SELFU.

```
C      CALCULATION OF SELF-ATTENUATION FACTOR FOR SODIUM
C      CHROMATE IN THE BLANKET NO.2 AT MITR.
C
 1000 CONTINUE
      READ (5,1) EN,XNA,XC,XU,MO
    1 FORMAT (4F10.5,I5)
C      INPUT ARGUEMENTS
C      EN - ENERGY OF THE PEAK OF INTEREST (MEV)
C      XNA,XC,XU - LINEAR ATTENUATION COEFFICIENTS OF SODIUM
C      CHROMATE, IRON, AND URANIUM AT THE GAMMA-RAY ENERGY
C      EN (1/CM), RESPECTIVELY.
C
      WRITE (6,10) EN
   10 FORMAT ('1',14X,'SELF-ATTENUATION ANALYSIS FOR',F10.5,
     1' MEV GAMMA')
      WRITE (6,11)
   11 FORMAT ('0',14X,'THE LINEAR ATTENUATION COEFFICIENTS (1/CM)')
      WRITE (6,12) XNA
   12 FORMAT (15X,'SODIUM CHROMATE ',E10.5)
      WRITE (6,13) XC
   13 FORMAT (15X,'IRON CLADDING   ',E10.5)
      WRITE (6,14) XU
   14 FORMAT (15X,'URANIUM         ',E10.5)
C
      X1=14.304
      X2=1.906
      PIE=3.141592
      RO=0.397
      RI=0.351
      R=0.3175
      RN=0.649
      X2A=0.643
      X3=0.238
      EL=14.78
      GAMMA=0.0621
      VT=(15.24*X1)-132*PIE*RO*RO
```

```
C
C      VOLUME FRACTION CALCULATION
C
       V1=X1*X2/VT
       V2A=3*RO*X2A/VT
       V2B=4*(4*RO*RN-RO*RO*PIE)/VT
       WRITE (6,15)
   15 FORMAT ('0',14X,'VOLUME FRACTIONS OF SODIUM CHROMATE')
       WRITE (6,16) V1
   16 FORMAT (15X,'PART 1           ',E10.5)
       WRITE (6,17) V2A
   17 FORMAT (15X,'PART 2A          ',E10.5)
       WRITE (6,18) V2B
   18 FORMAT (15X,'PART 2B          ',E10.5)
C
C      TRANSMISSION FACTOR CALCULATION
C
       T1=EXP(-XNA*X1)
       T2A=EXP(-XNA*X2A)
       T3=EXP(-XC*X3)
C
C      NORMALIZATION OF NEUTRON FLUX IN THE BLANKET NO.2
C
       FLU=(1-EXP(-3*GAMMA*EL))/GAMMA
C
C      SELF-ATTENUATION FACTOR OF PART 1
C
       EX1=EXP(-GAMMA*EL)
       EX2=EXP(-2*GAMMA*EL)
       EX3=EXP(-3*GAMMA*EL)
       S1=(T3**5)*T1*T1+T3*T3*T3*T1*EX1+T3*EX2
       S1=V1*S1/FLU
       S1=S1*(EX1-T1)/(XNA-GAMMA)
C
C      T2B AND SN CALCULATION IN THE UNIT CELL.  NUMERICAL
C      INTEGRATION DONE BY SIMPSON'S RULE.
```

```
C
      N=41
      YD=RO/(N-1)
      T2B=(EXP(-2*(XNA*(RN-RO)+XC*(RO-RI)+XU*R)))*YD/3.
      SN=(RN-RO)*(1.+EXP(-2*(XC*(RO-RI)+XU*R)-XNA*(RN-RO)))*YD/(3*FLU)
      I1=2
      DO 100 I=2,N
      Y=YD*FLOAT(I-1)
      YNO=RO*RO-Y*Y
      YNI=RI*RI-Y*Y
      YNR=R*R-Y*Y
      IF (YNO.LE.0.) YNO=0.
      IF (YNI.LE.0.) YNI=0.
      IF (YNR.LE.0.) YNR=0.
      YN=RN-SQRT(YNO)
      YC=SQRT(YNO)-SQRT(YNI)
      YU=SQRT(YNR)
      L=1
      DO 101 J=1,I
  101 L=(-1)*L
      I1=I1+2*L
      IF (I.EQ.N) I1=1
      T=I1*EXP(-2*(XNA*YN+XC*YC+XU*YU))*YD/3.
      S=I1*YN*(1.+EXP(-2*(XC*YC+XU*YU)-XNA*YN))*YD/(3*FLU)
      T2B=T2B+T
      SN=SN+S
  100 CONTINUE
C
      T2B=T2B/RO
      SN=SN/RO
      TT=(T2B**11)*T2A*T2A*T3*T3
      EXL=(EXP(-GAMMA*X2A)-EXP(-XNA*X2A))/(XNA-GAMMA)
C
C     SELF-ATTENUATION FACTOR OF PART 2A
C
      S2A=V2A*X2A*(TT*TT*TT/(T2A*T3)+EX1*TT*TT*(T3+1/(T2A+T3))
```

```
     1+EX2*TT*(T3+1/(T2A+T3))+EX3*T3)/FLU
C
C      SELF-ATTENUATION FACTOR OF PART 2B
C
       S2B=0.
       TB=1.
       DO 102 I=1,11
       X=42.81+1.298*FLOAT(I-1)
       EX=EXP(-GAMMA*X)
       EX=EX*TB
       S2B=S2B+EX
       TB=TB*T2B
  102  CONTINUE
C
       S2B=V2B*SN*S2B*T2A*T3
       S2B=S2B*(1.+TT*EX1/EX2+TT*TT/EX2)
       S2=S2A+S2B
       S12=S1+S2
       WRITE (6,19)
    19 FORMAT ('0',14X,'TRANSMISSION FACTORS')
       WRITE (6,20) T1
    20 FORMAT (15X,'PART 1           ',E10.5)
       WRITE (6,21) T2A
    21 FORMAT (15X,'PART 2A          ',E10.5)
       WRITE (6,22) T2B
    22 FORMAT (15X,'PART 2B          ',E10.5)
       WRITE (6,23) T3
    23 FORMAT (15X,'STEEL PLATE      ',E10.5)
       WRITE (6,24)
    24 FORMAT ('0',14X,'SELF-ATTENUATION FACTOR')
       WRITE (6,25) S1
    25 FORMAT (15X,'SELF-ATTENUATION FACTOR FOR PART 1 ',E10.5)
       WRITE (6,26) S2A
    26 FORMAT (15X,'SELF-ATTENUATION FACTOR FOR PART 2A',E10.5)
       WRITE (6,27) S2B
    27 FORMAT (15X,'SELF-ATTENUATION FACTOR FOR PART 2B',E10.5)
```

```
      WRITE (6,28) S12
   28 FORMAT (15X,'TOTAL SELF-ATTENUATION FACTOR       ',E10.5)
      IF (MO.GT.0) GO TO 1000
      CALL EXIT
      END
```

INPUT DATA

0.20980	0.20700	1.06000	25.50000	1
0.22820	0.20400	1.01400	20.60000	1
0.27760	0.20200	0.89000	13.00000	1
0.31590	0.19900	0.81500	10.40000	1
0.33430	0.19700	0.79500	8.51000	1
0.43800	0.18800	0.69500	4.25300	1
0.51500	0.18300	0.64300	3.17900	1
0.83510	0.15800	0.51200	1.71800	1
1.17300	0.12600	0.43300	1.29000	1
1.27400	0.12200	0.41400	1.13000	1
1.33250	0.12100	0.40500	1.04000	1
1.36850	0.12000	0.40100	1.00000	-1

SELF-ATTENUATION ANALYSIS FOR 0.20980 MEV GAMMA

THE LINEAR ATTENUATION COEFFICIENTS (1/CM)

SODIUM CHROMATE	.20700E 00
IRON CLADDING	.10600E 01
URANIUM	.25500E 02

VOLUME FRACTIONS OF SODIUM CHROMATE

PART 1	.17862E 00
PART 2A	.13379E-01
PART 2B	.14033E-01

TRANSMISSION FACTORS

PART 1	.51771E-01
PART 2A	.87538E 00
PART 2B	.13402E 00
STEEL PLATE	.77703E 00

SELF-ATTENUATION FACTOR

SELF-ATTENUATION FACTOR FOR PART 1 .38197E-02
SELF-ATTENUATION FACTOR FOR PART 2A.28244E-04
SELF-ATTENUATION FACTOR FOR PART 2B.20712E-04
TOTAL SELF-ATTENUATION FACTOR .38687E-02

OUTPUT DATA

SELF-ATTENUATION ANALYSIS FOR 0.22820 MEV GAMMA

THE LINEAR ATTENUATION COEFFICIENTS (1/CM)

SODIUM CHROMATE	.20400E 00
IRON CLADDING	.10140E 01
URANIUM	.20600E 02

VOLUME FRACTIONS OF SODIUM CHROMATE

PART 1	.17862E-01
PART 2A	.13379E 01
PART 2B	.14033E-01

TRANSMISSION FACTORS

PART 1	.54041E-01
PART 2A	.87707E 00
PART 2B	.13655E 00
STEEL PLATE	.78558E 00

SELF-ATTENUATION FACTOR

SELF-ATTENUATION FACTOR FOR PART 1 .39396E-02
SELF-ATTENUATION FACTOR FOR PART 2A.28555E-04
SELF-ATTENUATION FACTOR FOR PART 2B.21096E-04
TOTAL SELF-ATTENUATION FACTOR .39893E-02

SELF-ATTENUATION ANALYSIS FOR 0.27760 MEV GAMMA

THE LINEAR ATTENUATION COEFFICIENTS (1/CM)

SODIUM CHROMATE	.20200E 00
IRON CLADDING	.89000E 00
URANIUM	.13000E 02

VOLUME FRACTIONS OF SODIUM CHROMATE

PART 1	.17862E 00
PART 2A	.13379E-01
PART 2B	.14033E-01

TRANSMISSION FACTORS

PART 1	.55609E-01
PART 2A	.87820E 00
PART 2B	.14539E 00
STEEL PLATE	.80911E 00

SELF-ATTENUATION FACTOR

SELF-ATTENUATION FACTOR FOR PART 1	.41307E-02
SELF-ATTENUATION FACTOR FOR PART 2A	.29410E-04
SELF-ATTENUATION FACTOR FOR PART 2B	.22176E-04
TOTAL SELF-ATTENUATION FACTOR	.41823E-02

OUTPUT DATA

SELF-ATTENUATION ANALYSIS FOR 0.31590 MEV GAMMA

THE LINEAR ATTENUATION COEFFICIENTS (1/CM)

SODIUM CHROMATE	.19900E 00
IRON CLADDING	.81500E 00
URANIUM	.10400E 02

VOLUME FRACTIONS OF SODIUM CHROMATE

PART 1	.17862E 00
PART 2A	.13379E-01
PART 2B	.14033E-01

TRANSMISSION FACTORS

PART 1	.58047E-01
PART 2A	.87989E 00
PART 2B	.15375E 00
STEEL PLATE	.82368E 00

SELF-ATTENUATION FACTOR

SELF-ATTENUATION FACTOR FOR PART 1 .43102E-02
SELF-ATTENUATION FACTOR FOR PART 2A.29940E-04
SELF-ATTENUATION FACTOR FOR PART 2B.23016E-04
TOTAL SELF-ATTENUATION FACTOR .43541E-02

OUTPUT DATA

SELF-ATTENUATION ANALYSIS FOR 0.33430 MEV GAMMA

THE LINEAR ATTENUATION COEFFICIENTS (1/CM)

SODIUM CHROMATE	.19700E 00
IRON CLADDING	.79500E 00
URANIUM	.85100E 01

VOLUME FRACTIONS OF SODIUM CHROMATE

PART 1	.17862E 00
PART 2A	.13379E-01
PART 2B	.14033E-01

TRANSMISSION FACTORS

PART 1	.59732E-01
PART 2A	.88102E 00
PART 2B	.16295E 00
STEEL PLATE	.82761E 00

SELF-ATTENUATION FACTOR

SELF-ATTENUATION FACTOR FOR PART 1 .43823E-02
SELF-ATTENUATION FACTOR FOR PART 2A.30083E-04
SELF-ATTENUATION FACTOR FOR PART 2B.23581E-04
TOTAL SELF-ATTENUATION FACTOR .44359E-02

SELF-ATTENUATION ANALYSIS FOR 0.43800 MEV GAMMA

THE LINEAR ATTENUATION COEFFICIENTS (1/CM)

SODIUM CHROMATE	.18800E 00
IRON CLADDING	.69500E 00
URANIUM	.42530E 01

VOLUME FRACTIONS OF SODIUM CHROMATE

PART 1	.17862E 00
PART 2A	.13379E-01
PART 2B	.14033E-01

TRANSMISSION FACTORS

PART 1	.67939E-01
PART 2A	.88614E 00
PART 2B	.23951E 00
STEEL PLATE	.84755E 00

SELF-ATTENUATION FACTOR

SELF-ATTENUATION FACTOR FOR PART 1	.47944E-02
SELF-ATTENUATION FACTOR FOR PART 2A	.30807E-04
SELF-ATTENUATION FACTOR FOR PART 2B	.28156E-04
TOTAL SELF-ATTENUATION FACTOR	.48534E-02

THE LINEAR ATTENUATION COEFFICIENTS (1/CM)
SODIUM CHROMATE .18300E 00
IRON CLADDING .64300E 00
URANIUM .31790E 01

VOLUME FRACTIONS OF SODIUM CHROMATE
PART 1 .17862E 00
PART 2A .13379E-01
PART 2B .14033E-01

TRANSMISSION FACTORS
PART 1 .72976E-01
PART 2A .88899E 00
PART 2B .29649E 00
STEEL PLATE .85810E 00

SELF-ATTENUATION FACTOR
SELF-ATTENUATION FACTOR FOR PART 1 .50460E-02
SELF-ATTENUATION FACTOR FOR PART 2A.31191E-04
SELF-ATTENUATION FACTOR FOR PART 2B.31945E-04
TOTAL SELF-ATTENUATION FACTOR .51092E-02

OUTPUT DATA

SELF-ATTENUATION ANALYSIS FOR 0.83510 MEV GAMMA

THE LINEAR ATTENUATION COEFFICIENTS (1/CM)
SODIUM CHROMATE .15800E 00
IRON CLADDING .51200E 00
URANIUM .17180E 01

VOLUME FRACTIONS OF SODIUM CHROMATE
PART 1 .17862E 00
PART 2A .13379E-01
PART 2B .14033E-01

TRANSMISSION FACTORS
PART 1 .10435E 00
PART 2A .90340E 00
PART 2B .45224E 00
STEEL PLATE .88528E 00

SELF-ATTENUATION FACTOR
SELF-ATTENUATION FACTOR FOR PART 1 .64161E-02
SELF-ATTENUATION FACTOR FOR PART 2A.32193E-04
SELF-ATTENUATION FACTOR FOR PART 2B.46149E-04
TOTAL SELF-ATTENUATION FACTOR .64945E-02

SELF-ATTENUATION ANALYSIS FOR 1.17300 MEV GAMMA

THE LINEAR ATTENUATION COEFFICIENTS (1/CM)

SODIUM CHROMATE	.12600E 00
IRON CLADDING	.43300E 00
URANIUM	.12900E 01

VOLUME FRACTIONS OF SODIUM CHROMATE

PART 1	.17862E 00
PART 2A	.13379E-01
PART 2B	.14033E-01

TRANSMISSION FACTORS

PART 1	.16492E 00
PART 2A	.92218E 00
PART 2B	.53714E 00
STEEL PLATE	.90208E 00

SELF-ATTENUATION FACTOR

SELF-ATTENUATION FACTOR FOR PART 1 .90625E-02
SELF-ATTENUATION FACTOR FOR PART 2A.32888E-04
SELF-ATTENUATION FACTOR FOR PART 2B.58269E-04
TOTAL SELF-ATTENUATION FACTOR .91537E-02

OUTPUT DATA

SELF-ATTENUATION ANALYSIS FOR 1.27400 MEV GAMMA

THE LINEAR ATTENUATION COEFFICIENTS (1/CM)
SODIUM CHROMATE .12200E 00
IRON CLADDING .41400E 00
URANIUM .11300E 01

VOLUME FRACTIONS OF SODIUM CHROMATE
PART 1 .17862E 00
PART 2A .13379E-01
PART 2B .14033E-01

TRANSMISSION FACTORS
PART 1 .17463E 00
PART 2A .92455E 00
PART 2B .57010E 00
STEEL PLATE .90617E 00

SELF-ATTENUATION FACTOR
SELF-ATTENUATION FACTOR FOR PART 1 .95600E-02
SELF-ATTENUATION FACTOR FOR PART 2A.33131E-04
SELF-ATTENUATION FACTOR FOR PART 2B.63686E-04
TOTAL SELF-ATTENUATION FACTOR .96568E-02

SELF-ATTENUATION ANALYSIS FOR 1.33250 MEV GAMMA

THE LINEAR ATTENUATION COEFFICIENTS (1/CM)

SODIUM CHROMATE	.12100E 00
IRON CLADDING	.40500E 00
URANIUM	.10400E 01

VOLUME FRACTIONS OF SODIUM CHROMATE

PART 1	.17862E 00
PART 2A	.13379E-01
PART 2B	.14033E-01

TRANSMISSION FACTORS

PART 1	.17715E 00
PART 2A	.92515E 00
PART 2B	.58923E 00
STEEL PLATE	.90811E 00

SELF-ATTENUATION FACTOR

SELF-ATTENUATION FACTOR FOR PART 1	.97093E-02
SELF-ATTENUATION FACTOR FOR PART 2A	.33288E-04
SELF-ATTENUATION FACTOR FOR PART 2B	.67117E-04
TOTAL SELF-ATTENUATION FACTOR	.98097E-02

OUTPUT DATA

```
SELF-ATTENUATION ANALYSIS FOR   1.36850 MEV GAMMA

THE LINEAR ATTENUATION COEFFICIENTS (1/CM)
SODIUM CHROMATE .12000E 00
IRON CLADDING   .40100E 00
URANIUM         .10000E 01

VOLUME FRACTIONS OF SODIUM CHROMATE
PART 1          .17862E 00
PART 2A         .13379E-01
PART 2B         .14033E-01

TRANSMISSION FACTORS
PART 1          .17970E 00
PART 2A         .92574E 00
PART 2B         .59827E 00
STEEL PLATE     .90897E 00

SELF-ATTENUATION FACTOR
SELF-ATTENUATION FACTOR FOR PART 1 .98405E-02
SELF-ATTENUATION FACTOR FOR PART 2A.33372E-04
SELF-ATTENUATION FACTOR FOR PART 2B.68861E-04
TOTAL SELF-ATTENUATION FACTOR      .99428E-02
```

```
C      CALCULATION OF SELF-ATTENUATION FACTOR FOR URANIUM
C      IN THE BLANKET NO.2 AT MITR.
C
 1000 CONTINUE
      READ (5,1) EN,XNA,XC,XU,T2C,MO
    1 FORMAT (5F10.5,I5)
C      INPUT ARGUEMENTS
C      EN - ENERGY OF THE PEAK OF INTEREST (MEV)
C      XNA,XC,XU - LINEAR ATTENUATION COEFFICIENTS OF SODIUM
C      CHROMATE, IRON, AND URANIUM AT THE GAMMA-RAY ENERGY
C      EN (1/CM), RESPECTIVELY.
C      T2C   -  MEASURED ATTENUATION COEFFICIENT OF THE CELL
C
      WRITE (6,10) EN
   10 FORMAT ('1',14X,'SELF-ATTENUATION ANALYSIS FOR',F10.5,
     1' MEV GAMMA')
      WRITE (6,11)
   11 FORMAT ('0',14X,'THE LINEAR ATTENUATION COEFFICIENTS (1/CM)')
      WRITE (6,12) XNA
   12 FORMAT (15X,'SODIUM CHROMATE ',E10.5)
      WRITE (6,13) XC
   13 FORMAT (15X,'IRON CLADDING   ',E10.5)
      WRITE (6,14) XU
   14 FORMAT (15X,'URANIUM         ',E10.5)
C
      X1=14.304
      PIE=3.141592
      RO=0.397
      RI=0.351
      R=0.3175
      RN=0.649
      X2A=0.643
      X3=0.238
      EL=14.78
      GAMMA=0.0621
C
```

```
C     TRANSMISSION FACTOR CALCULATION
C
      T2A=EXP(-XNA*X2A)
      T3=EXP(-XC*X3)
C
C     NORMALIZATION OF NEUTRON FLUX IN THE BLANKET NO.2
C
      FLU=(1-EXP(-3*GAMMA*EL))/GAMMA
C
      EX1=EXP(-GAMMA*EL)
      EX2=EXP(-2*GAMMA*EL)
      EX3=EXP(-3*GAMMA*EL)
C
C     T2B AND SN CALCULATION IN THE UNIT CELL.  NUMERICAL
C     INTEGRATION DONE BY SIMPSON'S RULE.
C
      N=41
      YD=R/(N-1)
      T2B=(EXP(-2*(XNA*(RN-RO)+XC*(RO-RI)+XU*R)))*YD/3.
      SN=(EXP(-2*GAMMA*R-XC*(RO-RI)-XNA*(RN-RO))-EXP(-2*XU*R
     1-XC*(RO-RI)-XNA*(RN-RO)))*YD/(3*FLU*(XNA-GAMMA))
      I1=2
      DO 100 I=2,N
      Y=YD*FLOAT(I-1)
      YNO=RO*RO-Y*Y
      YNI=RI*RI-Y*Y
      YNR=R*R-Y*Y
      IF (YNO.LE.0.) YNO=0.
      IF (YNI.LE.0.) YNI=0.
      IF (YNR.LE.0.) YNR=0.
      YN=RN-SQRT(YNO)
      YC=SQRT(YNO)-SQRT(YNI)
      YU=SQRT(YNR)
      L=1
      DO 101 J=1,I
  101 L=(-1)*L
```

```
      I1=I1+2*L
      IF (I.EQ.N) I1=1
      T=I1*EXP(-2*(XNA*YN+XC*YC+XU*YU))*YD/3.
      S=(EXP(-2*GAMMA*YU-XC*YC-XNA*YN)-EXP(-2*XU*YU-XC*YC
     1-XNA*YN))*YD/(3*FLU*(XNA-GAMMA))
      T2B=T2B+T
      SN=SN+S
  100 CONTINUE
C
      T2B=T2B/R
      SN=SN/R
      TTB=(T2B**11)*T2A*T2A*T3*T3
      TTC=(T2C**11)*T2A*T2A*T3*T3
      EXL=(EXP(-GAMMA*X2A)-EXP(-XNA*X2A))/(XNA-GAMMA)
C
C     SELF-ATTENUATION FACTOR OF PART 2B
C
      S2B=0.
      S2C=0.
      TB=1.
      TC=1.
      DO 102 I=1,11
      X=42.81+1.298*FLOAT(I-1)
      EX=EXP(-GAMMA*X)
      EXB=EX*TB
      EXC=EX*TC
      S2B=S2B+EXB
      S2C=S2C+EXC
      TB=TB*T2B
      TC=TC*T2C
  102 CONTINUE
C
      S2B=SN*S2B*T2A*T3/33.
      S2C=SN*S2C*T2A*T3/33.
      S2B=S2B*(1.+TTB*EX1/EX2+TTB*TTB/EX2)
      S2C=S2C*(1.+TTC*EX1/EX2+TTC*TTC/EX2)
```

```
      WRITE (6,19)
   19 FORMAT ('0',14X,'TRANSMISSION FACTORS')
      WRITE (6,21) T2A
   21 FORMAT (15X,'PART 2A          ',E10.5)
      WRITE (6,22) T2B
   22 FORMAT (15X,'PART 2B (CALCULATED)',E10.5)
      WRITE (6,25) T2C
   25 FORMAT (15X,'PART 2B (MEASURED)  ',E10.5)
      WRITE (6,23) T3
   23 FORMAT (15X,'STEEL PLATE      ',E10.5)
      WRITE (6,24)
   24 FORMAT ('0',14X,'SELF-ATTENUATION FACTOR')
      WRITE (6,28) S2B
   28 FORMAT (15X,'SELF-ATTENUATION FACTOR (CALCULATED)',E10.5)
      WRITE (6,26) S2C
   26 FORMAT (15X,'SELF-ATTENUATION FACTOR (MEASURED)  ',E10.5)
      IF (MO.GT.0) GO TO 1000
      CALL EXIT
      END
```

INPUT DATA

0.20980	0.20700	1.06000	25.50000	0.24600	1
0.22820	0.20400	1.01400	20.60000	0.25100	1
0.27760	0.20200	0.89000	13.00000	0.26450	1
0.31590	0.19900	0.81500	10.40000	0.27490	1
0.33430	0.19700	0.79500	8.51000	0.27990	1
0.43800	0.18800	0.69500	4.25300	0.30810	1
0.51500	0.18300	0.64300	3.17900	0.32910	1
0.83510	0.15800	0.51200	1.71800	0.41620	-1

OUTPUT DATA

SELF-ATTENUATION ANALYSIS FOR 0.20980 MEV GAMMA

THE LINEAR ATTENUATION COEFFICIENTS (1/CM)
SODIUM CHROMATE .20700E 00
IRON CLADDING .10600E 01
URANIUM .25500E 02

TRANSMISSION FACTORS
PART 2A .87538E 00
PART 2B (CALCULATED).65581E-02
PART 2B (MEASURED) .24600E 00
STEEL PLATE .77703E 00

SELF-ATTENUATION FACTOR
TOTAL SELF-ATTENUATION FACTOR (CALCULATED).19050E-03
TOTAL SELF-ATTENUATION FACTOR (MEASURED) .24493E-03

OUTPUT DATA

SELF-ATTENUATION ANALYSIS FOR 0.22820 MEV GAMMA

THE LINEAR ATTENUATION COEFFICIENTS (1/CM)
SODIUM CHROMATE .20400E 00
IRON CLADDING .10140E 01
URANIUM .20600E 02

TRANSMISSION FACTORS
PART 2A .87707E 00
PART 2B (CALCULATED).76489E-02
PART 2B (MEASURED) .25100E 00
STEEL PLATE .78558E 00

SELF-ATTENUATION FACTOR
TOTAL SELF-ATTENUATION FACTOR (CALCULATED).19766E-03
TOTAL SELF-ATTENUATION FACTOR (MEASURED) .25541E-03

OUTPUT DATA

SELF-ATTENUATION ANALYSIS FOR 0.27760 MEV GAMMA

THE LINEAR ATTENUATION COEFFICIENTS (1/CM)
SODIUM CHROMATE .20200E 00
IRON CLADDING .89000E 00
URANIUM .13000E 00

TRANSMISSION FACTORS
PART 2A .87820E 00
PART 2B (CALCULATED).13941E-01
PART 2B (MEASURED) .26450E 00
STEEL PLATE .80911E 00

SELF-ATTENUATION FACTOR
TOTAL SELF-ATTENUATION FACTOR (CALCULATED).20791E-03
TOTAL SELF-ATTENUATION FACTOR (MEASURED) .27148E-03

SELF-ATTENUATION ANALYSIS FOR 0.31590 MEV GAMMA

THE LINEAR ATTENUATION COEFFICIENTS (1/CM)
SODIUM CHROMATE .19900E 00
IRON CLADDING .81500E 00
URANIUM .10400E 00

TRANSMISSION FACTORS
PART 2A .87989E 00
PART 2B (CALCULATED).21088E-01
PART 2B (MEASURED) .27490E 00
STEEL PLATE .82368E 00

SELF-ATTENUATION FACTOR
TOTAL SELF-ATTENUATION FACTOR (CALCULATED).21732E-03
TOTAL SELF-ATTENUATION FACTOR (MEASURED) .28549E-03

OUTPUT DATA

SELF-ATTENUATION ANALYSIS FOR 0.33430 MEV GAMMA

THE LINEAR ATTENUATION COEFFICIENTS (1/CM)
SODIUM CHROMATE .19700E 00
IRON CLADDING .79500E 00
URANIUM .85100E 01

TRANSMISSION FACTORS
PART 2A .88102E 00
PART 2B (CALCULATED).31573E-01
PART 2B (MEASURED) .27990E 00
STEEL PLATE .82761E 00

SELF-ATTENUATION FACTOR
TOTAL SELF-ATTENUATION FACTOR (CALCULATED).22146E-03
TOTAL SELF-ATTENUATION FACTOR (MEASURED) .28986E-03

OUTPUT DATA

SELF-ATTENUATION ANALYSIS FOR 0.43800 MEV GAMMA

THE LINEAR ATTENUATION COEFFICIENTS (1/CM)
SODIUM CHROMATE .18800E 00
IRON CLADDING .69500E 00
URANIUM .42530E 01

TRANSMISSION FACTORS
PART 2A .88614E 00
PART 2B (CALCULATED).12200E 00
PART 2B (MEASURED) .30810E 00
STEEL PLATE .84755E 00

SELF-ATTENUATION FACTOR
TOTAL SELF-ATTENUATION FACTOR (CALCULATED).23827E-03
TOTAL SELF-ATTENUATION FACTOR (MEASURED) .29542E-03

OUTPUT DATA

SELF-ATTENUATION ANALYSIS FOR 0.51500 MEV GAMMA

THE LINEAR ATTENUATION COEFFICIENTS (1/CM)
SODIUM CHROMATE .18300E 00
IRON CLADDING .64300E 00
URANIUM .31790E 01

TRANSMISSION FACTORS
PART 2A .88899E 00
PART 2B (CALCULATED).19028E 00
PART 2B (MEASURED) .32910E 00
STEEL PLATE .85810E 00

SELF-ATTENUATION FACTOR
TOTAL SELF-ATTENUATION FACTOR (CALCULATED).24585E-03
TOTAL SELF-ATTENUATION FACTOR (MEASURED) .29106E-03

OUTPUT DATA

SELF-ATTENUATION ANALYSIS FOR 0.83510 MEV GAMMA

THE LINEAR ATTENUATION COEFFICIENTS (1/CM)
SODIUM CHROMATE .15800E 00
IRON CLADDING .51200E 00
URANIUM .17180E 01

TRANSMISSION FACTORS
PART 2A .90340E 00
PART 2B (CALCULATED).37496E 00
PART 2B (MEASURED) .41620E 00
STEEL PLATE .88528E 00

SELF-ATTENUATION FACTOR
TOTAL SELF-ATTENUATION FACTOR (CALCULATED).29920E-03
TOTAL SELF-ATTENUATION FACTOR (MEASURED) .31770E-03

Appendix F

Computer Program SPECT

The computer code SPECT calculates the neutron energy spectra from Blanket No. 2 given the broadened Ge 691.4 KeV spectral line as input. The subroutine SMOOTH smooths the input data and the subroutine SPLINE interpolates among the given data using the cubic spline function (G9). The standard broadened spectrum 691.4 KeV for Cf-252 (Run No. 91) and the broadened $\bar{6}91.4$ KeV spectrum from Blanket No. 2 (Run No. 105) were used to unfold the blanket neutron spectrum. Typical input and output data immediately follow the code listing. Input data consist of the number of runs, the number of channels the minimum channel at which the analysis begins, the degree of freedom of smoothing, the energy per channel and the spectral data for the standard source run and the same input data for the blanket run follow.

```
C      NEUTRON ENERGY SPECTRA ANALYSIS FROM 691.4 KEV INTERNAL
C      CONVERSION LINE.
C
       REAL DATA(8200),E(100),W(100),FLUX(100),CFLUX(100),
      1X(500),Y(500),T(500),DELY(500),S2(500),S3(500),SS(500),B(500)
C
       WRITE (6,25)
    25 FORMAT ('1',14X,'THE ANALYSIS OF STANDARD NEUTRON SOURCE CF-252')
  1000 CONTINUE
       READ (5,1) NRUN,NCHAN,IMAX,LT,IDIST,EDELT,LIM
     1 FORMAT (5I5,F10.5,I5)
       READ (5,2) (DATA(I),I=1,NCHAN)
     2 FORMAT (7X,7(F6.0,1X)/(8(F6.0,1X)))
C      BACKGROUND SUBTRACTION
       DO  200 I=1,NCHAN
       DATA(I)=DATA(I)-DATA(NCHAN)
       IF (DATA(I).LE.0.) NCHAN=I
   200 CONTINUE
C
C      FORMING THE VECTOR FOR THE MEASURED 691.4 KEV SPECTRA.
C
       QVALUE=691.4
       GEMASS=72.0
       EMIN=QVALUE/(1.0+GEMASS)
       EMIN=-1.77196+1.16293*ALOG(EMIN)
       EMIN=EXP(EMIN)
       EMIN=EMIN+IDIST*EDELT
C
       WRITE (6,10) NRUN,NCHAN
    10 FORMAT ('0',14X,'PARAMETERS AND INPUT DATA FOR RUN',I5,
      11X,I5,' CHANNELS')
       WRITE (6,11) IMAX
    11 FORMAT ('0',14X,'LOW CHANNEL NUMBER WHICH BEGINS ANALYSIS',I5)
       WRITE (6,13) EDELT
    13 FORMAT (15X,'ENERGY PER CHANNEL NUMBER (KEV)',F7.5)
       CALL SMOOTH (IMAX,NCHAN,IDIST,DATA,W,FLUX,NOUT)
```

```
      N=2*IDIST*(NOUT-1)+1
      DO 204 I=1,N
  204 T(I)=FLOAT(IDIST+I-1)
C
      CALL SPLINE (FLUX,W,T,DATA,NOUT,N)
C
      NCHAN=IMAX+(2*NOUT-1)*IDIST
      IMAX=IMAX+IDIST
      DO 109 I=1,N
  109 W(I)=DATA(I)*100
      DO 205 I=1,N
      K=I+IMAX-1
      DATA(K)=W(I)
  205 CONTINUE
      NOUT=(NCHAN-IMAX)/IDIST
      WRITE (6,12) NOUT
   12 FORMAT (15X,'DIMENSION OF MATRIX',I5)
C
      DO 100 I=1,NOUT
      IU=IMAX+IDIST*I
      IL=IMAX+IDIST*(I-1)
      IP=IU-IDIST/2
      E(I)=EMIN+(IP-IMAX)*EDELT
      E(I)=1.52370+0.85990*ALOG(E(I))
      E(I)=EXP(E(I))/1000.
      WT=DATA(IL)
      IL=IL+1
      I1=2
      IK=2
      DO 101 J=IL,IU
      L=1
      DO 102 K=1,IK
  102 L=(-1)*L
      I1=I1+2*L
      IK=IK+1
      IF (J.EQ.IU) I1=1
```

```
      WT=WT+DATA(J)*I1
  101 CONTINUE
      W(I)=WT/(3*IDIST)
  100 CONTINUE
C
C     FORMING THE RESPONSE MATRIX
C
      IT=1
      DO 103 I=1,NOUT
      DO 104 J=I,NOUT
      IP=IMAX+IDIST*J-IDIST/2
      ER=EMIN+(IP-IMAX)*EDELT
      EP=1.52370+0.85990*ALOG(ER)
      EP=EXP(EP)/1000.
      EP=(EP*(1.+GEMASS)+QVALUE/1000.)*(EP*(1.+GEMASS)+QVALUE/1000.)/
     1(4*GEMASS*EP)
      DELTA=SQRT(1.-(GEMASS+1.)*QVALUE/(GEMASS*EP*1000))
      EL=GEMASS*(DELTA+1.)*(DELTA+1.)/((GEMASS+1.)*(GEMASS+1.))
      EL=ER/EL
      EU=GEMASS*(DELTA-1.)*(DELTA-1.)/((GEMASS+1.)*(GEMASS+1.))
      EU=ER/EU
      EDIST=(EU-EL)/NOUT
      NI=NOUT+1
      CT=(GEMASS+1.)*(GEMASS+1.)/(4*GEMASS*EL*DELTA)
      I1=2
      DO 105 K=2,NI
      EM=EL+EDIST*(K-1)
      L=1
      DO 106 K1=1,K
  106 L=(-1)*L
      I1=I1+2*L
      IF (K.EQ.NI) I1=1
      C=(GEMASS+1.)*(GEMASS+1.)/(4*GEMASS*EM*DELTA)
      CT=CT+C
  105 CONTINUE
      DATA(IT)=CT*EDIST/3.
```

```
      IT=IT+1
  104 CONTINUE
      E(I)=(1000*E(I)*(1.+GEMASS)+QVALUE)*(1000*E(I)*(1.+GEMASS)
     1+QVALUE)/(4000*GEMASS*E(I))
      FLUX(I)=W(I)
  103 CONTINUE
C
      WRITE (6,18)
   18 FORMAT ('0',14X,'THE ENERGY ARRAY OF NEUTRON IN KEV')
      WRITE (6,17) (E(I),I=1,NOUT)
   17 FORMAT (1X,6E12.5)
      IF (LIM.EQ.1) GO TO 2000
C
C     SOLVING THE MATRIX EQUATION BY THE ITERATIVE UNFOLDING METHOD
C
      DO 108 I=1,NOUT
  108 FLUX(I)=W(I)/DATA(I)
C
      WRITE (6,21)
   21 FORMAT ('0',14X,'THE MEASURED NEUTRON FLUX OF CF-252')
      WRITE (6,17) (FLUX(I),I=1,NOUT)
C
C     CORRECTION FUNCTION FOR RESPONSE MATRIX
C
      DO 111 I=1,NOUT
      W(I)=SQRT(E(I))*EXP(-E(I)/1390.)
      CFLUX(I)=FLUX(I)/W(I)
      X(I)=E(I)
  111 CONTINUE
      WRITE (6,23)
   23 FORMAT ('1',14X,'THE CALCULATED NEUTRON FLUX OF CF-252')
      WRITE (6,17) (W(I),I=1,NOUT)
      WRITE (6,24)
   24 FORMAT ('0',14X,'THE CORRECTION DIAGONAL MATRIX FOR THE SYSTEM')
      WRITE (6,17) (CFLUX(I),I=1,NOUT)
C
```

```
      ECMIN=E(1)
      ECMAX=E(NOUT)
      NCF=NOUT
C
      WRITE (6,26)
   26 FORMAT ('1',14X,'THE ANALYSIS OF UNKNOWN NEUTRON ENERGY SPECTRA')
C
      GO TO 1000
C
 2000 CONTINUE
C
      CALL SPLINE (X,CFLUX,E,SS,NCF,NOUT)
C
      DO 116 I=1,NOUT
      DATA(I)=DATA(I)*SS(I)
      FLUX(I)=W(I)/DATA(I)
  116 CONTINUE
      WRITE (6,19)
   19 FORMAT ('0',14X,'THE CORRECTED DIAGONAL RESPONSE MATRIX')
      WRITE (6,17) (DATA(I),I=1,NOUT)
      WRITE(6,27)
   27 FORMAT ('1',14X,'THE NEUTRON ENERGY SPECTRA FROM BLANKET')
      WRITE(6,17) (FLUX(I),I=1,NOUT)
      CALL EXIT
      END
```

```
      SUBROUTINE SMOOTH (IMAX,NCHAN,IDIST,DATA,W,X,NOUT)
C
      REAL DATA(500),W(500),X(500)
      NOUT=(NCHAN-IMAX)/(2*IDIST)
      DO 1 I=1,NOUT
      IU=IMAX+2*IDIST*I
      IL=IMAX+2*IDIST*(I-1)
      WT=DATA(IL)/100.
      IL=IL+1
      I1=2
      IK=2
      DO 2 J=IL,IU
      L=1
      DO 3 K=1,IK
    3 L=(-1)*L
      I1=I1+2*L
      IK=IK+1
      IF (J.EQ.IU) I1=1
      WT=WT+DATA(J)*I1/100.
    2 CONTINUE
      W(I)=WT/(6*IDIST)
      X(I)=FLOAT((2*I-1)*IDIST)
    1 CONTINUE
      RETURN
      END
```

```
      SUBROUTINE SPLINE (X,Y,T,SS,N,M)
C     NUMERICAL INTERPOLATION BY USING SPLINE FUNCTIONS
      REAL X(500),Y(500),T(500),DELY(500),S2(500),S3(500),
     1SS(500),B(500)
C     N               NUMBER OF DATA POINTS
C
C     M               NUMBER OF OUTPUT ARGUMENTS
C
C     EPSLN           ERROR CRITERION IN ITERATIVE SOLUTION OF EQUATIONS
C                     FOR SPLINE FUNCTION PARAMETERS
C
C     X(I),Y(I)       INPUT DATA POINTS
C                     I CHANGES FROM 1 TO N
C                     NOTE THAT THE ABSCISSAS X(I) MUST BE DISTINCT AND IN
C                     ALGEBRAICALLY INCREASING SEQUENCE.
    2 N1=N-1
    3 DO 51 I=1,N1
      SS(I)=X(I+1)-X(I)
   51 DELY(I)=(Y(I+1)-Y(I))/SS(I)
    4 DO 52 I=2,N1
      SS1=SS(I-1)+SS(I)
      S3(I)=.5*SS(I-1)/SS1
      DELSQY=(DELY(I)-DELY(I-1))/SS1
      S2(I)=2.*DELSQY
   52 B(I)=3.*DELSQY
      S2(1)=0.
      S2(N)=0.
      OMEGA=1.0717968
    5 ETA=0.
    6 DO 10 I=2,N1
    7 W=(B(I)-S3(I)*S2(I-1)-(.5-S3(I))*S2(I+1)-S2(I))*OMEGA
    8 IF (ABS(W)-ETA) 10,10,9
    9 ETA=ABS(W)
   10 S2(I)=S2(I)+W
      EPSLN=0.0001
   13 IF (ETA-EPSLN) 14,5,5
```

```
   14 DO 53 I=1,N1
   53 S3(I)=(S2(I+1)-S2(I))/SS(I)
   15 DO 61 J=1,M
   16 I=1
C     T(J)            OUTPUT ARGUMENTS
C                     THESE QUANTITIES NEED NOT BE IN ANY PARTICULAR ORDER.
C                     HOWEVER, EVERY T(J) MUST SATISFY X(1)<=T(J)<=X(N),
C                     THAT IS, EXTRAPOLATION IS NOT PROVIDED FOR.
   54 IF (T(J)-X(1)) 58,17,55
   55 IF (T(J)-X(N)) 57,59,58
   56 IF (T(J)-X(I)) 60,17,57
   57 I=I+1
      GO TO 56
   58 WRITE (6,44) J
   44 FORMAT (I4,24HTH ARGUMENT OUT OF RANGE)
      GO TO 61
   59 I=N
   60 I=I-1
   17 HT1=T(J)-X(I)
      HT2=T(J)-X(I+1)
      PROD=HT1*HT2
      SS(J)=S2(I)+HT1*S3(I)
      DELSQS=(S2(I)+S2(I+1)+SS(J))/6.
      SS(J)=Y(I)+HT1*DELY(I)+PROD*DELSQS
   61 CONTINUE
C     SS(J)           SPLINE FUNCTIONS
      RETURN
      END
```

INPUT DATA OF CF-252 SPECTRA

```
   91  215     2  200     4    0.42470     0
002236 002261 002357 002228 002112 002133 002077 002011 001599
002046 001990 001927 001928 001755 001785 001896 001875 001607
001716 001718 001744 001722 001725 001591 001637 001514 001615
001568 001608 001682 001520 001491 001499 001550 001539 001623
001423 001526 001483 001482 001495 001422 001384 001431 001631
001317 001341 001318 001365 001290 001299 001303 001308 001639
001239 001274 001294 001208 001194 001202 001237 001241 001647
001187 001288 001261 001181 001138 001170 001184 001196 001655
001137 001179 001143 001130 001144 001180 001121 001125 001663
001174 001102 001172 001143 001129 001126 001159 001185 001671
001064 001143 001107 001059 001100 001048 001066 001158 001679
001086 001079 001133 001031 001051 001082 001054 001028 001687
001013 001046 001034 001071 001014 001065 001018 001034 001695
001027 001075 001047 001088 000989 001026 001085 001057 001703
001050 001049 001068 001032 001013 000999 001009 001004 001711
001009 001027 001079 001047 000974 000939 001025 001023 001719
001022 001097 001018 000999 001011 001010 001014 000949 001727
000967 000964 001010 000943 000967 000988 000993 000990 001735
000993 000938 001008 000984 000992 000967 001025 000980 001743
000974 000993 001043 000954 000966 000994 000910 001033 001751
000969 000936 000990 000981 000968 000955 001021 001069 001759
000960 000994 000952 000962 000971 000978 000938 000976 001767
000962 000990 001013 001045 001011 000957 000982 001028 001775
001020 001041 000914 000934 000956 000924 000946 000931 001783
000927 000971 000941 000931 000879 000907 000915 000932 001791
000890 000928 000959 000930 000881 000919 000955 000907 001799
000945 000929 000920 000920 000885 000946 000896 000877 001807
```

INPUT DATA OF BLANKET SPECTRA

```
  106  100     7  100     2    0.90200     1
003920 004106 004033 004281 004098 004545 004728 005073 000719
004935 005060 004907 004742 004598 004600 004660 004580 000727
004389 004531 004366 004474 004224 004343 004327 004306 000735
004183 004334 004284 004064 003982 004063 004112 003918 000743
003895 004028 004022 003734 003797 003851 003867 003955 000751
003806 003824 003886 003899 003636 003790 003791 003820 000759
003627 003799 003852 003724 003653 003787 003741 003751 000767
003658 003784 003769 003595 003528 003600 003604 003693 000775
003592 003660 003679 003643 003465 003675 003588 003770 000783
003681 003572 003675 003513 003597 003600 003548 003693 000791
003618 003768 003709 003590 003544 003523 003533 003720 000799
003725 003636 003731 003469 003550 003630 003591 003637 000807
003538 003642 003510 003528 003409 003606 003425 003472 000815
```

OUTPUT DATA

THE ANALYSIS OF STANDARD NEUTRON SOURCE CF-252

PARAMETERS AND INPUT DATA FOR RUN 91 215 CHANNELS

LOW CHANNEL NUMBER WHICH BEGINS ANALYSIS 2
ENERGY PER CHANNEL NUMBER (KEV)0.42470
DIMENSION OF MATRIX 50

THE ENERGY ARRAY OF NEUTRON IN KEV

0.77452E 03 0.85070E 03 0.93155E 03 0.10139E 04 0.10964E 04 0.11786E 04
0.12604E 04 0.13415E 04 0.14219E 04 0.15017E 04 0.15808E 04 0.16593E 04
0.17372E 04 0.18145E 04 0.18913E 04 0.19675E 04 0.20433E 04 0.21185E 04
0.21933E 04 0.22676E 04 0.23415E 04 0.24150E 04 0.24881E 04 0.25609E 04
0.26332E 04 0.27053E 04 0.27769E 04 0.28483E 04 0.29194E 04 0.29901E 04
0.30605E 04 0.31307E 04 0.32006E 04 0.32702E 04 0.33396E 04 0.34087E 04
0.34776E 04 0.35462E 04 0.36146E 04 0.36828E 04 0.37507E 04 0.38185E 04
0.38860E 04 0.39533E 04 0.40204E 04 0.40874E 04 0.41541E 04 0.42207E 04
0.42870E 04 0.43532E 04

THE MEASURED NEUTRON FLUX OF CF-252

0.43678E 02 0.36996E 02 0.31381E 02 0.26994E 02 0.23743E 02 0.21285E 02
0.19103E 02 0.16937E 02 0.14781E 02 0.12772E 02 0.11134E 02 0.98788E 01
0.88333E 01 0.78934E 01 0.70437E 01 0.63899E 01 0.61040E 01 0.59971E 01
0.55959E 01 0.48554E 01 0.41208E 01 0.35967E 01 0.33232E 01 0.32544E 01
0.32764E 01 0.32312E 01 0.29545E 01 0.25623E 01 0.23864E 01 0.23944E 01
0.22401E 01 0.18808E 01 0.15600E 01 0.14144E 01 0.14499E 01 0.15420E 01
0.14844E 01 0.13282E 01 0.13328E 01 0.14495E 01 0.13715E 01 0.11722E 01
0.12417E 01 0.14819E 01 0.13757E 01 0.91384E 00 0.55184E 00 0.44518E 00
0.44540E 00 0.46150E 00

OUTPUT DATA

THE CALCULATED NEUTRON FLUX OF CF-252

0.15941E 02 0.15816E 02 0.15615E 02 0.15354E 02 0.15046E 02 0.14704E 02
0.14337E 02 0.13953E 02 0.13557E 02 0.13155E 02 0.12750E 02 0.12346E 02
0.11944E 02 0.11546E 02 0.11155E 02 0.10770E 02 0.10393E 02 0.10025E 02
0.96666E 01 0.93172E 01 0.89776E 01 0.86478E 01 0.83280E 01 0.80181E 01
0.77181E 01 0.74279E 01 0.71474E 01 0.68764E 01 0.66148E 01 0.63622E 01
0.61187E 01 0.58838E 01 0.56573E 01 0.54392E 01 0.52290E 01 0.50266E 01
0.48317E 01 0.46441E 01 0.44635E 01 0.42898E 01 0.41226E 01 0.39618E 01
0.38072E 01 0.36585E 01 0.35154E 01 0.33780E 01 0.32458E 01 0.31187E 01
0.29966E 01 0.28792E 01

THE CORRECTION DIAGONAL MATRIX FOR THE SYSTEM

0.27399E 01 0.23392E 01 0.20096E 01 0.17581E 01 0.15780E 01 0.14476E 01
0.13324E 01 0.12139E 01 0.10902E 01 0.97087E 00 0.87320E 00 0.80017E 00
0.73957E 00 0.68363E 00 0.63146E 00 0.59330E 00 0.58729E 00 0.59819E 00
0.57889E 00 0.52112E 00 0.45901E 00 0.41591E 00 0.39904E 00 0.40589E 00
0.42451E 00 0.43501E 00 0.41337E 00 0.37262E 00 0.36077E 00 0.37635E 00
0.36611E 00 0.31966E 00 0.27575E 00 0.26005E 00 0.27728E 00 0.30677E 00
0.30722E 00 0.28599E 00 0.29859E 00 0.33789E 00 0.33269E 00 0.29587E 00
0.32615E 00 0.40505E 00 0.39132E 00 0.27053E 00 0.17002E 00 0.14274E 00
0.14863E 00 0.16029E 00

OUTPUT DATA

THE ANALYSIS OF UNKNOWN NEUTRON ENERGY SPECTRA

PARAMETERS AND INPUT DATA FOR RUN 106 100 CHANNELS

LOW CHANNEL NUMBER WHICH BEGINS ANALYSIS 7
ENERGY PER CHANNEL NUMBER (KEV)0.90200
DIMENSION OF MATRIX 44

THE ENERGY ARRAY OF NEUTRON IN KEV

0.78122E 03 0.86303E 03 0.94932E 03 0.10369E 04 0.11244E 04 0.12116E 04
0.12981E 04 0.13839E 04 0.14689E 04 0.15532E 04 0.16368E 04 0.17197E 04
0.18019E 04 0.18835E 04 0.19645E 04 0.20449E 04 0.21248E 04 0.22041E 04
0.22830E 04 0.23614E 04 0.24393E 04 0.25168E 04 0.25939E 04 0.26705E 04
0.27468E 04 0.28227E 04 0.28983E 04 0.29735E 04 0.30484E 04 0.31229E 04
0.31972E 04 0.32711E 04 0.33448E 04 0.34181E 04 0.34912E 04 0.35640E 04
0.36366E 04 0.37089E 04 0.37810E 04 0.38528E 04 0.39244E 04 0.39958E 04
0.40669E 04 0.41378E 04

THE CORRECTED DIAGONAL RESPONSE MATRIX

0.71213E 02 0.62625E 02 0.55688E 02 0.50539E 02 0.47178E 02 0.44786E 02
0.42318E 02 0.39365E 02 0.36072E 02 0.33114E 02 0.31002E 02 0.29420E 02
0.27960E 02 0.26526E 02 0.25571E 02 0.26099E 02 0.27431E 02 0.27079E 02
0.24780E 02 0.22419E 02 0.21170E 02 0.21409E 02 0.22886E 02 0.24687E 02
0.25067E 02 0.23367E 02 0.22473E 02 0.24010E 02 0.24568E 02 0.22189E 02
0.19471E 02 0.18791E 02 0.20791E 02 0.23639E 02 0.23814E 02 0.23025E 02
0.25956E 02 0.29293E 02 0.27478E 02 0.27065E 02 0.34740E 02 0.39123E 02
0.30299E 02 0.18782E 02

OUTPUT DATA

THE NEUTRON ENERGY SPECTRA FROM BLANKET

0.20349E 02 0.20619E 02 0.20854E 02 0.21009E 02 0.20790E 02 0.20509E 02
0.20917E 02 0.21803E 02 0.21821E 02 0.20531E 02 0.19395E 02 0.19936E 02
0.18168E 02 0.16864E 02 0.16820E 02 0.17101E 02 0.15520E 02 0.13534E 02
0.13538E 02 0.15280E 02 0.15983E 02 0.14780E 02 0.13729E 02 0.12959E 02
0.10996E 02 0.85498E 01 0.81424E 01 0.92685E 01 0.91198E 01 0.82690E 01
0.96176E 01 0.12393E 02 0.11037E 02 0.77528E 01 0.82079E 01 0.11075E 02
0.93189E 01 0.57040E 01 0.61847E 01 0.92813E 01 0.78205E 01 0.52599E 01
0.49173E 01 0.74507E 01

Appendix G

COMPUTER PROGRAM COMPT

The computer code COMPT performs the analysis of the Compton continuum gamma-ray spectrum from Blanket No. 2. The integration is done by an iterative unfolding method. Input data are the smoothed background output data from GAMANL. Output data consist of the upper triangular response matrix as well as the photon flux spectrum from Blanket No. 2

```
C     COMPTON SCATTERING ANALYSIS OF GAMMA-RAY SPECTRA.
C
C     FORMING THE VECTOR FOR THE MEASURED COMPTON CONTINUUM
C     BY GE(LI) DETECTOR.
C
      REAL DATA(8200),E(100),W(100),FLUX(100)
C
      READ (5,1) NRUN,NCHAN,IMAX,LT,IDIST,ICH1,ICH2,EN1,EN2
    1 FORMAT (7I5,2F10.5)
      READ (5,2) (DATA(I),I=1,NCHAN)
    2 FORMAT (7X,7(F6.0,1X)/(8(F6.0,1X)))
C
      NOUT=(NCHAN-IMAX)/IDIST
      EDELT=(EN2-EN1)/(ICH2-ICH1)
C
      WRITE (6,10) NRUN,NCHAN
   10 FORMAT ('1',14X,'PARAMETERS AND INPUT DATA FOR RUN',I5,
     11X,I5,' CHANNELS')
      WRITE (6,11) IMAX
   11 FORMAT ('0',14X,'LOW CHANNEL NUMBER WHICH BEGINS ANALYSIS
     1 (IMAX)',I5)
      WRITE (6,12) NOUT
   12 FORMAT (15X,'DIMENSION OF MATRIX',I5)
      WRITE (6,13) EDELT
   13 FORMAT (15X,'ENERGY PER CHANNEL NUMBER (KEV)',F7.5)
      WRITE (6,14) ICH1,EN1
   14 FORMAT (15X,'CALIBRATION 1   CH=',I5,'    E=',F7.2)
      WRITE (6,15) ICH2,EN2
   15 FORMAT (15X,'CALIBRATION 2   CH=',I5,'    E=',F7.2)
      WRITE (6,22) LT
   22 FORMAT (15X,'NUMBER OF ITERATION PERFORMED',I5)
C
      DO 100 I=1,NOUT
      IU=IMAX+IDIST*I
      IL=IMAX+IDIST*(I-1)
      IP=IU-IDIST/2
```

```
      E(I)=(EN1+(IP-ICH1)*EDELT)/511.
      WT=DATA(IL)
      IL=IL+1
      I1=2
      IK=2
      DO 101 J=IL,IU
      L=1
      DO 102 K=1,IK
  102 L=(-1)*L
      I1=I1+2*L
      IK=IK+1
      IF (J.EQ.IU) I1=1
      WT=WT+DATA(J)*I1
  101 CONTINUE
      W(I)=WT/(3*IDIST)
  100 CONTINUE
C
      WRITE (6,16)
   16 FORMAT ('0',14X,'THE MEASURED COMPTCN CONTINUUM VECTOR')
      WRITE (6,17) (W(I),I=1,NOUT)
   17 FORMAT (6E12.5)
C
C     FORMING THE RESPONSE MATRIX
C
      IT=1
      DO 103 I=1,NOUT
      DO 104 J=I,NOUT
      IU=IMAX+IDIST*J
      EU=(EN1+(IU-ICH1)*EDELT)/511.
      EU=EU*(1.+SQRT(1.+2./EU))/2.
      IL=IMAX+IDIST*(J-1)
      EL=(EN1+(IL-ICH1)*EDELT)/511.
      EL=EL*(1.+SQRT(1.+2./EL))/2.
      EDIST=(EU-EL)/IDIST
      NI=IDIST+1
      CT=EL-E(I)
```

```
      CT=E(I)*E(I)/(EL*EL*EL*EL*CT*CT)+2./(EL*EL)
     1+((E(I)-1)*(E(I)-1)-1)/(EL*EL*EL*CT)
      I1=2
      DO 105 K=2,NI
      EM=EL+EDIST*(K-1)
      L=1
      DO 106 K1=1,K
  106 L=(-1)*L
      I1=I1+2*L
      IF (K.EQ.NI) I1=1
      C=EM-E(I)
      C=E(I)*E(I)/(EM*EM*EM*EM*C*C)+2./(EM*EM)
     1+((E(I)-1)*(E(I)-1)-1)/(EM*EM*EM*C)
      CT=CT+C
  105 CONTINUE
      DATA(IT)=CT*EDIST/3.
      IT=IT+1
  104 CONTINUE
      E(I)=511.*E(I)*(1.+SQRT(1+2./E(I)))/2.
  103 CONTINUE
C
      WRITE (6,18)
   18 FORMAT ('1',14X,'THE ENERGY ARRAY OF PHOTON IN KEV')
      WRITE (6,17) (E(I),I=1,NOUT)
      WRITE (6,19)
   19 FORMAT ('0',14X,'THE UPPER TRIANGULAR RESPONSE MATRIX')
      J1=1
      J2=NOUT
      DO 107 I=1,NOUT
      WRITE (6,20) I
   20 FORMAT (15X,'I=',I5)
      WRITE (6,17) (DATA(J),J=J1,J2)
      J1=J2+1
      J2=J1+(NOUT-I)-1
      FLUX(I)=1.
  107 CONTINUE
```

```
C
C      SOLVING THE MATRIX EQUATION BY THE  ITERATIVE UNFOLDING METHOD
C
       DO 108 L=1,LT
       IT=1
       DO 109 I=1,NOUT
       CT=0.
       DO 110 J=I,NOUT
       C=DATA(IT)*FLUX(J)
       CT=CT+C
       IT=IT+1
  110  CONTINUE
       FLUX(I)=FLUX(I)/CT
       FLUX(I)=FLUX(I)*W(I)
  109  CONTINUE
  108  CONTINUE
C
       WRITE (6,21)
   21  FORMAT ('1',14X,'THE PHOTON FLUX FROM THE BLANKET NO.2')
       WRITE (6,17) (FLUX(I),I=1,NOUT)
       WRITE (7,17) (FLUX(I),I=1,NOUT)
       CALL EXIT
       END
```

INPUT DATA

```
  105 4095    81   128    50  184   522 511.00001293.60000
          0.     0.     0.     0.     0.     0.     0.
    0.    0.     0.     0.     0.     0.     0.     0.
    0.    0.     0.     0.     0.     0.     0.     0.
    0.    0.     0.     0.     0.     0.     0.     0.
    0.    0.     0.     0.     0.     0.     0.     0.
    0.    0.     0.     0.     0.     0.     0.     0.
    0.    0.     0.     0.     0.     0.     0.     0.
    0.    0.     0.     0.     0.     0.     0.     0.
    0.    0.     0.     0.     0.     0.     0.     0.
    0.    0.     0.     0.     0.     0.     0.     0.
    0. 93902. 91291. 88386. 85751. 83845. 82715. 81988.
81143. 79830. 78034. 76045. 74276. 73039. 72363. 71963.
71408. 70405. 68998. 67506. 66260. 65361. 64667. 63978.
63220. 62462. 61801. 61255. 60770. 60274. 59710. 59006.
58069. 56851. 55431. 54035. 52916. 52194. 51780. 51436.
50939. 50206. 49321. 48461. 47789. 47374. 47166. 47022.
46773. 46318. 45677. 44989. 44423. 44082. 43940. 43874.
43729. 43399. 42875. 42263. 41740. 41583. 41293. 41003.
40713. 40423. 40133. 39842. 39552. 39262. 38972. 38791.
38610. 38429. 38248. 38067. 37886. 37705. 37523. 37342.
37161. 36980. 36799. 36618. 36437. 36256. 36107. 35958.
35808. 35659. 35510. 35360. 35211. 35061. 34912. 34437.
33962. 33486. 33011. 32536. 32171. 31806. 31441. 31076.
.30711. 30345. 29980. 29615. 29250. 28885. 28882. 28879.
28876. 28872. 28869. 28866. 28863. 28860. 28857. 28854.
28850. 28847. 28844. 28841. 28838. 28835. 28831. 28828.
28825. 28822. 28819. 28816. 28813. 28809. 28806. 28803.
28717. 28631. 28544. 28458. 28372. 28285. 28199. 28113.
28027. 27940. 27854. 27768. 27682. 27595. 27509. 27423.
27336. 27250. 27164. 27078. 26991. 26905. 26819. 26698.
26578. 26457. 26337. 26217. 26096. 25976. 25878. 25780.
25683. 25585. 25487. 25389. 25292. 25253. 25214. 25175.
```

25137. 25098. 25059. 24989. 24918. 24848. 24778. 24708.
24637. 24567. 24497. 24427. 24356. 24286. 24216. 24146.
24075. 24005. 23935. 23865. 23794. 23724. 23654. 23584.
23513. 23443. 23373. 23303. 23232. 23150. 23067. 22984.
22901. 22818. 22735. 22652. 22569. 22486. 22437. 22387.
22337. 22287. 22237. 22187. 22137. 22087. 22057. 22026.
21995. 21964. 21934. 21903. 21872. 21802. 21731. 21660.
21589. 21519. 21448. 21377. 21306. 21252. 21198. 21144.
21090. 21036. 20982. 20928. 20874. 20819. 20765. 20711.
20657. 20603. 20549. 20495. 20441. 20387. 20376. 20366.
20356. 20346. 20336. 20326. 20316. 20305. 20296. 20286.
20276. 20266. 20256. 20247. 20237. 20229. 20221. 20214.
20206. 20198. 20190. 20183. 20175. 20167. 20097. 20026.
19955. 19885. 19814. 19743. 19673. 19671. 19669. 19667.
19665. 19664. 19662. 19660. 19658. 19647. 19635. 19623.
19612. 19600. 19589. 19577. 19566. 19554. 19522. 19490.
19458. 19426. 19394. 19362. 19330. 19298. 19279. 19260.
19241. 19222. 19204. 19185. 19166. 19080. 18994. 18907.
18821. 18735. 18648. 18562. 18476. 18389. 18303. 18217.
18130. 18044. 17958. 17871. 17785. 17699. 17612. 17526.
17440. 17353. 17267. 17181. 17094. 17008. 16922. 16835.
16749. 16663. 16576. 16490. 16404. 16317. 16231. 16145.
16059. 15972. 15886. 15800. 15713. 15627. 15542. 15458.
15374. 15289. 15205. 15120. 15036. 14952. 14867. 14786.
14704. 14623. 14541. 14460. 14378. 14297. 14208. 14120.
14031. 13942. 13853. 13765. 13676. 13557. 13584. 13612.
13588. 13515. 13496. 13404. 13312. 13220. 13128. 13036.
12944. 12852. 12760. 12668. 12576. 12484. 12446. 12407.
12369. 12330. 12292. 12253. 12215. 12176. 12138. 12099.
12060. 12022. 11983. 11945. 11906. 11868. 11829. 11801.
11774. 11746. 11718. 11690. 11662. 11634. 11606. 11578.
11550. 11508. 11466. 11424. 11382. 11339. 11297. 11255.
11052. 10850. 10647. 10444. 10242. 10039. 9952. 9865.
9778. 9691. 9604. 9517. 9430. 9343. 9256. 9169.
9169. 9169. 9169. 9168. 9168. 9168. 9168. 9168.
9168. 9168. 9168. 9168. 9168. 9168. 9168. 9167.

9167.	9167.	9167.	9167.	9167.	9167.	9167.	9167.
9167.	9167.	9167.	9167.	9166.	9166.	9166.	9166.
9166.	9166.	9166.	9166.	9166.	9166.	9166.	9166.
9165.	9165.	9165.	9165.	9165.	9165.	9165.	9165.
9165.	9165.	9165.	9165.	9164.	9150.	9135.	9121.
9106.	9092.	9077.	9063.	9048.	9034.	9033.	9033.
9033.	9033.	9033.	9033.	9033.	9033.	9033.	9033.
9031.	9041.	9038.	9000.	8947.	8917.	8928.	8959.
8968.	8928.	8850.	8773.	8760.	8723.	8687.	8651.
8614.	8578.	8542.	8505.	8469.	8433.	8429.	8426.
8422.	8419.	8416.	8412.	8409.	8405.	8368.	8331.
8293.	8256.	8219.	8181.	8144.	8107.	8088.	8069.
8050.	8031.	8012.	7993.	7974.	7930.	7936.	7964.
7977.	7955.	7901.	7843.	7815.	7833.	7880.	7914.
7901.	7845.	7826.	7808.	7790.	7773.	7755.	7737.
7719.	7701.	7683.	7665.	7647.	7616.	7585.	7553.
7522.	7491.	7459.	7428.	7396.	7365.	7334.	7315.
7295.	7276.	7257.	7238.	7219.	7200.	7194.	7187.
7181.	7175.	7168.	7162.	7156.	7150.	7137.	7124.
7111.	7098.	7085.	7073.	7060.	7047.	7033.	7019.
7005.	6991.	6977.	6963.	6949.	6936.	6922.	6908.
6894.	6880.	6866.	6852.	6838.	6824.	6816.	6807.
6799.	6790.	6781.	6773.	6764.	6735.	6739.	6762.
6766.	6738.	6744.	6723.	6702.	6681.	6659.	6638.
6617.	6596.	6575.	6554.	6532.	6511.	6502.	6493.
6484.	6475.	6466.	6457.	6448.	6439.	6430.	6421.
6412.	6403.	6394.	6385.	6375.	6362.	6349.	6336.
6322.	6309.	6296.	6283.	6269.	6256.	6236.	6216.
6197.	6177.	6157.	6137.	6117.	6107.	6097.	6087.
6076.	6066.	6056.	6046.	6021.	6033.	6041.	6036.
6026.	6022.	6026.	6031.	6025.	6008.	5989.	5981.
5984.	5988.	5976.	5946.	5915.	5938.	5926.	5913.
5901.	5889.	5876.	5864.	5852.	5839.	5808.	5827.
5843.	5838.	5809.	5770.	5741.	5734.	5748.	5769.
5780.	5770.	5739.	5699.	5666.	5651.	5648.	5645.
5630.	5602.	5571.	5546.	5531.	5516.	5492.	5460.

5431.	5416.	5410.	5400.	5373.	5330.	5288.	5266.
5262.	5259.	5235.	5190.	5149.	5182.	5164.	5145.
5126.	5108.	5089.	5071.	5012.	5049.	5082.	5079.
5042.	4996.	4965.	4973.	4959.	4944.	4929.	4914.
4899.	4885.	4870.	4855.	4840.	4825.	4810.	4796.
4781.	4766.	4751.	4736.	4722.	4717.	4713.	4709.
4705.	4701.	4696.	4692.	4688.	4684.	4675.	4665.
4656.	4647.	4638.	4628.	4619.	4610.	4599.	4588.
4577.	4566.	4555.	4543.	4532.	4523.	4514.	4505.
4495.	4486.	4477.	4467.	4458.	4449.	4440.	4430.
4421.	4412.	4402.	4393.	4384.	4379.	4373.	4368.
4363.	4358.	4353.	4348.	4343.	4334.	4325.	4316.
4307.	4298.	4290.	4281.	4272.	4263.	4254.	4243.
4232.	4221.	4210.	4199.	4188.	4177.	4177.	4178.
4179.	4179.	4180.	4180.	4181.	4164.	4146.	4129.
4112.	4095.	4078.	4060.	4018.	4033.	4052.	4064.
4068.	4067.	4059.	4044.	4023.	4007.	4006.	4020.
4036.	4035.	4011.	3971.	3937.	3954.	3936.	3917.
3899.	3881.	3862.	3844.	3826.	3807.	3815.	3822.
3829.	3837.	3844.	3852.	3859.	3858.	3856.	3854.
3853.	3851.	3849.	3848.	3846.	3834.	3823.	3811.
3800.	3788.	3776.	3765.	3753.	3742.	3730.	3728.
3727.	3725.	3723.	3722.	3720.	3718.	3717.	3715.
3713.	3712.	3710.	3708.	3707.	3696.	3686.	3675.
3665.	3655.	3644.	3634.	3623.	3613.	3603.	3592.
3574.	3578.	3581.	3574.	3558.	3542.	3540.	3559.
3587.	3603.	3593.	3563.	3533.	3522.	3529.	3541.
3540.	3524.	3506.	3513.	3502.	3491.	3480.	3469.
3458.	3446.	3435.	3424.	3413.	3402.	3391.	3379.
3345.	3367.	3399.	3417.	3412.	3396.	3389.	3402.
3425.	3433.	3412.	3370.	3334.	3351.	3344.	3337.
3330.	3323.	3316.	3309.	3302.	3295.	3287.	3268.
3276.	3286.	3288.	3279.	3262.	3243.	3230.	3227.
3234.	3245.	3252.	3246.	3225.	3199.	3180.	3173.
3172.	3161.	3131.	3088.	3055.	3070.	3073.	3075.
3078.	3081.	3084.	3087.	3090.	3089.	3087.	3086.

3085.	3083.	3082.	3081.	3058.	3077.	3105.	3125.
3126.	3113.	3094.	3074.	3055.	3040.	3033.	3036.
3044.	3044.	3030.	3005.	2985.	3001.	3002.	3004.
3005.	3007.	3008.	3009.	3011.	3012.	2997.	2982.
2968.	2953.	2938.	2923.	2909.	2894.	2889.	2884.
2879.	2874.	2869.	2864.	2860.	2855.	2850.	2851.
2852.	2854.	2855.	2856.	2858.	2841.	2855.	2880.
2901.	2906.	2892.	2862.	2834.	2826.	2845.	2876.
2892.	2877.	2839.	2807.	2822.	2820.	2818.	2816.
2814.	2812.	2811.	2809.	2807.	2805.	2803.	2801.
2799.	2797.	2795.	2774.	2776.	2793.	2812.	2814.
2791.	2753.	2722.	2714.	2727.	2741.	2737.	2714.
2684.	2665.	2664.	2674.	2680.	2679.	2687.	2677.
2667.	2656.	2646.	2636.	2625.	2615.	2605.	2575.
2579.	2601.	2621.	2625.	2614.	2601.	2599.	2613.
2632.	2645.	2646.	2640.	2654.	2650.	2646.	2642.
2638.	2634.	2630.	2626.	2622.	2618.	2614.	2610.
2606.	2602.	2597.	2593.	2589.	2579.	2579.	2584.
2590.	2590.	2579.	2560.	2540.	2527.	2524.	2529.
2537.	2543.	2545.	2542.	2537.	2530.	2522.	2515.
2508.	2504.	2516.	2509.	2502.	2494.	2487.	2480.
2472.	2465.	2458.	2451.	2443.	2442.	2440.	2438.
2437.	2435.	2434.	2432.	2431.	2429.	2412.	2425.
2439.	2438.	2422.	2401.	2391.	2399.	2421.	2441.
2447.	2439.	2438.	2428.	2417.	2407.	2396.	2386.
2376.	2365.	2355.	2345.	2334.	2331.	2327.	2324.
2320.	2317.	2314.	2310.	2307.	2303.	2300.	2297.
2294.	2291.	2288.	2285.	2282.	2283.	2284.	2284.
2285.	2286.	2287.	2288.	2288.	2285.	2283.	2280.
2277.	2274.	2271.	2268.	2265.	2262.	2259.	2256.
2253.	2251.	2248.	2245.	2222.	2225.	2243.	2261.
2264.	2254.	2255.	2257.	2260.	2263.	2265.	2268.
2270.	2273.	2260.	2268.	2293.	2308.	2295.	2261.
2228.	2214.	2216.	2215.	2203.	2185.	2177.	2184.
2196.	2200.	2195.	2190.	2195.	2210.	2223.	2222.
2206.	2184.	2168.	2164.	2170.	2179.	2181.	2175.

2162.	2147.	2133.	2122.	2116.	2114.	2116.	2120.
2121.	2116.	2106.	2097.	2095.	2107.	2130.	2155.
2170.	2167.	2151.	2133.	2125.	2127.	2132.	2131.
2124.	2132.	2126.	2120.	2114.	2108.	2102.	2096.
2090.	2084.	2078.	2072.	2049.	2059.	2075.	2087.
2092.	2093.	2090.	2081.	2067.	2052.	2060.	2055.
2050.	2045.	2040.	2035.	2030.	2025.	2020.	2015.
2010.	2005.	2000.	1995.	1971.	1978.	1997.	2014.
2018.	2013.	2005.	2001.	2002.	2006.	2012.	2016.
2015.	2007.	1988.	1960.	1931.	1913.	1913.	1927.
1944.	1954.	1951.	1941.	1933.	1932.	1936.	1940.
1937.	1928.	1918.	1916.	1925.	1942.	1957.	1959.
1947.	1927.	1911.	1908.	1917.	1929.	1936.	1939.
1940.	1942.	1945.	1945.	1937.	1918.	1893.	1870.
1873.	1875.	1876.	1877.	1879.	1880.	1882.	1883.
1885.	1886.	1887.	1889.	1890.	1873.	1875.	1897.
1916.	1911.	1881.	1844.	1840.	1840.	1840.	1841.
1841.	1841.	1841.	1841.	1842.	1842.	1842.	1842.
1842.	1842.	1843.	1843.	1843.	1843.	1843.	1844.
1844.	1844.	1844.	1844.	1844.	1845.	1845.	1845.
1837.	1841.	1843.	1830.	1804.	1779.	1787.	1788.
1788.	1788.	1789.	1789.	1789.	1790.	1790.	1791.
1791.	1791.	1792.	1792.	1792.	1790.	1788.	1786.
1784.	1782.	1780.	1778.	1776.	1755.	1762.	1778.
1792.	1794.	1783.	1765.	1750.	1743.	1745.	1748.
1746.	1737.	1741.	1741.	1740.	1740.	1739.	1739.
1739.	1738.	1738.	1737.	1737.	1719.	1720.	1738.
1760.	1772.	1770.	1755.	1734.	1714.	1698.	1690.
1687.	1686.	1683.	1679.	1686.	1685.	1683.	1681.
1680.	1678.	1677.	1675.	1673.	1672.	1670.	1669.
1667.	1665.	1664.	1662.	1663.	1664.	1664.	1665.
1665.	1666.	1667.	1667.	1668.	1656.	1660.	1671.
1680.	1677.	1661.	1641.	1643.	1645.	1647.	1649.
1651.	1653.	1655.	1657.	1659.	1661.	1663.	1665.
1667.	1658.	1664.	1673.	1676.	1674.	1676.	1683.
1687.	1679.	1658.	1631.	1612.	1608.	1618.	1635.

1646.	1645.	1634.	1622.	1617.	1623.	1635.	1642.
1638.	1621.	1593.	1562.	1539.	1530.	1540.	1562.
1586.	1596.	1589.	1570.	1555.	1556.	1573.	1593.
1602.	1593.	1571.	1549.	1536.	1532.	1536.	1544.
1555.	1566.	1576.	1581.	1579.	1571.	1561.	1554.
1556.	1565.	1573.	1572.	1556.	1534.	1518.	1517.
1523.	1523.	1512.	1493.	1496.	1495.	1494.	1492.
1491.	1490.	1489.	1488.	1487.	1486.	1485.	1484.
1483.	1481.	1480.	1479.	1463.	1469.	1480.	1489.
1490.	1488.	1488.	1490.	1490.	1485.	1477.	1473.
1479.	1494.	1509.	1514.	1508.	1494.	1482.	1477.
1480.	1484.	1479.	1465.	1448.	1438.	1443.	1457.
1470.	1470.	1456.	1435.	1434.	1433.	1432.	1431.
1430.	1429.	1428.	1427.	1426.	1425.	1424.	1423.
1422.	1421.	1420.	1419.	1418.	1407.	1409.	1416.
1423.	1431.	1438.	1442.	1444.	1442.	1441.	1441.
1441.	1436.	1422.	1399.	1375.	1358.	1355.	1366.
1384.	1400.	1406.	1401.	1391.	1388.	1397.	1412.
1421.	1414.	1389.	1359.	1339.	1350.	1350.	1350.
1350.	1350.	1349.	1349.	1349.	1349.	1349.	1348.
1348.	1348.	1348.	1339.	1342.	1348.	1355.	1362.
1363.	1355.	1341.	1328.	1324.	1331.	1345.	1358.
1365.	1364.	1358.	1350.	1358.	1358.	1359.	1360.
1361.	1361.	1362.	1363.	1364.	1364.	1365.	1366.
1367.	1368.	1368.	1369.	1370.	1365.	1361.	1357.
1353.	1348.	1344.	1340.	1336.	1331.	1327.	1323.
1318.	1317.	1315.	1313.	1311.	1310.	1308.	1306.
1304.	1302.	1301.	1299.	1297.	1295.	1293.	1275.
1289.	1305.	1309.	1300.	1284.	1293.	1290.	1286.
1283.	1280.	1277.	1273.	1270.	1267.	1264.	1260.
1257.	1254.	1251.	1247.	1244.	1241.	1238.	1235.
1221.	1226.	1238.	1249.	1255.	1254.	1253.	1259.
1271.	1281.	1284.	1279.	1275.	1276.	1278.	1273.
1256.	1231.	1210.	1215.	1217.	1219.	1221.	1223.
1224.	1226.	1228.	1230.	1232.	1234.	1235.	1237.
1239.	1241.	1243.	1244.	1246.	1241.	1244.	1252.

1260.	1258.	1243.	1220.	1197.	1187.	1193.	1209.
1227.	1239.	1243.	1243.	1241.	1238.	1233.	1227.
1224.	1224.	1229.	1237.	1242.	1243.	1241.	1239.
1242.	1252.	1263.	1269.	1267.	1260.	1253.	1250.
1246.	1240.	1229.	1217.	1210.	1211.	1219.	1227.
1229.	1221.	1206.	1192.	1189.	1197.	1206.	1204.
1186.	1161.	1155.	1158.	1161.	1164.	1167.	1170.
1173.	1176.	1179.	1182.	1185.	1174.	1181.	1195.
1205.	1202.	1186.	1167.	1156.	1158.	1166.	1173.
1174.	1171.	1168.	1168.	1172.	1178.	1184.	1189.
1188.	1181.	1168.	1155.	1148.	1154.	1152.	1149.
1147.	1144.	1141.	1139.	1136.	1134.	1131.	1128.
1125.	1126.	1123.	1111.	1096.	1090.	1098.	1116.
1133.	1140.	1137.	1139.	1140.	1141.	1143.	1144.
1145.	1146.	1147.	1148.	1149.	1150.	1151.	1152.
1153.	1154.	1155.	1156.	1157.	1150.	1159.	1169.
1155.	1121.	1090.	1093.	1095.	1096.	1098.	1099.
1101.	1103.	1104.	1106.	1107.	1109.	1110.	1112.
1114.	1115.	1117.	1118.	1120.	1121.	1122.	1124.
1125.	1126.	1127.	1129.	1130.	1131.	1133.	1134.
1135.	1136.	1138.	1139.	1140.	1142.	1143.	1144.
1136.	1140.	1160.	1171.	1165.	1147.	1125.	1107.
1095.	1090.	1099.	1094.	1090.	1085.	1080.	1076.
1071.	1067.	1062.	1057.	1053.	1048.	1049.	1050.
1052.	1053.	1054.	1055.	1056.	1058.	1059.	1060.
1061.	1062.	1064.	1065.	1066.	1067.	1068.	1070.
1071.	1072.	1073.	1075.	1076.	1077.	1078.	1079.
1081.	1082.	1083.	1084.	1085.	1083.	1080.	1077.
1074.	1071.	1068.	1066.	1063.	1060.	1056.	1051.
1047.	1043.	1038.	1034.	1030.	1025.	1027.	1029.
1031.	1032.	1034.	1036.	1038.	1039.	1041.	1043.
1044.	1046.	1048.	1050.	1051.	1053.	1054.	1054.
1055.	1056.	1056.	1057.	1058.	1057.	1056.	1055.
1055.	1054.	1053.	1052.	1051.	1051.	1036.	1045.
1057.	1065.	1064.	1055.	1041.	1027.	1023.	1031.
1046.	1057.	1055.	1036.	1012.	1008.	1007.	1006.

1005.	1004.	1003.	1002.	1001.	1000.	999.	998.
997.	996.	995.	994.	980.	985.	1009.	1032.
1039.	1027.	1007.	997.	999.	1004.	1000.	983.
967.	974.	974.	974.	974.	974.	974.	974.
974.	974.	974.	974.	974.	974.	974.	974.
974.	974.	974.	973.	973.	962.	966.	983.
997.	998.	996.	991.	987.	982.	978.	973.
969.	964.	960.	955.	951.	946.	942.	938.
933.	929.	917.	918.	924.	932.	941.	946.
946.	939.	928.	919.	917.	925.	939.	952.
957.	950.	936.	924.	924.	938.	958.	974.
982.	982.	977.	969.	960.	968.	963.	959.
954.	949.	945.	940.	936.	931.	927.	922.
918.	913.	908.	904.	887.	892.	905.	919.
926.	925.	916.	905.	896.	891.	888.	886.
885.	886.	889.	895.	898.	898.	897.	899.
906.	914.	916.	911.	911.	910.	908.	907.
906.	904.	903.	901.	900.	892.	896.	900.
902.	903.	905.	908.	909.	908.	907.	905.
903.	897.	886.	873.	862.	859.	864.	874.
880.	880.	875.	869.	874.	873.	872.	871.
870.	869.	867.	866.	865.	864.	860.	856.
852.	848.	844.	841.	837.	833.	829.	823.
824.	824.	828.	828.	827.	826.	825.	824.
823.	822.	821.	811.	815.	832.	851.	861.
861.	853.	845.	853.	849.	845.	841.	837.
833.	829.	825.	821.	817.	813.	809.	797.
799.	808.	810.	799.	780.	776.	775.	775.
774.	774.	773.	772.	772.	771.	770.	770.
769.	768.	768.	767.	766.	766.	765.	764.
763.	762.	761.	760.	759.	758.	749.	756.
762.	760.	753.	749.	753.	765.	780.	793.
796.	789.	779.	772.	774.	782.	790.	795.
796.	796.	796.	791.	780.	769.	776.	776.
776.	776.	775.	775.	775.	775.	775.	774.
774.	774.	774.	774.	773.	773.	773.	773.

770.	771.	769.	763.	754.	748.	748.	753.
760.	763.	759.	751.	743.	740.	745.	755.
763.	765.	756.	740.	724.	726.	727.	729.
730.	732.	733.	735.	736.	738.	739.	741.
742.	744.	745.	747.	748.	750.	751.	753.
754.	756.	757.	747.	756.	767.	769.	760.
745.	735.	734.	741.	746.	748.	745.	742.
742.	745.	750.	757.	764.	770.	775.	776.
774.	769.	765.	762.	760.	758.	756.	755.
755.	756.	754.	748.	738.	731.	737.	737.
737.	737.	738.	738.	738.	739.	739.	739.
739.	740.	740.	731.	732.	742.	751.	754.
749.	742.	737.	737.	743.	753.	763.	768.
764.	751.	733.	721.	721.	732.	745.	749.
740.	723.	708.	715.	715.	715.	716.	716.
717.	717.	717.	718.	718.	718.	719.	719.
720.	720.	720.	721.	721.	721.	722.	722.
723.	723.	723.	724.	724.	724.	725.	725.
726.	726.	726.	727.	727.	727.	728.	728.
727.	727.	727.	726.	726.	726.	725.	725.
726.	727.	728.	730.	731.	732.	733.	734.
735.	736.	737.	739.	740.	741.	742.	743.
744.	745.	746.	748.	749.	750.	751.	752.
753.	754.	755.	757.	758.	759.	760.	761.
762.	764.	765.	766.	767.	768.	769.	771.
772.	773.	774.	775.	766.	771.	780.	791.
800.	802.	796.	785.	776.	772.	778.	787.
792.	788.	777.	767.	765.	770.	777.	782.
787.	795.	805.	811.	806.	790.	773.	769.
781.	802.	818.	817.	805.	795.	796.	810.
823.	823.	809.	789.	775.	770.	773.	775.
775.	773.	772.	771.	767.	759.	749.	742.
739.	741.	745.	749.	755.	763.	768.	770.
765.	755.	743.	730.	719.	722.	720.	718.
716.	714.	713.	711.	709.	707.	707.	708.
708.	708.	709.	709.	709.	710.	710.	710.

711.	711.	711.	712.	712.	712.	712.	713.
713.	713.	714.	714.	714.	715.	715.	715.
716.	716.	716.	717.	717.	717.	718.	718.
718.	718.	719.	719.	719.	720.	720.	720.
721.	721.	721.	722.	722.	722.	723.	723.
723.	723.	724.	724.	724.	725.	725.	725.
726.	726.	726.	727.	727.	727.	719.	732.
749.	755.	746.	731.	734.	730.	726.	722.
718.	713.	709.	705.	701.	699.	698.	696.
694.	693.	691.	689.	688.	686.	684.	683.
681.	679.	678.	665.	670.	679.	685.	682.
673.	663.	657.	655.	655.	657.	658.	658.
655.	646.	634.	622.	615.	616.	623.	634.
642.	645.	643.	640.	638.	639.	641.	643.
645.	646.	644.	638.	628.	617.	608.	607.
613.	622.	628.	630.	628.	628.	630.	632.
629.	622.	614.	612.	618.	629.	639.	643.
641.	644.	639.	634.	629.	624.	619.	614.
609.	605.	600.	595.	590.	585.	580.	575.
570.	565.	560.	556.	551.	546.	541.	536.
531.	526.	521.	516.	511.	507.	494.	497.
505.	510.	505.	494.	484.	480.	484.	490.
493.	488.	478.	466.	456.	452.	452.	453.
452.	448.	444.	441.	440.	440.	440.	436.
428.	416.	403.	393.	388.	390.	397.	404.
407.	405.	398.	389.	382.	378.	379.	382.
385.	385.	383.	382.	385.	391.	398.	401.
397.	386.	371.	359.	361.	360.	359.	357.
356.	354.	353.	351.	350.	348.	347.	346.
344.	343.	341.	340.	338.	337.	336.	334.
333.	331.	330.	328.	326.	327.	323.	316.
313.	316.	323.	327.	324.	316.	309.	309.
317.	329.	337.	336.	325.	312.	309.	308.
306.	305.	304.	302.	301.	300.	298.	297.
295.	294.	293.	291.	290.	285.	285.	289.
291.	291.	287.	282.	279.	280.	284.	287.

286.	280.	273.	267.	265.	265.	266.	268.
271.	276.	280.	283.	284.	282.	277.	271.
267.	267.	271.	275.	275.	270.	263.	256.
253.	254.	255.	255.	253.	251.	251.	255.
261.	267.	269.	263.	251.	239.	235.	243.
259.	273.	276.	269.	259.	256.	259.	264.
263.	258.	251.	247.	248.	250.	251.	250.
247.	241.	232.	223.	216.	214.	219.	224.
225.	220.	210.	200.	194.	192.	193.	194.
193.	189.	184.	182.	185.	191.	196.	195.
190.	184.	189.	187.	186.	185.	183.	182.
180.	179.	178.	176.	175.	174.	172.	171.
170.	168.	167.	166.	164.	162.	160.	158.
155.	153.	151.	149.	147.	144.	142.	140.
138.	135.	129.	131.	135.	138.	138.	132.
124.	115.	109.	106.	107.	110.	114.	117.
119.	119.	117.	114.	110.	108.	107.	109.
112.	115.	116.	115.	113.	111.	109.	108.
106.	102.	97.	93.	92.	95.	99.	103.
103.	101.	97.	94.	97.	96.	95.	95.
94.	94.	93.	93.	92.	92.	91.	91.
90.	90.	89.	89.	88.	88.	87.	86.
86.	85.	85.	84.	84.	80.	82.	85.
87.	86.	84.	83.	85.	89.	91.	91.
88.	85.	83.	83.	86.	89.	90.	89.
89.	88.	88.	88.	87.	87.	86.	86.
86.	85.	85.	81.	82.	84.	87.	89.
90.	88.	85.	82.	80.	79.	80.	80.
78.	76.	75.	75.	76.	75.	74.	74.
76.	81.	83.	82.	78.	73.	72.	73.
75.	75.	74.	72.	71.	73.	75.	76.
75.	72.	69.	67.	67.	70.	73.	77.
79.	77.	74.	77.	76.	75.	75.	74.
73.	72.	72.	71.	70.	70.	69.	68.
67.	67.	66.	65.	65.	64.	63.	59.
61.	66.	70.	73.	74.	75.	77.	79.

78.	75.	70.	66.	67.	72.	80.	86.
88.	85.	79.	75.	73.	74.	74.	73.
72.	70.	70.	70.	70.	69.	69.	69.
69.	68.	67.	65.	65.	67.	71.	73.
73.	70.	66.	62.	61.	65.	71.	75.
75.	72.	68.	65.	65.	67.	69.	69.
70.	69.	69.	69.	70.	73.	76.	79.
79.	75.	69.	64.	64.	67.	72.	76.
76.	72.	67.	62.	59.	59.	62.	64.
65.	65.	65.	65.	66.	65.	64.	61.
60.	60.	62.	64.	66.	67.	66.	64.
65.	66.	68.	69.	69.	68.	68.	68.
68.	66.	64.	64.	67.	71.	75.	73.
67.	61.	58.	59.	62.	65.	66.	65.
63.	61.	61.	62.	63.	63.	63.	62.
61.	62.	64.	66.	67.	66.	64.	62.
60.	59.	58.	58.	59.	60.	60.	58.
55.	52.	52.	53.	54.	53.	51.	50.
51.	53.	54.	54.	53.	53.	53.	53.
53.	53.	53.	52.	52.	52.	52.	52.
52.	51.	51.	51.	51.	51.	51.	50.
50.	50.	50.	50.	50.	47.	49.	51.
52.	52.	53.	53.	53.	54.	55.	54.
52.	50.	48.	49.	52.	57.	60.	60.
58.	54.	50.	53.	52.	52.	51.	51.
50.	50.	49.	49.	48.	48.	47.	47.
47.	46.	46.	44.	45.	45.	45.	44.
44.	44.	43.	44.	44.	45.	44.	43.
41.	39.	39.	40.	42.	44.	45.	44.
41.	37.	34.	34.	36.	39.	42.	42.
39.	36.	34.	35.	39.	45.	49.	50.
49.	45.	42.	41.	41.	42.	44.	45.
44.	41.	36.	31.	31.	31.	31.	31.
31.	32.	32.	32.	30.	30.	34.	38.
40.	39.	36.	34.	33.	33.	33.	33.
32.	32.	34.	36.	38.	40.	39.	38.

37.	37.	37.	37.	37.	38.	40.	41.
41.	39.	37.	36.	38.	41.	43.	43.
40.	36.	33.	33.	33.	33.	33.	32.
32.	31.	31.	30.	29.	27.	26.	27.
28.	28.	25.	23.	21.	22.	25.	27.
27.	26.	25.	25.	27.	30.	31.	31.
29.	30.	29.	29.	28.	28.	27.	27.
26.	26.	25.	25.	24.	24.	23.	23.
22.	22.	19.	20.	21.	23.	24.	24.
25.	25.	25.	24.	23.	22.	21.	21.
21.	20.	19.	18.	19.	19.	19.	19.
19.	19.	19.	19.	19.	19.	19.	19.
20.	20.	20.	20.	20.	20.	20.	20.
20.	20.	20.	19.	18.	16.	15.	14.
14.	14.	14.	15.	15.	16.	18.	20.
20.	19.	17.	14.	12.	12.	13.	15.
16.	17.	16.	15.	14.	14.	14.	15.
17.	18.	19.	20.	20.	20.	19.	17.
15.	14.	14.	14.	15.	15.	14.	13.
12.	11.	12.	12.	12.	11.	9.	8.
8.	10.	13.	16.	17.	17.	15.	13.
11.	10.	10.	9.	9.	10.	11.	13.
14.	14.	13.	10.	9.	8.	10.	12.
14.	14.	14.	13.	12.	12.	12.	12.
12.	12.	14.	17.	20.	21.	19.	16.
13.	11.	11.	13.	15.	15.	14.	11.
10.	10.	11.	12.	11.	10.	10.	10.
11.	12.	11.	10.	8.	7.	7.	8.
10.	11.	10.	8.	5.	4.	5.	8.
10.	10.	8.	6.	4.	4.	5.	6.
5.	5.	4.	4.	5.	7.	8.	9.
9.	9.	7.	6.	6.	6.	7.	8.
8.	8.	6.	5.	4.	4.	5.	7.
7.	7.	6.	4.	4.	4.	4.	6.
8.	8.	8.	7.	7.	8.	10.	13.
14.	13.	10.	6.	3.	3.	5.	6.

7.	6.	4.	2.	1.	2.	3.	5.
6.	6.	4.	3.	2.	3.	4.	5.
6.	7.	6.	5.	4.	4.	5.	8.
10.	10.	7.	5.	5.	4.	4.	4.
3.	3.	2.	2.	1.	2.	2.	7.
10.	8.	3.	2.	5.	3.	3.	11.
15.	13.	5.	4.	9.	7.	1.	2.
3.	3.	4.	7.	12.	8.	3.	3.
3.	2.	2.	2.	3.	3.	3.	3.
2.	1.	0.	2.	3.	4.	5.	5.
4.	4.	4.	6.	9.	11.	14.	15.
16.	18.	19.	0.	0.	0.	0.	0.

OUTPUT DATA

PARAMETERS AND INPUT DATA FOR RUN 105 4095 CHANNELS

LOW CHANNEL NUMBER WHICH BEGINS ANALYSIS (IMAX) 81
DIMENSION OF MATRIX 80
ENERGY PER CHANNEL NUMBER (KEV)2.31538
CALIBRATION 1 CH= 184 E= 511.00
CALIBRATION 2 CH= 522 E=1293.60
NUMBER OF ITERATION PERFORMED 128

THE MEASURED COMPTON CONTINUUM VECTOR

0.63536E 05 0.38270E 05 0.28850E 05 0.25258E 05 0.21883E 05 0.20011E 05
0.18160E 05 0.14130E 05 0.11007E 05 0.91663E 04 0.88160E 04 0.78077E 04
0.69780E 04 0.63519E 04 0.58221E 04 0.50254E 04 0.44872E 04 0.40780E 04
0.37547E 04 0.34651E 04 0.31670E 04 0.29353E 04 0.27542E 04 0.25898E 04
0.24171E 04 0.22723E 04 0.21684E 04 0.20497E 04 0.19216E 04 0.18395E 04
0.17592E 04 0.16671E 04 0.16044E 04 0.15066E 04 0.14335E 04 0.13616E 04
0.13238E 04 0.12461E 04 0.12310E 04 0.11654E 04 0.11271E 04 0.11063E 04
0.10596E 04 0.10372E 04 0.98354E 03 0.93907E 03 0.89929E 03 0.84662E 03
0.77717E 03 0.76796E 03 0.74971E 03 0.73797E 03 0.72536E 03 0.76558E 03
0.77383E 03 0.71387E 03 0.71419E 03 0.63904E 03 0.54737E 03 0.38979E 03
0.31334E 03 0.26655E 03 0.20870E 03 0.13037E 03 0.90380E 02 0.81267E 02
0.71420E 02 0.71087E 02 0.66027E 02 0.58060E 02 0.51473E 02 0.42333E 02
0.35747E 02 0.26747E 02 0.19407E 02 0.14573E 02 0.12360E 02 0.65867E 01
0.59067E 01 0.43067E 01

OUTPUT DATA

THE ENERGY ARRAY OF PHOTON IN KEV

0.49943E 03 0.62776E 03 0.75269E 03 0.87549E 03 0.99685E 03 0.11172E 04
0.12368E 04 0.13558E 04 0.14743E 04 0.15925E 04 0.17104E 04 0.18280E 04
0.19455E 04 0.20627E 04 0.21799E 04 0.22969E 04 0.24137E 04 0.25305E 04
0.26473E 04 0.27639E 04 0.28805E 04 0.29970E 04 0.31134E 04 0.32299E 04
0.33462E 04 0.34626E 04 0.35789E 04 0.36951E 04 0.38114E 04 0.39276E 04
0.40438E 04 0.41600E 04 0.42761E 04 0.43922E 04 0.45083E 04 0.46244E 04
0.47405E 04 0.48566E 04 0.49726E 04 0.50887E 04 0.52047E 04 0.53207E 04
0.54367E 04 0.55527E 04 0.56687E 04 0.57847E 04 0.59007E 04 0.60166E 04
0.61326E 04 0.62485E 04 0.63645E 04 0.64804E 04 0.65964E 04 0.67123E 04
0.68282E 04 0.69441E 04 0.70600E 04 0.71760E 04 0.72919E 04 0.74078E 04
0.75237E 04 0.76395E 04 0.77554E 04 0.78713E 04 0.79872E 04 0.81031E 04
0.82190E 04 0.83348E 04 0.84507E 04 0.85666E 04 0.86824E 04 0.87983E 04
0.89142E 04 0.90300E 04 0.91459E 04 0.92617E 04 0.93776E 04 0.94934E 04
0.96093E 04 0.97251E 04

THE UPPER TRIANGULAR RESPONSE MATRIX

I = 1

0.43571E 00 0.93011E-01 0.59835E-01 0.45710E-01 0.36446E-01 0.29734E-01
0.24689E-01 0.20806E-01 0.17759E-01 0.15329E-01 0.13361E-01 0.11747E-01
0.10407E-01 0.92826E-02 0.83308E-02 0.75178E-02 0.68180E-02 0.62114E-02
0.56823E-02 0.52178E-02 0.48081E-02 0.44448E-02 0.41212E-02 0.38315E-02
0.35715E-02 0.33371E-02 0.31248E-02 0.29324E-02 0.27571E-02 0.25971E-02
0.24506E-02 0.23163E-02 0.21926E-02 0.20786E-02 0.19732E-02 0.18758E-02
0.17853E-02 0.17012E-02 0.16229E-02 0.15500E-02 0.14818E-02 0.14180E-02
0.13583E-02 0.13022E-02 0.12496E-02 0.12001E-02 0.11534E-02 0.11095E-02
0.10680E-02 0.10288E-02 0.99171E-03 0.95661E-03 0.92331E-03 0.89175E-03
0.86178E-03 0.83329E-03 0.80616E-03 0.78033E-03 0.75578E-03 0.73234E-03
0.70998E-03 0.68862E-03 0.66821E-03 0.64872E-03 0.63004E-03 0.61214E-03
0.59503E-03 0.57859E-03 0.56286E-03 0.54773E-03 0.53330E-03 0.51926E-03
0.50594E-03 0.49299E-03 0.48063E-03 0.46867E-03 0.45720E+03 0.44607E-03
0.43542E-03 0.42506E-03

I = 2

0.26677E 00 0.73779E-01 0.47049E-01 0.36148E-01 0.29287E-01 0.24320E-01
0.20530E-01 0.17556E-01 0.15179E-01 0.13249E-01 0.11662E-01 0.10341E-01
0.92315E-02 0.82904E-02 0.74855E-02 0.67919E-02 0.61901E-02 0.56647E-02
0.52032E-02 0.47959E-02 0.44345E-02 0.41124E-02 0.38241E-02 0.35650E-02
0.33315E-02 0.31200E-02 0.29282E-02 0.27534E-02 0.25939E-02 0.24477E-02
0.23137E-02 0.21904E-02 0.20766E-02 0.19714E-02 0.18742E-02 0.17838E-02
0.16999E-02 0.16217E-02 0.15489E-02 0.14808E-02 0.14171E-02 0.13575E-02
0.13015E-02 0.12489E-02 0.11994E-02 0.11528E-02 0.11090E-02 0.10675E-02
0.10284E-02 0.99129E-03 0.95622E-03 0.92295E-03 0.89141E-03 0.86146E-03
0.83299E-03 0.80588E-03 0.78008E-03 0.75554E-03 0.73212E-03 0.70976E-03
0.68842E-03 0.66802E-03 0.64854E-03 0.62988E-03 0.61199E-03 0.59489E-03
0.57846E-03 0.56273E-03 0.54760E-03 0.53318E-03 0.51915E-03 0.50584E-03
0.49289E-03 0.48054E-03 0.46858E-03 0.45712E-03 0.44599E-03 0.43534E-03
0.42499E-03

I = 3

0.19113E 00 0.61874E-01 0.39332E-01 0.30141E-01 0.24566E-01 0.20592E-01
0.17560E-01 0.15165E-01 0.13231E-01 0.11645E-01 0.10327E-01 0.92193E-02
0.82804E-02 0.74773E-02 0.67852E-02 0.61846E-02 0.56602E-02 0.51995E-02
0.47928E-02 0.44319E-02 0.41102E-02 0.38222E-02 0.35634E-02 0.33302E-02
0.31189E-02 0.29272E-02 0.27526E-02 0.25931E-02 0.24471E-02 0.23132E-02
0.21899E-02 0.20761E-02 0.19710E-02 0.18738E-02 0.17835E-02 0.16996E-02
0.16215E-02 0.15487E-02 0.14806E-02 0.14169E-02 0.13573E-02 0.13013E-02
0.12488E-02 0.11993E-02 0.11527E-02 0.11089E-02 0.10674E-02 0.10283E-02
0.99121E-03 0.95615E-03 0.92288E-03 0.89135E-03 0.86140E-03 0.83294E-03
0.80584E-03 0.78003E-03 0.75550E-03 0.73208E-03 0.70973E-03 0.68839E-03
0.66799E-03 0.64851E-03 0.62985E-03 0.61196E-03 0.59486E-03 0.57843E-03
0.56271E-03 0.54758E-03 0.53317E-03 0.51914E-03 0.50582E-03 0.49288E-03
0.48052E-03 0.46856E-03 0.45711E-03 0.44597E-03 0.43533E-03 0.42498E-03

I = 4

0.14869E 00 0.53625E-01 0.34133E-01 0.26044E-01 0.21251E-01 0.17897E-01
0.15356E-01 0.13348E-01 0.11722E-01 0.10380E-01 0.92575E-02 0.83088E-02
0.74990E-02 0.68022E-02 0.61982E-02 0.56712E-02 0.52085E-02 0.48003E-02
0.44382E-02 0.41155E-02 0.38267E-02 0.35674E-02 0.33336E-02 0.31218E-02
0.29298E-02 0.27549E-02 0.25951E-02 0.24489E-02 0.23148E-02 0.21913E-02
0.20774E-02 0.19721E-02 0.18748E-02 0.17845E-02 0.17005E-02 0.16223E-02
0.15494E-02 0.14813E-02 0.14175E-02 0.13578E-02 0.13018E-02 0.12493E-02

0.11998E-02 0.11531E-02 0.11093E-02 0.10677E-02 0.10286E-02 0.99150E-03
0.95642E-03 0.92313E-03 0.89158E-03 0.86162E-03 0.83315E-03 0.80603E-03
0.78021E-03 0.75567E-03 0.73224E-03 0.70988E-03 0.68853E-03 0.66813E-03
0.64864E-03 0.62997E-03 0.61207E-03 0.59497E-03 0.57853E-03 0.56281E-03
0.54767E-03 0.53325E-03 0.51922E-03 0.50590E-03 0.49295E-03 0.48059E-03
0.46863E-03 0.45717E-03 0.44603E-03 0.43539E-03 0.42503E-03

I = 5

0.12165E 00 0.47496E-01 0.30356E-01 0.23070E-01 0.18808E-01 0.15871E-01
0.13666E-01 0.11931E-01 0.10525E-01 0.93619E-02 0.83865E-02 0.75583E-02
0.68485E-02 0.62349E-02 0.57008E-02 0.52327E-02 0.48203E-02 0.44549E-02
0.41296E-02 0.38387E-02 0.35776E-02 0.33424E-02 0.31294E-02 0.29364E-02
0.27607E-02 0.26002E-02 0.24534E-02 0.23187E-02 0.21948E-02 0.20806E-02
0.19750E-02 0.18774E-02 0.17868E-02 0.17025E-02 0.16242E-02 0.15511E-02
0.14829E-02 0.14189E-02 0.13592E-02 0.13030E-02 0.12504E-02 0.12008E-02
0.11541E-02 0.11101E-02 0.10685E-02 0.10293E-02 0.99218E-03 0.95705E-03
0.92372E-03 0.89213E-03 0.86213E-03 0.83362E-03 0.80647E-03 0.78063E-03
0.75606E-03 0.73260E-03 0.71022E-03 0.68885E-03 0.66843E-03 0.64892E-03
0.63024E-03 0.61233E-03 0.59521E-03 0.57876E-03 0.56302E-03 0.54788E-03
0.53344E-03 0.51940E-03 0.50607E-03 0.49312E-03 0.48075E-03 0.46878E-03
0.45731E-03 0.44617E-03 0.43552E-03 0.42516E-03

I = 6

0.10294E 00 0.42728E-01 0.27459E-01 0.20805E-01 0.16934E-01 0.14296E-01
0.12334E-01 0.10798E-01 0.95560E-02 0.85290E-02 0.76658E-02 0.69315E-02
0.63003E-02 0.57531E-02 0.52751E-02 0.48551E-02 0.44838E-02 0.41539E-02
0.38592E-02 0.35950E-02 0.33573E-02 0.31423E-02 0.29476E-02 0.27704E-02
0.26088E-02 0.24609E-02 0.23254E-02 0.22008E-02 0.20859E-02 0.19797E-02
0.18816E-02 0.17906E-02 0.17060E-02 0.16273E-02 0.15539E-02 0.14854E-02
0.14213E-02 0.13613E-02 0.13050E-02 0.12522E-02 0.12024E-02 0.11556E-02
0.11115E-02 0.10698E-02 0.10305E-02 0.99328E-03 0.95807E-03 0.92467E-03
0.89301E-03 0.86296E-03 0.83439E-03 0.80719E-03 0.78130E-03 0.75668E-03
0.73319E-03 0.71077E-03 0.68937E-03 0.66891E-03 0.64938E-03 0.63067E-03
0.61273E-03 0.59559E-03 0.57912E-03 0.56336E-03 0.54820E-03 0.53375E-03
0.51969E-03 0.50634E-03 0.49337E-03 0.48099E-03 0.46901E-03 0.45753E-03
0.44638E-03 0.43572E-03 0.42535E-03

I = 7

0.89245E-01 0.38890E-01 0.25147E-01 0.19014E-01 0.15449E-01 0.13039E-01

0.11260E-01 0.98754E-02 0.87588E-02 0.78365E-02 0.70616E-02 0.64016E-02
0.58334E-02 0.53398E-02 0.49078E-02 0.45273E-02 0.41901E-02 0.38896E-02
0.36208E-02 0.33793E-02 0.31613E-02 0.29640E-02 0.27847E-02 0.26212E-02
0.24718E-02 0.23350E-02 0.22093E-02 0.20934E-02 0.19864E-02 0.18877E-02
0.17960E-02 0.17109E-02 0.16317E-02 0.15579E-02 0.14890E-02 0.14246E-02
0.13643E-02 0.13077E-02 0.12547E-02 0.12047E-02 0.11577E-02 0.11135E-02
0.10716E-02 0.10322E-02 0.99483E-03 0.95950E-03 0.92600E-03 0.89425E-03
0.86410E-03 0.83546E-03 0.80819E-03 0.78223E-03 0.75756E-03 0.73401E-03
0.71154E-03 0.69009E-03 0.66959E-03 0.65001E-03 0.63126E-03 0.61329E-03
0.59612E-03 0.57962E-03 0.56383E-03 0.54864E-03 0.53417E-03 0.52009E-03
0.50672E-03 0.49373E-03 0.48133E-03 0.46933E-03 0.45784E-03 0.44667E-03
0.43599E-03 0.42561E-03

I = 8

0.78783E-01 0.35723E-01 0.23247E-01 0.17556E-01 0.14241E-01 0.12012E-01
0.10377E-01 0.91100E-02 0.80921E-02 0.72532E-02 0.65488E-02 0.59487E-02
0.54317E-02 0.49822E-02 0.45881E-02 0.42405E-02 0.39318E-02 0.36564E-02
0.34095E-02 0.31871E-02 0.29862E-02 0.28040E-02 0.26381E-02 0.24866E-02
0.23480E-02 0.22207E-02 0.21036E-02 0.19955E-02 0.18957E-02 0.18032E-02
0.17174E-02 0.16375E-02 0.15632E-02 0.14938E-02 0.14289E-02 0.13683E-02
0.13113E-02 0.12580E-02 0.12078E-02 0.11605E-02 0.11160E-02 0.10740E-02
0.10344E-02 0.99684E-03 0.96137E-03 0.92773E-03 0.89586E-03 0.86560E-03
0.83685E-03 0.80949E-03 0.78344E-03 0.75869E-03 0.73507E-03 0.71253E-03
0.69102E-03 0.67046E-03 0.65084E-03 0.63204E-03 0.61402E-03 0.59681E-03
0.58027E-03 0.56444E-03 0.54922E-03 0.53471E-03 0.52060E-03 0.50721E-03
0.49420E-03 0.48177E-03 0.46975E-03 0.45823E-03 0.44705E-03 0.43635E-03
0.42595E-03

I = 9

0.70532E-01 0.33060E-01 0.21649E-01 0.16340E-01 0.13236E-01 0.11155E-01
0.96369E-02 0.84654E-02 0.75273E-02 0.67558E-02 0.61087E-02 0.55578E-02
0.50832E-02 0.46702E-02 0.43079E-02 0.39878E-02 0.37034E-02 0.34493E-02
0.32210E-02 0.30153E-02 0.28290E-02 0.26598E-02 0.25056E-02 0.23647E-02
0.22354E-02 0.21166E-02 0.20070E-02 0.19060E-02 0.18124E-02 0.17256E-02
0.16450E-02 0.15699E-02 0.14999E-02 0.14344E-02 0.13733E-02 0.13159E-02
0.12622E-02 0.12116E-02 0.11640E-02 0.11192E-02 0.10770E-02 0.10371E-02
0.99937E-03 0.96371E-03 0.92989E-03 0.89786E-03 0.86746E-03 0.83859E-03
0.81110E-03 0.78495E-03 0.76010E-03 0.73638E-03 0.71376E-03 0.69217E-03

0.67155E-03 0.65185E-03 0.63300E-03 0.61492E-03 0.59766E-03 0.58107E-03
0.56520E-03 0.54993E-03 0.53539E-03 0.52124E-03 0.50781E-03 0.49477E-03
0.48231E-03 0.47027E-03 0.45872E-03 0.44751E-03 0.43679E-03 0.42637E-03

I= 10

0.63859E-01 0.30783E-01 0.20281E-01 0.15307E-01 0.12385E-01 0.10430E-01
0.90081E-02 0.79153E-02 0.70428E-02 0.63269E-02 0.57274E-02 0.52175E-02
0.47782E-02 0.43960E-02 0.40604E-02 0.37639E-02 0.35002E-02 0.32642E-02
0.30522E-02 0.28608E-02 0.26873E-02 0.25294E-02 0.23855E-02 0.22538E-02
0.21328E-02 0.20213E-02 0.19188E-02 0.18238E-02 0.17358E-02 0.16541E-02
0.15781E-02 0.15074E-02 0.14412E-02 0.13794E-02 0.13215E-02 0.12673E-02
0.12162E-02 0.11682E-02 0.11232E-02 0.10806E-02 0.10404E-02 0.10024E-02
0.96654E-03 0.93252E-03 0.90030E-03 0.86972E-03 0.84069E-03 0.81306E-03
0.78678E-03 0.76180E-03 0.73797E-03 0.71525E-03 0.69357E-03 0.67286E-03
0.65308E-03 0.63415E-03 0.61601E-03 0.59868E-03 0.58203E-03 0.56610E-03
0.55079E-03 0.53620E-03 0.52200E-03 0.50854E-03 0.49545E-03 0.48296E-03
0.47088E-03 0.45931E-03 0.44806E-03 0.43732E-03 0.42687E-03

I= 11

0.58348E-01 0.28812E-01 0.19092E-01 0.14415E-01 0.11654E-01 0.98067E-02
0.84667E-02 0.74401E-02 0.66228E-02 0.59536E-02 0.53941E-02 0.49187E-02
0.45094E-02 0.41532E-02 0.38407E-02 0.35644E-02 0.33183E-02 0.30982E-02
0.29001E-02 0.27212E-02 0.25589E-02 0.24112E-02 0.22762E-02 0.21525E-02
0.20388E-02 0.19343E-02 0.18376E-02 0.17482E-02 0.16652E-02 0.15881E-02
0.15164E-02 0.14493E-02 0.13868E-02 0.13282E-02 0.12734E-02 0.12218E-02
0.11733E-02 0.11278E-02 0.10849E-02 0.10444E-02 0.10061E-02 0.96991E-03
0.93563E-03 0.90318E-03 0.87240E-03 0.84317E-03 0.81537E-03 0.78893E-03
0.76381E-03 0.73985E-03 0.71701E-03 0.69521E-03 0.67440E-03 0.65453E-03
0.63550E-03 0.61728E-03 0.59988E-03 0.58316E-03 0.56717E-03 0.55180E-03
0.53715E-03 0.52290E-03 0.50938E-03 0.49625E-03 0.48372E-03 0.47160E-03
0.45999E-03 0.44871E-03 0.43794E-03 0.42746E-03

I= 12

0.53721E-01 0.27087E-01 0.18047E-01 0.13635E-01 0.11017E-01 0.92642E-02
0.79953E-02 0.70255E-02 0.62551E-02 0.56258E-02 0.51004E-02 0.46545E-02
0.42708E-02 0.39371E-02 0.36444E-02 0.33853E-02 0.31549E-02 0.29485E-02
0.27627E-02 0.25946E-02 0.24423E-02 0.23034E-02 0.21764E+02 0.20598E-02
0.19529E-02 0.18541E-02 0.17629E-02 0.16784E-02 0.15999E-02 0.15270E-02
0.14589E-02 0.13955E-02 0.13361E-02 0.12806E-02 0.12284E-02 0.11793E-02

0.11333E-02 0.10899E-02 0.10490E-02 0.10103E-02 0.97385E-03 0.93927E-03
0.90655E-03 0.87553E-03 0.84608E-03 0.81807E-03 0.79144E-03 0.76615E-03
0.74204E-03 0.71905E-03 0.69712E-03 0.67618E-03 0.65620E-03 0.63708E-03
0.61876E-03 0.60127E-03 0.58447E-03 0.56840E-03 0.55296E-03 0.53824E-03
0.52394E-03 0.51036E-03 0.49718E-03 0.48460E-03 0.47243E-03 0.46078E-03
0.44946E-03 0.43865E-03 0.42813E-03

I = 13

0.49779E-01 0.25564E-01 0.17120E-01 0.12946E-01 0.10455E-01 0.87871E-02
0.75806E-02 0.66601E-02 0.59306E-02 0.53356E-02 0.48397E-02 0.44191E-02
0.40577E-02 0.37437E-02 0.34679E-02 0.32242E-02 0.30072E-02 0.28128E-02
0.26378E-02 0.24796E-02 0.23358E-02 0.22047E-02 0.20848E-02 0.19749E-02
0.18737E-02 0.17802E-02 0.16939E-02 0.16138E-02 0.15395E-02 0.14702E-02
0.14057E-02 0.13453E-02 0.12889E-02 0.12360E-02 0.11863E-02 0.11397E-02
0.10957E-02 0.10544E-02 0.10153E-02 0.97840E-03 0.94348E-03 0.91044E-03
0.87913E-03 0.84942E-03 0.82118E-03 0.79433E-03 0.76884E-03 0.74455E-03
0.72139E-03 0.69931E-03 0.67824E-03 0.65813E-03 0.63888E-03 0.62045E-03
0.60286E-03 0.58596E-03 0.56981E-03 0.55429E-03 0.53950E-03 0.52512E-03
0.51148E-03 0.49824E-03 0.48560E-03 0.47338E-03 0.46168E-03 0.45032E-03
0.43946E-03 0.42890E-03

I = 14

0.46381E-01 0.24208E-01 0.16290E-01 0.12330E-01 0.99559E-02 0.83636E-02
0.72124E-02 0.63357E-02 0.56419E-02 0.50769E-02 0.46066E-02 0.42084E-02
0.38665E-02 0.35693E-02 0.33088E-02 0.30784E-02 0.28732E-02 0.26895E-02
0.25241E-02 0.23744E-02 0.22384E-02 0.21142E-02 0.20008E-02 0.18966E-02
0.18006E-02 0.17120E-02 0.16300E-02 0.15540E-02 0.14833E-02 0.14175E-02
0.13560E-02 0.12986E-02 0.12448E-02 0.11943E-02 0.11471E-02 0.11025E-02
0.10605E-02 0.10210E-02 0.98362E-03 0.94829E-03 0.91489E-03 0.88324E-03
0.85323E-03 0.82472E-03 0.79762E-03 0.77191E-03 0.74740E-03 0.72406E-03
0.70180E-03 0.68056E-03 0.66031E-03 0.64093E-03 0.62237E-03 0.60466E-03
0.58766E-03 0.57141E-03 0.55579E-03 0.54091E-03 0.52646E-03 0.51275E-03
0.49943E-03 0.48673E-03 0.47445E-03 0.46269E-03 0.45128E-03 0.44037E-03
0.42977E-03

I = 15

0.43421E-01 0.22992E-01 0.15542E-01 0.11777E-01 0.95082E-02 0.79844E-02
0.68833E-02 0.60453E-02 0.53832E-02 0.48447E-02 0.43972E-02 0.40186E-02
0.36936E-02 0.34116E-02 0.31644E-02 0.29458E-02 0.27512E-02 0.25770E-02

0.24200E-02 0.22780E-02 0.21488E-02 0.20311E-02 0.19233E-02 0.18242E-02
0.17330E-02 0.16488E-02 0.15708E-02 0.14983E-02 0.14310E-02 0.13683E-02
0.13097E-02 0.12549E-02 0.12035E-02 0.11554E-02 0.11101E-02 0.10676E-02
0.10274E-02 0.98955E-03 0.95375E-03 0.91993E-03 0.88791E-03 0.85755E-03
0.82872E-03 0.80134E-03 0.77536E-03 0.75062E-03 0.72706E-03 0.70461E-03
0.68319E-03 0.66276E-03 0.64322E-03 0.62453E-03 0.60669E-03 0.58956E-03
0.57320E-03 0.55748E-03 0.54250E-03 0.52796E-03 0.51416E-03 0.50077E-03
0.48800E-03 0.47565E-03 0.46383E-03 0.45235E-03 0.44139E-03 0.43074E-03

I = 16

0.40819E-01 0.21896E-01 0.14864E-01 0.11275E-01 0.91038E-02 0.76427E-02
0.65867E-02 0.57838E-02 0.51499E-02 0.46352E-02 0.42079E-02 0.38466E-02
0.35369E-02 0.32683E-02 0.30328E-02 0.28247E-02 0.26397E-02 0.24739E-02
0.23245E-02 0.21892E-02 0.20665E-02 0.19543E-02 0.18516E-02 0.17573E-02
0.16704E-02 0.15901E-02 0.15156E-02 0.14466E-02 0.13823E-02 0.13224E-02
0.12664E-02 0.12140E-02 0.11649E-02 0.11188E-02 0.10755E-02 0.10347E-02
0.99624E-03 0.95992E-03 0.92562E-03 0.89316E-03 0.86241E-03 0.83322E-03
0.80552E-03 0.77925E-03 0.75424E-03 0.73043E-03 0.70775E-03 0.68612E-03
0.66550E-03 0.64579E-03 0.62694E-03 0.60895E-03 0.59169E-03 0.57520E-03
0.55935E-03 0.54427E-03 0.52963E-03 0.51574E-03 0.50226E-03 0.48941E-03
0.47698E-03 0.46509E-03 0.45355E-03 0.44252E-03 0.43181E-03

I = 17

0.38514E-01 0.20901E-01 0.14246E-01 0.10819E-01 0.87363E-02 0.73327E-02
0.63180E-02 0.55467E-02 0.49385E-02 0.44452E-02 0.40357E-02 0.36902E-02
0.33941E-02 0.31374E-02 0.29125E-02 0.27140E-02 0.25373E-02 0.23790E-02
0.22364E-02 0.21076E-02 0.19903E-02 0.18833E-02 0.17853E-02 0.16952E-02
0.16122E-02 0.15354E-02 0.14643E-02 0.13982E-02 0.13368E-02 0.12794E-02
0.12258E-02 0.11757E-02 0.11286E-02 0.10845E-02 0.10429E-02 0.10038E-02
0.96684E-03 0.93199E-03 0.89904E-03 0.86785E-03 0.83826E-03 0.81019E-03
0.78358E-03 0.75827E-03 0.73418E-03 0.71125E-03 0.68939E-03 0.66856E-03
0.64865E-03 0.62961E-03 0.61146E-03 0.59404E-03 0.57741E-03 0.56144E-03
0.54624E-03 0.53147E-03 0.51748E-03 0.50391E-03 0.49096E-03 0.47845E-03
0.46648E-03 0.45486E-03 0.44377E-03 0.43300E-03

I = 18

0.36457E-01 0.19995E-01 0.13679E-01 0.10401E-01 0.84005E-02 0.70499E-02
0.60729E-02 0.53308E-02 0.47460E-02 0.42717E-02 0.38788E-02 0.35472E-02
0.32633E-02 0.30173E-02 0.28022E-02 0.26121E-02 0.24430E-02 0.22915E-02

0.21553E-02 0.20319E-02 0.19197E-02 0.18174E-02 0.17236E-02 0.16374E-02
0.15579E-02 0.14844E-02 0.14163E-02 0.13531E-02 0.12941E-02 0.12391E-02
0.11878E-02 0.11396E-02 0.10945E-02 0.10521E-02 0.10122E-02 0.97458E-03
0.93911E-03 0.90561E-03 0.87391E-03 0.84386E-03 0.81538E-03 0.78840E-03
0.76274E-03 0.73835E-03 0.71513E-03 0.69301E-03 0.67194E-03 0.65181E-03
0.63257E-03 0.61423E-03 0.59664E-03 0.57985E-03 0.56374E-03 0.54840E-03
0.53351E-03 0.51940E-03 0.50572E-03 0.49267E-03 0.48007E-03 0.46801E-03
0.45631E-03 0.44514E-03 0.43430E-03

I = 19

0.34610E-01 0.19166E-01 0.13157E-01 0.10016E-01 0.80922E-02 0.67905E-02
0.58486E-02 0.51332E-02 0.45694E-02 0.41129E-02 0.37348E-02 0.34160E-02
0.31432E-02 0.29071E-02 0.27005E-02 0.25181E-02 0.23558E-02 0.22108E-02
0.20801E-02 0.19617E-02 0.18542E-02 0.17561E-02 0.16662E-02 0.15835E-02
0.15073E-02 0.14368E-02 0.13715E-02 0.13107E-02 0.12541E-02 0.12014E-02
0.11520E-02 0.11058E-02 0.10624E-02 0.10216E-02 0.98321E-03 0.94705E-03
0.91291E-03 0.88064E-03 0.85009E-03 0.82114E-03 0.79374E-03 0.76770E-03
0.74295E-03 0.71941E-03 0.69700E-03 0.67567E-03 0.65530E-03 0.63583E-03
0.61728E-03 0.59951E-03 0.58254E-03 0.56626E-03 0.55077E-03 0.53575E-03
0.52151E-03 0.50771E-03 0.49455E-03 0.48184E-03 0.46969E-03 0.45790E-03
0.44665E-03 0.43572E-03

I = 20

0.32943E-01 0.18404E-01 0.12676E-01 0.96611E-02 0.78076E-02 0.65516E-02
0.56423E-02 0.49512E-02 0.44073E-02 0.39668E-02 0.36022E-02 0.32950E-02
0.30325E-02 0.28052E-02 0.26065E-02 0.24310E-02 0.22753E-02 0.21358E-02
0.20102E-02 0.18965E-02 0.17933E-02 0.16990E-02 0.16126E-02 0.15332E-02
0.14599E-02 0.13922E-02 0.13294E-02 0.12709E-02 0.12166E-02 0.11658E-02
0.11183E-02 0.10738E-02 0.10321E-02 0.99281E-03 0.95585E-03 0.92101E-03
0.88810E-03 0.85697E-03 0.82750E-03 0.79963E-03 0.77316E-03 0.74803E-03
0.72413E-03 0.70140E-03 0.67977E-03 0.65913E-03 0.63941E-03 0.62063E-03
0.60265E-03 0.58549E-03 0.56903E-03 0.55337E-03 0.53819E-03 0.52381E-03
0.50988E-03 0.49660E-03 0.48378E-03 0.47152E-03 0.45963E-03 0.44828E-03
0.43727E-03

I = 21

0.31430E-01 0.17701E-01 0.12229E-01 0.93317E-02 0.75442E-02 0.63309E-02
0.54514E-02 0.47834E-02 0.42575E-02 0.38319E-02 0.34797E-02 0.31834E-02
0.29301E-02 0.27109E-02 0.25192E-02 0.23505E-02 0.22003E-02 0.20660E-02

0.19451E-02 0.18358E-02 0.17364E-02 0.16456E-02 0.15625E-02 0.14860E-02
0.14156E-02 0.13503E-02 0.12898E-02 0.12337E-02 0.11812E-02 0.11324E-02
0.10866E-02 0.10437E-02 0.10035E-02 0.96561E-03 0.92997E-03 0.89635E-03
0.86457E-03 0.83452E-03 0.80612E-03 0.77918E-03 0.75361E-03 0.72932E-03
0.70623E-03 0.68427E-03 0.66332E-03 0.64333E-03 0.62430E-03 0.60608E-03
0.58871E-03 0.57205E-03 0.55621E-03 0.54086E-03 0.52633E-03 0.51224E-03
0.49883E-03 0.48588E-03 0.47351E-03 0.46151E-03 0.45006E-03 0.43896E-03

I = 22

0.30051E-01 0.17051E-01 0.11814E-01 0.90255E-02 0.72996E-02 0.61257E-02
0.52746E-02 0.46278E-02 0.41187E-02 0.37068E-02 0.33664E-02 0.30798E-02
0.28350E-02 0.26232E-02 0.24384E-02 0.22754E-02 0.21305E-02 0.20010E-02
0.18844E-02 0.17790E-02 0.16831E-02 0.15957E-02 0.15155E-02 0.14419E-02
0.13738E-02 0.13109E-02 0.12527E-02 0.11985E-02 0.11480E-02 0.11008E-02
0.10566E-02 0.10152E-02 0.97640E-03 0.93987E-03 0.90545E-03 0.87295E-03
0.84225E-03 0.81326E-03 0.78579E-03 0.75973E-03 0.73501E-03 0.71151E-03
0.68919E-03 0.66791E-03 0.64762E-03 0.62830E-03 0.60983E-03 0.59221E-03
0.57534E-03 0.55930E-03 0.54376E-03 0.52906E-03 0.51482E-03 0.50126E-03
0.48817E-03 0.47566E-03 0.46355E-03 0.45199E-03 0.44078E-03

I = 23

0.28789E-01 0.16447E-01 0.11428E-01 0.87400E-02 0.70712E-02 0.59349E-02
0.51101E-02 0.44831E-02 0.39896E-02 0.35907E-02 0.32609E-02 0.29833E-02
0.27463E-02 0.25418E-02 0.23629E-02 0.22053E-02 0.20654E-02 0.19402E-02
0.18277E-02 0.17258E-02 0.16333E-02 0.15488E-02 0.14715E-02 0.14003E-02
0.13346E-02 0.12740E-02 0.12176E-02 0.11653E-02 0.11165E-02 0.10710E-02
0.10283E-02 0.98833E-03 0.95079E-03 0.91547E-03 0.88216E-03 0.85073E-03
0.82110E-03 0.79303E-03 0.76644E-03 0.74123E-03 0.71729E-03 0.69456E-03
0.67292E-03 0.65229E-03 0.63266E-03 0.61390E-03 0.59603E-03 0.57891E-03
0.56266E-03 0.54692E-03 0.53202E-03 0.51761E-03 0.50388E-03 0.49065E-03
0.47800E-03 0.46576E-03 0.45408E-03 0.44276E-03

I = 24

0.27628E-01 0.15885E-01 0.11066E-01 0.84725E-02 0.68581E-02 0.57567E-02
0.49565E-02 0.43481E-02 0.38695E-02 0.34823E-02 0.31624E-02 0.28933E-02
0.26639E-02 0.24656E-02 0.22924E-02 0.21398E-02 0.20044E-02 0.18834E-02
0.17744E-02 0.16759E-02 0.15864E-02 0.15048E-02 0.14300E-02 0.13611E-02
0.12978E-02 0.12390E-02 0.11846E-02 0.11340E-02 0.10868E-02 0.10427E-02
0.10015E-02 0.96282E-03 0.92650E-03 0.89229E-03 0.86005E-03 0.82968E-03

0.80096E-03 0.77378E-03 0.74802E-03 0.72360E-03 0.70042E-03 0.67837E-03
0.65737E-03 0.63741E-03 0.61833E-03 0.60018E-03 0.58280E-03 0.56630E-03
0.55033E-03 0.53523E-03 0.52062E-03 0.50672E-03 0.49333E-03 0.48053E-03
0.46814E-03 0.45634E-03 0.44489E-03

I = 25

0.26559E-01 0.15362E-01 0.10727E-01 0.82220E-02 0.66582E-02 0.55896E-02
0.48127E-02 0.42220E-02 0.37570E-02 0.33810E-02 0.30703E-02 0.28094E-02
0.25866E-02 0.23942E-02 0.22263E-02 0.20785E-02 0.19473E-02 0.18299E-02
0.17244E-02 0.16290E-02 0.15424E-02 0.14633E-02 0.13908E-02 0.13243E-02
0.12629E-02 0.12061E-02 0.11534E-02 0.11044E-02 0.10587E-02 0.10160E-02
0.97608E-03 0.93862E-03 0.90340E-03 0.87027E-03 0.83909E-03 0.80963E-03
0.78179E-03 0.75544E-03 0.73047E-03 0.70681E-03 0.68431E-03 0.66289E-03
0.64256E-03 0.62314E-03 0.60467E-03 0.58700E-03 0.57024E-03 0.55403E-03
0.53870E-03 0.52389E-03 0.50979E-03 0.49622E-03 0.48325E-03 0.47071E-03
0.45876E-03 0.44718E-03

I = 26

0.25570E-01 0.14871E-01 0.10409E-01 0.79864E-02 0.64702E-02 0.54327E-02
0.46780E-02 0.41037E-02 0.36515E-02 0.32859E-02 0.29842E-02 0.27305E-02
0.25141E-02 0.23273E-02 0.21643E-02 0.20209E-02 0.18935E-02 0.17797E-02
0.16773E-02 0.15849E-02 0.15009E-02 0.14242E-02 0.13541E-02 0.12895E-02
0.12300E-02 0.11749E-02 0.11238E-02 0.10763E-02 0.10320E-02 0.99067E-03
0.95195E-03 0.91561E-03 0.88146E-03 0.84938E-03 0.81911E-03 0.79053E-03
0.76352E-03 0.73796E-03 0.71375E-03 0.69075E-03 0.66889E-03 0.64814E-03
0.62835E-03 0.60954E-03 0.59155E-03 0.57450E-03 0.55802E-03 0.54245E-03
0.52740E-03 0.51310E-03 0.49933E-03 0.48619E-03 0.47348E-03 0.46138E-03
0.44965E-03

I = 27

0.24651E-01 0.14412E-01 0.10110E-01 0.77644E-02 0.62932E-02 0.52853E-02
0.45512E-02 0.39924E-02 0.35523E-02 0.31969E-02 0.29032E-02 0.26564E-02
0.24460E-02 0.22644E-02 0.21061E-02 0.19666E-02 0.18429E-02 0.17323E-02
0.16331E-02 0.15432E-02 0.14616E-02 0.13873E-02 0.13191E-02 0.12565E-02
0.11988E-02 0.11454E-02 0.10958E-02 0.10497E-02 0.10067E-02 0.96660E-03
0.92899E-03 0.89372E-03 0.86063E-03 0.82946E-03 0.80008E-03 0.77233E-03
0.74610E-03 0.72129E-03 0.69776E-03 0.67540E-03 0.65420E-03 0.63399E-03
0.61480E-03 0.59647E-03 0.57910E-03 0.56233E-03 0.54649E-03 0.53120E-03
0.51667E-03 0.50268E-03 0.48935E-03 0.47646E-03 0.46418E-03 0.45230E-03

I= 28

0.23798E-01 0.13980E-01 0.98273E-02 0.75548E-02 0.61264E-02 0.51461E-02
0.44316E-02 0.38873E-02 0.34592E-02 0.31128E-02 0.28268E-02 0.25866E-02
0.23819E-02 0.22052E-02 0.20510E-02 0.19154E-02 0.17951E-02 0.16877E-02
0.15911E-02 0.15038E-02 0.14247E-02 0.13523E-02 0.12862E-02 0.12253E-02
0.11692E-02 0.11173E-02 0.10692E-02 0.10244E-02 0.98270E-03 0.94368E-03
0.90715E-03 0.87294E-03 0.84077E-03 0.81048E-03 0.78192E-03 0.75496E-03
0.72949E-03 0.70535E-03 0.68245E-03 0.66076E-03 0.64010E-03 0.62049E-03
0.60178E-03 0.58407E-03 0.56698E-03 0.55084E-03 0.53528E-03 0.52050E-03
0.50629E-03 0.49274E-03 0.47965E-03 0.46719E-03 0.45514E-03

I= 29

0.23001E-01 0.13573E-01 0.95604E-02 0.73570E-02 0.59685E-02 0.50144E-02
0.43184E-02 0.37886E-02 0.33711E-02 0.30335E-02 0.27549E-02 0.25208E-02
0.23214E-02 0.21492E-02 0.19992E-02 0.18671E-02 0.17501E-02 0.16455E-02
0.15515E-02 0.14667E-02 0.13895E-02 0.13193E-02 0.12549E-02 0.11958E-02
0.11412E-02 0.10907E-02 0.10439E-02 0.10004E-02 0.95981E-03 0.92187E-03
0.88641E-03 0.85311E-03 0.82182E-03 0.79237E-03 0.76460E-03 0.73840E-03
0.71360E-03 0.69009E-03 0.66785E-03 0.64670E-03 0.62664E-03 0.60752E-03
0.58942E-03 0.57198E-03 0.55553E-03 0.53967E-03 0.52463E-03 0.51016E-03
0.49638E-03 0.48308E-03 0.47042E-03 0.45819E-03

I= 30

0.22257E-01 0.13190E-01 0.93084E-02 0.71694E-02 0.58189E-02 0.48896E-02
0.42118E-02 0.36949E-02 0.32877E-02 0.29586E-02 0.26868E-02 0.24587E-02
0.22640E-02 0.20963E-02 0.19500E-02 0.18214E-02 0.17073E-02 0.16054E-02
0.15140E-02 0.14313E-02 0.13563E-02 0.12879E-02 0.12252E-02 0.11676E-02
0.11145E-02 0.10654E-02 0.10199E-02 0.97751E-03 0.93800E-03 0.90114E-03
0.86660E-03 0.83419E-03 0.80374E-03 0.77507E-03 0.74807E-03 0.72254E-03
0.69837E-03 0.67553E-03 0.65383E-03 0.63328E-03 0.61370E-03 0.59520E-03
0.57737E-03 0.56058E-03 0.54440E-03 0.52905E-03 0.51432E-03 0.50029E-03
0.48675E-03 0.47388E-03 0.46145E-03

I= 31

0.21559E-01 0.12829E-01 0.90693E-02 0.69914E-02 0.56767E-02 0.47718E-02
0.41104E-02 0.36061E-02 0.32088E-02 0.28876E-02 0.26224E-02 0.23996E-02
0.22099E-02 0.20461E-02 0.19036E-02 0.17781E-02 0.16668E-02 0.15676E-02
0.14784E-02 0.13978E-02 0.13247E-02 0.12580E-02 0.11970E-02 0.11409E-02
0.10892E-02 0.10414E-02 0.99697E-03 0.95568E-03 0.91726E-03 0.88133E-03

0.84769E-03 0.81613E-03 0.78647E-03 0.75856E-03 0.73223E-03 0.70734E-03
0.68384E-03 0.66154E-03 0.64044E-03 0.62037E-03 0.60141E-03 0.58318E-03
0.56600E-03 0.54947E-03 0.53381E-03 0.51878E-03 0.50447E-03 0.49069E-03
0.47759E-03 0.46494E-03

I = 32

0.20904E-01 0.12486E-01 0.88422E-02 0.68220E-02 0.55423E-02 0.46595E-02
0.40141E-02 0.35219E-02 0.31339E-02 0.28203E-02 0.25612E-02 0.23437E-02
0.21584E-02 0.19987E-02 0.18594E-02 0.17369E-02 0.16285E-02 0.15315E-02
0.14446E-02 0.13660E-02 0.12947E-02 0.12296E-02 0.11701E-02 0.11154E-02
0.10650E-02 0.10184E-02 0.97510E-03 0.93492E-03 0.89744E-03 0.86241E-03
0.82962E-03 0.79886E-03 0.76997E-03 0.74274E-03 0.71705E-03 0.69283E-03
0.66987E-03 0.64818E-03 0.62756E-03 0.60811E-03 0.58942E-03 0.57183E-03
0.55492E-03 0.53891E-03 0.52356E-03 0.50896E-03 0.49490E-03 0.48155E-03
0.46866E-03

I = 33

0.20288E-01 0.12161E-01 0.86261E-02 0.66616E-02 0.54140E-02 0.45526E-02
0.39226E-02 0.34418E-02 0.30628E-02 0.27562E-02 0.25031E-02 0.22906E-02
0.21096E-02 0.19534E-02 0.18174E-02 0.16979E-02 0.15918E-02 0.14973E-02
0.14123E-02 0.13357E-02 0.12660E-02 0.12026E-02 0.11445E-02 0.10912E-02
0.10420E-02 0.99644E-03 0.95429E-03 0.91506E-03 0.87849E-03 0.84433E-03
0.81234E-03 0.78236E-03 0.75415E-03 0.72757E-03 0.70255E-03 0.67887E-03
0.65652E-03 0.63531E-03 0.61532E-03 0.59614E-03 0.57810E-03 0.56077E-03
0.54438E-03 0.52868E-03 0.51376E-03 0.49941E-03 0.48579E-03 0.47265E-03

I = 34

0.19707E-01 0.11853E-01 0.84214E-02 0.65082E-02 0.52916E-02 0.44509E-02
0.38354E-02 0.33656E-02 0.29949E-02 0.26953E-02 0.24478E-02 0.22401E-02
0.20630E-02 0.19104E-02 0.17775E-02 0.16606E-02 0.15571E-02 0.14646E-02
0.13817E-02 0.13067E-02 0.12388E-02 0.11768E-02 0.11201E-02 0.10680E-02
0.10199E-02 0.97555E-03 0.93437E-03 0.89607E-03 0.86038E-03 0.82703E-03
0.79582E-03 0.76653E-03 0.73897E-03 0.71307E-03 0.68860E-03 0.66553E-03
0.64367E-03 0.62309E-03 0.60336E-03 0.58483E-03 0.56706E-03 0.55026E-03
0.53418E-03 0.51891E-03 0.50424E-03 0.49032E-03 0.47691E-03

I = 35

0.19158E-01 0.11561E-01 0.82258E-02 0.63619E-02 0.51750E-02 0.43538E-02
0.37524E-02 0.32927E-02 0.29304E-02 0.26372E-02 0.23952E-02 0.21919E-02
0.20187E-02 0.18695E-02 0.17394E-02 0.16252E-02 0.15239E-02 0.14335E-02

```
0.13524E-02 0.12792E-02 0.12128E-02 0.11522E-02 0.10968E-02 0.10458E-02
0.99893E-03 0.95555E-03 0.91531E-03 0.87790E-03 0.84303E-03 0.81048E-03
0.77997E-03 0.75133E-03 0.72446E-03 0.69912E-03 0.67526E-03 0.65268E-03
0.63145E-03 0.61113E-03 0.59207E-03 0.57380E-03 0.55655E-03 0.54006E-03
0.52442E-03 0.50940E-03 0.49516E-03 0.48145E-03
                I=   36
0.18641E-01 0.11283E-01 0.80390E-02 0.62224E-02 0.50636E-02 0.42612E-02
0.36728E-02 0.32234E-02 0.28687E-02 0.25819E-02 0.23449E-02 0.21458E-02
0.19765E-02 0.18303E-02 0.17031E-02 0.15913E-02 0.14922E-02 0.14038E-02
0.13245E-02 0.12529E-02 0.11879E-02 0.11286E-02 0.10744E-02 0.10247E-02
0.97881E-03 0.93640E-03 0.89706E-03 0.86050E-03 0.82644E-03 0.79459E-03
0.76475E-03 0.73681E-03 0.71049E-03 0.68577E-03 0.66240E-03 0.64046E-03
0.61950E-03 0.59985E-03 0.58105E-03 0.56331E-03 0.54637E-03 0.53032E-03
0.51492E-03 0.50033E-03 0.48631E-03
                I=   37
0.18149E-01 0.11017E-01 0.78609E-02 0.60889E-02 0.49571E-02 0.41723E-02
0.35969E-02 0.31569E-02 0.28099E-02 0.25288E-02 0.22968E-02 0.21021E-02
0.19360E-02 0.17930E-02 0.16684E-02 0.15590E-02 0.14619E-02 0.13754E-02
0.12978E-02 0.12277E-02 0.11641E-02 0.11061E-02 0.10531E-02 0.10044E-02
0.95954E-03 0.91805E-03 0.87958E-03 0.84383E-03 0.81049E-03 0.77932E-03
0.75019E-03 0.72281E-03 0.69712E-03 0.67290E-03 0.65018E-03 0.62850E-03
0.60821E-03 0.58882E-03 0.57055E-03 0.55313E-03 0.53663E-03 0.52082E-03
0.50586E-03 0.49149E-03
                I=   38
0.17683E-01 0.10764E-01 0.76905E-02 0.59613E-02 0.48548E-02 0.40875E-02
0.35242E-02 0.30935E-02 0.27534E-02 0.24781E-02 0.22510E-02 0.20600E-02
0.18974E-02 0.17573E-02 0.16353E-02 0.15280E-02 0.14330E-02 0.13483E-02
0.12722E-02 0.12035E-02 0.11412E-02 0.10846E-02 0.10327E-02 0.98499E-03
0.94106E-03 0.90045E-03 0.86283E-03 0.82782E-03 0.79516E-03 0.76471E-03
0.73615E-03 0.70941E-03 0.68423E-03 0.66065E-03 0.63820E-03 0.61720E-03
0.59718E-03 0.57833E-03 0.56037E-03 0.54339E-03 0.52714E-03 0.51178E-03
0.49703E-03
                I=   39
0.17241E-01 0.10523E-01 0.75276E-02 0.58386E-02 0.47571E-02 0.40060E-02
0.34546E-02 0.30326E-02 0.26993E-02 0.24297E-02 0.22069E-02 0.20198E-02
0.18604E-02 0.17231E-02 0.16034E-02 0.14984E-02 0.14053E-02 0.13222E-02
```

0.12477E-02 0.11804E-02 0.11195E-02 0.10639E-02 0.10130E-02 0.96636E-03
0.92334E-03 0.88359E-03 0.84672E-03 0.81241E-03 0.78049E-03 0.75062E-03
0.72271E-03 0.69647E-03 0.67196E-03 0.64865E-03 0.62689E-03 0.60616E-03
0.58668E-03 0.56814E-03 0.55064E-03 0.53390E-03 0.51809E-03 0.50294E-03

I = 40

0.16820E-01 0.10292E-01 0.73710E-02 0.57213E-02 0.46632E-02 0.39281E-02
0.33877E-02 0.29741E-02 0.26477E-02 0.23831E-02 0.21647E-02 0.19812E-02
0.18250E-02 0.16903E-02 0.15730E-02 0.14700E-02 0.13787E-02 0.12972E-02
0.12242E-02 0.11583E-02 0.10985E-02 0.10440E-02 0.99422E-03 0.94847E-03
0.90634E-03 0.86737E-03 0.83121E-03 0.79765E-03 0.76633E-03 0.73712E-03
0.70972E-03 0.68417E-03 0.65992E-03 0.63731E-03 0.61582E-03 0.59564E-03
0.57648E-03 0.55840E-03 0.54114E-03 0.52485E-03 0.50926E-03

I = 41

0.16420E-01 0.10071E-01 0.72213E-02 0.56085E-02 0.45733E-02 0.38530E-02
0.33234E-02 0.29182E-02 0.25978E-02 0.23385E-02 0.21242E-02 0.19443E-02
0.17909E-02 0.16588E-02 0.15438E-02 0.14427E-02 0.13531E-02 0.12732E-02
0.12017E-02 0.11370E-02 0.10784E-02 0.10250E-02 0.97613E-03 0.93130E-03
0.88997E-03 0.85174E-03 0.81635E-03 0.78341E-03 0.75275E-03 0.72407E-03
0.69737E-03 0.67209E-03 0.64855E-03 0.62622E-03 0.60528E-03 0.58542E-03
0.56672E-03 0.54888E-03 0.53208E-03 0.51601E-03

I = 42

0.16037E-01 0.98594E-02 0.70774E-02 0.55005E-02 0.44866E-02 0.37808E-02
0.32620E-02 0.28642E-02 0.25501E-02 0.22956E-02 0.20854E-02 0.19087E-02
0.17583E-02 0.16286E-02 0.15157E-02 0.14165E-02 0.13286E-02 0.12503E-02
0.11800E-02 0.11166E-02 0.10590E-02 0.10067E-02 0.95877E-03 0.91477E-03
0.87420E-03 0.83676E-03 0.80200E-03 0.76974E-03 0.73963E-03 0.71165E-03
0.68523E-03 0.66067E-03 0.63741E-03 0.61564E-03 0.59503E-03 0.57564E-03
0.55718E-03 0.53981E-03 0.52322E-03

I = 43

0.15673E-01 0.96564E-02 0.69395E-02 0.53962E-02 0.44031E-02 0.37117E-02
0.32025E-02 0.28125E-02 0.25041E-02 0.22544E-02 0.20479E-02 0.18746E-02
0.17269E-02 0.15996E-02 0.14887E-02 0.13913E-02 0.13051E-02 0.12281E-02
0.11591E-02 0.10969E-02 0.10404E-02 0.98906E-03 0.94203E-03 0.89882E-03
0.85907E-03 0.82228E-03 0.78823E-03 0.75653E-03 0.72714E-03 0.69945E-03
0.67375E-03 0.64948E-03 0.62680E-03 0.60536E-03 0.58522E-03 0.56608E-03
0.54809E-03 0.53094E-03

I = 44

0.15325E-01 0.94622E-02 0.68065E-02 0.52959E-02 0.43233E-02 0.36448E-02
0.31455E-02 0.27626E-02 0.24599E-02 0.22146E-02 0.20120E-02 0.18417E-02
0.16967E-02 0.15716E-02 0.14627E-02 0.13671E-02 0.12824E-02 0.12069E-02
0.11391E-02 0.10780E-02 0.10226E-02 0.97208E-03 0.92588E-03 0.88352E-03
0.84444E-03 0.80838E-03 0.77490E-03 0.74394E-03 0.71484E-03 0.68790E-03
0.66251E-03 0.63882E-03 0.61647E-03 0.59551E-03 0.57563E-03 0.55696E-03
0.53920E-03

I = 45

0.14992E-01 0.92750E-02 0.66786E-02 0.51998E-02 0.42458E-02 0.35806E-02
0.30904E-02 0.27146E-02 0.24173E-02 0.21764E-02 0.19774E-02 0.18101E-02
0.16675E-02 0.15446E-02 0.14377E-02 0.13438E-02 0.12605E-02 0.11863E-02
0.11198E-02 0.10598E-02 0.10053E-02 0.95569E-03 0.91038E-03 0.86872E-03
0.83039E-03 0.79493E-03 0.76221E-03 0.73155E-03 0.70322E-03 0.67658E-03
0.65178E-03 0.62843E-03 0.60657E-03 0.58588E-03 0.56648E-03 0.54804E-03

I = 46

0.14673E-01 0.90952E-02 0.65560E-02 0.51066E-02 0.41715E-02 0.35186E-02
0.30374E-02 0.26682E-02 0.23762E-02 0.21396E-02 0.19440E-02 0.17795E-02
0.16394E-02 0.15188E-02 0.14136E-02 0.13213E-02 0.12395E-02 0.11666E-02
0.11012E-02 0.10422E-02 0.98864E-03 0.93995E-03 0.89536E-03 0.85449E-03
0.81678E-03 0.78210E-03 0.74970E-03 0.71983E-03 0.69181E-03 0.66578E-03
0.64133E-03 0.61849E-03 0.59689E-03 0.57669E-03 0.55752E-03

I = 47

0.14367E-01 0.89230E-02 0.64372E-02 0.50171E-02 0.40996E-02 0.34588E-02
0.29861E-02 0.26235E-02 0.23366E-02 0.21040E-02 0.19117E-02 0.17500E-02
0.16124E-02 0.14937E-02 0.13904E-02 0.12996E-02 0.12192E-02 0.11475E-02
0.10832E-02 0.10252E-02 0.97262E-03 0.92470E-03 0.88093E-03 0.84070E-03
0.80381E-03 0.76945E-03 0.73786E-03 0.70832E-03 0.68093E-03 0.65526E-03
0.63132E-03 0.60875E-03 0.58765E-03 0.56768E-03

I = 48

0.14075E-01 0.87564E-02 0.63230E-02 0.49306E-02 0.40303E-02 0.34009E-02
0.29367E-02 0.25804E-02 0.22984E-02 0.20697E-02 0.18805E-02 0.17217E-02
0.15863E-02 0.14696E-02 0.13679E-02 0.12786E-02 0.11996E-02 0.11291E-02
0.10658E-02 0.10088E-02 0.95709E-03 0.91003E-03 0.86693E-03 0.82755E-03
0.79100E-03 0.75749E-03 0.72623E-03 0.69733E-03 0.67031E-03 0.64517E-03
0.62151E-03 0.59945E-03 0.57859E-03

I = 49

0.13793E-01 0.85964E-02 0.62127E-02 0.48471E-02 0.39632E-02 0.33451E-02
0.28890E-02 0.25387E-02 0.22614E-02 0.20364E-02 0.18506E-02 0.16943E-02
0.15611E-02 0.14463E-02 0.13463E-02 0.12585E-02 0.11807E-02 0.11113E-02
0.10491E-02 0.99297E-03 0.94214E-03 0.89579E-03 0.85358E-03 0.81456E-03
0.77889E-03 0.74572E-03 0.71513E-03 0.68661E-03 0.66014E-03 0.63528E-03
0.61214E-03 0.59033E-03

I = 50

0.13523E-01 0.84419E-02 0.61063E-02 0.47663E-02 0.38985E-02 0.32912E-02
0.28428E-02 0.24983E-02 0.22256E-02 0.20045E-02 0.18215E-02 0.16677E-02
0.15367E-02 0.14237E-02 0.13254E-02 0.12389E-02 0.11623E-02 0.10941E-02
0.10329E-02 0.97771E-03 0.92763E-03 0.88220E-03 0.84038E-03 0.80227E-03
0.76696E-03 0.73448E-03 0.70429E-03 0.67633E-03 0.65015E-03 0.62583E-03
0.60295E-03

I = 51

0.13263E-01 0.82931E-02 0.60033E-02 0.46883E-02 0.38359E-02 0.32390E-02
0.27980E-02 0.24592E-02 0.21911E-02 0.19734E-02 0.17934E-02 0.16421E-02
0.15131E-02 0.14019E-02 0.13051E-02 0.12200E-02 0.11447E-02 0.10775E-02
0.10173E-02 0.96288E-03 0.91377E-03 0.86876E-03 0.82789E-03 0.79016E-03
0.75557E-03 0.72351E-03 0.69390E-03 0.66625E-03 0.64062E-03 0.61656E-03

I = 52

0.13014E-01 0.81492E-02 0.59040E-02 0.46128E-02 0.37752E-02 0.31884E-02
0.27547E-02 0.24216E-02 0.21576E-02 0.19434E-02 0.17662E-02 0.16172E-02
0.14903E-02 0.13808E-02 0.12854E-02 0.12017E-02 0.11275E-02 0.10614E-02
0.10021E-02 0.94871E-03 0.90005E-03 0.85604E-03 0.81557E-03 0.77859E-03
0.74444E-03 0.71298E-03 0.68369E-03 0.65660E-03 0.63125E-03

I = 53

0.12772E-01 0.80104E-02 0.58078E-02 0.45397E-02 0.37164E-02 0.31393E-02
0.27129E-02 0.23850E-02 0.21252E-02 0.19143E-02 0.17399E-02 0.15932E-02
0.14682E-02 0.13603E-02 0.12665E-02 0.11839E-02 0.11109E-02 0.10458E-02
0.98752E-03 0.93467E-03 0.88706E-03 0.84348E-03 0.80380E-03 0.76728E-03
0.73375E-03 0.70263E-03 0.67393E-03 0.64713E-03

I = 54

0.12541E-01 0.78763E-02 0.57148E-02 0.44688E-02 0.36594E-02 0.30920E-02
0.26723E-02 0.23495E-02 0.20937E-02 0.18861E-02 0.17144E-02 0.15699E-02
0.14467E-02 0.13406E-02 0.12480E-02 0.11668E-02 0.10948E-02 0.10308E-02

```
0.97312E-03 0.92138E-03 0.87424E-03 0.83149E-03 0.79229E-03 0.75642E-03
0.72324E-03 0.69273E-03 0.66433E-03
                I=   55
0.12317E-01 0.77466E-02 0.56245E-02 0.44001E-02 0.36044E-02 0.30460E-02
0.26329E-02 0.23151E-02 0.20633E-02 0.18589E-02 0.16896E-02 0.15473E-02
0.14260E-02 0.13213E-02 0.12302E-02 0.11501E-02 0.10794E-02 0.10160E-02
0.95948E-03 0.90824E-03 0.86198E-03 0.81974E-03 0.78123E-03 0.74574E-03
0.71320E-03 0.68300E-03
                I=   56
0.12101E-01 0.76209E-02 0.55370E-02 0.43338E-02 0.35509E-02 0.30014E-02
0.25947E-02 0.22818E-02 0.20338E-02 0.18323E-02 0.16656E-02 0.15254E-02
0.14058E-02 0.13027E-02 0.12129E-02 0.11342E-02 0.10641E-02 0.10020E-02
0.94600E-03 0.89569E-03 0.84997E-03 0.80845E-03 0.77034E-03 0.73552E-03
0.70331E-03
                I=   57
0.11892E-01 0.74992E-02 0.54527E-02 0.42693E-02 0.34990E-02 0.29580E-02
0.25576E-02 0.22495E-02 0.20050E-02 0.18065E-02 0.16423E-02 0.15041E-02
0.13863E-02 0.12846E-02 0.11963E-02 0.11183E-02 0.10496E-02 0.98809E-03
0.93309E-03 0.88338E-03 0.83842E-03 0.79734E-03 0.75993E-03 0.72545E-03
                I=   58
0.11691E-01 0.73819E-02 0.53706E-02 0.42067E-02 0.34486E-02 0.29160E-02
0.25217E-02 0.22180E-02 0.19771E-02 0.17816E-02 0.16196E-02 0.14834E-02
0.13672E-02 0.12673E-02 0.11798E-02 0.11033E-02 0.10352E-02 0.97479E-03
0.92044E-03 0.87154E-03 0.82705E-03 0.78670E-03 0.74966E-03
                I=   59
0.11497E-01 0.72679E-02 0.52910E-02 0.41460E-02 0.33997E-02 0.28752E-02
0.24866E-02 0.21874E-02 0.19501E-02 0.17572E-02 0.15977E-02 0.14633E-02
0.13490E-02 0.12500E-02 0.11641E-02 0.10884E-02 0.10215E-02 0.96175E-03
0.90827E-03 0.85986E-03 0.81616E-03 0.77621E-03
                I=   60
0.11309E-01 0.71574E-02 0.52137E-02 0.40869E-02 0.33522E-02 0.28355E-02
0.24525E-02 0.21577E-02 0.19237E-02 0.17337E-02 0.15762E-02 0.14440E-02
0.13308E-02 0.12336E-02 0.11486E-02 0.10741E-02 0.10080E-02 0.94919E-03
0.89626E-03 0.84869E-03 0.80541E-03
                I=   61
0.11127E-01 0.70501E-02 0.51386E-02 0.40297E-02 0.33060E-02 0.27968E-02
```

```
0.24195E-02 0.21288E-02 0.18982E-02 0.17107E-02 0.15557E-02 0.14248E-02
0.13136E-02 0.12174E-02 0.11337E-02 0.10601E-02 0.99501E-03 0.93680E-03
0.88476E-03 0.83765E-03
                  I=   62
0.10950E-01 0.69461E-02 0.50659E-02 0.39739E-02 0.32609E-02 0.27593E-02
0.23873E-02 0.21007E-02 0.18732E-02 0.16886E-02 0.15352E-02 0.14066E-02
0.12965E-02 0.12018E-02 0.11191E-02 0.10466E-02 0.98217E-03 0.92493E-03
0.87339E-03
                  I=   63
0.10780E-01 0.68452E-02 0.49950E-02 0.39195E-02 0.32173E-02 0.27227E-02
0.23560E-02 0.20733E-02 0.18492E-02 0.16666E-02 0.15157E-02 0.13884E-02
0.12801E-02 0.11865E-02 0.11050E-02 0.10333E-02 0.96988E-03 0.91319E-03
                  I=   64
0.10614E-01 0.67470E-02 0.49259E-02 0.38669E-02 0.31746E-02 0.26872E-02
0.23255E-02 0.20470E-02 0.18253E-02 0.16457E-02 0.14964E-02 0.13711E-02
0.12640E-02 0.11717E-02 0.10911E-02 0.10205E-02 0.95771E-03
                  I=   65
0.10453E-01 0.66514E-02 0.48590E-02 0.38154E-02 0.31332E-02 0.26524E-02
0.22961E-02 0.20207E-02 0.18026E-02 0.16249E-02 0.14779E-02 0.13540E-02
0.12484E-02 0.11571E-02 0.10778E-02 0.10078E-02
                  I=   66
0.10297E-01 0.65590E-02 0.47936E-02 0.37656E-02 0.30927E-02 0.26191E-02
0.22668E-02 0.19958E-02 0.17800E-02 0.16049E-02 0.14596E-02 0.13375E-02
0.12330E-02 0.11431E-02 0.10645E-02
                  I=   67
0.10146E-01 0.64686E-02 0.47303E-02 0.37167E-02 0.30539E-02 0.25858E-02
0.22390E-02 0.19709E-02 0.17583E-02 0.15853E-02 0.14420E-02 0.13211E-02
0.12182E-02 0.11292E-02
                  I=   68
0.99994E-02 0.63812E-02 0.46683E-02 0.36699E-02 0.30150E-02 0.25541E-02
0.22112E-02 0.19471E-02 0.17370E-02 0.15663E-02 0.14245E-02 0.13055E-02
0.12036E-02
                  I=   69
0.98570E-02 0.62956E-02 0.46088E-02 0.36229E-02 0.29781E-02 0.25225E-02
0.21846E-02 0.19235E-02 0.17163E-02 0.15475E-02 0.14078E-02 0.12899E-02
                  I=   70
```

```
0.97183E-02 0.62136E-02 0.45493E-02 0.35785E-02 0.29413E-02 0.24923E-02
0.21583E-02 0.19009E-02 0.16959E-02 0.15294E-02 0.13912E-02
                I =   71
0.95849E-02 0.61314E-02 0.44928E-02 0.35341E-02 0.29060E-02 0.24624E-02
0.21330E-02 0.18783E-02 0.16762E-02 0.15115E-02
                I =   72
0.94522E-02 0.60537E-02 0.44365E-02 0.34915E-02 0.28712E-02 0.24336E-02
0.21078E-02 0.18567E-02 0.16567E-02
                I =   73
0.93262E-02 0.59761E-02 0.43825E-02 0.34495E-02 0.28376E-02 0.24049E-02
0.20837E-02 0.18352E-02
                I =   74
0.92010E-02 0.59018E-02 0.43292E-02 0.34089E-02 0.28042E-02 0.23774E-02
0.20597E-02
                I =   75
0.90809E-02 0.58284E-02 0.42777E-02 0.33686E-02 0.27721E-02 0.23501E-02
                I =   76
0.89625E-02 0.57575E-02 0.42266E-02 0.33299E-02 0.27402E-02
                I =   77
0.88486E-02 0.56874E-02 0.41776E-02 0.32914E-02
                I =   78
0.87355E-02 0.56200E-02 0.41289E-02
                I =   79
0.86275E-02 0.55532E-02
                I =   80
0.85201E-02
```

OUTPUT DATA

THE PHOTON FLUX FROM THE BLANKET NO.2

0.84949E 05 0.63603E 05 0.54138E 05 0.61731E 05 0.61825E 05 0.71540E 05
0.89881E 05 0.74696E 05 0.55368E 05 0.38823E 05 0.48860E 05 0.45496E 05
0.42083E 05 0.40914E 05 0.44068E 05 0.36788E 05 0.32835E 05 0.30216E 05
0.28906E 05 0.28216E 05 0.25645E 05 0.23837E 05 0.23117E 05 0.22892E 05
0.21513E 05 0.20080E 05 0.20441E 05 0.20246E 05 0.18342E 05 0.18270E 05
0.18487E 05 0.17296E 05 0.18398E 05 0.16922E 05 0.16486E 05 0.14975E 05
0.16439E 05 0.13624E 05 0.15982E 05 0.14384E 05 0.13770E 05 0.15151E 05
0.14053E 05 0.15703E 05 0.14915E 05 0.14522E 05 0.14940E 05 0.14948E 05
0.10992E 05 0.11715E 05 0.11452E 05 0.11633E 05 0.94130E 04 0.13238E 05
0.18029E 05 0.14561E 05 0.20160E 05 0.20449E 05 0.22444E 05 0.13884E 05
0.10616E 05 0.10534E 05 0.10328E 05 0.56667E 04 0.26071E 04 0.24569E 04
0.16557E 04 0.20989E 04 0.22571E 04 0.20321E 04 0.20974E 04 0.17191E 04
0.17457E 04 0.13684E 04 0.96811E 03 0.65377E 03 0.85667E 03 0.28395E 03
0.35928E 03 0.50547E 03

Appendix H

INPUT DATA OF RUNS NO. 38, 39, and 40

These data were used to determine the moisture content in Na_2CrO_4. The irradiation facility was 4TH1 at the MITR. The descriptions of each run are in Table H-1. Immediately after the table the input data follows.

TABLE H-1

Descriptions of Runs No. 38, 39, and 40

Run Number		38	39	40
Irradiation Time (min.)		468	463	468
Weight of Samples (gm)	Na_2CrO_4	12.3718	0	12.3718
	Mylar	0.7710	0	0
	Al-can	11.6660	11.4248	11.6660
Percent Loss Due to Counting Dead Time		3.5	<1.0	3.0
Diameter of Collimators (inch)		3/4	3/4	3/4

Run numbers and line numbers are labeled at the end of printing lines.

003316	002466	002416	002491	002485	002443	002479	002492	001031	38- 0001
002454	002429	002347	002321	002252	002354	002413	002417	001039	38- 0002
002343	002460	002443	002466	002341	002388	002404	002411	001047	38- 0003
002278	002460	002444	002417	002305	002433	002301	002406	001055	38- 0004
002391	002462	002358	002280	002326	002322	002354	002437	001063	38- 0005
002232	002446	002372	002342	002343	002326	002345	002425	001071	38- 0006
002467	002545	002659	002571	002617	002834	002868	002901	001079	38- 0007
002725	002725	002549	002380	002267	002310	002342	002312	001087	38- 0008
002323	002505	002476	002435	002450	002450	002434	002281	001095	38- 0009
002266	002447	002247	002303	002310	002304	002166	002348	001103	38- 0010
002209	002354	002308	002324	002203	002219	002329	002290	001111	38- 0011
002344	002325	002258	002266	002171	002278	002261	002324	001119	38- 0012
002296	002284	002276	002264	002268	002320	002214	002301	001127	38- 0013
002133	002222	002251	002199	002237	002197	002267	002262	001135	38- 0014
002159	002188	002222	002191	002176	002158	002229	002272	001143	38- 0015
002224	002289	002117	002143	002198	002203	002185	002217	001151	38- 0016
002226	002167	002199	002127	002107	002263	002167	002300	001159	38- 0017
002119	002197	002288	002251	002244	002313	002360	002449	001167	38- 0018
002312	002246	002249	002189	002147	002227	002184	002172	001175	38- 0019
002127	002187	002237	002156	002021	002095	002110	002247	001183	38- 0020
002158	002137	002108	002107	002126	002175	002162	002148	001191	38- 0021
002012	002179	002185	002123	002011	002117	002094	002145	001199	38- 0022
002127	002165	002157	002111	002039	002139	002151	002170	001207	38- 0023
002069	002122	002110	002124	001983	002134	002028	002161	001215	38- 0024
002097	002210	002155	002039	002025	002102	002085	002236	001223	38- 0025
002095	002136	002078	002104	002122	002273	002202	002263	001231	38- 0026
002227	002177	002166	002016	001983	002158	002007	002147	001239	38- 0027
002113	002078	002061	002075	002065	002055	002085	002123	001247	38- 0028
002041	002063	002080	002103	002070	002192	002100	002092	001255	38- 0029
001900	002051	002028	001961	001965	002062	001972	002117	001263	38- 0030
001957	002050	002043	001980	001877	002023	002008	002064	001271	38- 0031
001972	001964	002043	001935	001937	001931	001938	002050	001279	38- 0032

000604	000585	000599	000541	000569	000571	000603	000597	001031	39- 0001
000594	000571	000559	000614	000558	000610	000574	000617	001039	39- 0002
000569	000592	000545	000592	000585	000598	000544	000560	001047	39- 0003
000548	000567	000582	000572	000550	000572	000554	000608	001055	39- 0004
000566	000602	000581	000558	000519	000550	000552	000541	001063	39- 0005
000549	000581	000590	000581	000549	000568	000561	000604	001071	39- 0006
000553	000596	000583	000533	000592	000558	000604	000591	001079	39- 0007
000574	000648	000603	000565	000508	000527	000562	000571	001087	39- 0008
000529	000568	000561	000521	000506	000537	000528	000523	001095	39- 0009
000545	000528	000525	000524	000560	000567	000516	000533	001103	39- 0010
000551	000535	000552	000528	000544	000527	000550	000522	001111	39- 0011
000527	000540	000559	000530	000530	000545	000529	000566	001119	39- 0012
000556	000555	000546	000547	000559	000535	000548	000568	001127	39- 0013
000554	000552	000552	000573	000544	000522	000565	000520	001135	39- 0014
000592	000512	000527	000569	000524	000478	000499	000550	001143	39- 0015
000486	000537	000582	000530	000489	000551	000539	000556	001151	39- 0016
000505	000520	000498	000505	000509	000525	000503	000528	001159	39- 0017
000553	000567	000582	000531	000483	000489	000514	000516	001167	39- 0018
000527	000551	000508	000471	000473	000551	000522	000561	001175	39- 0019
000492	000502	000518	000515	000504	000508	000502	000495	001183	39- 0020
000522	000530	000502	000506	000517	000491	000529	000474	001191	39- 0021
000513	000473	000473	000543	000495	000491	000523	000503	001199	39- 0022
000463	000524	000520	000465	000515	000493	000505	000520	001207	39- 0023
000486	000469	000488	000494	000462	000523	000485	000497	001215	39- 0024
000505	000519	000512	000528	000460	000471	000520	000520	001223	39- 0025
000504	000520	000514	000530	000403	000515	000518	000444	001231	39- 0026
000500	000521	000529	000493	000464	000514	000469	000503	001239	39- 0027
000494	000530	000464	000500	000432	000483	000494	000452	001247	39- 0028
000468	000510	000510	000465	000445	000472	000462	000483	001255	39- 0029
000486	000497	000470	000470	000465	000469	000468	000472	001263	39- 0030
000508	000477	000515	000467	000477	000470	000517	000541	001271	39- 0031
000470	000493	000504	000454	000471	000525	000483	000469	001279	39- 0032

001975	002066	001952	001988	001896	001886	001992	001925	001031	40- 0001
001876	001966	001876	001869	001789	001879	001820	001884	001039	40- 0002
001867	001921	001842	001863	001765	001932	001742	001852	001047	40- 0003
001743	001812	001883	001842	001797	001789	001738	001818	001055	40- 0004
001726	001821	001773	001850	001701	001841	001790	001869	001063	40- 0005
001847	001838	001846	001770	001790	001940	001787	001845	001071	40- 0006
001800	001830	001816	001845	001806	001858	001997	001912	001079	40- 0007
001908	001931	001879	001915	001834	001844	001794	001885	001087	40- 0008
001748	001857	001920	001976	001868	001860	001856	001811	001095	40- 0009
001685	001784	001678	001750	001654	001719	001752	001789	001103	40- 0010
001763	001750	001718	001730	001671	001745	001752	001851	001111	40- 0011
001734	001787	001773	001779	001719	001778	001673	001814	001119	40- 0012
001732	001814	001750	001785	001659	001691	001713	001758	001127	40- 0013
001693	001747	001729	001663	001615	001709	001616	001760	001135	40- 0014
001692	001698	001648	001669	001666	001719	001719	001689	001143	40- 0015
001675	001679	001697	001741	001661	001652	001703	001678	001151	40- 0016
001708	001702	001665	001619	001514	001604	001648	001663	001159	40- 0017
001665	001787	001702	001724	001632	001718	001734	001835	001167	40- 0018
001805	001849	001678	001683	001649	001650	001648	001623	001175	40- 0019
001521	001682	001583	001691	001587	001599	001593	001708	001183	40- 0020
001680	001603	001649	001572	001660	001602	001636	001608	001191	40- 0021
001547	001629	001678	001708	001559	001628	001588	001650	001199	40- 0022
001612	001612	001664	001628	001658	001620	001697	001676	001207	40- 0023
001579	001660	001546	001631	001506	001607	001618	001709	001215	40- 0024
001572	001699	001621	001632	001511	001609	001583	001670	001223	40- 0025
001605	001709	001756	001722	001631	001772	001825	001836	001231	40- 0026
001787	001677	001743	001563	001612	001584	001587	001619	001239	40- 0027
001566	001626	001618	001519	001567	001538	001616	001633	001247	40- 0028
001582	001642	001622	001558	001543	001595	001572	001561	001255	40- 0029
001558	001511	001629	001640	001526	001561	001580	001589	001263	40- 0030
001501	001610	001625	001513	001620	001605	001488	001651	001271	40- 0031
001483	001558	001492	001560	001495	001588	001581	001576	001279	40- 0032

Appendix I

GAMANL OUTPUT DATA AND THEIR SPECTRAL FIGURES OF RUNS NO. 99, 102, 103, 104, AND 105

PKANAL output data from GAMANL are reported. Original data plots done by the CAL-COMP at the MIT Information Processing Center follow immediately after the data.

Runs No. 99, 102, and 103 are decay gamma-ray spectra in Blanket No. 2. The identifying characteristics of these gamma-ray spectra is given in Table I-1.

TABLE I-1

DESCRIPTIONS OF RUNS NO. 99, 102, and 103

Run Number	99	102	103
Irradiation Time (min.)	1424	1372	1372
Cooling Time (min.)	106	288	1509
Counting Time (min.)	949	1187	2589
Diameter of Collimator (inch)	None	None	None

Runs No. 104 and 105 are prompt gamma-ray spectra in Blanket No. 2. The description of these runs is given in Table I-2.

TABLE I-2

DESCRIPTIONS OF RUNS NO. 104 and 105

Run Number	104	105
Irradiation Time (min.)	1380	1380
Diameter of Collimators (inch)	5/16	3/16

Run numbers and line numbers are labeled at the end of printing lines.

NO.	ENERGY(KEV)	INT(GAUS)	PC ERR	AREAG	AREAS	
1	213.179	0.008	10.215	2185.908	1803.234	99- 0001
2	230.928	0.053	2.082	12710.273	12485.074	99- 0002
4	251.546	0.005	16.975	1032.542	1297.477	99- 0003
5	264.872	0.003	29.531	548.368	411.492	99- 0004
8	296.527	0.004	18.232	764.832	618.344	99- 0005
9	304.299	0.005	17.073	796.529	565.570	99- 0006
10	317.174	0.014	6.321	2311.401	3017.425	99- 0007
11	335.219	0.018	5.610	2581.519	2478.785	99- 0008
14	378.109	0.005	20.575	534.859	367.550	99- 0009
15	385.227	0.003	36.900	287.285	178.970	99- 0010
3	240.598	0.007	10.953	1708.567	1399.023	99- 0011
6	279.294	0.094	1.469	18275.953	18789.246	99- 0012
7	287.872	0.009	8.936	1722.252	1244.609	99- 0013
12	350.438	0.003	33.040	351.183	205.263	99- 0014
13	371.009	0.003	26.784	410.167	234.385	99- 0015
17	511.000	0.023	6.743	1622.857	1756.907	99- 0016
16	435.124	0.003	31.287	317.083	276.097	99- 0017
18	530.557	0.015	9.930	1002.059	1112.492	99- 0018
19	541.595	0.004	35.640	240.631	158.561	99- 0019
20	556.301	0.011	14.156	641.306	671.860	99- 0020
21	585.002	0.010	15.488	552.237	489.808	99- 0021
22	592.583	0.007	21.206	384.741	374.947	99- 0022
23	658.195	0.033	6.343	1534.855	1861.594	99- 0023
24	667.134	0.014	12.589	655.797	797.844	99- 0024
25	725.275	0.006	31.917	222.122	261.589	99- 0025
26	743.282	0.024	8.956	948.259	1014.743	99- 0026
27	761.174	0.007	26.548	258.653	224.519	99- 0027
28	772.207	0.019	11.094	703.500	607.910	99- 0028
29	811.786	0.009	22.388	300.782	265.597	99- 0029
30	816.542	0.008	24.367	273.771	232.267	99- 0030
31	824.820	0.010	19.604	343.249	425.135	99- 0031
32	831.531	0.012	17.416	392.970	497.056	99- 0032
33	846.776	0.065	4.816	2071.415	2552.007	99- 0033
34	912.462	0.007	31.253	208.065	134.707	99- 0034
35	946.443	0.007	34.137	187.467	112.623	99- 0035
						99- 0036

36	961.593	0.008	29.805	217.064	193.209	99- 0037
37	1024.770	0.015	19.289	354.856	328.490	99- 0038
38	1039.246	0.011	25.730	254.732	157.101	99- 0039
39	1076.386	0.012	23.993	270.727	197.927	99- 0040
40	1147.574	0.010	28.750	192.113	144.234	99- 0041
41	1173.098	0.066	6.328	1245.071	1352.769	99- 0042
42	1261.327	0.016	17.082	279.039	207.467	99- 0043
43	1282.542	0.009	27.577	148.538	155.771	99- 0044
44	1293.600	0.221	3.205	3641.353	3719.141	99- 0045
45	1332.499	0.063	6.735	987.227	1029.501	99- 0046
46	1368.656	0.166	3.924	2508.201	2613.879	99- 0047
47	1384.916	0.016	17.662	232.396	208.447	99- 0048
48	1408.287	0.008	32.237	107.772	68.135	99- 0049
49	1451.560	0.011	24.171	144.621	155.647	99- 0050
50	1460.339	0.070	6.748	935.603	993.641	99- 0051
51	1509.873	0.007	34.670	93.760	89.726	99- 0052
52	1522.522	0.010	26.256	127.285	80.339	99- 0053
53	1587.584	0.010	29.591	113.215	106.813	99- 0054
54	1595.705	0.021	16.584	238.908	243.432	99- 0055
55	1677.864	0.010	30.932	104.157	55.147	99- 0056
56	1731.830	0.177	4.693	1815.599	2004.511	99- 0057
57	1758.910	0.011	28.007	114.223	61.037	99- 0058
58	1780.660	0.013	25.569	124.087	140.891	99- 0059
59	1794.482	0.013	24.632	130.241	149.747	99- 0060
60	1810.563	0.033	13.104	315.250	361.954	99- 0061
61	1875.021	0.016	23.338	140.300	100.923	99- 0062
62	1938.818	0.014	25.580	121.382	111.408	99- 0063
63	2208.377	0.019	24.802	122.236	114.710	99- 0064
64	2243.532	0.041	14.818	266.767	405.016	99- 0065
65	2320.183	0.019	25.773	123.628	110.379	99- 0066
66	2614.956	0.021	21.751	121.774	95.720	99- 0067
67	2754.157	0.235	5.844	1320.215	1404.004	99- 0068

NO.	ENERGY(KEV)	INT(GAUS)	PC ERR	AREAG	AREAS	
1	107.858	0.319	3.738	12658.344	11278.125	102-0001
2	178.878	0.028	33.816	853.693	561.543	102-0002
3	186.421	0.025	38.140	725.901	483.043	102-0003
4	210.091	0.106	9.582	2805.354	2621.332	102-0004
5	228.847	0.368	3.379	8981.672	9109.719	102-0005
6	238.492	0.062	15.272	1438.431	2029.882	102-0006
7	251.461	0.036	26.813	793.019	1114.336	102-0007
8	278.094	0.657	2.364	12779.559	13058.969	102-0008
9	285.619	0.055	17.448	1029.788	808.255	102-0009
10	316.181	0.079	13.302	1279.738	1301.717	102-0010
11	334.477	0.127	9.138	1871.112	1685.291	102-0011
12	352.833	0.041	26.151	551.740	479.755	102-0012
13	511.000	0.211	8.958	1489.964	1868.859	102-0013
14	529.719	0.155	12.055	1027.708	942.272	102-0014
15	556.052	0.082	22.017	496.031	419.747	102-0015
16	609.172	0.079	25.150	404.487	334.801	102-0016
17	658.015	0.228	10.908	1051.729	1126.235	102-0017
18	667.085	0.117	19.178	531.150	465.293	102-0018
19	723.314	0.059	37.568	239.785	207.711	102-0019
20	743.414	0.218	12.438	846.204	1037.701	102-0020
21	772.468	0.155	17.074	565.732	479.758	102-0021
22	846.781	0.214	14.481	679.912	730.439	102-0022
23	954.023	0.117	29.203	306.800	218.570	102-0023
24	1000.612	0.111	31.360	268.834	348.419	102-0024
25	1023.907	0.102	35.788	239.309	164.438	102-0025
26	1164.807	0.153	23.693	293.421	299.851	102-0026
27	1172.460	1.838	4.344	3492.289	3569.862	102-0027
28	1260.326	0.128	26.122	218.017	176.644	102-0028
29	1293.000	2.372	4.020	3905.453	4163.172	102-0029
30	1331.524	1.954	4.553	3075.983	3013.378	102-0030
31	1367.919	1.384	5.591	2086.798	2167.485	102-0031
32	1460.040	0.965	7.219	1296.068	1426.822	102-0032
33	1594.063	0.306	15.609	350.966	506.235	102-0033
34	1731.299	1.357	7.109	1393.540	1408.743	102-0034
35	1763.154	0.139	29.355	139.010	100.990	102-0035
						102-0036

36	1810.703	0.185	24.946	177.481	146.414	102-0037
37	2240.785	0.314	23.599	204.104	196.744	102-0038
38	2613.130	0.220	28.986	128.471	107.409	102-0039
39	2751.601	2.113	8.313	1185.930	1262.056	102-0040

NO.	ENERGY(KEV)	INT(GAUS)	PC ERR	AREAG	AREAS	
1	108.594	0.483	3.219	19112.602	16959.477	103-0001
2	117.238	0.069	19.644	2628.319	1732.488	103-0002
3	210.687	0.170	7.787	4488.375	4189.754	103-0003
4	229.332	0.577	2.792	14042.230	14680.539	103-0004
5	239.324	0.165	7.940	3836.449	4358.730	103-0005
6	270.759	0.047	26.216	947.367	694.797	103-0006
7	278.464	0.965	2.032	18747.805	19007.934	103-0007
8	286.107	0.078	15.947	1467.226	936.248	103-0008
9	296.432	0.052	23.593	933.570	1402.842	103-0009
10	317.845	0.135	10.237	2157.691	3232.302	103-0010
11	334.925	0.163	9.034	2384.022	2393.234	103-0011
12	353.092	0.075	18.836	994.345	837.214	103-0012
13	377.540	0.038	37.780	444.695	287.482	103-0013
14	486.014	0.071	26.116	546.845	472.229	103-0014
15	511.000	0.232	9.616	1636.404	2288.453	103-0015
16	529.241	0.122	17.401	808.996	701.763	103-0016
17	558.240	0.058	36.552	347.389	217.407	103-0017
18	582.955	0.119	19.981	651.587	548.469	103-0018
19	608.826	0.163	15.700	828.796	824.666	103-0019
20	657.686	0.204	13.570	942.732	1096.937	103-0020
21	666.913	0.236	12.201	1069.776	1261.304	103-0021
22	743.211	0.173	17.722	669.804	551.592	103-0022
23	771.864	0.291	11.872	1064.555	871.063	103-0023
24	909.753	0.271	15.138	766.142	1806.896	103-0024
25	947.162	0.223	18.876	592.073	1398.600	103-0025
26	953.553	0.206	20.482	539.235	1273.746	103-0026
27	1112.481	0.276	17.667	569.922	898.044	103-0027
28	1170.832	4.510	2.709	8589.191	8939.211	103-0028
29	1286.564	0.112	30.599	186.500	151.564	103-0029
30	1329.505	5.076	2.761	8007.551	8325.996	103-0030
31	1337.234	0.123	26.711	191.632	85.425	103-0031
32	1365.532	0.935	7.006	1413.162	1466.850	103-0032
33	1457.761	2.169	4.655	2922.282	3189.874	103-0033
34	1591.575	0.618	10.011	711.620	1181.397	103-0034
35	1727.941	0.974	8.275	1002.937	1205.884	103-0035
						103-0036

36	2237.318	0.227	27.567	147.612	150.204	103-0037
37	2607.338	0.503	16.779	294.811	301.718	103-0038
38	2746.359	1.258	11.630	707.311	778.368	103-0039

NO.	ENERGY(KEV)	INT(GAUS)	PC ERR	AREAG	AREAS	
1	459.106	0.014	33.872	1145.985	804.066	104-0001
2	477.202	0.049	9.989	3938.426	3284.523	104-0002
3	493.330	0.089	5.961	6677.461	4220.941	104-0003
4	511.000	0.939	0.996	66322.750	66928.500	104-0004
5	529.796	0.146	3.958	9628.043	15835.121	104-0005
6	546.501	0.096	6.002	5985.398	9879.695	104-0006
7	596.450	0.275	2.830	14432.184	23677.652	104-0007
8	627.373	0.022	29.980	1083.390	757.430	104-0008
9	644.570	0.022	30.526	1044.138	776.910	104-0009
10	662.763	0.022	30.577	1025.351	993.633	104-0010
11	695.240	0.275	3.206	11735.730	20149.082	104-0011
12	812.257	0.025	33.600	851.739	738.270	104-0012
13	832.721	0.094	9.780	3049.276	3385.102	104-0013
14	846.946	0.102	9.285	3225.928	3611.931	104-0014
15	867.458	0.111	8.792	3386.718	3220.375	104-0015
16	886.066	0.038	25.029	1119.021	1099.067	104-0016
17	902.678	0.036	26.932	1037.552	1034.893	104-0017
18	959.601	0.043	24.896	1111.435	991.355	104-0018
19	996.144	0.047	24.098	1142.966	957.023	104-0019
20	1016.647	0.102	11.126	2418.334	5632.043	104-0020
21	1038.990	0.176	6.991	4032.968	9390.566	104-0021
22	1066.548	0.278	4.870	6114.258	14234.102	104-0022
23	1173.157	0.156	8.043	2969.536	2951.820	104-0023
24	1200.894	0.118	10.372	2155.152	2419.078	104-0024
25	1221.134	0.033	35.105	582.835	446.753	104-0025
26	1259.855	0.058	20.424	993.602	917.462	104-0026
27	1275.950	0.244	5.492	4097.801	2759.040	104-0027
28	1293.600	2.935	1.038	48282.281	48718.508	104-0028
29	1311.706	0.342	4.043	5513.652	18504.961	104-0029
30	1331.080	0.375	3.840	5907.156	20438.359	104-0030
31	1346.816	0.200	6.383	3087.626	10674.215	104-0031
32	1588.797	0.040	35.208	465.583	494.744	104-0032
33	1728.436	0.070	22.042	722.646	633.059	104-0033
34	1780.983	0.061	25.746	601.157	537.754	104-0034
35	2225.275	0.363	6.589	2366.207	2509.977	104-0035
						104-0036

36	2391.301	0.073	25.784	455.274	512.573	104-0037
37	2828.953	0.057	32.534	314.547	433.933	104-0038
38	3201.317	0.123	17.184	592.713	553.619	104-0039
39	3388.760	0.077	26.340	347.753	304.936	104-0040
40	3709.047	0.069	31.087	270.374	392.802	104-0041
41	3794.903	0.067	33.061	254.578	204.502	104-0042
42	3929.173	0.092	25.382	339.277	321.601	104-0043
43	4905.406	0.519	7.641	1794.648	2203.894	104-0044
44	5003.273	0.458	8.305	1583.407	1598.050	104-0045
45	5181.020	0.058	35.610	199.871	139.861	104-0046
46	5365.992	0.121	19.483	417.134	330.225	104-0047
47	5419.438	0.067	31.111	232.200	194.890	104-0048
48	5513.121	0.085	25.346	293.007	328.364	104-0049
49	6266.563	0.172	17.244	595.818	716.847	104-0050
50	6619.016	1.004	14.283	3469.903	4073.336	104-0051
51	6631.465	0.765	14.528	2644.042	3100.268	104-0052
52	6710.379	0.208	18.665	717.824	764.592	104-0053
53	7130.902	0.155	22.997	536.525	1005.655	104-0054
54	7645.598	0.061	32.750	210.083	330.517	104-0055
55	7874.633	0.040	38.944	136.763	202.895	104-0056
56	8286.094	0.088	40.916	304.016	288.207	104-0057
57	9410.453	0.031	71.868	106.301	35.291	104-0058
58	9419.777	0.038	71.184	130.607	41.234	104-0059
59	9428.664	0.059	69.929	202.948	67.456	104-0060
60	9437.887	0.081	69.462	279.650	91.339	104-0061

NO.	ENERGY(KEV)	INT(GAUS)	PC ERR	AREAG	AREAS	
1	417.102	0.048	13.709	4684.965	3811.945	105-0001
2	438.149	0.041	16.675	3716.072	3515.562	105-0002
3	476.293	0.141	5.600	11263.141	10858.082	105-0003
4	493.339	0.149	5.476	11212.000	7046.477	105-0004
5	511.000	1.785	0.743	126096.688	127862.313	105-0005
6	529.730	0.246	3.674	16233.375	16877.094	105-0006
7	545.923	0.119	7.590	7411.738	7686.652	105-0007
8	566.065	0.086	11.024	5016.242	5177.730	105-0008
9	596.773	0.410	2.841	21465.652	31547.719	105-0009
10	625.209	0.044	24.534	2178.910	3233.853	105-0010
11	643.627	0.032	34.041	1524.977	1028.855	105-0011
12	660.651	0.040	27.813	1846.275	1317.770	105-0012
13	676.491	0.037	30.769	1651.373	936.465	105-0013
14	695.369	0.478	2.830	20409.566	32519.555	105-0014
15	753.166	0.054	23.835	2051.695	1634.184	105-0015
16	809.600	0.070	20.055	2384.745	2186.516	105-0016
17	830.554	0.190	7.884	6201.418	6778.723	105-0017
18	846.049	0.359	4.488	11417.621	12530.359	105-0018
19	866.682	0.208	7.618	6367.727	5838.023	105-0019
20	883.918	0.059	26.401	1752.930	1196.043	105-0020
21	901.426	0.059	27.436	1684.218	1460.090	105-0021
22	938.270	0.054	31.604	1441.885	1110.078	105-0022
23	957.719	0.072	24.370	1878.025	1836.441	105-0023
24	977.875	0.053	34.173	1326.465	1014.531	105-0024
25	1034.255	0.325	6.190	7489.391	14392.059	105-0025
26	1054.952	0.517	4.175	11572.813	22301.027	105-0026
27	1067.645	0.574	3.871	12608.277	24302.781	105-0027
28	1141.293	0.056	34.843	1116.852	815.367	105-0028
29	1173.794	0.128	15.817	2436.137	2210.672	105-0029
30	1200.595	0.286	7.477	5229.129	5770.645	105-0030
31	1260.790	0.086	24.346	1462.256	1061.445	105-0031
32	1275.678	0.458	4.965	7685.953	5281.680	105-0032
33	1293.599	5.825	0.773	95830.375	96194.250	105-0033
34	1312.006	0.597	3.918	9607.844	17398.445	105-0034
35	1329.545	0.493	4.691	7781.234	14378.695	105-0035
						105-0036

36	1362.635	0.280	8.055	4244.570	7786.570	105-0037
37	1433.938	0.169	14.042	2344.647	2114.301	105-0038
38	1459.761	0.148	16.431	1983.029	2066.344	105-0039
39	1546.060	0.070	35.983	850.533	622.398	105-0040
40	1565.016	0.083	30.895	979.491	792.594	105-0041
41	1615.142	0.114	23.387	1285.466	1041.934	105-0042
42	1658.895	0.085	31.254	926.239	692.707	105-0043
43	1676.159	0.085	31.585	910.679	673.961	105-0044
44	1694.106	0.084	32.253	887.369	670.344	105-0045
45	1712.429	0.139	19.918	1445.831	1496.601	105-0046
46	1728.494	0.285	10.210	2937.366	3043.073	105-0047
47	1749.065	0.093	29.914	940.388	720.344	105-0048
48	1780.853	0.262	11.325	2580.231	2438.645	105-0049
49	2206.265	0.118	29.790	775.973	545.992	105-0050
50	2224.811	0.894	4.768	5830.555	5468.355	105-0051
51	2242.717	0.143	24.703	929.709	617.422	105-0052
52	2334.394	0.103	33.640	650.070	477.921	105-0053
53	2352.069	0.107	32.253	675.756	457.131	105-0054
54	2390.025	0.150	23.474	936.441	892.917	105-0055
55	2418.660	0.107	32.491	661.987	757.961	105-0056
56	2572.258	0.127	27.395	753.227	656.872	105-0057
57	2756.356	0.198	17.950	1107.347	905.167	105-0058
58	3115.814	0.116	30.831	578.524	509.044	105-0059
59	3138.850	0.137	26.239	676.434	529.914	105-0060
60	3173.018	0.105	33.818	515.365	377.698	105-0061
61	3198.591	0.419	9.592	2027.268	2446.778	105-0062
62	3388.608	0.198	19.533	892.370	870.829	105-0063
63	3444.674	0.187	20.692	823.701	864.017	105-0064
64	3793.810	0.257	16.748	978.871	1008.996	105-0065
65	3863.431	0.119	34.403	444.311	609.046	105-0066
66	3884.296	0.110	37.081	410.288	385.396	105-0067
67	3929.704	0.403	11.396	1485.245	1706.624	105-0068
68	4227.730	0.144	28.981	498.411	908.489	105-0069
69	4510.117	0.177	23.014	611.121	741.236	105-0070
70	4904.563	1.359	4.443	4696.270	5694.051	105-0071
71	4949.297	0.127	29.659	438.659	727.118	105-0072

72	5002.707	1.316	4.555	4548.410	5443.262	105-0073
73	5053.020	0.115	32.129	397.463	378.422	105-0074
74	5076.387	0.127	29.253	438.831	574.279	105-0075
75	5091.199	0.236	16.718	814.146	1072.372	105-0076
76	5236.230	0.178	21.439	614.725	508.369	105-0077
77	5367.492	0.350	11.623	1209.005	1533.405	105-0078
78	5381.563	0.162	22.595	559.650	711.659	105-0079
79	5417.109	0.213	17.718	737.851	979.849	105-0080
80	5514.445	0.176	20.783	609.300	564.425	105-0081
81	5693.570	0.139	24.727	480.055	378.155	105-0082
82	5767.234	0.124	27.230	427.656	501.934	105-0083
83	6145.758	0.118	27.224	408.997	346.203	105-0084
84	6228.984	0.184	18.415	634.417	1019.083	105-0085
85	6264.684	0.599	7.725	2070.156	3383.674	105-0086
86	6299.227	0.100	31.647	344.702	240.179	105-0087
87	6350.875	0.123	26.435	424.899	536.964	105-0088
88	6618.664	3.193	5.080	11035.141	15793.465	105-0089
89	6630.148	2.469	5.267	8533.848	12244.852	105-0090
90	6711.113	1.203	6.209	4156.922	5936.016	105-0091
91	6772.184	0.132	24.383	457.168	578.554	105-0092
92	6928.914	0.108	27.246	372.375	446.167	105-0093
93	7131.711	0.512	9.211	1769.952	2405.972	105-0094
94	7142.641	0.375	10.429	1297.652	1765.784	105-0095
95	7221.762	0.193	14.704	667.512	842.306	105-0096
96	7471.832	0.048	35.556	165.629	289.243	105-0097
97	7643.750	0.155	14.885	535.448	1257.325	105-0098
98	7730.398	0.058	25.399	201.787	195.259	105-0099
99	7874.367	0.222	13.888	766.958	1237.986	105-0100
100	8285.500	0.271	15.699	937.831	1499.682	105-0101
101	8384.594	0.037	32.251	126.778	195.058	105-0102
102	8523.141	0.026	36.535	91.565	66.424	105-0103
103	8706.859	0.039	29.878	134.729	218.583	105-0104
104	8794.793	0.046	27.809	159.517	193.156	105-0105
105	9304.563	0.021	37.610	72.526	54.094	105-0106
106	9358.992	0.020	38.345	70.260	32.448	105-0107
107	9377.188	0.028	35.418	95.470	44.085	105-0108

108	9386.203	0.025	36.470	85.940	36.755	105-0109
109	9395.434	0.040	32.677	139.382	64.550	105-0110
110	9404.285	0.042	32.587	146.139	64.376	105-0111
111	9413.488	0.059	31.086	202.861	91.715	105-0112
112	9422.270	0.063	31.058	219.084	91.949	105-0113
113	9431.379	0.086	30.163	296.619	124.337	105-0114

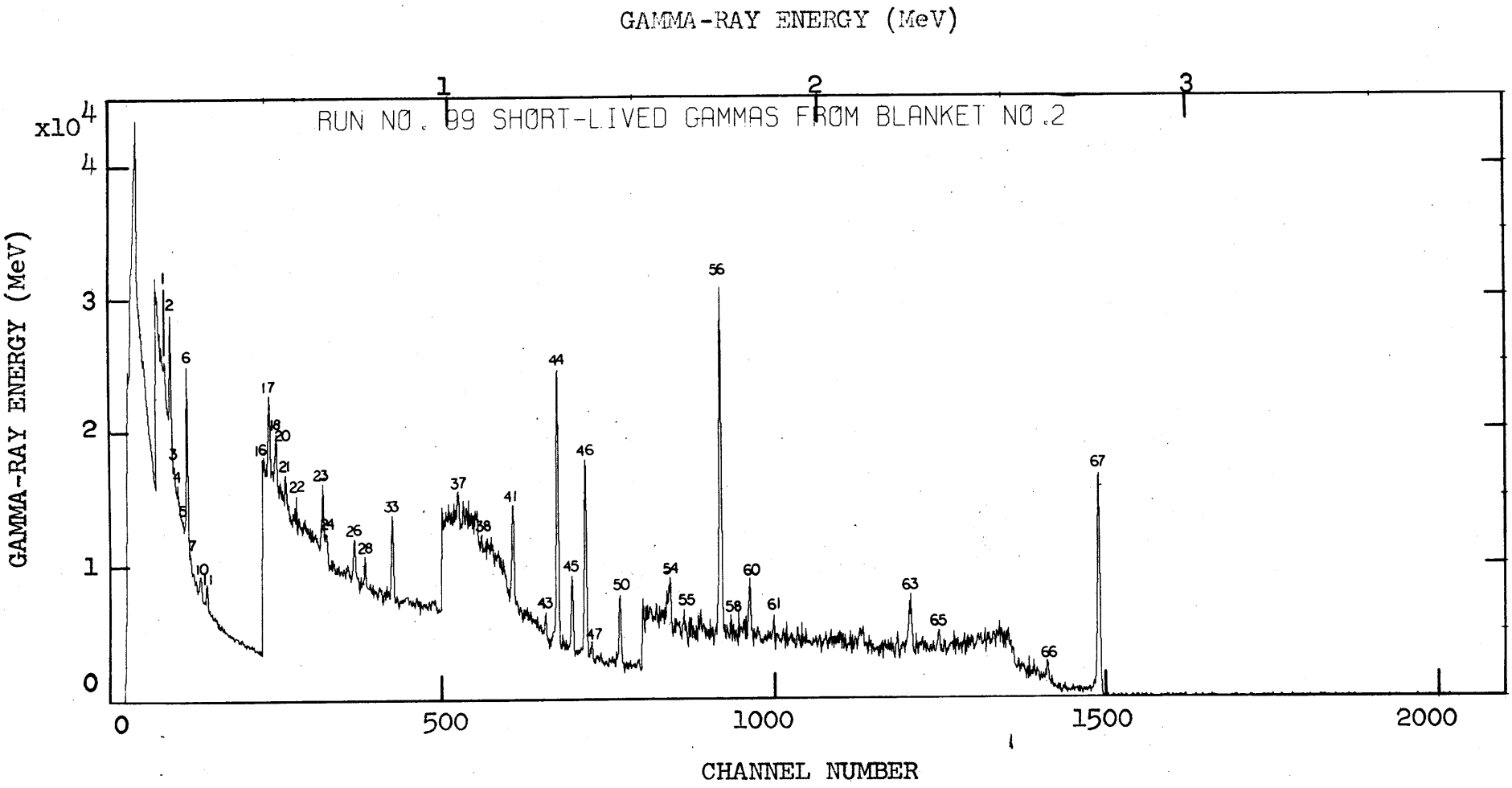

Fig. I-1 Run No. 99, Short-Lived Gamma-Rays from Blanket No. 2

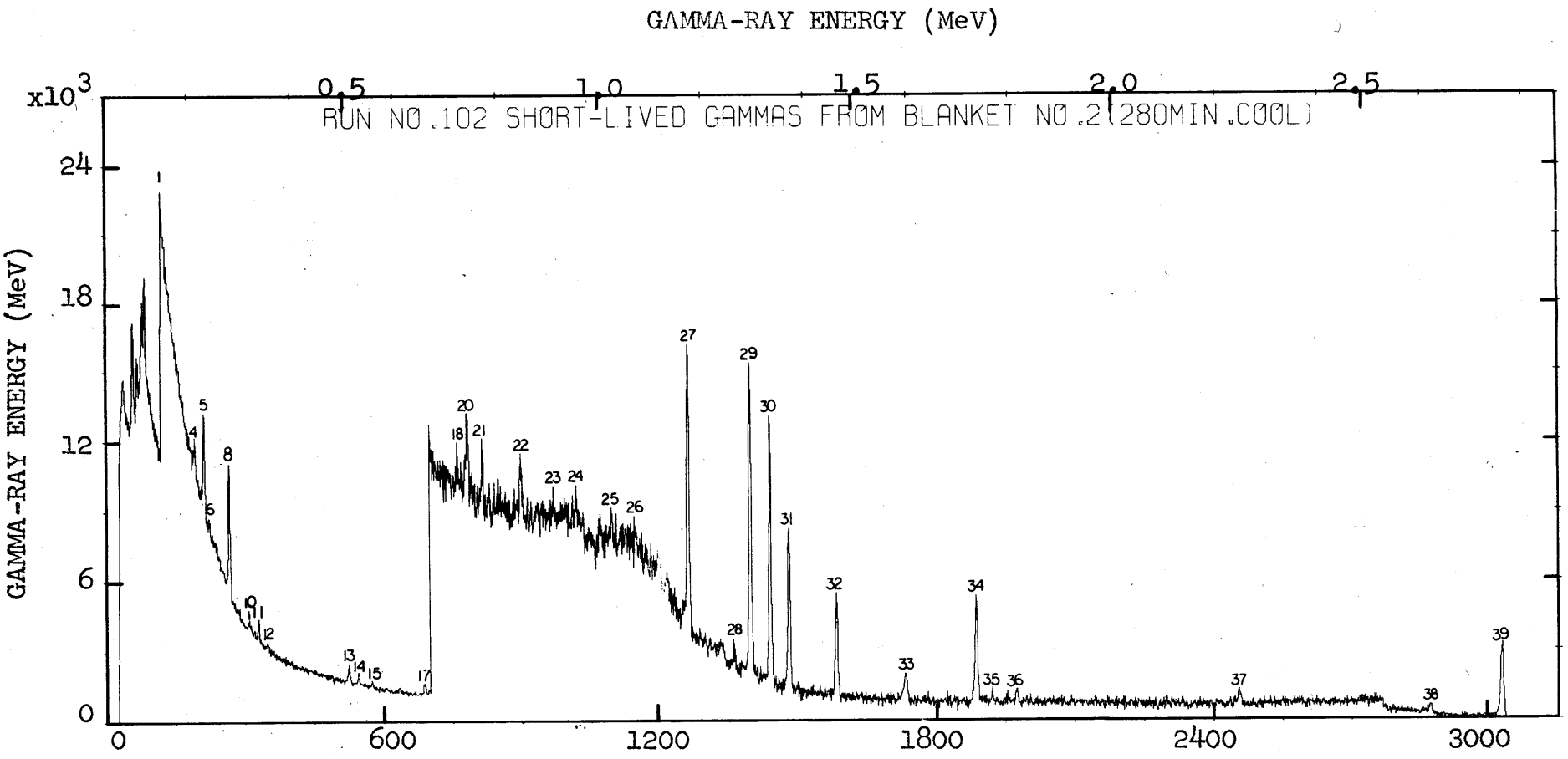

Fig. I-2 Run No. 102, Short-Lived Gammas

(280 min. Cooling)

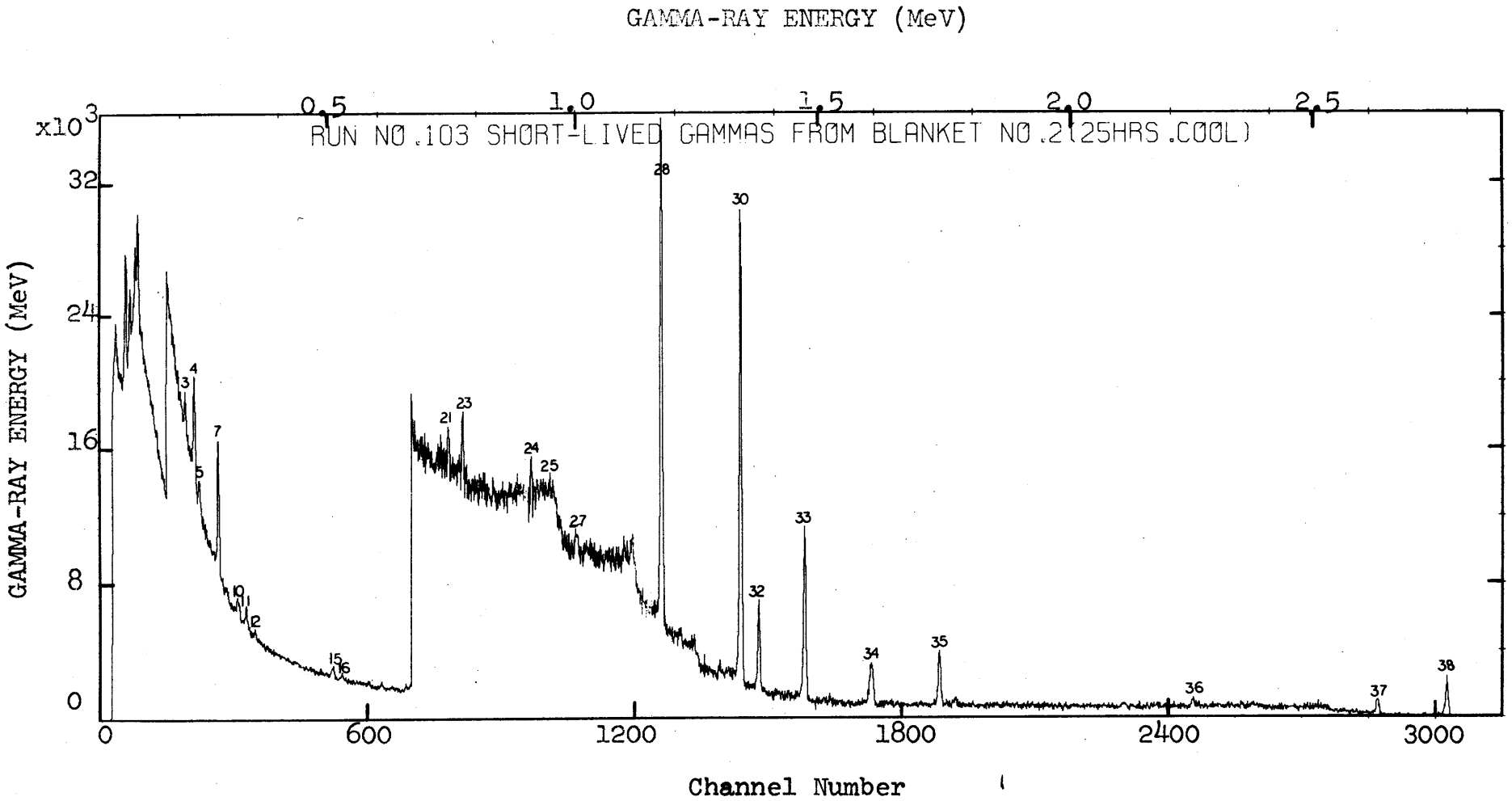

Fig. I-3 Run No. 103, Short-Lived Gammas
(25 Hrs. Cooling)

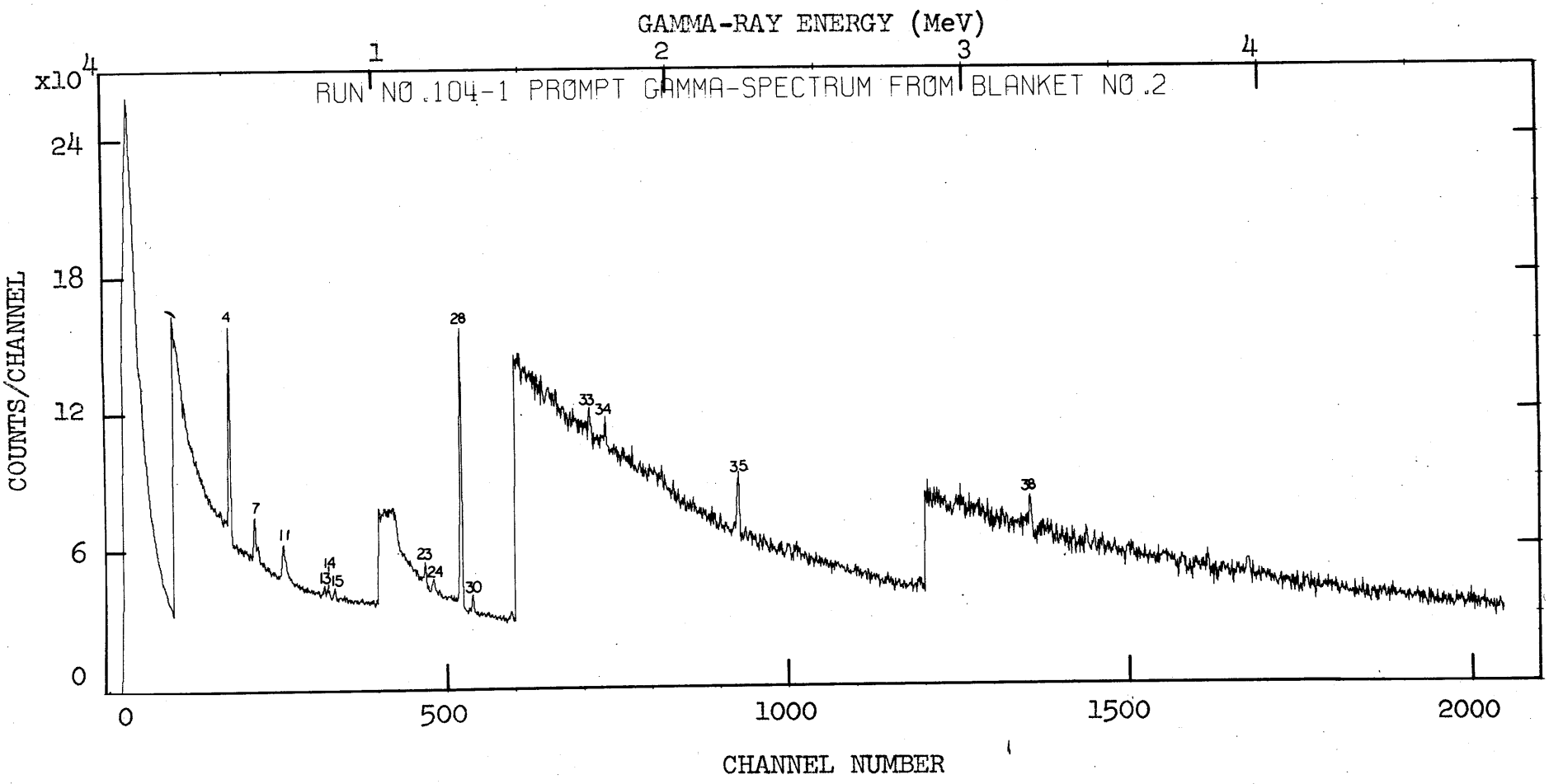

Fig. I-4 Run No. 104-1, Prompt Gamma-Spectrum from Blanket No. 2

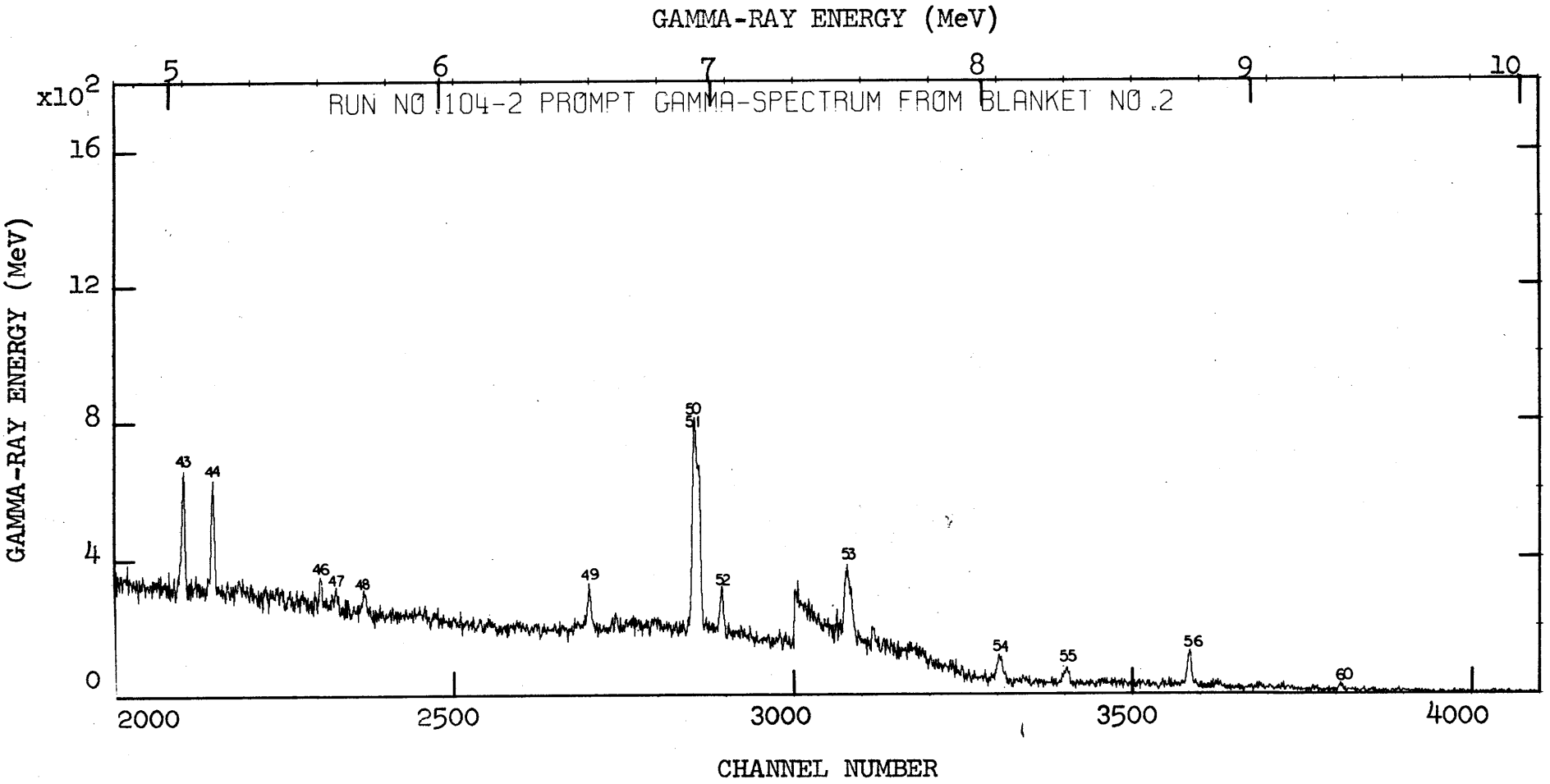

Fig. I-5 Run No. 104-2, Prompt Gamma-Spectrum from Blanket No. 2

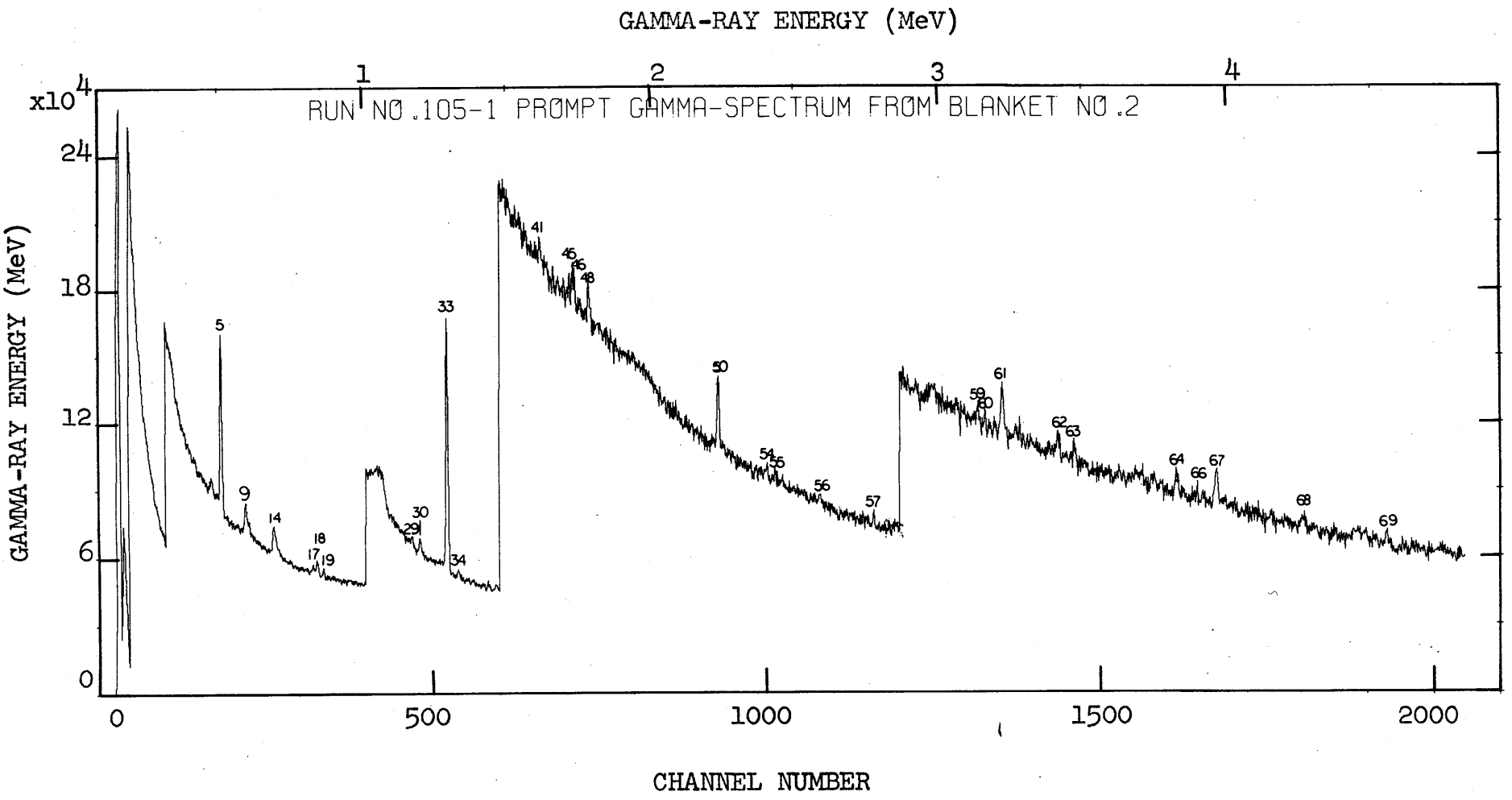

Fig. I-6 Run No. 105-1, Prompt Gamma-Spectrum from Blanket No. 2

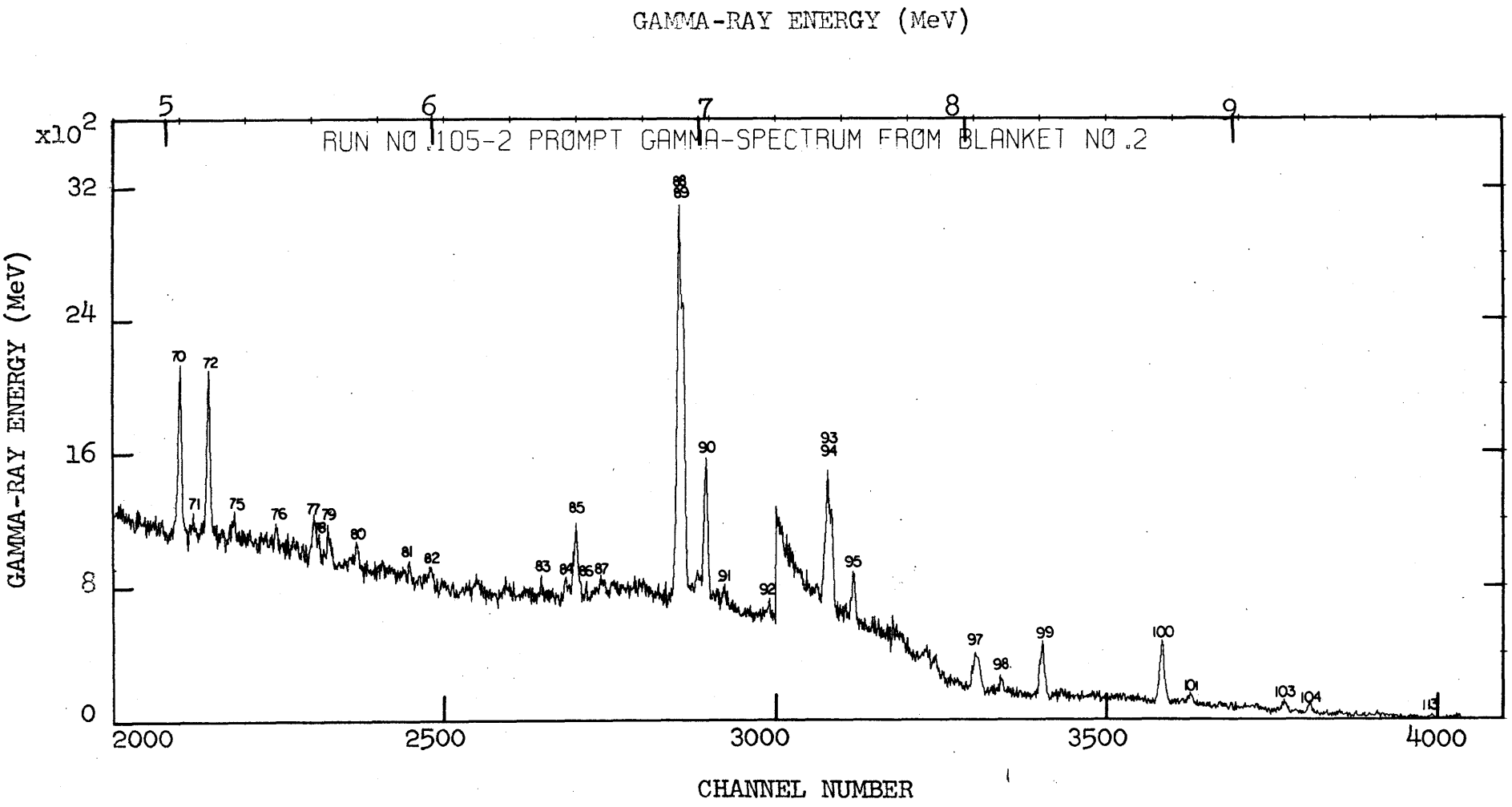

Fig. I-7 Run No. 105-2, Prompt Gamma-Spectrum from Blanket No. 2